Article:
González-Cuest, Manuel, Sidhu, Peter, Ashmus, Roger A. et al. (10 more authors) (2022) Bicyclic picomolar OGA inhibitors enable chemoproteomic mapping of its endogenous post-translational modifications. Journal of the American Chemical Society. 832–844. ISSN 1520-5126

https://doi.org/10.1021/jacs.1c10504

Bicyclic picomolar OGA inhibitors enable chemoproteomic mapping of its endogenous post-translational modifications.

Manuel González-Cuesta,[a] Peter Sidhu,[b,c] Roger A. Ashmus,[b] Alexandra Males,[d] Cameron Proceviat,[b] Zarina Madden,[b] Jason C. Rogalski,[c] Jil A. Busmann,[e] Leonard J. Foster,[c] José M. García Fernández,[f] Gideon J. Davies,[d,*] Carmen Ortiz Mellet,[a,*] David J. Vocadlo[b,e,*]

[a] Departamento de Química Orgánica, Facultad de Química, Universidad de Sevilla, 41012, Sevilla, Spain.
[b] Department of Chemistry, Simon Fraser University, Burnaby V5A 1S6, British Columbia, Canada.
[c] Department of Biochemistry and Molecular Biology, University of British Columbia, Vancouver, British Columbia, V6T 1Z4, Canada.
[d] Department of Chemistry. University of York, York YO10 5DD, United Kingdom.
[e] Department of Molecular Biology and Biochemistry, Simon Fraser University, V5A 1S6, Burnaby, British Columbia, Canada.
[f] Instituto de Investigaciones Químicas (IIQ), CSIC - Universidad de Sevilla, 41092 Sevilla, Spain.

ABSTRACT:

Owing to its roles in human health and disease, the modification of nuclear, cytoplasmic, and mitochondrial proteins with O-linked N-acetylglucosamine residues (O-GlcNAc) has emerged as a topic of great interest. Despite the presence of O-GlcNAc on hundreds of proteins within cells, only two enzymes regulate this modification. One of these enzymes is O-GlcNAcase (OGA), a dimeric glycoside hydrolase that has a deep active site cleft in which diverse substrates are accommodated. Chemical tools to control OGA are emerging as essential resources for helping to decode the biochemical and cellular functions of the O-GlcNAc pathway. Here we describe rationally designed bicyclic thiazolidine inhibitors that exhibit superb selectivity and picomolar inhibition of human OGA. Structures of these inhibitors in complex with human OGA reveal the basis for their exceptional potency and show that they extend out of the enzyme active site cleft. Leveraging this structure, we create a high affinity chemoproteomic probe that enables simple one-step purification of endogenous OGA from brain and targeted proteomic mapping of its post-translational modifications. These data uncover a range of new modifications including some that are less-known, such as O-ubiquitination and N-formylation. We expect that these inhibitors and chemoproteomics probes will prove useful as fundamental tools to decipher the mechanisms by which OGA is regulated and directed to its diverse cellular substrates. Moreover, the inhibitors and structures described here lay out a blueprint that will enable the creation of chemical probes and tools to interrogate OGA and other carbohydrate active enzymes.

KEYWORDS:

O-GlcNAc, glycoside hydrolase, inhibitor, affinity probe, chemoproteomics, post-translational modifications,

INTRODUCTION:

The incorporation of single N-acetylglucosamine (GlcNAc) residues O-linked to serine and threonine residues of nuclear and cytoplasmic proteins (O-GlcNAcylation)[1] is a widespread modification conserved among all multicellular eukaryotes. Only two enzymes regulate this process; the glycosyltransferase O-GlcNAc transferase (OGT)[2] acts to install O-GlcNAc and the glycoside hydrolase (OGA)[3] acts to cleave this modification off from proteins.[4] Levels of O-GlcNAc vary depending on nutrient availability, and even at basal levels O-GlcNAc is notably abundant, with well over a thousand proteins modified.[5] In line with its extensive distribution, O-GlcNAc has been shown to play fundamental roles on proteins including, for example, blocking ubiquitin-mediated degradation[6] and controlling protein subcellular localization[7]. Within cells, O-GlcNAc coordinates adaptive responses including helping to cope with diverse stresses[8] and regulating transcription.[9] In accord with its biochemical and physiological roles, enhancing O-GlcNAc levels has been shown to be protective in various animal models of disease. Within brain in particular, increased O-GlcNAc levels are protective against ischemic injuries[10,11] and various neurodegenerative disorders.[12-15]

Given the importance of O-GlcNAc in the vital processes of organisms, the molecular mechanisms by which O-GlcNAc is regulated by its cycling enzymes and how it exerts its molecular roles in controlling cellular processes are of great interest.[4] Considerable effort is being directed toward the development of chemical biology tools[16,17] to aid in understanding the O-GlcNAc cycling pathway from the molecular to the organismal level. Prominent among these chemical tools are inhibitors that have afforded structural insights into the molecular details of the O-GlcNAc regulatory enzymes.[18-24] OGA is a two-domain enzyme comprising an inactive acetyltransferase domain and a glycoside hydrolase CAZy family 84 (GH84) domain. Inhibitors binding to the active site of this GH84 domain of human OGA enable control over the levels of O-GlcNAc in cells and tissues and have gained significant attention. Some of these have been advanced as tool compounds[20,25] and even entered into the clinic.[15] Among known OGA inhibitors are polyhydroxylated compounds that have the basic carbon skeleton shared by GlcNAc. These carbohydrate-inspired inhibitors are generally thought to derive their potency against OGA by virtue of their resemblance to the transition state structures, or tightly bound intermediate,[20,26,27] found in the reaction mechanism of the OGA-catalyzed hydrolysis of β-*N*-acetylglucosaminides.

The catalytic mechanism used by OGA involves two distinct chemical steps (Figure 1) leading to hydrolysis with retention of configuration at the anomeric center. Experimental[28,29] and modelling[30] studies show that this reaction mechanism involves nucleophilic participation of the 2-acetamido group of the substrate to form a transient and tightly bound oxazoline intermediate. Such studies have also shown that the transition states flanking this bicyclic intermediate bear significant delocalized positive charge at both the anomeric center and endocyclic oxygen. This charge delocalization is enabled by a flattening of the pyranose ring to adopt a $^{4}H_{3}/^{4}E$ conformation (Figure 1). Accordingly, potent carbohydrate-based inhibitors of OGA typically manifest one or more of these features. Among carbohydrate-based OGA inhibitors is 1,2-dideoxy-2'-methyl-α-D-glucopyranoso[2,1-d]-Δ2'-thiazoline (NAG-thiazoline, Figure 1, K_i = 70 nM)[28], which resembles the oxazoline intermediate found in the reaction pathway. Building on these thiazolines, aminothiazolines that are more hydrolytically stable have been generated, including 1,2-dideoxy-2'-ethylamino-α-D-glucopyranoso-[2,1-d]-Δ2'-thiazoline (Thiamet-G, K_i = 2.1 nM). The increased basicity of this aminothiazoline as compared to the analogous thiazoline, favors its protonation at physiological pH values and enables formation of a favorable ionic interaction with the key catalytic residue Asp[174].[26]

Other potent carbohydrate-based inhibitors of OGA are known, including *O*-(2-acetamido-2-deoxy-D-glucopyranosylidene)-amino-*N*-phenylcarbamate (PUGNAc, K_i = 46 nM, Figure 1).[3] PUGNAc has a sp^2-hybridized carbon at the pseudo-anomeric center and a ^4E conformation resembling the OGA transition states (Figure 1). GlcNAcstatin C (K_i = 4 nM, Figure 1) is a potent analog of the natural product NAGstatin that manifests this same ^4E conformation and bears a pendent group that mimics the aglycone portion of a glycoside. Notably, such compounds have been modified to make them of value as fluorescence polarization probes for use in screening for new inhibitors of OGA.[24] Iminosugars that bear a formal positive charge at the nitrogen atom that occupies the position of the endocyclic ring oxygen in GlcNAc have also demonstrated activity against OGA, albeit with notably lower potency. 2-Acetamido-1,2-dideoxy-nojirimycin (DNJNAc), for example, is moderately active (K_i = 23 μM)[31] whereas the related, but more rigid, bicyclic 6-acetamido-6-deoxy-castanospermine (6-Ac-Cas, K_i = 300 nM) (Figure 1) is a much better inhibitor of OGA.[32] Less intuitively, tailoring the configurational and substitution pattern about a pyrrolidine core, coupled with introduction of a mimic of the aglycone, led to a potent cationic OGA inhibitor *N*-(*p*-fluorophenylpropyl) iminocyclitol derivative NFPI (K_i = 9 nM, Figure 1).[21]

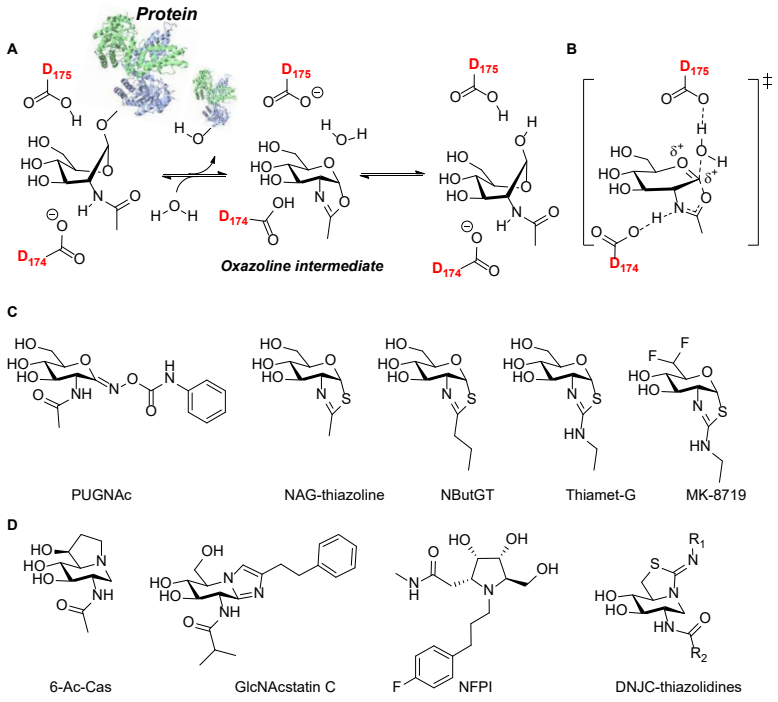

Figure 1. The substrate-assisted catalytic mechanism used by OGA to cleave O-GlcNAc from protein substrates and carbohydrate-based inhibitors of this enzyme. A) The catalytic mechanism of OGA involves two carboxyl residues within the enzyme active site (D174 and D175) that catalyze a two-step process proceeding through an oxazoline intermediate. B) The proposed ^4E envelope or $^4H_3$ half-chair conformation for the transition states for formation and breakdown of the oxazoline intermediate. C) Structures of carbohydrate-based hOGA inhibitors PUGNAc, NAG-thiazoline, NButGT, Thiamet-G, MK-8719. D) Structures of iminosugar-type inhibitors of hOGA including 6-Ac-Cas, GlcNAcstatin C, NFPI and the general structure of the DNJC-thiazolidines reported in this work.

One challenge associated with creating rationally designed carbohydrate-based inhibitors of OGA as tool compounds has been their selectivity toward OGA over other functionally related glycoside hydrolases. In humans, the lysosomal hexosaminidases HexA and HexB from family GH20 and *N*-acetyl-α-

glucosaminidase NAGLU from family GH89 play important roles in regulating levels of various glycoconjugates and their concomitant inhibition is accordingly undesirable. Underscoring this problem, NAG-Thiazoline, PUGNAc, and 6Ac-CAS all lack selectivity for OGA.[28,32] Selectivity has been realized by incorporating a slightly larger N-acyl substituent at the position typically occupied by the N-acetyl group of the natural substrate, which is tolerated by a pocket found within the active site of OGA but that is not present in these other functionally related enzymes.[21-23,33] This approach was demonstrated for 1,2-dideoxy-2′-propyl-α-D-glucopyranoso[2,1-d]-Δ2′-thiazoline (NButGT, Figure 1) to provide 700-fold selectivity for OGA. A similar strategy applied to GlcNAcstatin-G afforded 150-fold selectivity, however, when applied to PUGNAc, this approach yielded only modest selectivity of 10-fold. Thiamet-G exploits this approach to yield excellent 37,000-fold selectivity, which led to a search for improved analogues that could be used clinically. The result of a major chemistry effort led to MK-8719[15] (K_i = 7.9 nM, Figure 1), a less polar difluoromethyl derivative of Thiamet-G having excellent properties as a tool compound with no significant measurable activity against lysosomal hexosaminidases and NAGLU. This work stresses the need for potent carbohydrate-based OGA inhibitors that can be readily tailored to tune their molecular properties. The subsequent advance of MK-8719 to first-in-human phase I clinical trials for potential treatment of neurodegeneration highlights the interest and potential of such inhibitors, not only as tool compounds for basic biology, but also as potential first-in-class therapeutics.[15]

Here we describe rationally conceived iminosugar inhibitors of OGA that combine advantageous structural features seen in various known OGA inhibitors. These inhibitors show exceptional potency and selectivity toward OGA over functionally related human enzymes. In particular, we incorporated a rigid bicyclic core with an embedded basic isothiourea moiety that confers mimicry of the cationic nature of the transition state. Appended to this core we link an aryl moiety to mimic the aglycone leaving group. These 6*S*,5*N*-alkyliminomethylidene-2-carboxamido-1,2-dideoxynojirimycin (DNJC-thiazolidine) derivatives are new representatives of the class of sp^2-iminosugar glycomimetics that are characterized by the presence of a pseudoamide functionality in their core structure.[34-38] We further define the molecular basis of this inhibition through structural studies with human OGA and with a bacterial orthologue of hOGA. We then take advantage of this information to optimize the structure in terms of inhibition potency and selectivity towards hOGA. We additionally show that these compounds exhibit superb cell-based potency and are also brain permeable. Using this new structural class of inhibitors, we create a chemoproteomic probe that enables convenient isolation of endogenous OGA from brain tissue with high efficiency. Finally, using this tool we have identified a diverse set of native post-translational modifications on endogenous OGA from brain, most of which have been identified for the first time.

RESULTS AND DISCUSSION:

We were motivated by interest in OGA inhibitors and chemical probes to identify a carbohydrate-based inhibitor that could have its molecular properties readily tuned. An underexplored area are bicyclic sp^2-iminosugars that bear an isothiourea group to which various substituents can be appended.[36,39-41] The dimeric nature of hOGA, in which the active site is located at the base of a cleft found at the dimer interface, has suggested that compounds having a pendant group can reach the complementary monomer and may be able to derive binding potency in this manner.[21,22] We therefore reasoned that tuning the substituent on the exocyclic nitrogen could provide a convenient way to tune these inhibitors in a way that cannot readily be accomplished for Thiamet-G[25] or the GlcNAcstatins[20] (Figure 1). Modification of

these later two compounds requires complex synthetic manipulations as seen, for example, in the generation of MK-8719.[15] With regard to selectivity for OGA over functionally related enzymes, we reasoned that modifying the 2-acetamido group might afford selectivity for hOGA over functionally related enzymes such as HexA and HexB, which have more constrained active site pockets.[33]

With the above considerations in mind, we set out to synthesize new sp^2-iminosugars having a common 2-acetamido-1,2-dideoxynojirimycin (DNJNAc) core with the piperidine nitrogen engaged in a five-membered cyclic isothiourea moiety. We therefore implemented a simple two-step synthetic strategy to generate 6*S*,5*N*-alkyliminomethylidene-2-carboxamido-1,2-dideoxynojirimycin (DNJC-thiazolidine) using as an advanced intermediate the iminosugar DNJNAc. We accessed DNJNAc using a conveniently scalable procedure from commercially available D-glucuronolactone.[42] We first focused on using a series of simple alkyl and aryl isothiocyanates that could help test the potential value of extending the pseudo-aglycone moiety by measuring the resulting effects on inhibition of hOGA. Straightforward coupling of DNJNAc with a series of isothiocyanates afforded, with total chemoselectivity, the DNJNAc-thioureas **1-12**. These intermediates were in turn smoothly transformed through acid-catalyzed intramolecular nucleophilic cyclization to furnish us with the desired DNJNAc-thiazolidines **13**-**24** (Scheme 1A). In agreement with data for analogous systems,[35] we observed only a single set of signals in the NMR spectra of the 2-imino-1,3-thiazolidine derivatives. These spectra therefore indicated that only the more stable *Z*-diastereomer at the C=N double bond, devoid of unfavorable 1,3-parallel steric interactions, is formed.[35,43]

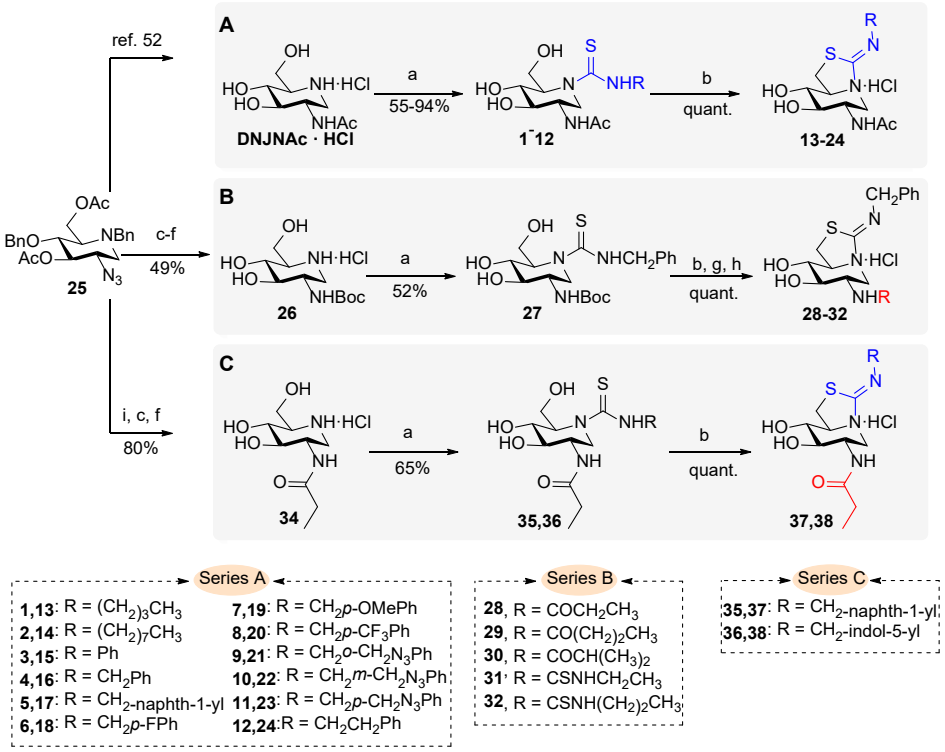

Scheme 1. Synthesis of DNJNAc-thioureas **1-12** and DNJNAc-thiazolidines **13-38**. a. Et_3N, R-NCS, DMF, RT, 18 h, 55-94%. b. HCl(conc), MeOH, RT, 18 h, quant. c. NaOMe, MeOH, RT, 18 h; d. PPh_3, THF-NH_4OH, 60 ºC,18 h; e. Boc_2O, Et_3N, dioxane, RT, 18 h; f. H_2, Pd/C, MeOH, RT, 18 h; g.TFA, 1:1 DCM-H_2O; h. RCOCl or RNCS, Et_3N, MeOH, RT, 18 h, quant; i. Zn, $CuSO_4$ (aq), THF-PrOH-Pr_2O, RT, 20 min.

We next evaluated these compounds (**13**-**24**) as inhibitors of hOGA using 4-methylumbelliferyl 2-acetamido-2-deoxy-D-glucopyranoside (MU-GlcNAc)[3] as a substrate. We found, however, that the potency of these compounds was such that the K_i values were lower than the enzyme concentration needed to perform the assay. We therefore turned to using the more sensitive substrate resorufin 2-acetamido-2-deoxy-D-glucopyranoside (Res-GlcNAc) in combination with analysis using the Morrison equation.[44] These data (Table 1) revealed that the identity of the group appended to the exocyclic *N*'-nitrogen had a major influence on the inhibitory potency of these molecules. We found that while the aliphatic *N*'-alkyl derivatives **13** (K_i = 24 ± 8 nM) and **14** (K_i 20 ± 7 nM) were more potent that their *N*'-phenyl counterpart **15** (K_i 400 ± 130 nM), positioning the aromatic ring further from the endocyclic nitrogen as in the *N*'-benzyl derivatives **16** (K_i = 3 ± 1 nM), *N*'-(1-naphthylmethyl) **17** (K_i = 0.3 ± 0.1 nM) and *N*'-phenethyl **24** (K_i = 0.9 ± 0.3 nM) markedly enhanced their potency against hOGA. Finally, various groups at the aromatic moiety in compounds **18**-**20** were detrimental (K_i = 30-50 nM), whereas electron donating azidomethyl substituents in **21**-**23** enhanced the inhibition potency (K_i = 0.22-0.40 nM).

Given these observations we sought to understand the molecular basis of inhibition of OGA by these bicyclic inhibitors. We initially obtained structures of the complex with the bacterial orthologue of hOGA from *Bacteroides thetaiotamicron* (*Bt*GH84),[45] at 1.50 Å resolution, then subsequently with the recently described dimeric catalytic domain of hOGA,[21-23] at 2.41 Å resolution. Analysis of the diffraction data obtained from crystals of the catalytic domain of hOGA soaked with **16** showed unambiguous electron density within the active site of hOGA (Figure 2A). The catalytic residues, D174 and D175, engage compound **16** with D174 hydrogen bonding to the 2-acetamido group and D175 hydrogen bonding to the exocyclic nitrogen. As seen in complexes with substrates and transition state analogues,[26,29,32,45] the 2-acetamido group is oriented and stabilised by interactions with W278, Y219, and N280 (Figure 2B). The hydroxyl groups at the C3 and C4 position of the piperidine ring form hydrogen bonds with the backbone oxygen of G67 and the sidechains of K98, D285, and N313. A hydrophobic pocket formed by the residues of F223, from one monomer, and P678' and W679', from the second monomer, interacts with the phenyl group of **16** through π-stacking interactions.

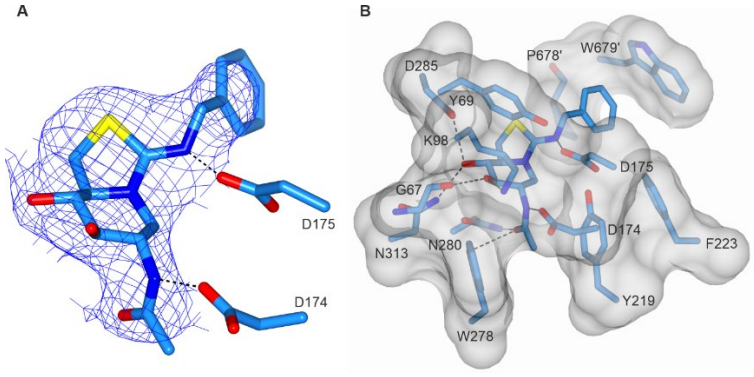

Figure 2. Compound **16** in complex with hOGA. Active site residues of hOGA are shown in blue. (A) **16** is shown in blue with the corresponding REFMAC maximum-likelihood/σA-weighted $2F_o$-F_c map, shown in dark blue, contoured at 0.11 electrons Å^{-3}. (B) Surface representation of the active site pocket of hOGA with neighbouring residues and hydrogen bond interactions highlighted by dashed lines.

A higher resolution structure of compound **16** in complex with *Bt*GH84 was sought to gain more precise insights into the interactions of **16** with GH84 enzymes. Compound **16** also shows good inhibition of BtGH84 (K_i = 733 nM), consistent with its structurally conserved active site making it a useful model of

hOGA. The piperidine ring of **16** was observed to bind in an unambiguous $^4C_1$ conformation in complex with *Bt*GH84 and the thiazolidine ring was observed in a ^1E conformation. The conformation of the piperidine ring corresponds to that of the pyranose ring seen for the GalNAc-oxazoline intermediate in the reaction coordinate of β-*N*-acetylglucosaminide hydrolysis catalyzed by GH84 enzymes (Figure 1A). Similarly, when bound in the active site of hOGA, the pyranose ring of the **16** was also bound in a $^4C_1$ conformation and engages in a similar set of protein contacts. The high resolution *Bt*GH84 structure also clearly shows the *N*-alkyl imine of **16** in the *Z*-configuration, which is consistent with the weaker electron density observed for this substituent in the complex of **16** with hOGA. Within the *Bt*GH84 structure we note, however, some features that are distinct from those seen in the hOGA complex. The position of the phenyl group of the *N*-alkyl substituent in *Bt*GH84 has shifted to be pointing out of the active site pocket, possibly due to a steric clash with H433 and the absence of an equivalent residue in place of W679' of hOGA. Also, the sulfur atom of the thiazolidine ring is in close proximity to and interacts with H433 and two water molecules, whereas the residue in the equivalent position of hOGA, P678', is not within bonding distance (Supplemental Figure 13). Finally, a common feature in these two structures that likely confers affinity is interaction of the isothiourea group through a hydrogen bond between the exocyclic nitrogen and the catalytic residue D175 in hOGA and D243 *Bt*GH84, respectively (Supplemental Figure 13). This bond would not be present if the moiety adopted an *E*-configuration, where the endocyclic sulfur atom and the exocyclic benzylic methyl are in a quasi-*trans* disposition.

Comparing the structure of hOGA in complex with **16** to complexes with Thiamet-G,[21,23] PUGNAc,[23] and PUGNAc-imidazole hybrid inhibitors[21] shows that the six-membered ring and 2-acetamido group adopt the same position in all cases (Figure 3). The phenyl moiety of the PUGNAc inhibitors shows a degree of movement compared to **16** that is tolerated within the active site (Figure 3). The phenyl group of **16** adopts a more compact position than that of phenyl group of the PUGNAc-imidazole type inhibitor. This movement allows the protein backbone to lie closer to the active site as can be seen for W679' where the Cα has moved 5.4 Å closer to the active site. The position of the backbone seen in the complex with **16** would cause a clash with the benzyl group of PUGNAc, however, the residues between R664-R682 are not observed in this structure, suggesting they adopt a flexible disordered state further away from the active site.[23] Thiamet-G binds in the same $^4C_1$ conformation, whereas PUGNAc binds in a ^4E conformation and PUGNAc-imidazole binds in a $^4E/^4H_3$ conformation.

The 5,6-fused ring structure of **16** bears resemblance to the bicyclic iminosugar 6-Ac-Cas and, to a lesser extent, that of NAG-thiazoline (Figure 3D and E). Known complexes of 6-Ac-Cas and NAG-thiazoline in complex with *Bt*GH84[32] allowed us to compare the orientations of these molecules with that seen for compound **16**. The general position of the inhibitors 6-Ac-Cas and NAG-thiazoline in the active site of *Bt*GH84 are the same. However, in comparison to 6-Ac-Cas where the five-membered ring lies in the same plane as the six-membered ring, the five-membered ring of **16** is pointing ~70° away from the plane aligning to the C6 hydroxyl of NAG-thiazoline. This may arise due to introduction of the phenyl moiety appended to the five-membered ring needing to avoid a steric clash with the sidechain of V314. Strikingly, the puckering of the 5-membered ring of **16** allows it to access a different ring conformation. 6-Ac-Cas adopts a $^{1,4}B/^1S_3$ conformation, whereas Thiamet-G and NAG-thiazoline adopt a $^4C_1$ conformation. In summary, we find that bicyclic compound **16** binds to both hOGA and *Bt*GH84 with its 5-membered ring adopting a similar position as seen for the analogous ring of 6-Ac-Cas and the 6-membered ring adopting an undistorted $^4C_1$ conformation like NAG-thiazoline. These two features of **16**, coupled with the additional bonding to the exocyclic nitrogen and the optimal positioning of the pendent aryl ring

within the active site, likely account for its picomolar inhibition constant as compared to the ~300 nM K_i values seen for NAG-thiazoline and 6-Ac-Cas with hOGA.[32]

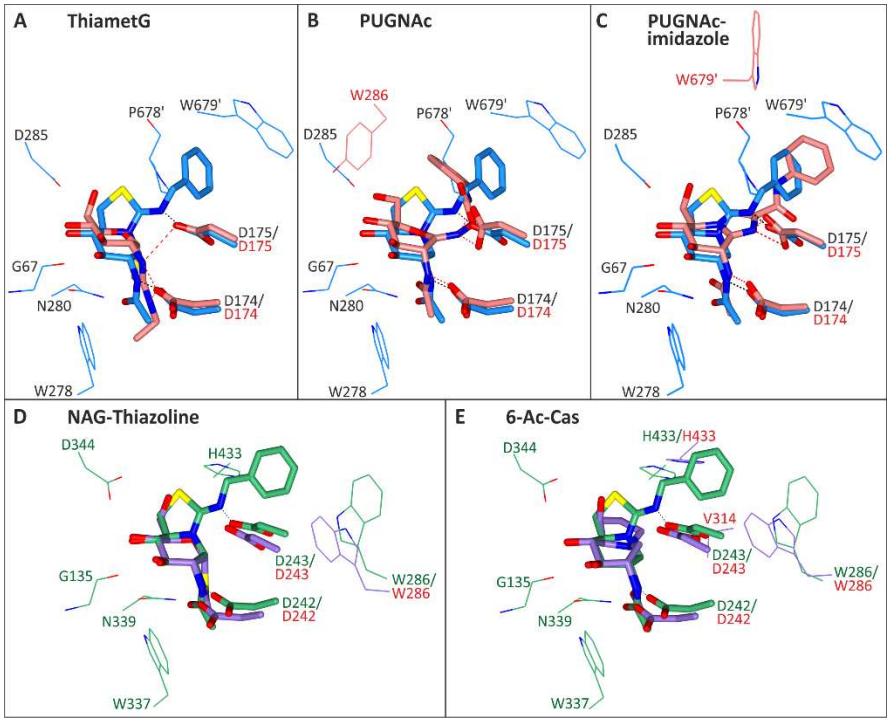

Figure 3. Superimposition of **16** bound to hOGA and *Bt*GH84 with various characterised OGA inhibitors. The general acid/general base residues, D174/D175 from hOGA and D242/D243 from *Bt*GH84, are represented with thicker bond widths compared to the surrounding active site residues. Residues in the overlaid structures that occupy different positions and that make important interactions are highlighted. Panels A-C compare compound **16** bound to hOGA and panels D-E compare **16** bound to *Bt*GH84. (A) Thiamet-G, shown in orange, in complex with hOGA (PDB ID: 5M7S)[21]. (B) PUGNAc, shown in orange, in complex with hOGA (PDB ID: 5UHO)[23]. (C) PUGNAc-imidazole hybrid inhibitor, shown in orange, in complex with hOGA (PDB ID: 5M7T)[21]. (D) NAG-thiazoline, shown in purple, in complex with *Bt*GH84 (PDB ID: 2CHN)[45]. (E) 6-Ac-Cas, shown in purple, in complex with *Bt*GH84 (PDB ID: 2XJ7)[32].

The structure of **16** in complex with hOGA and its comparison to that of known selective and non-selective inhibitors of hOGA suggested that these compounds may also be effective inhibitors of human GH20 hexosaminidases, which as noted above use a similar catalytic mechanism and also processes GalNAc-configured substrates. We therefore assessed the inhibition of HexA by DNJNAc-thiazolidines **13**-**24** (Table 1) and, in parallel, commercial hexosaminidases (Supplemental Table 1). While these arylalkylimino DNJNAc-thiazolidines, which all contain a simple 2-acetamido group as seen for the natural substrate, rank among the most potent hOGA inhibitors reported to date, their potency toward HexA was good but not exceptional. The resulting selectivity of these inhibitors for hOGA over HexA (K_i hOGA/K_i Hex) was quite promising, being up to ~30000-fold for some of the picomolar hOGA inhibitors including **17**, **21**, and **22** (Table 1). Nevertheless, we judged that improving on this selectivity would be valuable to deliver highly selective tool compounds that would be convenient to use and avoid potential off-target effects.

Table 1. Inhibition constants (K_i) of inhibitors **13-24** for hHex*A* K_i (μM) and hOGA K_i (nM).[a]

Compound	NHR group	=N-R group	hHexA K_i (μM)	hOGA K_i (nM)	Selectivity ratio K_i Hex/ K_i hOGA
Series A - Potency					
13	Ac	$(CH_2)_3CH_3$	4.2 ± 1	24 ± 8	175
14	Ac	$(CH_2)_7CH_3$	3.8 ± 1	20 ± 7	190
15	Ac	Ph	14 ± 4	400 ± 130	35
16	Ac	CH_2Ph	9.9 ± 4	3 ± 1	3300
17	Ac	CH_2-1-naphthyl	9.0 ± 4	0.3 ± 0.1	30000
18	Ac	CH_2p-FPh	4.2 ± 1	50 ± 20	84
19	Ac	CH_2p-OMePh	8.8 ± 4	30 ± 10	293
20	Ac	CH_2p-CF_3Ph	3.0 ± 1	50 ± 20	60
21	Ac	CH_2o-CH_2N_3Ph	5.0 ± 3	0.27 ± 0.09	18518
22	Ac	CH_2m-CH_2N_3Ph	5.0 ± 3	0.22 ± 0.07	22727
23	Ac	CH_2p-CH_2N_3Ph	3.7 ± 1	0.4 ± 0.2	9250
24	Ac	CH_2CH_2Ph	21 ± 7	0.9 ± 0.3	23333
Series B - Selectivity					
28	$COCH_2CH_3$	CH_2Ph	>100	8 ± 3	>10000
29	$CO(CH_2)_2CH_3$	CH_2Ph	>100	900 ± 300	>100
30	$COCH(CH_3)_2$	CH_2Ph	>100	300 ± 100	>300
31	$CSNHCH_2CH_3$	CH_2Ph	>100	1000 ± 400	>100
32	$CSNH(CH_2)_2CH_3$	CH_2Ph	>100	800 ± 300	>100
Series C - Combined					
37	$COCH_2CH_3$	CH_2-1-naphthyl	>100	0.8 ± 0.2	>120000
38	$COCH_2CH_3$	CH_2-5-indolyl	>100	2.4 ± 0.9	>40000

Inhibition was competitive in all cases. [a] Human HexA and human OGA enzyme inhibition were measured as described (SI) and K_i values are from ≥ 2 assays with standard deviation of ≤ 35% of the reported mean.

Inspired by work showing the improvement on selectivity against hOGA for inhibitors bearing extended N-acyl groups,[20,25,28] we therefore devised a second series of DNJC-thiazolidines that retained a benzyl substituent at the imino center as in compound **16**, but the 2-acetamido group was replaced by propionamido **28**, butyramido **29**, isobutyramido **30**, *N*'-ethylthioureido **31**, or *N*'-propylthioureido **32** functionalities (Scheme 1B). We made the choice to retain the benzyl group based on the data showing favorable contribution of an aromatic substituent located several bonds away from the sugar-like core for hOGA inhibition. We implemented a divergent synthetic strategy starting from the known 2-azido-2-deoxy DNJ derivative **25**, a synthetic intermediate in the route leading to DNJNAc (Scheme 1B).[42] Deacetylation using Zemplen conditions followed by Staudinger reduction of the azido group with *in situ* Boc-protection of the resulting amine, followed by Pd-catalyzed hydrogenolysis, delivered iminosugar **26** in 60% yield over three steps. Reaction of **26** with benzyl isothiocyanate afforded us the pivotal thiourea **27**, which was transformed into our target 2-benzyliminothiazolidines through parallel three-step, one-purification reaction sequences. This series of reactions involved: (i) acid-catalyzed cyclization to form the five-membered isothiourea ring, (ii) TFA-induced hydrolysis of the carbamate, and (iii) N-acylation (**28**-**30**) or isothiocyanation reaction (**31** and **32**) of the free amine with the corresponding acyl chloride or alkyl isothiocyanate (Scheme 1B).We assayed these candidate inhibitors and found that modifications of this group completely eliminated inhibition of HexA at concentrations up to 100 μM. In contrast, hOGA was relatively tolerant to these structural variations. Nevertheless, the scope of changes that were well tolerated was limited. Replacement of the acetamido group of **16** (K_i = 3.0 ± 1 nM) by butyramido, isobutyramido, *N*'-ethylthioureido, or *N*'-propylthioureido, as incorporated into compounds **29**-**32**, resulted in a drop of potency of approximately two orders of magnitude (K_i = 800-1000 nM). A subtle change to a propionamido group as in **28**, however, only slightly affected inhibitory potency (K_i = 8 ± 3

nM) with an over 10,000-fold selectivity for hOGA (Table 1). These collective inhibition data advised generating an hOGA inhibitor that would exhibit high selectivity by virtue of incorporating a 2-propionamido group as in **28**, as compared to the 2-acetamido group of **16**. We also reasoned that it would be beneficial to install a pendent polycyclic aromatic group, since for **17** we see a 10-fold improvement in potency over compound **16** that has a simple pendant phenyl group. Towards this end, we prepared 2-deoxy-2-propionamido-DNJ derivative **34** from the common intermediate **25** in a three-step procedure (Scheme 1C). We then N-acylated **34** using 1-naphthylmethyl isothiocyanate or 5-indolylmethyl isothiocyanate and converted the thiourea adducts, **35** and **36**, under acidic conditions to the desired bicyclic sp^2-iminosugars **37** and **38** (Scheme 1C). We found these compounds to be potent, showing high pM (**37**) to low nM (**38**) K_i values (Table 1, Figure 4), as well as being highly selective for hOGA (>40,000 to >120,000 fold). Given their properties, we judged that both **37** and **38** could serve as useful tool compounds for studying O-GlcNAc. We therefore examined the dose-dependent effect of these compounds on protein O-GlcNAcylation using the convenient neuronal cell model SK-N-SH. Using as a benchmark the compound Thiamet-G, which has similar potency (K_i = 2.1 nM),[26] we found **37** was equally effective at increasing cellular O-GlcNAc levels. **37** Was active at nM concentrations as assessed in immunoblot assays both by using pan-specific anti-O-GlcNAc and anti-OGA antibodies to monitor levels of O-GlcNAc and OGA (Figure 4).

The high potency of these compounds, coupled with tolerance to various pendent aryl groups that can extend out of the immediate active site cleft (Figure 2), suggested to us that modification of these inhibitors could yield useful affinity-based chemoproteomics probes. Previous non-covalent chemoproteomic probes have been reported for other enzyme classes including, for example, Src multidomain kinases,[46] casein kinases,[47] heat shock protein (HSP) chaperones,[48] protease complexes,[49] histone deacetylases,[50] as well as the non-lysosomal glycosidase β-glucosidase 2 (GBA2)[51]. Few, however, have been applied to identify the post-translational modification state of specific proteins of interest. We felt that such a tool could prove useful for enriching OGA from various tissues to allow a detailed analysis of the properties of endogenous OGA, including identifying sites of post-translational modifications. We envisioned that we could tether a biotin affinity tag through a long linker to the phenyl group of inhibitor **23**, which exhibits pM potency against hOGA, such that the biotin moiety could still reach a streptavidin-presenting matrix even with the inhibitor bound within the deep active site cleft of OGA. We elected to use a disulphide-containing linker that could be cleaved using gentle conditions. We were inspired in this regard by the work of Teranishi *et al.* on proteases[49], who used a 70 Å polyethylene glycol (PEG) linker within an affinity probe.

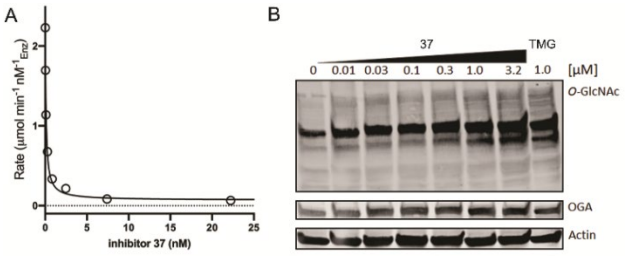

Figure 4: In vitro and in cell potency of **37**. (A) K_i value determined using the Morrison equation and (B) cell-based assays obtained using SK-N-SH neuroblastoma cells treated with **37** for 24 h using immunoblot of cell lysates for dose-dependent effects of cell-based inhibition of OGA on global O-GlcNAc levels and OGA levels. A comparison of the effects of 37 compared to Thiamet-G (TMG) is made.

During the synthesis of our target probe, we found that using large quantities of PEG linkers, which are hygroscopic, proved troublesome during amide coupling reactions. To circumvent this problem, we elected to couple together suitably functionalized inhibitor and biotin components using a copper azide-alkyne cycloaddition (CuAAC) reaction. We therefore reduced the azide of inhibitor **23** and coupled it with alkyne-functionalized PEG_4-acid (Figure 5A). The resulting alkyne intermediate **39** was then coupled to disulfide biotin azide using CuAAC to give **40** (DNJNAc-6S-NBn-Biotin). We then determined the inhibitory potency of DNJNAc-6S-NBn-Biotin toward OGA and found it showed an IC_{50} value of 7.6 ± 0.5 nM (Figure 5C), which we reasoned was suitably potent binding to enable its intended use as a chemoproteomic probe. We envisioned a workflow (Figure 5B) in which the probe would be first bound to OGA within clarified tissue lysates, after which the binary OGA-Probe complex would be precipitated using magnetic streptavidin beads. After washing of the beads, elution under mild reducing conditions with dithiothreitol (DTT) would release the enriched OGA. We first used recombinant hOGA to determine how effective our proposed workflow would be in precipitating OGA. Success of the probe in capturing of hOGA, using this protocol, was verified by detection of hOGA in the eluate by anti-OGA immunoblot (Supplemental Figure 14). Furthermore, we found that five rounds of washing of the beads still resulted in retention of hOGA bound to immobilized DNJNAc-6S-NBn-Biotin on the beads. These data collectively show that DNJNAc-6S-NBn-Biotin has sufficient affinity to bind hOGA and enable its high-level enrichment.

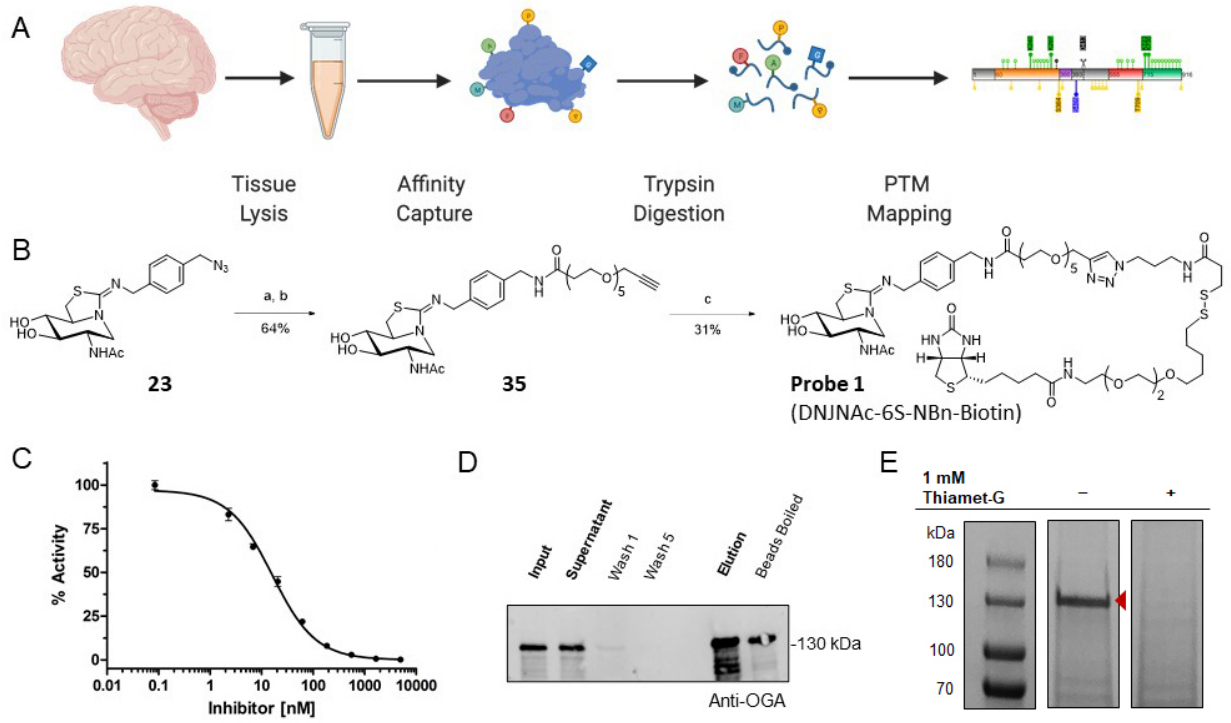

Figure 5: Chemoproteomic enrichment workflow with probe design, synthesis, in vitro evaluation, and use for precipitation of bovine OGA from brain tissue. (A) Scheme showing the chemoproteomic strategy used to enrich bovine OGA from brain. (B) Scheme showing the chemical synthesis of cleavable DNJNAc-6S-NBn-Biotin using **23** as a starting material. Reagents and conditions: a) PPh_3, THF/H_2O, RT, 21 h. b) alkyne-PEG4-acid, HBTU, DIPEA, DMF, RT, 22 h; c) biotin-azide, sodium ascorbate, $CuSO_4 \cdot 5H_2O$, DMF/H_2O, RT, 17 h. (C) In vitro IC_{50} value determined for DNJNAc-6S-NBn-Biotin toward hOGA reveals an IC_{50} value of 7.6 nM. (D) Small scale validation experiment showing DNJNAc-6S-NBn-Biotin enables enrichment of bovine OGA from brain as determined using immunoblot assay. (E) Large scale chemoproteomic enrichment of bovine OGA from brain tissue followed by analysis of the elution by SDS-PAGE with detection using Coomassie stain in parallel with a Thiamet-G blocking control.

We next used DNJNAc-6S-NBn-Biotin to precipitate OGA from bovine brain tissue (bOGA). We selected bovine brain because OGA was first isolated from this tissue,[52] where the enzyme is particularly abundant, in view of the therapeutic potential of OGA inhibition in various neurodegenerative diseases.[12-15] We used DNJNAc-6S-NBn-Biotin concentrations that would be maximized but not exceed available sites of streptavidin on a convenient volume of beads (100 µL). Following the precipitation experiment, for which we performed a parallel control involving blocking of bOGA binding by adding the potent inhibitor Thiamet-G, analysis of the OGA immunoreactivity by immunoblot (Figure 5D) showed that DTT elution resulted in release of OGA from the resin. Released OGA was observed as having an approximate mass of 130 kDa, consistent with the initial report on its biochemical purification.[3] Analysis of the eluates showed efficient and high-level enrichment of OGA (Figure 5E) that was blocked by Thiamet-G. Given the efficiency of the pull-down, we focused on excising the band corresponding to OGA and identifying OGA-derived peptides that were post-translationally modified. Tryptic in-gel digestion of the isolated OGA and analysis of the resulting tryptic fragments by LC-MS/MS sequencing and analysis using Byonic revealed 436 unique peptides that covered 62% of full-length bOGA. Several of these peptides were found to bear various post-translational modifications. We performed a targeted search of the data using Byonic for the 30 most common protein modifications and, using this strategy, identified 1676 peptide spectral matches, with 339 peptides bearing modifications. We elected to focus on those PTMs that are known to be enzymatically installed as we felt these would be of wider interest and more likely to have regulatory functions. To focus on candidate enzymatic modifications, we therefore tabulated such modifications that also met our false discovery rate (FDR) criterion to be considered a modification on a peptide of having a |Log Prob|>1.52 (3% FDR). We assigned high-confidence modifications as those with |Log Prob|>2.0 (1% FDR), which corresponded to a total of nine modifications including O-GlcNAcylation (2), lysine acetylation (2), lysine N-formylation (2), and both O- and N-ubiquitination (3) (Table 2).

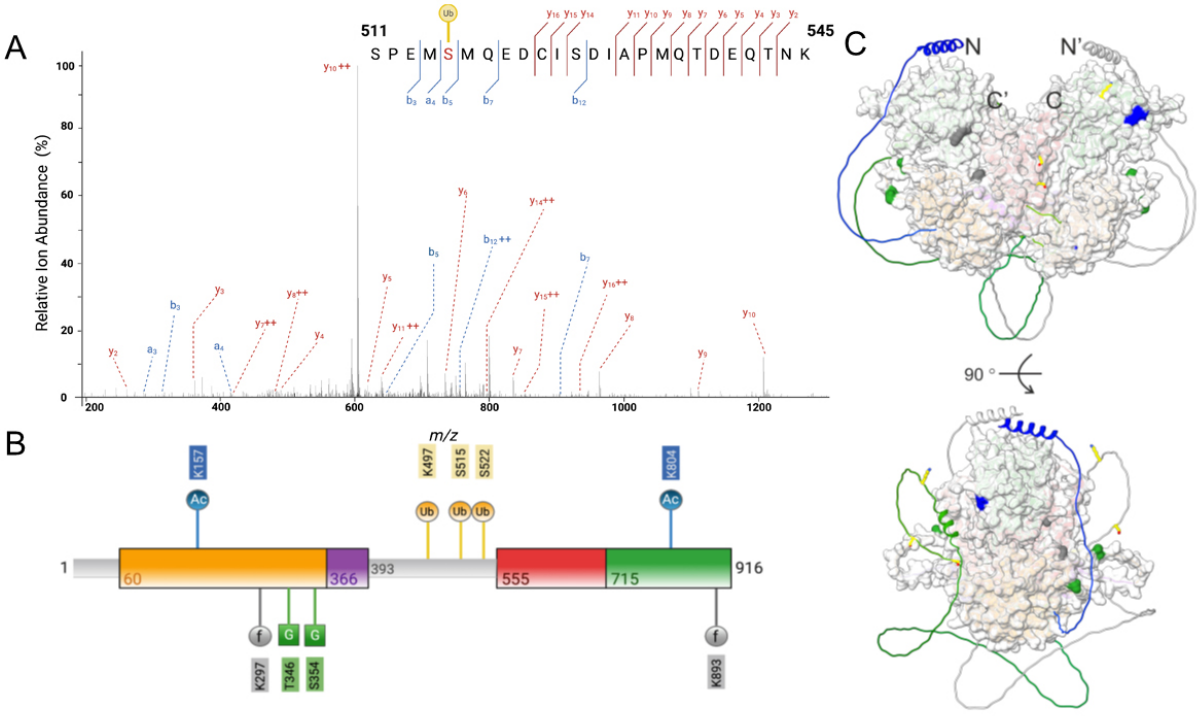

Figure 6: Mapping of post-translational modifications on endogenous OGA from bovine brain. A) Representative MS/MS peptide sequencing data showing B and Y ion-series that enable mapping of O-ubiquitination to Ser515 of OGA. B) Domain structure of bovine OGA with sites of identified post-translational modifications noted. Domains are coloured orange (GH84 domain), red (stalk domain), purple (hinge domain), green (acetyltransferase-like domain), grey (intrinsically disordered regions). Modifications are colour coded (Grey = Formylation, Blue = Acetylation, Green = O-GlcNAcylation, Yellow = Ubiquitination). C) Identified sites of post-translational modifications marked on a homodimeric bovine OGA model (sequence according to UNIPROT entry E1BQ16), built using an AlphaFold[55] predicted monomeric structure of bovine OGA with the second monomer guided into place using the crystal structure of hOGA (PDB ID: 7OU6). Post-translational modification sites are colour coded the same as Panel B on a surface representation of the structured regions. Domains are represented by ribbons with the colour from panel B applied; the disordered regions of one monomer are coloured by Jones' rainbow (N-terminus: blue, C-terminus: red). Although AlphaFold predicts the lowest energy monomeric 3D fold, regions 1-29 and 715-916 were manually moved in coot[56] due to steric clashes of the disordered regions with the second monomer.

The MS/MS sequencing data for these modified tryptic peptides (Figure 6A, Supplemental Figures 15-23, Supplemental Tables 3-11) allowed us to identify the sites of these modifications, which we mapped onto the domain structure and a three-dimensional model of bOGA (Figure 6B and C). Most of these modification sites were previously unknown (Table 2) and almost all are found on the surface of the protein. They include a ubiquitination site at K497 within the intervening disordered region between the catalytic domain and the stalk domain, as well as the much less studied O-ubiquitination odification[53] at S515 and S522. In addition, we observed new O-GlcNAcylation sites at T346 and S354. We also found acetyl groups at K157 and K804 within the C-terminal putative acetyltransferase domain between residues 716-916, as well as the relatively little understood formyl modification[54] at K297 and K893. Interestingly, K157, which is acetylated, is not surface exposed but instead is buried in the catalytic domain where it is locked in place by three hydrogen bond interactions by the backbone oxygen atoms of K102, W107, and E109. The human and bovine OGA 3-D coordinate sets do not contain any post-translational modifications due to the production of hOGA in *Escherichia coli* and the use of structure prediction software for the available bovine OGA model. Perhaps, when produced endogenously in mammals, acetylation of the lysine could cause it to flip to be surface exposed or, alternatively, this region of the protein may have some flexibility. Collectively, these targeted sequencing data confirm several sites of modification previously identified using high-throughput proteomic analyses and uncovers multiple new sites of post-translational modification on OGA from bovine brain.

Table 2. Post-translational modification data acquired for analysis of endogenous OGA.

Modification	Site	Residues	Peptide Sequence	Log Probability	Score	Site Annotated
Acetyl	K157	156 – 167	R(**KAc**)LDQVSQFGCR	3.3	359	*[Ub][57]
Acetyl	K804	795 - 804	ISWIPFMQE(**KAc**)	2.99	299.7	
Formyl	K297	291 - 299	LFLGPY(**Kf**)GR	1.7	286.7	*[Ub][57]
Formyl	K893	887 - 893	ILEFYS(**Kf**)	1.67	237.7	*[Ub][57]
O-GlcNAc	T346	343 - 359	DVVM(**Tg**)DSEDSTVSIQIK	1.8	177	
O-GlcNAc	S354	343 - 359	DVVMTDSEDSTV(**Sg**)IQIK	6.38	304.3	
Ubiquitin	K497	492 - 510	MAEEL**(KUb)**PMDTDKESIAESK	2.24	237	
Ubiquitin	S515	510 - 545	SPEM**(SUb)**MQEDCISDIAPMQTDEQTNK	5.39	411.1	*[P][58]
Ubiquitin	S522	510 - 545	SPEMSMQEDCI**(SUb)**DIAPMQTDEQTNK	3.44	200.2	*[P][57]

Modifications are denoted on peptide sequence: (Ac) – Acetylation; (f) – Formylation; (g) – O-GlcNAcylation; (Ub) – Ubiquitination; (P) - Phosphorylation. * Site has been previously annotated for a modification.

CONCLUSION:

Small molecule inhibitors of the O-GlcNAc cycling enzyme OGA are proving widely useful in evaluating its functional roles in a range of physiological and pathophysiological processes. Tuning the properties of these inhibitors to enable their ready use in vivo has emerged as an important consideration. One challenge for carbohydrate-based inhibitors of OGA such as Thiamet-G, however, has been the synthetic difficulty associated with modifying the structure of the inhibitor.[15] An emerging approach[21] has been to exploit OGA inhibitors having features that extend outside of the active site pocket. Here we report a class of picomolar OGA inhibitors that we show, through structural analyses of their binding to human OGA, exploit the presence of such a pendent group to drive binding. These inhibitors are highly active in cell systems with cell potencies that are equivalent to that of Thiamet-G. Notably, these inhibitors and are also brain permeable (Supplemental Figures 24 and 25). Accordingly, we anticipate that such compounds should prove useful for evaluating the neuroprotective effects of OGA inhibition in different preclinical animal models. Such compounds may also serve as valuable leads for eventual clinical development.

The presence of only two O-GlcNAc cycling enzymes and their apparent constitutive activity makes the regulation of O-GlcNAc on target proteins a major puzzle for the field. Emerging data suggests that targeting of OGA and OGT to specific complexes may be one mechanism that dictates their activities. In this regard, the post-translational modifications of these proteins are topics of considerable interest since targeting may be controlled through such modifications. Indeed, this has been shown in the case of OGT, where phosphorylation was shown to affect nuclear import in myotubes, altering binding partners, increased activity, and stability from proteasomal degradation, as well O-GlcNAcylation affecting cellular localization.[4,7] The available information regarding the repertoire of post-translational modifications on OGT is, however, limited and even less is known for OGA (Table 2). Accordingly, deeper knowledge regarding endogenous modifications found on these proteins is needed to understand their regulation and the control of cellular O-GlcNAcylation.

One often used approach to mapping post-translational modifications is to overexpress proteins of interest fused to various peptide epitope tags. Alternatively, to avoid potential artifacts associated with overexpression, high affinity antibodies are sometimes used to immunoprecipitate proteins from tissues. However, the limited availability of high-quality antibodies validated for immunoprecipitation, and their cost, can deter the pursuit of such experiments. High affinity chemoproteomic probes offer a less explored, yet powerful, strategy to accomplish this goal. We exploited the high affinity bicyclic inhibitors reported here to develop a chemoproteomic affinity probe that could be used to enrich endogenous OGA from homogenized tissues. The initial report on purification of OGA from bovine brain was a heroic effort involving eight steps of purification from one kg of bovine brain that enabled detection of OGA in polyacrylamide gel by silver stain. In contrast, DNJNAc-6S-NBn-Biotin enabled highly efficient one-step purification of OGA, allowing ready detection of OGA by simple Coomassie staining within a polyacrylamide gel. The ability to rapidly isolate μg quantities of OGA has allowed us to map for the first time, in a targeted manner, post-translational modifications on this enzyme. Previous mapping of post-translational modifications to OGA in various high-throughput proteomic studies used cancer tissues rather than healthy tissues.[57,59-61] Furthermore, most of the modifications identified have only been observed once and such assignments are often not unambiguous. In addition, these previous studies have principally focused on specific modifications, such as phosphorylation and ubiquitination, rather than adopting a modification agnostic strategy. Here we identified a range of different modifications on OGA

from endogenous brain tissue including, for example, sites of formylation[54] (Table 2). The roles of this modification on cytoplasmic proteins remain poorly understood.

We expect that application of this OGA chemoproteomic probe, or other suitably functionalized high affinity OGA ligands, should allow comparative assessment of post-translational modifications from different tissues and species. Such data are expected to enable understanding which modification sites are most relevant to regulation of OGA localization and activity. Moreover, though O-GlcNAc is ubiquitous in tissues its abundance and that of the cycling enzymes that control this modification vary widely, suggesting that tissue-specific post-translational modification of OGA may contribute to its regulation. Targeted cell and biochemical studies will aid our understanding of the physiological roles of these modification sites on OGA function. Finally, though applied here to OGA, we also expect that this approach should be readily amenable to the study of other glycan processing enzymes that are likely to be regulated through various post-translational modifications.

ASSOCIATED CONTENT

Supporting Information

The supporting Information is available free of charge on the ACS Publications website:

- Methods for chemical syntheses, proteomic analyses, enzyme kinetic analyses, and X-ray structure determinations.
- Supplementary figures for proteomic data, characterization data for compounds, brain permeability data, and K_i determinations.
- Tables summarizing inhibition data, fragment ion series of modified peptides, and data collection and refinement statistics for X-ray structures.
- An .xls file with source data for MS-proteomics experiments.

AUTHOR INFORMATION

Corresponding Authors

*Gideon J. Davies: gideon.davies@york.ac.uk *Carmen Ortiz Mellet: mellet@us.es *David J. Vocadlo: dvocadlo@sfu.ca

Acknowledgements

The authors are grateful for support from the Ministerio de Ciencia, Innovación y Universidades, the Ministerio de Ciencia e Innovación, the Agencia Estatal de Investigación, the European Regional Development Funds (projects RTI2018-097609-B-C21 and PID2019-105858RB-I00), the Junta de Andalucía, the Canada Foundation for Innovation, the British Columbia Knowledge Development Fund, Genome Canada/Genome BC (264PRO), and the Canadian Institutes of Health Research (CIHR; PJT-148732, PJT-156202). DJV thanks the Canada Research Chairs program for support as a Tier I Canada Research Chair in Chemical Biology. RAA is supported by a trainee award from the Michael Smith

Foundation Health Research (MSFHR). MG-C is a FPI fellow. Technical assistance from the research support services of the University of Seville (CITIUS) is also acknowledged.

Notes

The authors declare a patent covering inhibitors of OGA related to this work has been filed.

REFERENCES:

(1) Carmen-Rosa, T.; Hart, G. W. Topography and polypeptide distribution of terminal N-Acetylglucosamine residues on the surfaces of intact lymphocytes. *J. Biol. Chem.* **1984**, *259*, 3308-3317.

(2) Kreppel, L. K.; Blomberg, M. A.; Hart, G. W. Dynamic glycosylation of nuclear and cytosolic proteins cloning and characterization of a unique O-GlcNAc transferase with multiple tetratricopeptide repeats. *J. Biol. Chem.* **1997**, *272*, 9308-9315.

(3) Gao, Y.; Wells, L.; Comer, F. I.; Parker, G. J.; Hart, G. W. Dynamic O-glycosylation of nuclear and cytosolic proteins Cloning and characterization of a neutral, cytosolic Î²-N-acetylglucosaminidase from human brain. *J. Biol. Chem.* **2001**, *276*, 9838-9845.

(4) King, D. T.; Males, A.; Davies, G. J.; Vocadlo, D. J. Molecular mechanisms regulating O-linked N-acetylglucosamine (O-GlcNAc)–processing enzymes. *Curr. Opin. Chem. Biol.* **2019**, *53*, 131-144.

(5) Wulff-Fuentes, E.; Berendt, R. R.; Massman, L.; Danner, L.; Malard, F.; Vora, J.; Kahsay, R.; Olivier-Van Stichelen, S. The human O-GlcNAcome database and meta-analysis. *Sci. Data* **2021**, *8*, 25.

(6) Ruan, H. B.; Nie, Y.; Yang, X. Regulation of protein degradation by O-GlcNAcylation: crosstalk with ubiquitination. *Mol. Cel. Proteom.* **2013**, *12*, 3489-3497.

(7) Yang, X.; Qian, K. Protein O-GlcNAcylation: emerging mechanisms and functions. *Nat. Rev. Molec. Cell Biol.* **2017**, *18*, 452-465.

(8) Martinez, M. R.; Dias, T. B.; Natov, P. S.; Zachara, N. E. Stress-induced O-GlcNAcylation: an adaptive process of injured cells. *Biochem. Soc. Trans.* **2017**, *45*, 237-249.

(9) Hart, G. W. Nutrient regulation of signaling and transcription. *J. Biol. Chem.* **2019**, *294*, 2211-2231.

(10) Jiang, M.; Yu, S.; Yu, Z.; Sheng, H.; Li, Y.; Liu, S.; Warner, D. S.; Paschen, W.; Yang, W. XBP1 (X-box-binding protein-1)-dependent O-GlcNAcylation Is neuroprotective in ischemic stroke in young mice and its impairment in aged mice Is rescued by thiamet-G. *Stroke* **2017**, *48*, 1646-1654.

(11) Jensen, R. V.; Andreadou, I.; Hausenloy, D. J.; Botker, H. E. The Role of O-GlcNAcylation for Protection against Ischemia-Reperfusion Injury. *Int. J. Mol. Sci.* **2019**, *20*, 404.

(12) Park, J.; Lai, M. K. P.; Arumugam, T. V.; Jo, D. G. O-GlcNAcylation as a Therapeutic Target for Alzheimer's Disease. *Neuromol. Med.* **2020**, *22*, 171-193.

(13) Zhao, M. J.; Yao, X.; Wei, P.; Zhao, C.; Cheng, M.; Zhang, D.; Xue, W.; He, W. T.; Xue, W.; Zuo, X.; Jiang, L. L.; Luo, Z.; Song, J.; Shu, W. J.; Yuan, H. Y.; Liang, Y.; Sun, H.; Zhou, Y.; Zhou, Y.; Zheng, L.; Hu, H. Y.; Wang, J.; Du, H. N. O-GlcNAcylation of TDP-43 suppresses proteinopathies and promotes TDP-43's mRNA splicing activity. *EMBO Rep.* **2021**, *22*, e51649.

(14) Wang, X.; Li, W.; Marcus, J.; Pearson, M.; Song, L.; Smith, K.; Terracina, G.; Lee, J.; Hong, K.-L. K.; Lu, S. X. MK-8719, a novel and selective O-GlcNAcase inhibitor that reduces the formation of pathological tau and ameliorates neurodegeneration in a mouse model of tauopathy. *J. Pharmacol. Exp. Ther.* **2020**, *374*, 252-263.

(15) Selnick, H. G.; Hess, J. F.; Tang, C.; Liu, K.; Schachter, J. B.; Ballard, J. E.; Marcus, J.; Klein, D. J.; Wang, X.; Pearson, M. Discovery of MK-8719, a potent O-GlcNAcase inhibitor as a potential treatment for tauopathies. *J. Med. Chem.* **2019**, *62*, 10062-10097.

(16) Groenevelt, J. M.; Corey, D. J.; Fehl, C. Chemical Synthesis and Biological Applications of O-GlcNAcylated Peptides and Proteins. *Chembiochem* **2021**, *22*, 1854-1870.

(17) Ju Kim, E. O-GlcNAc Transferase: Structural Characteristics, Catalytic Mechanism and Small-Molecule Inhibitors. *Chembiochem* **2020**, *21*, 3026-3035.

(18) Lazarus, M. B.; Jiang, J.; Gloster, T. M.; Zandberg, W. F.; Whitworth, G. E.; Vocadlo, D. J.; Walker, S. Structural snapshots of the reaction coordinate for O-GlcNAc transferase. *Nat. Chem. Biol.* **2012**, *8*, 966-968.

(19) Lazarus, M. B.; Jiang, J.; Kapuria, V.; Bhuiyan, T.; Janetzko, J.; Zandberg, W. F.; Vocadlo, D. J.; Herr, W.; Walker, S. HCF-1 is cleaved in the active site of O-GlcNAc transferase. *Science* **2013**, *342*, 1235-1239.
(20) Dorfmueller, H. C.; Borodkin, V. S.; Schimpl, M.; Zheng, X.; Kime, R.; Read, K. D.; van Aalten, D. M. Cell-penetrant, nanomolar O-GlcNAcase inhibitors selective against lysosomal hexosaminidases. *Chem. Biol.* **2010**, *17*, 1250-1255.
(21) Roth, C.; Chan, S.; Offen, W. A.; Hemsworth, G. R.; Willems, L. I.; King, D. T.; Varghese, V.; Britton, R.; Vocadlo, D. J.; Davies, G. J. Structural and functional insight into human O-GlcNAcase. *Nat. Chem. Biol.* **2017**, *13*, 610-612.
(22) Li, B.; Li, H.; Lu, L.; Jiang, J. Structures of human O-GlcNAcase and its complexes reveal a new substrate recognition mode. *Nat. Struct. Mol. Biol.* **2017**, *24*, 362-369.
(23) Elsen, N. L.; Patel, S. B.; Ford, R. E.; Hall, D. L.; Hess, F.; Kandula, H.; Kornienko, M.; Reid, J.; Selnick, H.; Shipman, J. M.; Sharma, S.; Lumb, K. J.; Soisson, S. M.; Klein, D. J. Insights into activity and inhibition from the crystal structure of human O-GlcNAcase. *Nat. Chem. Biol.* **2017**, *13*, 613-615.
(24) Borodkin, V. S.; Rafie, K.; Selvan, N.; Aristotelous, T.; Navratilova, I.; Ferenbach, A. T.; Van Aalten, D. M. O-GlcNAcase fragment discovery with fluorescence polarimetry. *ACS Chem. Biol.* **2018**, *13*, 1353-1360.
(25) Yuzwa, S. A.; Macauley, M. S.; Heinonen, J. E.; Shan, X.; Dennis, R. J.; He, Y.; Whitworth, G. E.; Stubbs, K. A.; McEachern, E. J.; Davies, G. J. A potent mechanism-inspired O-GlcNAcase inhibitor that blocks phosphorylation of tau in vivo. *Nat. Chem. Biol.* **2008**, *4*, 483-490.
(26) Cekic, N.; Heinonen, J.; Stubbs, K.; Roth, C.; He, Y.; Bennet, A.; McEachern, E.; Davies, G.; Vocadlo, D. Analysis of transition state mimicry by tight binding aminothiazoline inhibitors provides insight into catalysis by human O-GlcNAcase. *Chem. Sci.* **2016**, *7*, 3742-3750.
(27) Bergeron-Brlek, M.; Meanwell, M.; Britton, R. Direct synthesis of imino-C-nucleoside analogues and other biologically active iminosugars. *Nat. Commun.* **2015**, *6*, 6903.
(28) Macauley, M. S.; Whitworth, G. E.; Debowski, A.; Chin, D.; Vocadlo, D. J. O-GlcNAcase uses substrate-assisted catalysis: kinetic analysis and development of highly selective mechanism-inspired inhibitors. *J. Biol. Chem.* **2005**, *280*, 25313-25322.
(29) He, Y.; Macauley, M. S.; Stubbs, K. A.; Vocadlo, D. J.; Davies, G. J. Visualizing the reaction coordinate of an O-GlcNAc hydrolase. *J. Am. Chem. Soc.* **2010**, *132*, 1807-1809.
(30) Xiong, J.; Xu, D. Mechanistic Insights into the Hydrolysis of O-GlcNAcylation Catalyzed by Human O-GlcNAcase. *J. Phys. Chem. B* **2020**, *124*, 9310-9322.
(31) Stubbs, K. A.; Bacik, J. P.; Perley-Robertson, G. E.; Whitworth, G. E.; Gloster, T. M.; Vocadlo, D. J.; Mark, B. L. The development of selective inhibitors of NagZ: increased susceptibility of Gram-negative bacteria to beta-lactams. *Chembiochem* **2013**, *14*, 1973-1981.
(32) Macauley, M. S.; He, Y.; Gloster, T. M.; Stubbs, K. A.; Davies, G. J.; Vocadlo, D. J. Inhibition of O-GlcNAcase using a potent and cell-permeable inhibitor does not induce insulin resistance in 3T3-L1 adipocytes. *Chem. Biol.* **2010**, *17*, 937-948.
(33) Mark, B. L.; Mahuran, D. J.; Cherney, M. M.; Zhao, D.; Knapp, S.; James, M. N. Crystal structure of human beta-hexosaminidase B: understanding the molecular basis of Sandhoff and Tay-Sachs disease. *J. Mol. Biol.* **2003**, *327*, 1093-1109.
(34) Tiscornia, G.; Vivas, E. L.; Matalonga, L.; Berniakovich, I.; Barragan Monasterio, M.; Eguizabal, C.; Gort, L.; Gonzalez, F.; Ortiz Mellet, C.; Garcia Fernandez, J. M.; Ribes, A.; Veiga, A.; Izpisua Belmonte, J. C. Neuronopathic Gaucher's disease: induced pluripotent stem cells for disease modelling and testing chaperone activity of small compounds. *Hum. Mol. Genet.* **2013**, *22*, 633-645.

(35) Suzuki, H.; Ohto, U.; Higaki, K.; Mena-Barragan, T.; Aguilar-Moncayo, M.; Ortiz Mellet, C.; Nanba, E.; Garcia Fernandez, J. M.; Suzuki, Y.; Shimizu, T. Structural basis of pharmacological chaperoning for human beta-galactosidase. *J. Biol. Chem.* **2014**, *289*, 14560-14568.
(36) Yu, Y.; Mena-Barragan, T.; Higaki, K.; Johnson, J. L.; Drury, J. E.; Lieberman, R. L.; Nakasone, N.; Ninomiya, H.; Tsukimura, T.; Sakuraba, H.; Suzuki, Y.; Nanba, E.; Mellet, C. O.; Garcia Fernandez, J. M.; Ohno, K. Molecular basis of 1-deoxygalactonojirimycin arylthiourea binding to human alpha-galactosidase a: pharmacological chaperoning efficacy on Fabry disease mutants. *ACS Chem. Biol.* **2014**, *9*, 1460-1469.
(37) de la Mata, M.; Cotan, D.; Oropesa-Avila, M.; Garrido-Maraver, J.; Cordero, M. D.; Villanueva Paz, M.; Delgado Pavon, A.; Alcocer-Gomez, E.; de Lavera, I.; Ybot-Gonzalez, P.; Paula Zaderenko, A.; Ortiz Mellet, C.; Garcia Fernandez, J. M.; Sanchez-Alcazar, J. A. Pharmacological Chaperones and Coenzyme Q10 Treatment Improves Mutant beta-Glucocerebrosidase Activity and Mitochondrial Function in Neuronopathic Forms of Gaucher Disease. *Sci. Rep.* **2015**, *5*, 10903.
(38) Risquez-Cuadro, R.; Matsumoto, R.; Ortega-Caballero, F.; Nanba, E.; Higaki, K.; Garcia Fernandez, J. M.; Ortiz Mellet, C. Pharmacological Chaperones for the Treatment of alpha-Mannosidosis. *J. Med. Chem.* **2019**, *62*, 5832-5843.
(39) Aguilar-Moncayo, M.; Takai, T.; Higaki, K.; Mena-Barragan, T.; Hirano, Y.; Yura, K.; Li, L.; Yu, Y.; Ninomiya, H.; Garcia-Moreno, M. I.; Ishii, S.; Sakakibara, Y.; Ohno, K.; Nanba, E.; Ortiz Mellet, C.; Garcia Fernandez, J. M.; Suzuki, Y. Tuning glycosidase inhibition through aglycone interactions: pharmacological chaperones for Fabry disease and GM1 gangliosidosis. *Chem.Commun.* **2012**, *48*, 6514-6516.
(40) Mena-Barragan, T.; Narita, A.; Matias, D.; Tiscornia, G.; Nanba, E.; Ohno, K.; Suzuki, Y.; Higaki, K.; Garcia Fernandez, J. M.; Ortiz Mellet, C. pH-Responsive Pharmacological Chaperones for Rescuing Mutant Glycosidases. *Angew. Chem. Int. Ed. Engl.* **2015**, *54*, 11696-11700.
(41) Mena-Barragan, T.; Garcia-Moreno, M. I.; Sevsek, A.; Okazaki, T.; Nanba, E.; Higaki, K.; Martin, N. I.; Pieters, R. J.; Fernandez, J. M. G.; Mellet, C. O. Probing the Inhibitor versus Chaperone Properties of sp(2)-Iminosugars towards Human beta-Glucocerebrosidase: A Picomolar Chaperone for Gaucher Disease. *Molecules* **2018**, *23*, 927.
(42) Glawar, A. F.; Best, D.; Ayers, B. J.; Miyauchi, S.; Nakagawa, S.; Aguilar-Moncayo, M.; Garcia Fernandez, J. M.; Ortiz Mellet, C.; Crabtree, E. V.; Butters, T. D.; Wilson, F. X.; Kato, A.; Fleet, G. W. Scalable syntheses of both enantiomers of DNJNAc and DGJNAc from glucuronolactone: the effect of N-alkylation on hexosaminidase inhibition. *Eur. J. Chem.* **2012**, *18*, 9341-9359.
(43) Anitha, M.; Swamy, K. C. K. Synthesis of thiazolidine-thiones, imino-thiazolidines and oxazolidines via the base promoted cyclisation of epoxy-sulfonamides and heterocumulenes. *Org. Biomol. Chem.* **2018**, *16*, 402-413.
(44) Murphy, D. J. Determination of accurate KI values for tight-binding enzyme inhibitors: an in silico study of experimental error and assay design. *Anal. Biochem.* **2004**, *327*, 61-67.
(45) Dennis, R. J.; Taylor, E. J.; Macauley, M. S.; Stubbs, K. A.; Turkenburg, J. P.; Hart, S. J.; Black, G. N.; Vocadlo, D. J.; Davies, G. J. Structure and mechanism of a bacterial beta-glucosaminidase having O-GlcNAcase activity. *Nat. Struct. Mol. Biol.* **2006**, *13*, 365-371.
(46) Fang, L.; Chakraborty, S.; Dieter, E. M.; Potter, Z. E.; Lombard, C. K.; Maly, D. J. Chemoproteomic Method for Profiling Inhibitor-Bound Kinase Complexes. *J. Am. Chem. Soc.* **2019**, *141*, 11912-11922.
(47) Duncan, J. S.; Gyenis, L.; Lenehan, J.; Bretner, M.; Graves, L. M.; Haystead, T. A.; Litchfield, D. W. An unbiased evaluation of CK2 inhibitors by chemoproteomics: characterization of inhibitor effects on CK2 and identification of novel inhibitor targets. *Mol. Cell Proteom.* **2008**, *7*, 1077-1088.
(48) Moulick, K.; Ahn, J. H.; Zong, H.; Rodina, A.; Cerchietti, L.; Gomes DaGama, E. M.; Caldas-Lopes, E.; Beebe, K.; Perna, F.; Hatzi, K.; Vu, L. P.; Zhao, X.; Zatorska, D.; Taldone, T.; Smith-Jones, P.; Alpaugh, M.; Gross, S. S.; Pillarsetty, N.; Ku, T.; Lewis, J. S.; Larson, S. M.; Levine, R.; Erdjument-Bromage, H.;

644 Guzman, M. L.; Nimer, S. D.; Melnick, A.; Neckers, L.; Chiosis, G. Affinity-based proteomics reveal cancer-
645 specific networks coordinated by Hsp90. *Nat. Chem. Biol.* **2011**, *7*, 818-826.
646 (49) Teranishi, Y.; Hur, J. Y.; Welander, H.; Frånberg, J.; Aoki, M.; Winblad, B.; Frykman, S.; Tjernberg,
647 L. O. Affinity pulldown of γ-secretase and associated proteins from human and rat brain. *J. Cell Mol.*
648 *Med.* **2010**, *14*, 2675-2686.
649 (50) Becher, I.; Dittmann, A.; Savitski, M. M.; Hopf, C.; Drewes, G.; Bantscheff, M. Chemoproteomics
650 reveals time-dependent binding of histone deacetylase inhibitors to endogenous repressor complexes.
651 *ACS Chem. Biol.* **2014**, *9*, 1736-1746.
652 (51) Cruz, I. N.; Barry, C. S.; Kramer, H. B.; Chuang, C. C.; Lloyd, S.; van der Spoel, A. C.; Platt, F. M.;
653 Yang, M.; Davis, B. G. Glycomimetic affinity-enrichment proteomics identifies partners for a clinically-
654 utilized iminosugar. *Chem. Sci.* **2013**, *4*, 3442-3446.
655 (52) Dong, D. L.; Hart, G. W. Purification and characterization of an *O*-GlcNAc selective *N*-acetyl-β-D-
656 glucosaminidase from rat spleen cytosol. *J. Biol. Chem.* **1994**, *269*, 19321-19330.
657 (53) Kelsall, I. R.; Zhang, J.; Knebel, A.; Arthur, J. S. C.; Cohen, P. The E3 ligase HOIL-1 catalyses ester
658 bond formation between ubiquitin and components of the Myddosome in mammalian cells. *Proc. Natl.*
659 *Acad. U.S.A.* **2019**, *116*, 13293-13298.
660 (54) Wisniewski, J. R.; Zougman, A.; Mann, M. Nepsilon-formylation of lysine is a widespread post-
661 translational modification of nuclear proteins occurring at residues involved in regulation of chromatin
662 function. *Nucl. Acid. Res.* **2008**, *36*, 570-577.
663 (55) Jumper, J.; Evans, R.; Pritzel, A.; Green, T.; Figurnov, M.; Ronneberger, O.; Tunyasuvunakool, K.;
664 Bates, R.; Zidek, A.; Potapenko, A.; Bridgland, A.; Meyer, C.; Kohl, S. A. A.; Ballard, A. J.; Cowie, A.;
665 Romera-Paredes, B.; Nikolov, S.; Jain, R.; Adler, J.; Back, T.; Petersen, S.; Reiman, D.; Clancy, E.; Zielinski,
666 M.; Steinegger, M.; Pacholska, M.; Berghammer, T.; Bodenstein, S.; Silver, D.; Vinyals, O.; Senior, A. W.;
667 Kavukcuoglu, K.; Kohli, P.; Hassabis, D. Highly accurate protein structure prediction with AlphaFold.
668 *Nature* **2021**, *596*, 583-589.
669 (56) Emsley, P.; Lohkamp, B.; Scott, W. G.; Cowtan, K. Features and development of Coot. *Acta Cryst.*
670 *D* **2010**, *66*, 486-501.
671 (57) Mertins, P.; Qiao, J. W.; Patel, J.; Udeshi, N. D.; Clauser, K. R.; Mani, D. R.; Burgess, M. W.;
672 Gillette, M. A.; Jaffe, J. D.; Carr, S. A. Integrated proteomic analysis of post-translational modifications by
673 serial enrichment. *Nat. Meth.* **2013**, *10*, 634-637.
674 (58) Wu, X.; Tian, L.; Li, J.; Zhang, Y.; Han, V.; Li, Y.; Xu, X.; Li, H.; Chen, X.; Chen, J.; Jin, W.; Xie, Y.;
675 Han, J.; Zhong, C. Q. Investigation of receptor interacting protein (RIP3)-dependent protein
676 phosphorylation by quantitative phosphoproteomics. *Mol. Cell Proteom.* **2012**, *11*, 1640-1651.
677 (59) Yi, T.; Zhai, B.; Yu, Y.; Kiyotsugu, Y.; Raschle, T.; Etzkorn, M.; Seo, H. C.; Nagiec, M.; Luna, R. E.;
678 Reinherz, E. L.; Blenis, J.; Gygi, S. P.; Wagner, G. Quantitative phosphoproteomic analysis reveals system-
679 wide signaling pathways downstream of SDF-1/CXCR4 in breast cancer stem cells. *Proc. Natl. Acad.*
680 *U.S.A.* **2014**, *111*, E2182-E2190.
681 (60) Elia, A. E.; Boardman, A. P.; Wang, D. C.; Huttlin, E. L.; Everley, R. A.; Dephoure, N.; Zhou, C.;
682 Koren, I.; Gygi, S. P.; Elledge, S. J. Quantitative Proteomic Atlas of Ubiquitination and Acetylation in the
683 DNA Damage Response. *Mol. Cell* **2015**, *59*, 867-881.
684 (61) Kim, W.; Bennett, E. J.; Huttlin, E. L.; Guo, A.; Li, J.; Possemato, A.; Sowa, M. E.; Rad, R.; Rush, J.;
685 Comb, M. J.; Harper, J. W.; Gygi, S. P. Systematic and quantitative assessment of the ubiquitin-modified
686 proteome. *Mol. Cell* **2011**, *44*, 325-340.

687

688

– Supporting Information –

Bicyclic picomolar OGA inhibitors enable chemoproteomic mapping of its endogenous post-translational modifications.

Manuel González-Cuesta,[a] Peter Sidhu,[b,c] Roger A. Ashmus,[b] Alexandra Males,[d] Cameron Proceviat,[b] Zarina Madden,[b] Jason C. Rogalski,[c] Jil A. Busmann,[e] Leonard J. Foster,[c] José M. García Fernández,[f] Gideon J. Davies,[d,*] Carmen Ortiz Mellet,[a,*] David J. Vocadlo[b,e,*]

[a] Departamento de Química Orgánica, Facultad de Química, Universidad de Sevilla, 41012, Sevilla, Spain.
[b] Department of Chemistry, Simon Fraser University, Burnaby V5A 1S6, British Columbia, Canada.
[c] Department of Biochemistry and Molecular Biology, University of British Columbia, Vancouver, British Columbia, V6T 1Z4, Canada.
[d] Department of Chemistry. University of York, York YO10 5DD, United Kingdom.
[e] Department of Molecular Biology and Biochemistry, Simon Fraser University, V5A 1S6, Burnaby, British Columbia, Canada.
[f] Instituto de Investigaciones Químicas (IIQ), CSIC - Universidad de Sevilla, 41092 Sevilla, Spain.

List of Contents

General methods

All reagents and solvents were purchased from commercial sources and used without further purification unless otherwise stated. Thin-layer chromatography (TLC) was carried out on aluminium sheets coated with *Sílica gel 60 F_{254} Merck* with visualization by UV light (λ 254 nm) and by charring with 10% ethanolic H_2SO_4, 0.1% ethanolic ninhydrin and heating at 100 ºC. With preparative purposes, column chromatography was carried out on *Silice 60 A.C.C. Chromagel* (SDS 70-200 and 35-70 μm). CombiFlash was performed on CombiFlash Rf 200 from Teledyne ISCO. In reference to 'dry load', the residue was dissolved in appropriate solvent then silica gel was added; this solvent was then evaporated to produce the residue adhered to silica which was loaded onto the column in dry form. HPLC was performed on Agilent 1100 series equipped with a variable wavelength UV-Vis detector using either an Eclipse XDB-C18 column (3.5 μm particle size, 3.0 × 150 mm for analytical runs and 5.0 μm, 9.4 × 250 mm for semi-preparative scale purifications) or ZORBAX 300SB C8 column (5.0 μm particle size, 9.4´ 250 mm for analytical runs and semi-preparative scale purifications) using HPLC grade solvents. Optical rotations were measured at 20 ± 2 ºC in 1 cm tubes on a Jasco P-2000 polarimeter using a sodium lamp (λ 589 nm). UV spectra were recorded on JASCO V-630 instrument; unit for ε values: $mm^{-1}cm^{-1}$. Elemental analyses were carried out at the Instituto de Investigaciones Químicas (Sevilla, Spain) using an elemental analyser *Leco CHNS-932* o *Leco TruSpec CHN*. NMR experiments were performed at 300 (75.5), 500 (125.7) and 600 (150) MHz with Bruker 300 ADVANCE, 500 DRX and Bruker Avance 600 equipped with a QNP or TCI cryoprobe (600 MHz). 1D TOCSY, 2D COSY, HMQC and HSQC experiments were used to assist on NMR assignments. The chemical shift values are given in ppm (part per million), using the solvent as internal standard, tetramethylsilane (for $CDCl_3$). The values of the coupling constant (*J*) are measured in Hz. Abbreviations to indicate the multiplicities of the signals are: s (singlet), bs (broad singlet), d (doublet), t (triplet), q (quartet) and m (multiplet). Mass spectra were carried out on Micromass AutoSpecQ (for chemical ionization, CI) or Bruker Daltonics Esquire6000™ (for electrospray ionization, ESI). For CI mass spectrometry, samples were introduced via solid probe heated from 30 to 280 ºC. In the case of ESI, methanol was used as the solvent. High resolution mass spectrometer (HRMS) spectra were recorded on a Bruker MaXis Impact or Agilent Technologies 6210 Time-of-Flight LC/MS spectrometers using positive or negative ESI.

Inhibition assays against commercial β-N-acetylglucosaminidases. Inhibition constant (K_i) values were determined by spectrophotometrically measuring the residual hydrolytic activities of the glycosidases against *p*-nitrophenyl *N*-acetyl-β-D-glucosaminide. The K_m values for the glycosidases used in the tests and the corresponding working pHs are listed herein: β-N-

acetylglucosaminidase (from human placenta), K_m = 0.34 mM (pH 5.5); β-N-acetylglucosaminidase (from bovine kidney), K_m = 0.48 mM (pH 5.5). Each assay was performed in phosphate-citrate buffer and the reactions were initiated by addition of the enzyme to a solution of the substrate in the absence or presence of various inhibitor concentrations. The mixture was incubated for 10-30 min at 37 ºC and the reaction was quenched by addition of 1 M Na_2CO_3. Reaction times were appropriate to obtain 10-20% conversion of the substrate in order to achieve linear rates. The absorbance of the resulting mixture was determined at 405 nm. Approximate values of K_i were determined using a fixed concentration of substrate (around the K_m value for the different glycosidases) and various inhibitor concentrations. Full K_i determinations and enzyme inhibition mode were determined from the slope of Lineweaver-Burk plots and double reciprocal analysis using a Microsoft Office Excel 2007 program.

Inhibition assays against hOGA. Inhibition constant (K_i) values for compounds against hOGA enzyme are determined by measuring the change in fluorescent signal corresponding to the rate of hydrolytic activity against the artificial substrate, Resorufin-N-acetyl-β-D-glucosaminide. hOGA activity assays were performed in a buffer of 20 mM HEPES, 5 mM EDTA, 150 mM KCl, pH 7.1 and 0.2 nM [hOGA]. K_m = 25uM was measured with these conditions. Inhibition assays were run at 0.2 nM [hOGA] in the same buffer, in the presence or absence of various concentrations of inhibitors and at a fixed substrate concentration of 25 μM and 1% DMSO. First, inhibitor was serially diluted to the desired range of concentrations in 2% DMSO buffer. Next, 50 μL of inhibitor solutions at various concentrations in 2% DMSO buffer was added to 50 μL of 0.8 nM enzyme and allowed to incubate at 25 °C for 5 minutes. 100 μL of 50 μM and 1% DMSO substrate was then added and reaction mixture was immediately mixed and aliquoted in 45 μL triplicates to a CORNING 384 well black plate. Fluorescence signal was measured continuously for 20 minutes at 37 °C in a BioTek Neo 2 Plate reader set at excitation and emission wavelengths of 572 and 610 nm, respectively. Maximal reaction rates for all inhibitor concentrations were calculated within Gen5 BioTek reader software. % A ctivity was subsequently calculated for each inhibitor concentration against the maximal reaction rate of uninhibited hOGA. GraphPad Prism 2016 was used to approximate the Morrison K_i values for each inhibitor.

Inhibition assays against rhHexA. Inhibition constant (K_i) values for compounds against recombinant human Hexosaminidase A (HexA) enzyme, purchased from R&D Systems (cat# 6237-GH-020), were determined by measuring the fluorescent signal corresponding to the rate of hydrolytic activity against the commercially available artificial substrate, 4-methylumbelliferone-N-acetyl-β-D-glucosaminide. HexA activity assays were performed in a buffer of 100 mM sodium citrate, 250 NaCl, pH 4.5 and 1.0 nM [HexA], then stopped after 20 minutes with a

solution of 1.0 M Tris, pH 9.5 to enhance fluorescent signal. Preliminary experiments have shown that reaction rates are linear for 20 min after substrate addition, and that 1.0 M Tris at pH 9.5 is sufficient for stopping activity, as signal is stable after stopping. Inhibition assays were run in the presence or absence of various concentrations of inhibitors and at a fixed substrate concentration of 100 μM and 1% DMSO. First, inhibitor was serially diluted to the desired range of concentrations in 2% DMSO buffer. Next, 25 μL of inhibitor solutions at various concentrations in 2% DMSO buffer was added to 25 μL of 4.0 nM enzyme and allowed to incubate at 25 °C for 5 min. 50 μL of 200 μM and 1% DMSO substrate was then added and allowed to react for 20 min. 100 μL of stop solution was added to reaction mixture, and immediately mixed and aliquoted in 45 μL triplicates to a CORNING 384 well black plate. Fluorescence signal was measured in a BioTek Neo 2 Plate reader set at excitation and emission wavelengths of 355 and 450 nm, respectively. % Activity was subsequently calculated for each inhibitor concentration against the fluorescence signal of uninhibited HexA. GraphPad Prism 2016 was used to approximate the Morrison K_i values for each inhibitor.

Inhibition assays against rhHexB. Inhibition constant (K_i) values against recombinant human Hexosaminidase B (HexB), purchased from R&D Systems (cat# 8907-GH-020) are determined by measuring the change in fluorescent signal corresponding to the rate of hydrolytic activity against the commercially available artificial substrate, 4-methylumbelliferone N-acetyl-β-D-galactosaminide. HexB activity assays were performed in 100 mM MES buffer at pH 5.5 and 5nM [HexB]. Inhibition assays were in the presence or absence of various concentrations of inhibitors and at a fixed substrate concentration of 150 μM and 1% DMSO. First, inhibitor was serially diluted to the desired range of concentrations in 2% DMSO buffer. Next, 50 μL of inhibitor solutions at various concentrations in 2% DMSO Buffer was added to 50 μL of 20 nM enzyme and allowed to incubate at 25 °C for 5 min. 100 μL of 300 μM and 1% DMSO substrate was then added and reaction mixture was immediately mixed and aliquoted in 45 μL triplicates to a CORNING 384 well black plate. Fluorescence signal was measured continuously for 20 min at 25 °C in a BioTek Neo 2 Plate reader set at excitation and emission wavelengths of 355 and 450 nm, respectively. Max reaction rates for all inhibitor concentrations were calculated within Gen5 BioTek reader software. % Activity was subsequently calculated for each inhibitor concentration against the max reaction rate of uninhibited HexB. GraphPad Prism 2016 was used to approximate the Morrison K_i values for each inhibitor.

Inhibition assays against *Bt*GH84. The inhibition constant (K_i) value for compound **16** against recombinant OGA from *Bacteriodes thetaiotaoicron* (*Bt*GH84), which was produced and purified according to Dennis *et al*, 2006, was determined spectrophotometrically by measuring the change

in absorbance at 405 nm upon hydrolysis of *p*-nitrophenyl *N*-acetyl-β-D-glucosaminide. A Biotek Epoch Microplate Spectrophotometer was used to monitor the enzyme assays that were performed in 384-well clear bottomed plates. The K_M value used in the tests was 1.09 mM at pH 6.5 (50 mM MES pH 6.5, 200 mM NaCl). The enzyme was incubated for 5 mins at 25 °C in the presence of various inhibitor concentrations after which the reaction was initiated by the addition of the substrate. The reaction was observed over 10 mins to achieve linear rates. An IC_{50} was conducted using a fixed concentration of substrate (around the K_M value) to approximate the K_i value. Full K_i determinations were obtained from the slope of Lineweaver-Burk plots and taking the reciprocal of the slope on a plot of K_{app} vs the inhibitor concentration.

Cell culture. All cells were cultured at 37°C in a humidified incubator with 5% CO_2 using standard procedures. Briefly, SK-N-SH cells (ATCC) were cultured in EMEM (M5650, Sigma) supplemented with 10% FBS (Gibco) and Pen/Strep antibiotics (Bioshop). Cells were expanded in T175 flasks and media was changed every 3 to 4 days until cells reached 80-90 % confluency. For each passage, cells were washed with warm PBS, treated with the minimal volume of Trypsin/EDTA, incubated for 3 to 5 minutes until cells were fully detached, and re-suspended in media containing FBS. Cells were counted using BioRad Automated Cell Counter TC20 with Trypan blue (Gibco), and either split into a new flask for sub-culturing (1:4 to 1:5 dilution) or plated for treatments. All experiments were carried out with cells having a passage number between P13 and P18.

Cell plating and treatment. After counting, the concentration of cells was adjusted and 2.5 x 10^6 cells were plated in 10 cm petri dishes (TC Dish-100, Sarstedt). Dishes were incubated for 2 days before medium was exchanged and inhibitors diluted in medium (final concentrations of 0–3.2 μM for **33** and 1 μM for Thiamet-G; <0.1% DMSO content) were added. The treated cells were incubated for 2 days before harvesting.

Cell harvesting. Culture plates were put on ice, the medium was aspirated, and cold PBS (4 °C, LonzaBioWhittaker) was added to all wells. The cells were scraped off and spun down at 300 g for 5 min at 4 °C (Sorvall Legend Micro 17R, Thermo Scientific). Cell pellets were resuspended in cold PBS buffer (3x the volume of the cell pellet) containing complete protease inhibitor cocktail tablets (Roche) prior to freeze-thaw-lysis. Samples were 3x plunged into liquid nitrogen and thawed in a water bath at 25 °C (280 series, Precision). Following, samples were spun down at 20,800 g at 4 °C for 30 min (centrifuge 5417 C, Eppendorf) and the supernatant was collected in fresh microcentrifuge tubes. The protein concentration of the samples was measured using the Quick Start Bradford 1x Dye Reagent (Biorad) and the Synergy neo2 plate reader (BioTek).

Immunoblotting. Samples were diluted in 5x SDS-PAGE loading buffer and heated at 90 °C for 3 min. Following, samples were quickly spun down and separated in Mini-PROTEAN TGX gels (4-15%, 10-well comb, 50 ul, Bio-Rad) at 70 V (PowerPac Basic, BioRad). Proteins were transferred to a 0.45 μm nitrocellulose membrane (Bio-Rad) by wet transfer at 110 V at 4 °C for 70 min. The membrane was incubated with 4% BSA (BioShop) in PBS buffer at 4 °C for 1 hour prior to incubation overnight (4 °C) on a rocking platform (Scilogex) with primary antibodies for fluorescent immunoblotting. Following primary antibodies were used: anti-OGA (1:5,000, rabbit, SAB4200311, Sigma-Aldrich), anti-*O*-GlcNAc clone CTD110.6 (1:3,000, mouse, MABS1254, EMD Millipore), and β-anti-Actin (1:10,000, rabbit, 926-42210, Li-Cor). On the following day, the membrane was washed 3x with PBS-T (0.1% tween 20, BioShop) for each 2 min. The membrane was then incubated with the secondary antibodies in 2% BSA in PBS-T at RT for 1 hour. Following secondary antibodies were used: Goat-anti-rabbit IRDye 800CW (1:20,000, 926-32211, Li-Cor) and Goat-anti-mouse IRDye 680LT (1:20,000, 926-68020, Li-Cor). Membranes were then washed 3x with PBS-T for each 2 min prior to imaging (Odyssey, Li-Cor).

Expression and purification of recombinant hOGA. *E. coli* cells that were transformed with a plasmid expressing hexahistidine tagged hOGA (full-length) were inoculated in lysogeny broth (LB) medium containing kanamycin (50 μg/mL), and were incubated aerobically at 37 °C overnight. The following day, 10 L of LB containing kanamycin (50 μg/mL), were inoculated with the overnight culture (1:100) and incubated aerobically at 37 °C to an OD600 of ~1.0. Once reached, cells were cold shocked at 4 °C for 30 min, then had IPTG added (0.1 mM) to induce protein synthesis, and expression induced at 21°C overnight. The cells were harvested by centrifugation (high-speed) at 20,000 RPM at 4°C for 20 min, and cells were flash frozen in liquid nitrogen, and stored at −80°C until needed.

For purification of hOGA, cells were thawed and resuspended in 25 mM HEPES, 500 mM NaCl, 1 mM DTT, pH 7.0, 5 mM imidazole (resuspension buffer), and rocked with lysozyme (1 mg/mL) at 4°C for 30 min. Cells were lysed using a sonic dismembrator at amplitude 60%, for 3 min (20 sec on, 40 sec off). The lysate was cleared by centrifugation (high-speed) at 20,000 RPM at 4 °C for 30 min, and again (ultra-speed) at 45,000 RPM at 4 °C for 40 min. The supernatant was passed through a pre-equilibrated HisTrap FF column (GE Healthcare) in suspension buffer using a peristaltic pump (flow rate 2mL/min). The column loaded with hOGA was purified by a gradient of 0% to 50% of elution buffer (25 mM HEPES, 500 mM NaCl, 1 mM DTT, pH 7.0, and 500 mM imidazole) over 50 mL of volume. Fractions containing hOGA were pooled and dialyzed using a molecular weight cut-off (MWCO) of 30 kDa in final buffer (10 mM HEPES, 250 mM NaCl, 1 mM DTT, pH 7.0). Dialyzed hOGA was concentrated using a Vivaspin of 70 kDa

MWCO, and had concentrations determined by Nanodrop 2000 UV-Vis spectrophotometer. Purified hOGA was aliquoted, flash frozen in liquid nitrogen, and stored at -80 °C until required.

Western blotting. Samples were diluted in 5x SDS-PAGE loading buffer and heated at 90°C for 3 min. Following, samples were quickly spun down and separated in Mini-PROTEAN TGX gels (4-15%, 10-well comb, 50 µl, Bio-Rad) at 70 V (PowerPac Basic, BioRad). Proteins were transferred to a 0.45 µm nitrocellulose membrane (Bio-Rad) by wet transfer at 110 V at 4 °C for 70 min. The membrane was incubated with 4% BSA (BioShop) in PBS buffer at 4 °C for 1 hour prior to incubation overnight (4 °C) on a rocking platform (Scilogex) with primary antibodies for fluorescent immunoblotting. Following primary antibodies were used: anti-OGA (1:5,000, rabbit, SAB4200311, Sigma-Aldrich), anti-*O*-GlcNAc clone CTD110.6 (1:3,000, mouse, MABS1254, EMD Millipore), and β-anti-Actin (1:10,000, rabbit, 926-42210, Li-Cor). On the following day, the membrane was washed 3x with PBS-T (0.1% tween 20, BioShop) for each 2 min. The membrane was then incubated with the secondary antibodies in 2% BSA in PBS-T at RT for 1 hour. Following secondary antibodies were used: Goat-anti-rabbit IRDye 800CW (1:20,000, 926-32211, Li-Cor) and Goat-anti-mouse IRDye 680LT (1:20,000, 926-68020, Li-Cor). Membranes were then washed 3x with PBS-T for each 2 min prior to imaging (Odyssey, Li-Cor).

Materials

2-Acetamido-1,2-dideoxynojirimicin hydrochloride (DNJNAc HCl), 2-azido-3,6-di-*O*-acetyl-4-*O*-benzyl-1,2,5-trideoxy-1,5-imino-D-glucitol (**25**),[1] 1,4-bis(azidomethyl)benzene[2] and 1-naphtylmethyl isothiocyanate[3] were prepared according to literature procedures. 1,5-Imino-2-propamido-1,2,5-trideoxy-D-glucitol (**34**)[4] was previously characterized. *o*-, *m*- and *p*-Azidomethylbenzylamines were obtained by cotrolled reduction of the corresponding *o*-, *m*- and *p*-bis(azidomethyl)benzene derivatives with triphenyphosphine, following the method reported by Lau *et al.*[5] They were used in the next isothiocyanation reaction without further purification. The non-commercial *p*-trifluoromethylbenzyl, *o*-, *m*-and *p*-azidomethylbenzyl and 5-indolyl isothiocyanates were synthesized by isothiocyanation of the corresponding amines as detailed hereinafter:

Synthesis of *p*-Trifluoromethylbenzyl isothiocyanate.

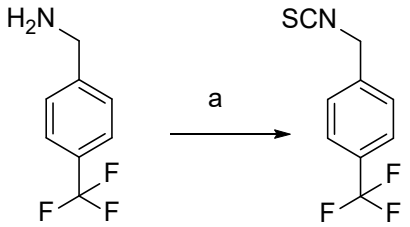

Supplemental scheme 1. Reagents and conditions: a. CS_2, Et_3N, Boc_2O, DMAP, EtOH, RT, 18 h.

To a solution of *p*-(trifluoromethyl)benzylamine (213 µL, 1.494 mM) in EtOH (8 mL), CS_2 (928 µL, 14.940 mM) and Et_3N (414 µL, 2.99 mM) were added. The mixture was stirred at RT for 30 min. Then di-*tert*-butyl dicarbonate (326 mg, 1.49 mmol) and 4-dimethylaminopyridine (3.7 mg, 0.029 mM) were added at 0 ºC and the reaction mixture was stirred for 18 h at RT. The solvent was evaporated under reduced pressure and the residue was dissolved with DCM (20 mL), washed with water (20 mL), brine (20 mL), dried ($MgSO_4$) and concentrated. The crude product was purified by column chromatography (1:8 → 1:3 EtOAc- cyclohexane). Yield: 128 mg (60%). R_f 0.66 (1:3 EtOAc-cyclohexane). $[\alpha]_D$ +5.6 (*c* 1.0 in DCM).

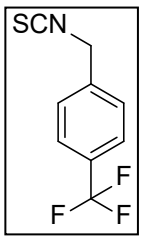

^{1}H NMR (300 MHz, $CDCl_3$): δ = 7.68 (d, 1 H, $^3J_{H,H}$ = 8.1 Hz, CH_{arom}), 7.47 (d, 1H, CH_{arom}), 4.81 (s, 2 H, CH_2NCS). **^{13}C NMR** (100.6 MHz, $CDCl_3$): δ = 138.2 (C-1), 130.9 (C-4), 127.0 (C-2), 126.0 ($J_{C,F}$ = 3.7 Hz, CF_3, C-3), 122.0 (NCS). **ESIMS**: *m/z* 215.8 $[M - H]^-$. Anal. Calcd. for $C_9H_6F_3NS$: C 49.77, H 2.78, F 26.24, N 6.45, S 14.76. Found C 49.63, H 2.56, N 6.27, S 14.49.

Synthesis of *o*-, *m*- and *p*-Azidomethylbenzyl isothiocyanates.

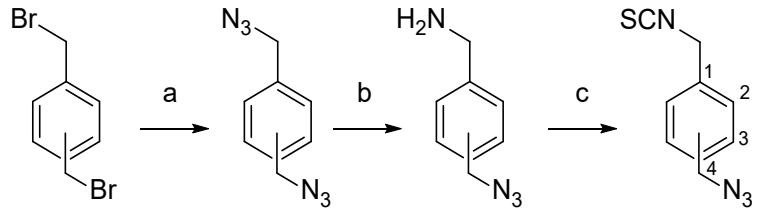

o,m,p-**ABNCS**

Supplemental scheme 2. Reagents and conditions: a. NaN_3, DMF, 60 ºC, 18 h; b. PPh_3, HCl 1M Et_2O, RT, 24 h; c. CS_2, $Cu_2SO_4 \cdot 5H_2O$, Et_3N, 2:1 EtOAc-H_2O, RT, 18 h.

General procedure for *o,m,p*-ABNCS synthesis. To a solution of the corresponding *o*-, *m*- or *p*-azidomethylbenzylamine (1.0 g, 6.5 mM) in EtOAc-H_2O (2:1, 18 mL), CS_2 (3.9 mL, 65 mM) and Et_3N (1.8 mL, 13 mM) were added and the mixture was stirred at r.t. for 1 h. Then, $Cu_2SO_4 \cdot 5H_2O$ (413 mg, 1.65 mM) was added and the mixture was further stirred at RT for 16 h. The crude product was filtered, diluted with EtOAc (20 mL), washed with H_2O (20 mL), dried ($MgSO_4$) and concentrated. The crude was purified by column chromatography (1:10 EtOAc-cyclohexane).

***o*-(Azidomethyl)benzyl isothiocyanate (*o*-ABNCS).** Yield: 0.97 g (72%). R_f 0.51 (1:8 EtOAc-cyclohexane). $[\alpha]_D$ -1.62 (*c* 1.00 in DCM).

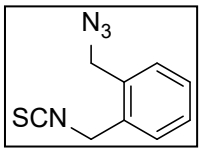

^{1}H NMR (300 MHz, $CDCl_3$): δ 7.49-7.33 (m, 4 H, CH_{arom}), 4.82 (s, 2 H, CH_2NCS), 4.42 (s, 2 H, CH_2N_3). **^{13}C NMR** (75.5 MHz, $CDCl_3$): δ = 133.2 (NCS), 132.9 (C-1), 132.8 (C-6), 130.2 (C-5), 129.4 (C-2), 129.0 (C-3), 128.8 (C-4), 52.4 (CH_2NCS), 46.3 (CH_2N_3). **ESIMS**: *m/z* 215.8 $[M - H]^-$. Anal. Calcd. for $C_9H_8N_4S$: C 52.92, H 3.95, N 27.43, S 15.70. Found C 53.23, H 4.21, N 27.31, S 15.48.

***m*-(Azidomethyl)benzyl isothiocyanate.** Yield: 0.92 g (68%). R_f 0.51 (1:8 EtOAc-cyclohexane). $[\alpha]_D$ -0.71 (*c* 1.00 in DCM).

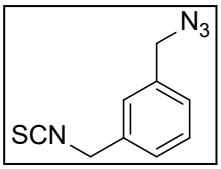

^{1}H NMR (300 MHz, $CDCl_3$): δ 7.46–7.28 (m, 4 H, CH_{arom}), 4.76 (s, 2 H, CH_2NCS), 4.40 (s, 2 H, CH_2N_3). **^{13}C NMR** (75.5 MHz, $CDCl_3$): δ = 136.4 (C-1), 135.0 (C-5), 132.8 (NCS), 129.5 (C-2), 128.1 (C-3), 126.7 (C-4), 126.4 (C-6), 54.4 (CH_2NCS), 48.4 (CH_2N_3). **ESIMS**: *m/z* = 215.8 $[M - H]^-$. Anal. Calcd. for $C_9H_8N_4S$: C 52.92, H 3.95, N 27.43, S 15.70. Found C 53.18, H 4.18, N 27.26, S 15.44.

***p*-(Azidomethyl)benzyl isothiocyanate.** Yield: 1.0 g (74%); R_f 0.51 (1:8 EtOAc-cyclohexane). $[\alpha]_D$ -2.51 (*c* 1.00 in DCM).

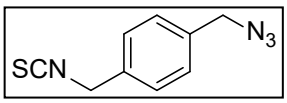

^{1}H NMR (300 MHz, $CDCl_3$): δ 7.36 (s, 4 H, CH_{arom}), 4.74 (s, 2 H, CH_2NCS), 4.37 (s, 2 H, CH_2N_3). **^{13}C NMR** (100.6 MHz, $CDCl_3$): δ = 135.7 (C-1), 134.3 (C-4), 129.7 (NCS), 128.7 (C-2), 127.3 (C-3), 54.3 (CH_2NCS), 48.3 (CH_2N_3). **ESIMS**: *m/z* = 215.8 [M - H]$^-$. Anal. calcd. for $C_9H_8N_4S$: C 52.92, H 3.95, N 27.43, S 15.70. Found C 53.04, H 3.99, N 27.17, S 15.39.

Synthesis of *tert*-butyl 5-(isothiocyanatomethyl)-1H-indole-1-carboxylate.

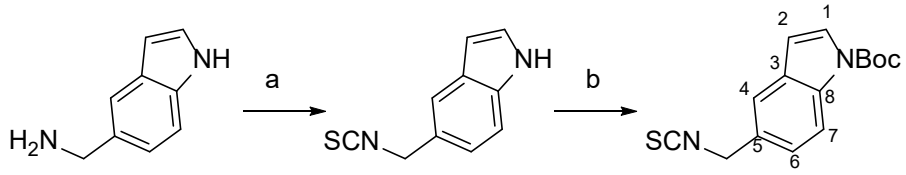

IBLNCS

Supplemental scheme 3. Reagents and conditions: a. CS_2, Et_3N, Boc_2O, DMAP, EtOH, RT, 18 h; b. Boc_2O, Et_3N, DCM, RT, 18 h.

To a solution of (1H-indol-5-yl)methanamine (600 mg, 2 mM) in EtOH (22 mL), CS_2 (2.4 mL, 20 mM) and Et_3N (1 mL, 4 mM) were added. The mixture was stirred at RT for 30 min. Then di-*tert*-butyl dicarbonate (875 mg, 2 mM) and 4-dimethylaminopyridine (10 mg, 0.04 mM) were added at 0 ºC and the reaction mixture was stirred for 18 h at RT. The solvent was evaporated under reduced pressure and the residue was dissolved with DCM (30 mL), washed with water (30 mL), brine (30 mL), dried ($MgSO_4$) and concentrated. The crude product was directly dissolved in DCM (15 mL) and Et_3N (0.5 mL) and Boc_2O (800 mg) were added and the mixture was stirred for 18 h at RT. The solvent was evaporated and the crude product purified by column chromatography (1:4 EtOAc-cyclohexane). Yield: 300 mg (50%, over 2 steps). R_f 0.50 (1:4 EtOAc-cyclohexane).

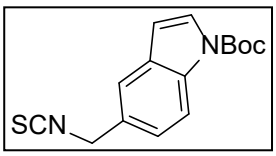

^{1}H NMR (300 MHz, $CDCl_3$): δ 8.08 (d, 1 H, H-4), 7.55 (d, 1 H, H-7), 7.43 (s, 1 H, H-6), 7.10 (dd, 1 H, H-1), 6.40 (d, 1 H, H-2), 4.71 (s, 2 H, CH_2NCS), 1.60 (s, 9 H, $C(CH_3)_3$). **^{13}C NMR** (75.5 MHz, $CDCl_3$): δ = 149.5 (CO), 134.9, 130.9, 128.5, 126.9, 123.1, 119.4, 115.6, 107.0 (NCS, C_{arom}), 84.0 ($C(CH_3)_3$), 48.9 (CH_2NCS), 28.1 ($C(CH_3)_3$). **ESIMS**: *m/z* = 287.40 [M - H]$^-$.

Synthesis of DNJNAc-thioureas 1-12

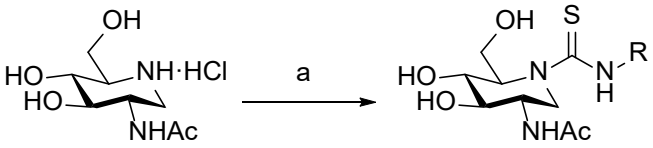

Supplemental scheme 4. Reagents and conditions: a. Et_3N, R-NCS, DMF, RT, 18 h.

General procedure for the preparation of the DNJNAc-thioureas 1-12. To a solution of 2-*N*-acetamido-1,2-dideoxynojirimicin hydrochloride (100 mg, 0.415 mM) in DMF (3.7 mL), Et_3N (0.115 mL, 0.830 mM) and the corresponding isothiocyanate (0.498 mM, 1.2 eq) were added. The mixture was stirred at RT for 18 h. Then, the solvent was coevapored with toluene and the resulting residue was purified by column chromatography using the eluent indicated in each case.

2-Acetamido-5-*N*-(*N'*-butylthiocarbamoyl)-1,2-dideoxynojirimycin (1). Column chromatography, eluent 80:10:1 DCM-MeOH-H_2O. Yield: 116 mg (86%). $[\alpha]_D$ -114.7 (*c* 1.04, MeOH). R_f 0.35 (70:10:1 DCM-MeOH-H_2O). UV (MeOH) 249 nm (ε_{mM} 12.5).

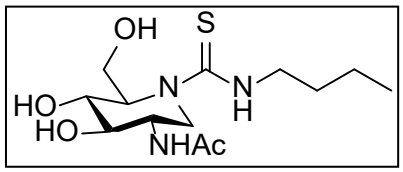

^{1}H NMR (500 MHz, CD_3OD): δ 4.83 (bd, 1 H, $J_{1a,1b}$ = 14.4 Hz, H-1a), 4.25 (m, 1 H, H-5), 3.92 (dd, 1 H, $J_{5,6a}$ = 8.6 Hz, $J_{6a,6b}$ = 11.4 Hz, H-6a), 3.90 (m, 1 H, H-2), 3.84 (dd, 1 H, $J_{5,6b}$ = 3.6 Hz, H-6b), 3.67 (dd, 1 H, $J_{3,4}$ = 6.1 Hz, $J_{4,5}$= 4.7 Hz, H-4), 3.57 (m, 2 H, C*H*$_2$NH, H-3), 3.47 (dd, 1 H, $J_{1b,2}$ = 4.0 Hz, H-1b), 1.95 (s, 1 H, $COCH_3$), 1.59 (m, 2 H, CH_2), 1.38 (m, 2 H, C*H*$_2$$CH_3$), 0.95 (t, 3 H, $J_{H,H}$ = 7.4 Hz, CH_3). **^{13}C NMR** (125.7 MHz, CD_3OD): δ 186.6 (CS), 173.0 (CO), 72.8 (C-3), 70.8 (C-4), 66.2 (C-5), 62.2 (C-6), 53.3 (C-2), 46.8 (CH_2N), 45.2 (C-1), 32.3 (CH_2), 23.0 (CO*C*H_3), 21.1 (*C*H_2CH_3), 14.1 (CH_3). **CIMS**: *m/z* 320 (10, $[M + H]^+$). Anal. Calcd for $C_{13}H_{25}N_3O_4S$: C, 48.88; H, 7.89; N, 13.16; S, 10.04. Found: C, 48.72; H, 7.69; N, 12.83; S, 9.69.

2-Acetamido-1,2-dideoxy-5-*N*-(*N'*-octylthiocarbamoyl)nojirimycin (2). Column chromatography, eluent 80:10:1 DCM-MeOH-H_2O. Yield: 124 mg (78%). $[\alpha]_D$ -73.8 (*c* 1.00, MeOH). R_f 0.39 (70:10:1 DCM-MeOH-H_2O). UV (MeOH) 248 nm (ε_{mM} 11.4).

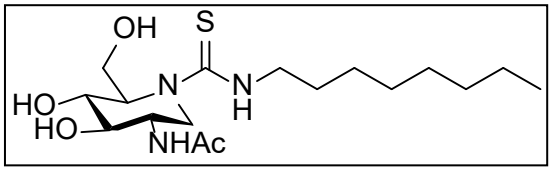

^{1}H NMR (500 MHz, CD_3OD): δ 4.83 (bd, 1 H, $J_{1a,1b}$ = 14.6 Hz, H-1a), 4.23 (m, 1 H, H-5), 3.92 (dd, 1 H, $J_{6a,6b}$ = 11.4 Hz, $J_{5,6a}$ = 8.8 Hz, H-6a), 3.88 (m, 1 H, H-2), 3.83 (dd, 1 H, $J_{5,6b}$ = 3.5 Hz, H-6b), 3.66 (t, 1 H, $J_{3,4}$ = $J_{4,5}$= 6.0 Hz, H-4), 3.56 (m, 2 H, C*H*$_2$NH, H-3), 3.46 (dd, 1 H, $J_{1b,2}$ = 4.1 Hz, H-1b), 1.94 (s, 1 H, $COCH_3$), 1.60 (m, 2 H, CH_2), 1.31 (m, 10 H, CH_2), 0.90 (t, 3 H, $^3J_{H,H}$ = 7.0 Hz, CH_3). **^{13}C NMR** (125.7 MHz, CD_3OD): δ 186.6 (CS), 173.0 (CO), 72.8 (C-3), 70.8 (C-4), 66.2 (C-5), 62.1 (C-6), 53.2 (C-2), 47.1 (CH_2N), 45.2 (C-1), 32.9, 30.4, 30.3, 30.1 28.0, 23.6 (CH_2), 23.0 (CO*C*H_3), 14.3(CH_3). **ESIMS**: *m/z* 376

[M + H]$^+$, 398 [M + Na]$^+$. Anal. Calcd for $C_{17}H_{33}N_3O_4S$: C, 54.37; H, 8.86; N, 11.19; S, 8.54. Found: C, 54.51; H, 8.91; N, 10.94; S 8.22.

2-Acetamido-1,2-dideoxy-5-*N*-(*N'*-phenylthiocarbamoyl)nojirimycin (3). Column chromatography, eluent 80:10:1 DCM-MeOH-H_2O. Yield: 118 mg (82%). $[\alpha]_D$ -132.8 (*c* 1.12, MeOH). R_f 0.29 (70:10:1 DCM-MeOH-H_2O). UV (MeOH) 258 nm (ε_{mM} 14.9).

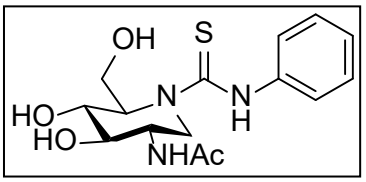

^{1}H NMR (400 MHz, acetone-d_6): δ 9.83 (bs, 1 H, NH), 7.88 (bd, 1 H, $J_{NH,2}$ = 6.4 Hz, NH), 7.67-7.08 (m, 5 H, CH_{arom}), 5.45 (bs, 1 H, OH), 5.03 (bs, 1 H, OH), 4.91 (d, 1 H, $J_{1a,1b}$ = 14.4 Hz, H-1a), 4.62 (bs, 1 H, OH), 4.40 (m, 1 H, H-5), 4.13 (t, 1 H, $J_{5,6a}$ = $J_{6a,6b}$ = 11.1 Hz, H-6a), 4.04 (dd, 1 H, $J_{5,6b}$ = 2.9 Hz, H-6b), 3.92 (m, 1 H, H-2), 3.75 (t, 1 H, $J_{3,4}$ = $J_{4,5}$ = 6.8 Hz, H-4), 3.63 (dd, 1 H, $J_{2,3}$ = 4.7 Hz, H-3), 3.57 (dd, 1 H, $J_{1b,2}$ = 4.4 Hz, H-1b), 1.93 (s, 1 H, $COCH_3$). **^{13}C NMR** (100.6 MHz, acetone-d_6): δ 185.8 (CS), 171.2 (CO), 141.8, 129.0, 124.9, 124.2 (C_{arom}), 74.6 (C-3), 70.5 (C-4), 66.6 (C-5), 62.7 (C-6), 54.4 (C-2), 44.5 (C-1), 23.2 ($COCH_3$). **ESIMS**: *m/z* 362 [M + Na]$^+$. Anal. Calcd for $C_{15}H_{21}N_3O_4S$: C, 53.08; H, 6.24; N, 12.38; S, 9.45. Found: C, 53.20; H, 6.28; N, 12.41; S 9.60.

2-Acetamido-5-*N*-(*N'*-benzylthiocarbamoyl)-1,2-dideoxynojirimycin (4). Column chromatography, eluent 80:10:1 DCM-MeOH-H_2O. Yield: 117 mg (78%). $[\alpha]_D$ -48.7 (*c* 0.46, MeOH). R_f 0.33 (70:10:1 DCM-MeOH-H_2O). UV (MeOH) 208 nm (ε_{mM} 18.0).

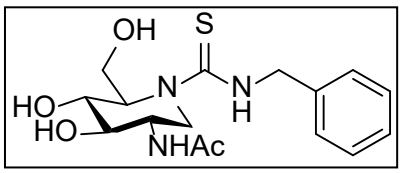

^{1}H NMR (500 MHz, CD_3OD): δ 7.37-7.21 (CH_{arom}), 4.89 (m, 2 H, H-1a, C*H*$_2$Ph), 4.78 (d, 1 H, $^2J_{H,H}$ = 15 Hz, C*H*$_2$Ph), 4.38 (m, 1 H, H-5), 3.95 (dd, 1 H, $J_{6a,6b}$ = 11.4 Hz, $J_{5,6a}$ = 8.7 Hz, H-6a), 3.93 (m, 1 H, H-2), 3.83 (dd, 1 H, $J_{5,6b}$ = 3.6 Hz, H-6b), 3.70 (t, 1 H, $J_{3,4}$ = $J_{4,5}$= 5.1 Hz, H-4), 3.60 (t, 1 H, $J_{2,3}$ = 5.1 Hz, H-3), 3.46 (dd, 1 H, $J_{1a,1b}$ = 14.3 Hz, $J_{1b,2}$ = 3.8 Hz, H-1b), 1.93 (s, 1 H, $COCH_3$). **^{13}C NMR** (125.7 MHz, CD_3OD): δ 186.9 (CS), 173.0 (CO), 140.0, 129.4, 128.6, 128.0 (C_{arom}), 72.3 (C-3), 70.6 (C-4), 66.0 (C-5), 61.8 (C-6), 53.0 (C-2), 50.5 (*C*H$_2$Ph), 45.3 (C-1), 23.0 ($COCH_3$). **ESIMS**: *m/z* 376 [M + Na]$^+$. Anal. Calcd for $C_{16}H_{23}N_3O_4S$: C, 54.37; H, 6.56; N, 11.89; S, 9.07. Found: C, 54.45; H, 6.69; N, 11.76; S 8.84.

2-Acetamido-5-*N*-(*N'*-1-naphthylmethylthiocarbamoyl)-1,2-dideoxynojirimycin (5). Column chromatography, eluent 100:10:1 DCM-MeOH-H_2O. Yield: 90 mg (60%). $[\alpha]_D$ -54.6 (*c* 1.00, MeOH). R_f 0.40 (70:10:1 DCM-MeOH-H_2O).

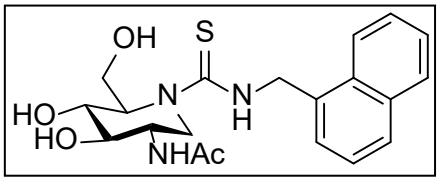

^{1}H NMR (300 MHz, CD_3OD): δ 8.10-7.41 (CH_{arom}), 5.27 (bs, 2 H, C*H*$_2$Naph), 4.95 (m, 1 H, H-1a), 4.30 (m, 1 H,

H-5), 3.93 (dd, 1 H, $J_{6a,6b}$ = 11.2 Hz, $J_{5,6a}$ = 8.8 Hz, H-6a), 3.92 (m, 1 H, H-2), 3.82 (dd, 1 H, $J_{5,6b}$ = 3.5 Hz, H-6b), 3.66 (t, 1 H, $J_{3,4}$ = $J_{4,5}$= 5.7 Hz, H-4), 3.61 (t, 1 H, $J_{2,3}$ = 5.4 Hz, H-3), 3.53 (dd, 1 H, $J_{1a,1b}$ = 14.1 Hz, $J_{1b,2}$ = 3.8 Hz, H-1b), 1.94 (s, 3 H, NHCOCH_3). **^{13}C NMR** (100.6 MHz, CD_3OD): δ 185.3 (CS), 171.6 (CO), 133.9-123.2 (C_{arom}), 70.9 (C-3), 69.2 (C-4), 64.8 (C-5), 60.4 (C-6), 51.6 (C-2), 48.4 (*C*H_2Naph), 43.9 (C-1), 21.6 (CO*C*H_3). **ESIMS**: *m/z* 401.9 $[M - H]^-$. Anal. Calcd for $C_{20}H_{25}N_3O_4S$: C 59.53, H 6.25, N 10.41, S 7.95. Found: C, 59.42; H, 6.13; N, 10.29; S 7.80.

2-Acetamido-5-*N*-(*N'*-*p*-fluorobenzylthiocarbamoyl)-1,2-dideoxynojirimycin (6). Column chromatography, eluent 100:10:1 DCM-MeOH-H_2O. Yield: 128 mg (83%). $[\alpha]_D$ -97.5 (*c* 1.00, MeOH). R_f 0.33 (70:10:1 DCM-MeOH-H_2O). UV (MeOH) 227 nm (ε_{mM} 4.8).

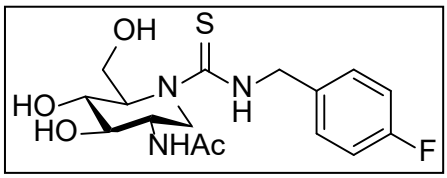

^{1}H NMR (500 MHz, CD_3OD): δ 7.36, 7.04 (CH_{arom}), 4.92 (m, 1 H, H-1a), 4.76 (d, 2 H, $^3J_{H,H}$ = 15 Hz, CH_2Ph), 4.38 (m, 1 H, H-5), 3.95 (dd, 1 H, $J_{6a,6b}$ = 11.1 Hz, $J_{5,6a}$ = 8.9 Hz, H-6a), 3.93 (m, 1 H, H-2), 3.83 (dd, 1 H, $J_{5,6b}$ = 3.7 Hz, H-6b), 3.70 (t, 1 H, $J_{3,4}$ = $J_{4,5}$= 5.2 Hz, H-4), 3.60 (t, 1 H, $J_{2,3}$ = $J_{3,4}$= 5.2 Hz, H-3), 3.46 (dd, 1 H, $J_{1a,1b}$ = 14.3 Hz, $J_{1b,2}$ = 3.8 Hz, H-1b), 1.95 (s, 3 H, NHCOCH_3). **^{13}C NMR** (125.7 MHz, CD_3OD): δ 185.4 (CS), 171.6 (CO), 162.2, 134.8, 129.0, 114.6 (C_{arom}), 70.9 (C-3), 69.2 (C-4), 64.5 (C-5), 60.4 (C-6), 51.6 (C-2), 48.2 (*C*H_2Ph), 43.9 (C-1), 21.6 (CO*C*H_3). **ESIMS**: *m/z* 394.1 $[M + Na]^+$. Anal. Calcd for $C_{16}H_{22}FN_3O_4S$: C 51.74, H 5.97, N 11.31, S 8.63. Found: C, 51.57; H, 6.10; N, 11.19; S 8.36.

2-Acetamido-5-*N*-(*N'*-*p*-methoxybenzylthiocarbamoyl)-1,2-dideoxynojirimycin (7). Column chromatography, eluent 100:10:1 DCM-MeOH-H_2O. Yield: 150 mg (94%). $[\alpha]_D$ –72.2 (*c* 1.00, MeOH). R_f 0.40 (70:10:1 DCM-MeOH-H_2O). UV (MeOH) 230 nm (ε_{mM} 31.4).

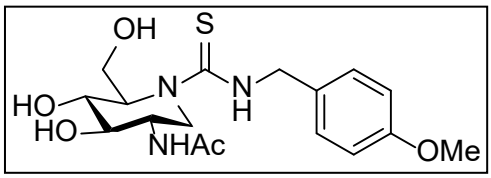

^{1}H NMR (500 MHz, CD_3OD): δ 7.27 (m, 2 H, CH_{arom}), 6.8 (m, 2 H, CH_{arom}), 4.91 (m, 1 H, H-1a), 4.76 (d, 2 H, $^3J_{H,H}$ = 15 Hz, CH_2Ph), 4.34 (m, 1 H, H-5), 3.95 (dd, 1 H, $J_{6a,6b}$ = 11.2 Hz, $J_{5,6a}$ = 8.7 Hz, H-6a), 3.93 (m, 1 H, H-2), 3.82 (dd, 1 H, $J_{5,6b}$ = 3.7 Hz, H-6b), 3.78 (s, 3 H, OCH_3), 3.69 (t, 1 H, $J_{3,4}$ = $J_{4,5}$= 5.4 Hz, H-4), 3.60 (t, 1 H, $J_{2,3}$ = $J_{3,4}$= 5.4 Hz, H-3), 3.46 (dd, 1 H, $J_{1a,1b}$ = 14.4 Hz, $J_{1b,2}$ = 3.7 Hz, H-1b), 1.95 (s, 3 H, NHCOCH_3). **^{13}C NMR** (125.7 MHz, CD_3OD): δ 185.2 (CS), 171.6 (CO), 158.9, 130.5, 128.5, 113.4 (C_{arom}), 71.0 (C-3), 69.2 (C-4), 64.6 (C-5), 60.4 (C-6), 54.2 (OCH_3), 51.6 (C-2), 48.7 (*C*H_2Ph), 43.9 (C-1), 21.6 (CO*C*H_3). **ESIMS**: *m/z* 406.2 $[M + Na]^+$. Anal. Calcd for $C_{17}H_{25}N_3O_5S$: C 53.25, H 6.57, N 10.96, S 8.36. Found: C, 53.35; H, 6.72; N, 10.80; S 8.09.

2-Acetamido-5-*N*-(*N'*-*p*-trifluoromethylbenzylthiocarbamoyl)-1,2-dideoxynojirimycin (8). Column chromatography, eluent 100:10:1 DCM-MeOH-H_2O. Yield: 87 mg (55%). $[\alpha]_D$ +4.2 (*c* 1.00, MeOH). R_f 0.31 (70:10:1 DCM-MeOH-H_2O). UV (MeOH) 223 nm (ε_{mM} 15.4).

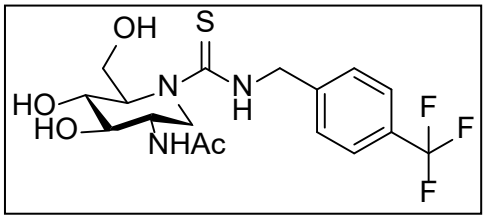

^{1}H NMR (500 MHz, CD_3OD): δ 7.61 (d, 2 H, $J_{H,H}$= 7.9 Hz, CH_{arom}), 7.52 (d, 2 H, CH_{arom}), 5.01 (d, 2 H, $^3J_{H,H}$ = 15 Hz, CH_2Ph), 4.91 (m, 1 H, H-1a), 4.47 (m, 1 H, H-5), 4.12 (m, 1 H, H-2), 3.99 (dd, 1 H, $J_{6a,6b}$ = 11.2 Hz, $J_{5,6a}$ = 8.7 Hz, H-6a), 3.86 (dd, 1 H, $J_{5,6b}$ = 3.8 Hz, H-6b), 3.75 (t, 1 H, $J_{3,4}$ = $J_{4,5}$= 5.2 Hz, H-4), 3.63 (dd, 1 H, $J_{2,3}$ = 7.2 Hz, $J_{3,4}$= 5.2 Hz, H-3), 3.46 (dd, 1 H, $J_{1a,1b}$ = 14.1 Hz, $J_{1b,2}$ = 3.4 Hz, H-1b), 1.93 (s, 3 H, COCH_3). **^{13}C NMR** (125.7 MHz, CD_3OD): δ 185.7 (CS), 171.6 (CO), 143.7, 127.5 (C_{arom}), 124.7 (q, CF_3), 113.4 (C_{arom}), 70.7 (C-3), 69.2 (C-4), 64.4 (C-5), 60.3 (C-6), 51.5 (C-2), 48.3 (*C*H_2Ph), 43.9 (C-1), 21.6 (CO*C*H_3). **ESIMS**: *m/z* 444.1 $[M + Na]^+$. Anal. Calcd for $C_{17}H_{22}F_3N_3O_4S$: C 48.45, H 5.26, N 9.97, S 7.61. Found: C, 48.36; H, 5.17; N, 9.72; S 7.36.

2-Acetamido-5-*N*-(*N'*-*o*-azidomethylbenzylthiocarbamoyl)-1,2-dideoxynojirimycin (9). Column chromatography, eluent 100:10:1 DCM-MeOH-H_2O. Yield: 114 mg (75%). $[\alpha]_D$ -44.0 (*c* 1.00, MeOH). R_f 0.40 (70:10:1 DCM-MeOH-H_2O). UV (MeOH) 230 nm (ε_{mM} 20.3).

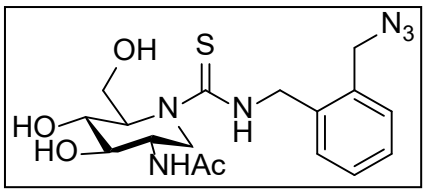

^{1}H NMR (300 MHz, CD_3OD): δ 7.43-7.28 (d, 4 H, CH_{arom}), 4.96 (bd, 1 H, H-1a), 4.91 (d, 2 H, CH_2Ph), 4.53 (s, 2 H, CH_2N_3), 4.37 (m, 1 H, H-5), 3.97 (dd, 1 H, $J_{6a,6b}$ = 11.3 Hz, $J_{5,6a}$ = 8.5 Hz, H-6a), 3.94 (m, 1 H, H-2), 3.82 (dd, 1 H, $J_{5,6b}$ = 3.8 Hz, H-6b), 3.70 (bdd, 1 H, $J_{3,4}$ = $J_{4,5}$= 5.4 Hz, H-4), 3.61 (t, 1 H, $J_{2,3}$ = 5.4 Hz, H-3), 3.52 (dd, 1 H, $J_{1a,1b}$ = 14.2 Hz, $J_{1b,2}$ = 3.7 Hz, H-1b), 1.95 (s, 3 H, COCH_3). **^{13}C NMR** (100.6 MHz, CD_3OD): δ 185.2 (CS), 171.6 (CO), 137.1, 133.5, 129.4, 128.6, 128.3, 127.1 (C_{arom}), 70.8 (C-3), 69.2 (C-4), 64.5 (C-5), 60.4 (C-6), 51.9 (CH_2N_3), 51.5 (C-2), 46.4 (*C*H_2Ph), 43.9 (C-1), 21.6 (CO*C*H_3). **ESIMS**: *m/z* 431.2 $[M + Na]^+$. Anal. Calcd for $C_{17}H_{24}N_6O_4S$: C 49.99, H 5.92, N 20.57, S 7.85. Found: C, 49.81; H, 5.80; N, 20.36; S 7.64.

2-Acetamido-5-*N*-(*N'*-*m*-azidomethylbenzylthiocarbamoyl)-1,2-dideoxynojirimycin (10). Column chromatography, eluent 100:10:1 DCM-MeOH-H_2O. Yield: 94 mg (65%). $[\alpha]_D$ -64.3 (*c* 1.00, MeOH). R_f 0.40 (70:10:1 DCM-MeOH-H_2O). UV (MeOH) 230 nm (ε_{mM} 31.4).

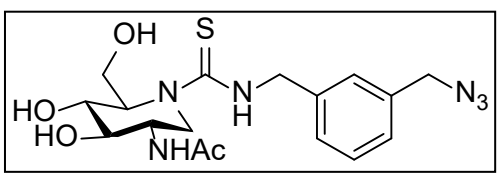

^{1}H NMR (300 MHz, CD_3OD): δ 7.27-7.11 (m, 4 H, CH_{arom}), 4.83 (bd, 1 H, H-1a), 4.78 (bd, 2 H, CH_2Ph), 4.29 (m, 1 H, H-5), 4.24 (s, 2 H, CH_2N_3), 3.86 (dd, 1

H, $J_{6a,6b}$ = 11.3 Hz, $J_{5,6a}$ = 8.6 Hz, H-6a), 3.83 (m, 1 H, H-2), 3.72 (dd, 1 H, $J_{5,6b}$ = 3.8 Hz, H-6b), 3.61 (bdd, 1 H, $J_{3,4}$ = $J_{4,5}$= 5.3 Hz, H-4), 3.50 (t, 1 H, $J_{2,3}$ = 5.3 Hz, H-3), 3.42 (dd, 1 H, $J_{1a,1b}$ = 14.2 Hz, $J_{1b,2}$ = 3.8 Hz, H-1b), 1.82 (s, 3 H, NHCOC*H*$_3$). **^{13}C NMR** (100.6 MHz, CD_3OD): δ 185.5 (CS), 171.6 (CO), 139.5, 135.9, 128.4, 127.1, 126.9, 126.6 (C_{arom}), 70.8 (C-3), 69.2 (C-4), 64.5 (C-5), 60.3 (C-6), 54.1 (CH_2N_3), 51.5 (C-2), 48.8 (*C*H_2Ph), 43.8 (C-1), 21.6 (CO*C*H_3). **ESIMS**: *m/z* 431.2 $[M + Na]^+$. Anal. Calcd for $C_{17}H_{24}N_6O_4S$: C 49.99, H 5.92, N 20.57, S 7.85. Found: C, 49.75; H, 5.67; N, 20.20; S 7.51.

2-Acetamido-5-*N*-(*N'*-*p*-azidomethylbenzylthiocarbamoyl)-1,2-dideoxynojirimycin (11). Column chromatography, eluent 100:10:1 DCM-MeOH-H_2O. Yield: 100 mg (60%). $[\alpha]_D$ -54.0 (*c* 1.00, MeOH). R_f 0.40 (70:10:1 DCM-MeOH-H_2O). UV (MeOH) 230 nm (ε_{mM} 31.4).

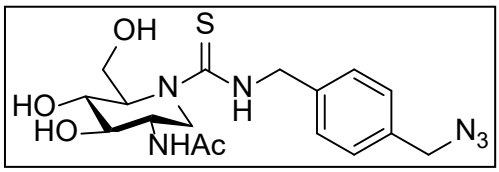

^{1}H NMR (400 MHz, CD_3OD): δ 7.39 (d, 2 H, $J_{H,H}$ = 8.2 Hz, CH_{arom}), 7.32 (d, 2 H, CH_{arom}), 4.94 (bd, 1 H, H-1a), 4.82 (d, 2 H, $^2J_{H,H}$ = 15.0 Hz, C*H*$_2$Ph), 4.43 (m, 1 H, H-5), 4.35 (s, 2 H, C*H*$_2$N$_3$), 3.98 (dd, 1 H, $J_{6a,6b}$ = 11.3 Hz, $J_{5,6a}$ = 8.5 Hz, H-6a), 3.94 (m, 1 H, H-2), 3.85 (dd, 1 H, $J_{5,6b}$ = 3.7 Hz, H-6b), 3.73 (bdd, 1 H, $J_{3,4}$ = $J_{4,5}$= 5.4 Hz, H-4), 3.62 (t, 1 H, $J_{2,3}$ = 5.4 Hz, H-3), 3.54 (dd, 1 H, $J_{1a,1b}$ = 14.2 Hz, $J_{1b,2}$ = 3.7 Hz, H-1b), 1.95 (s, 3 H, NHCOC*H*$_3$). **^{13}C NMR** (100.6 MHz, CD_3OD): δ 185.4 (CS), 171.6 (CO), 139.0, 134.4, 128.1, 127.1 (C_{arom}), 70.8 (C-3), 69.2 (C-4), 64.5 (C-5), 60.4 (C-6), 53.9 (CH_2N_3), 51.6 (C-2), 48.7 (*C*H_2Ph), 43.9 (C-1), 21.6 (CO*C*H_3). **ESIMS**: *m/z* 431.2 $[M + Na]^+$. Anal. Calcd for $C_{17}H_{24}N_6O_4S$: C 49.99, H 5.92, N 20.57, S 7.85. Found: C, 49.75; H, 5.67; N, 20.20; S 7.51.

2-Acetamido-5-*N*-(*N'*-2-phenylethylthiocarbamoyl)-1,2-dideoxynojirimycin (12). Column chromatography, eluent 100:10:1 DCM-MeOH-H_2O. Yield: 120 mg (78%). $[\alpha]_D$ +4.29 (*c* 1.00, MeOH). R_f 0.42 (70:10:1 DCM-MeOH-H_2O). UV (MeOH) 223 nm (ε_{mM} 15.4).

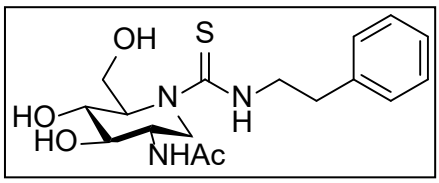

^{1}H NMR (300 MHz, CD_3OD): δ 7.33-7.17 (m, 5 H, CH_{arom}), 4.86 (bd, 1 H, H-1a), 4.25 (m, 1 H, H-5), 3.92 (m, 1 H, H-2), 3.91 (dd, 1 H, $J_{6a,6b}$ = 11.2 Hz, $J_{5,6a}$ = 8.3 Hz, H-6a), 3.81 (m, 3 H, H-6b, CH_2CH_2Ph), 3.69 (dd, 1 H, $J_{3,4}$ = 5.9 Hz, $J_{4,5}$= 4.6 Hz, H-4), 3.57 (bdd, 1 H, H-3), 3.48 (dd, 1 H, $J_{1a,1b}$ = 14.2 Hz, $J_{1b,2}$ = 3.9 Hz, H-1b), 2.92 (m, 2 H, C*H*$_2$CH$_2$Ph), 1.97 (s, 3 H, NHCOC*H*$_3$). **^{13}C NMR** (75.5 MHz, CD_3OD): δ 185.0 (CS), 171.6 (CO), 139.2, 128.4, 128.0, 125.9 (C_{arom}), 71.1 (C-3), 69.2 (C-4), 64.4 (C-5), 60.4 (C-6), 51.6 (C-2), 47.1 (CH_2CH_2Ph), 43.8 (C-1), 34.9 (*C*H_2CH$_2$Ph), 21.6 (CO*C*H_3). **ESIMS**: *m/z* 390.2 $[M + Na]^+$. Anal. Calcd for $C_{17}H_{25}N_3O_4S$: C 55.57, H 68.6, N 11.44, S 8.72. Found: C, 48.36; H, 5.17; N, 9.72; S 7.36.

Synthesis of DNJC-thiazolidines 13-24

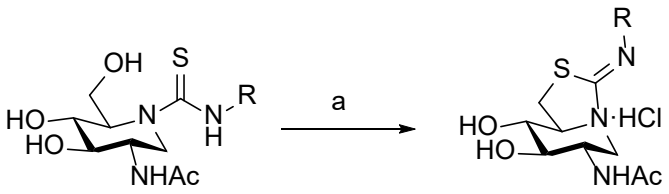

Supplemental scheme 5. Reagents and conditions: a. $HCl_{(conc)}$, MeOH, RT, 18 h, quant.

General procedure for the preparation of the DNJNAc-thiazolidines 13-24. The corresponding DNJNAc thiourea **1-12** (0.27 mM) was dissolved in MeOH (2 mL) and concentrated HCl was dropwise added until pH 1. The solution was stirred at RT until complete disappearance of the starting material (18-24 h). The solvent was removed under reduced pressure, the residue was coevaporated with MeOH (3 x 10 mL) and the product was purified by column chromatography using the eluent indicated in each case.

(*Z*)-2-Acetamido-5-*N*,6-*S*-(*N'*-butyliminomethylidene)-1,2-dideoxy-6-thionojirimycin Hydrochloride (13). Column chromatography, eluent: 60:10:1 → 50:10:1 → 40:10:1 DCM-MeOH-H_2O. Yield: 81 mg (quantitative). $[\alpha]_D$ +41.6 (*c* 0.88, MeOH). R_f 0.25 (70:10:1 DCM-MeOH-H_2O).

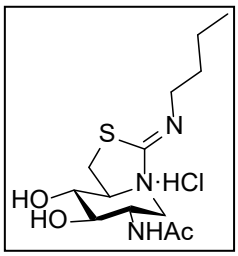

^{1}H NMR (500 MHz, CD_3OD): δ 4.11 (dd, 1 H, $J_{1a,1b}$ = 13.2 Hz, $J_{1a,2}$ = 5.3 Hz, H-1a), 3.99 (m, 1 H, H-5), 3.83 (m, 1 H, H-2), 3.76 (dd, 1 H, $J_{6a,6b}$ = 11.4 Hz, $J_{5,6a}$ = 7.7 Hz, H-6a), 3.51 (m, 2 H, H-3, H-6b), 3.43 (t, 1 H, $J_{3,4}$ = $J_{4,5}$ = 9.4, H-4), 3.37 (t, 2 H, C*H*$_2$NH), 3.01 (dd, 1 H, $J_{1b,2}$ = 11.7 Hz, H-1b), 2.01 (s, 1 H, $COCH_3$), 1.66 (m, 2 H, CH_2), 1.41 (m, 2 H, CH_2), 0.97 (t, 3 H, $^3J_{H,H}$ = 7.4 Hz, CH_3). **^{13}C NMR** (125.7 MHz, CD_3OD): δ 173.9 (CO), 171.8 (CN), 75.4 (C-3), 74.7 (C-4), 69.1 (C-5), 50.9 (CH_2N), 50.4 (C-2), 46.9 (C-1), 32.2 (C-6), 32.1 (CH_2), 22.7 (CO*C*H$_3$), 20.8 (CH_2), 13.9 (CH_3). **ESIMS**: *m/z* 302 $[M + H]^+$, 324 $[M + Na]^+$. Anal. Calcd for $C_{13}H_{23}N_3O_3S.HCl$: C, 46.21; H, 7.16; N, 12.44; S, 9.49. Found: C, 46.09; H, 7.22; N, 12.15; S, 9.13.

(*Z*)-2-Acetamido-1,2-dideoxy-5-*N*,6-*S*-(*N'*-octyliminomethylidene)-6-thionojirimycin Hydrochloride (14). Column chromatography, eluent: 70:10:1 → 60:10:1 → 50:10:1 DCM-MeOH-H_2O. Yield: 96 mg (quantitative). $[\alpha]_D$ +36.3 (*c* 0.98, MeOH). R_f 0.53 (40:10:1 DCM-MeOH-H_2O).

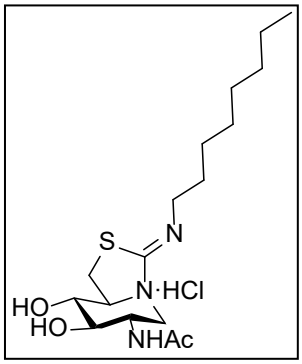

^{1}H NMR (500 MHz, CD_3OD): δ 4.10 (dd, 1 H, $J_{1a,1b}$ = 13.2 Hz, $J_{1a,2}$ = 5.3 Hz, H-1a), 3.96 (m, 1 H, H-5), 3.82 (m, 1 H, H-2), 3.73 (dd, 1 H, $J_{6a,6b}$ = 11.4 Hz, $J_{5,6a}$ = 7.7 Hz, H-6a), 3.49 (m, 2 H, H-6b, H-3), 3.42 (t, 1 H, $J_{3,4} = J_{4,5}$= 7.4 Hz, H-4), 3.35 (t, 2 H, CH_2NH), 2.98 (t, 1 H, $J_{1b,2} = J_{1a,1b}$ = 13.2 Hz, H-1b), 2.00 (s, 1 H, $COCH_3$), 1.67 (m, 2 H, CH_2), 1.33 (m, 10 H, CH_2), 0.91 (t, 3 H, $^3J_{H,H}$ = 6.8 Hz, CH_3). **^{13}C NMR** (125.7 MHz, CD_3OD): δ 173.9 (CO), 171.4 (CN), 75.5 (C-3), 74.8 (C-4), 67.0 (C-5), 50.9 (CH_2N), 50.9 (C-2), 46.9 (C-1), 32.9 (C-6), 32.0, 30.3, 30.3, 30.2, 27.7, 23.7 (CH_2), 22.7 (CO*C*H_3), 14.4 (CH_3). **ESIMS**: *m/z* 358 (100, $[M + H]^+$). Anal. Calcd for $C_{17}H_{31}N_3O_3S.HCl$: C, 51.83; H, 8.19; N, 10.67; S, 8.14. Found: C, 52.00; H, 8.31; N, 10.44; S, 7.97.

(*Z*)-2-Acetamido-1,2-dideoxy-5-*N*,6-*S*-(*N'*-phenyliminomethylidene)-6-thionojirimycin Hydrochloride (15). Column chromatography, eluent: 60:10:1 → 50:10:1 → 40:10:1 DCM-MeOH-H_2O. Yield: 86 mg (quantitative). $[\alpha]_D$ +12.2 (*c* 0.89, MeOH). R_f 0.23 (70:10:1 DCM-MeOH-H_2O).

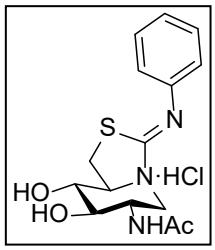

^{1}H NMR (500 MHz, 10:1 CD_3CN-D_2O): δ 7.32 (t, 2 H, $^3J_{H,H}$ = 7.6 Hz, CH-arom), 7.14 (t, 1 H, CH_{arom}), 7.0 (d, 2 H, CH_{arom}), 4.21 (dd, 1 H, $J_{1a,1b}$ = 13.1 Hz, $J_{1a,2}$ = 5.3 Hz, H-1a), 3.81 (m, 1 H, H-2), 3.65 (m, 1 H, H-5), 3.47 (t, 1 H, $J_{2,3} = J_{3,4}$ = 9.2 Hz, H-3), 3.43 (dd, 1 H, $J_{6a,6b}$ = 11.3 Hz, $J_{5,6a}$ = 7.2 Hz, H-6a), 3.39 (t, 1 H, $J_{4,5}$ = 9.2, H-4), 3.18 (dd, 1 H, $J_{5,6b}$= 6.9 Hz, H-6b), 2.79 (dd, 1 H, $J_{1b,2}$ = 11.5 Hz, H-1b), 1.94 (s, 1 H, $COCH_3$). **^{13}C NMR** (125.7 MHz, 10:1 CD_3CN-D_2O): δ 173.4 (CO), 164.1 (CN), 130.2-118.7 (C_{arom}), 75.8 (C-3), 74.3 (C-4), 65.9 (C-5), 50.8 (C-2), 46.7 (C-1), 30.9 (C-6), 23.1 (CO*C*H_3). **ESIMS**: *m/z* 322 $[M + H]^+$, 344 $[M + Na]^+$. Anal. Calcd for $C_{15}H_{19}N_3O_3S.HCl$: C, 50.35; H, 5.63; N, 11.74; S, 8.96. Found: C, 50.67; H, 5.81; N, 11.42; S, 8.35.

(*Z*)-2-Acetamido-5-*N*,6-*S*-(*N'*-benzyliminomethylidene)-1,2-dideoxy-6-thionojirimycin Hydrochloride (16). Column chromatography, eluent: 60:10:1 DCM-MeOH-H_2O. Yield: 90 mg (quantitative). $[\alpha]_D$ +36.2 (*c* 1.04, MeOH). R_f 0.39 (40:10:1 DCM-MeOH-H_2O).

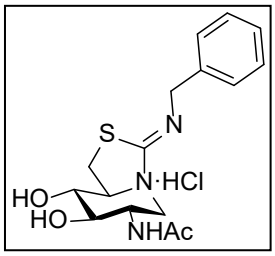

^{1}H NMR (500 MHz, CD_3OD): δ 7.37-7.27 (m, 5 H, CH_{arom}), 4.49 (m, 2 H, CH_2Ph), 4.16 (dd, 1 H, $J_{1a,1b}$ = 13.1 Hz, $J_{1a,2}$ = 5.3 Hz, H-1a), 3.85 (m, 1 H, H-2), 3.77 (m, 1 H, H-5), 3.63 (dd, 1 H, $J_{6a,6b}$ = 11.2 Hz, $J_{5,6a}$ = 7.3 Hz, H-6a), 3.48 (t, 1 H, $J_{2,3} = J_{3,4}$ = 9.6, H-3), 3.38 (m, 1 H, H-4, H-6b), 2.87 (dd, 1 H, $J_{1b,2}$ = 11.7 Hz, H-1b), 1.99 (s, 1 H, $COCH_3$). **^{13}C NMR** (125.7 MHz, CD_3OD): δ 173.8 (CO), 171.4 (CN), 138.5, 129.7, 128.8 (C_{arom}), 76.0 (C-3), 74.0 (C-4), 68.0 (C-5), 55.5 (CH_2Ph), 51.1 (C-2), 47.1 (C-1), 31.9 (C-6), 22.7 ($COCH_3$). **ESIMS**: *m/z* 336 $[M + H]^+$, 358 $[M + Na]^+$. Anal. Calcd for $C_{16}H_{22}N_3O_3S.HCl$: C, 51.68; H, 5.96; N, 11.30; S, 8.62. Found: C, 51.82; H, 6.14; N, 11.09; S, 8.37.

(*Z*)-2-Acetamido-5-*N*,6-*S*-(*N'*-1-naphthymethyliminomethylidene)-1,2-dideoxy-6-thionojirimycin Hydrochloride (17). Column chromatography, eluent: 70:10:1 DCM-MeOH-H_2O. Yield: 104 mg (quantitative). $[\alpha]_D$ +4.8 (*c* 1.00, 1:1 DCM-MeOH). R_f 0.62 (70:10:1 DCM-MeOH-H_2O).

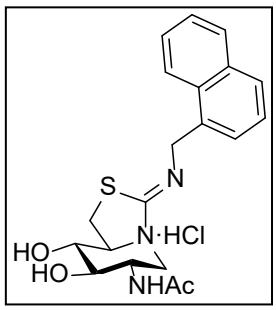

^{1}H NMR (300 MHz, 8:1 CD_3OD-$CDCl_3$): δ 8.03-7.43 (m, 2 H, CH_{arom}), 4.89 (bs, 2H, CH_2Naph), 4.20 (dd, 1 H, $J_{1a,1b}$ = 13.1 Hz, $J_{1a,2}$ = 5.2 Hz, H-1a), 3.86 (m, 1 H, H-2), 3.65 (m, 1 H, H-5), 3.58 (m, 1 H, H-6a), 3.46 (t, 1 H, $J_{2,3} = J_{3,4}$ = 9.7, H-3), 3.38 (m, 2 H, H-4, H-6b), 2.78 (dd, 1 H, $J_{1b,2}$ = 11.5 Hz, H-1b), 1.98 (s, 3 H, NHCOCH_3). **^{13}C NMR (**100.6 MHz, 8:1 CD_3OD-$CDCl_3$): δ 172.4 (CO), 165.5 (CN), 133.8-122.9 (C_{arom}), 75.0 (C-3), 73.7 (C-4), 65.9 (C-5), 53.3 (CH_2Naph), 49.8 (C-2), 45.8 (C-1), 30.4 (C-6), 21.5 (NHCO*C*H_3). **ESIMS**: *m/z* 386.2 $[M + H]^+$. Anal. Calcd for $C_{20}H_{23}N_3O_3S.HCl$: C 56.93, H 5.73, N 9.96, S 7.60. Found: C, 56.65; H, 5.48; N, 9.68; S 7.29.

(*Z*)-2-Acetamido-5-*N*,6-*S*-(*N'*-*p*-fluorobenzyliminomethylidene)-1,2-dideoxy-6-thionojirimycin Hydrochloride (18). Column chromatography, eluent: 60:10:1 DCM-MeOH-H_2O. Yield: 95 mg (quantitative). $[\alpha]_D$ +34.4 (*c* 1.00, MeOH). R_f 0.53 (40:10:1 DCM -MeOH-H_2O).

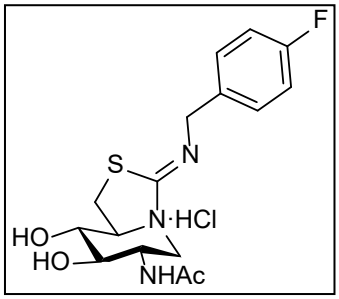

^{1}H NMR (500 MHz, CD_3OD): δ 7.42 (m, 2 H, CH_{arom}), 7.12 (bt, 2 H, $J_{H,H}$ = 8.7 Hz, CH_{arom}), 4.54 (bs, 2H, CH_2Ph), 4.17 (dd, 1 H, $J_{1a,1b}$ = 13.1 Hz, $J_{1a,2}$ = 5.2 Hz, H-1a), 3.94 (m, 1 H, H-2), 3.86 (m, 1 H, H-5), 3.72 (dd, 1 H, $J_{6a,6b}$ = 11.1 Hz, $J_{5,6a}$ = 7.5 Hz, H-6a), 3.53 (t,

1 H, $J_{2,3} = J_{3,4}$ = 9.4 Hz, H-3), 3.40 (m, 2 H, H-4, H-6b), 3.00 (dd, 1 H, $J_{1b,2}$ = 11.7 Hz, H-1b), 2.02 (s, 1 H, NHCOCH_3). **^{13}C NMR** (125.7 MHz, CD_3OD): δ 172.3 (CO), 169.5 (CN), 162, 128.6, 113.5 (C_{arom}), 74.2 (C-3), 73.4 (C-4), 67.2 (C-5), 52.1 (CH_2Ph), 49.5 (C-2), 45.6 (C-1), 30.7 (C-6), 21.3 (NHCOCH$_3$). **ESIMS**: *m/z* 354 $[M + H]^+$, 376 $[M + Na]^+$. Anal. Calcd for $C_{16}H_{20}FN_3O_3S.HCl$: C 49.29, H 5.43, N 10.78, S 8.22. Found: C, 49.14; H, 5.53; N, 10.62; S, 7.99.

(*Z*)-2-Acetamido-5-*N*,6-*S*-(*N'*-*p*-methoxybenzyliminomethylidene)-1,2-dideoxy-6-thionojirimycin Hydrochloride (19). Column chromatography, eluent: 60:10:1 DCM-MeOH-H_2O. Yield: 98 mg (quantitative). $[\alpha]_D$ +36.2 (*c* 1.00, MeOH). R_f 0.32 (40:10:1 DCM-MeOH-H_2O).

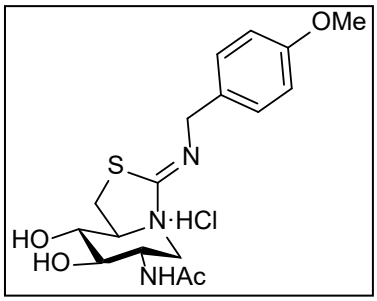

^{1}H NMR (500 MHz, CD_3OD): δ 7.26 (d, 2 H, $J_{H,H}$ = 8.5 Hz, CH_{arom}), 6.91 (d, 2 H, $J_{H,H}$ = 8.5 Hz, Ph), 4.41 (d, 2H, $^3J_{H,H}$ = 15 Hz, CH_2Ph), 4.15 (dd, 1 H, $J_{1a,1b}$ = 13.1 Hz, $J_{1a,2}$ = 5.4 Hz, H-1a), 3.84 (m, 1 H, H-2), 3.79 (s, 3 H, OCH_3), 3.69 (m, 1 H, H-5), 3.63 (dd, 1 H, $J_{6a,6b}$ = 11.1 Hz, $J_{5,6a}$ = 7.2 Hz, H-6a), 3.46 (t, 1 H, $J_{2,3} = J_{3,4}$ = 9.7, H-3), 3.38 (m, 2 H, H-4, H-6b), 2.87 (dd, 1 H, $J_{1b,2}$ = 11.7 Hz, H-1b), 2.00 (s, 3 H, NHCOCH_3). **^{13}C NMR** (125.7 MHz, CD_3OD): δ 172.3 (CO), 168.1 (CN), 159.2, 128.6, 113.5 (C_{arom}), 74.8 (C-3), 73.6 (C-4), 66.2 (C-5), 54.3 (CH_2Ph, CH_3O), 49.7 (C-2), 45.7 (C-1), 30.3 (C-6), 21.3 (NHCOCH$_3$). **ESIMS**: *m/z* 366.2 $[M + H]^+$, 388.1 $[M + Na]^+$. Anal. Calcd for $C_{17}H_{23}N_3O_4S.HCl$: C 50.80, H 6.02, N 10.46, S 7.98. Found: C, 50.53; H, 6.14; N, 10.33; S, 7.75.

(*Z*)-2-Acetamido-5-*N*,6-*S*-(*N'*-*p*-trifluoromethylbenzyliminomethylidene)-1,2-dideoxy-6-thionojirimycin Hydrochloride (20). Column chromatography, eluent: 60:10:1 DCM-MeOH-H_2O. Yield: 95 mg (quantitative). $[\alpha]_D$ +34.4 (*c* 1.00, MeOH). R_f 0.50 (40:10:1 DCM-MeOH-H_2O).

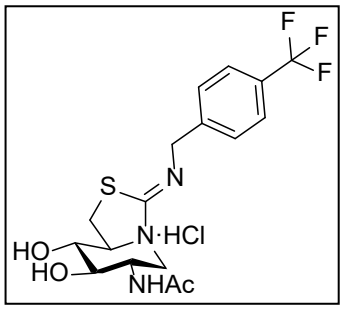

^{1}H NMR (500 MHz, CD_3OD): δ 7.42 (m, 2 H, CH_{arom}), 7.12 (bt, 2 H, $J_{H,H}$ = 8.7 Hz, CH_{arom}), 4.54 (bs, 2H, CH_2Ph), 4.17 (dd, 1 H, $J_{1a,1b}$ = 13.1 Hz, $J_{1a,2}$ = 5.2 Hz, H-1a), 3.94 (m, 1 H, H-2), 3.86 (m, 1 H, H-5), 3.72 (dd, 1 H, $J_{6a,6b}$ = 11.1 Hz, $J_{5,6a}$ = 7.5 Hz, H-6a), 3.53 (t, 1 H, $J_{2,3} = J_{3,4}$ = 9.4, H-3), 3.40 (m, 2 H, H-4, H-6b), 3.00 (dd, 1 H, $J_{1b,2}$ = 11.7 Hz, H-1b), 2.02 (s, 3 H, NHCOCH_3). **^{13}C NMR** (125.7 MHz, CD_3OD): δ 172.34 (CO), 163.7 (CN), 128.6, 113.5 (C_{arom}), 74.2 (C-3), 73.4 (C-4), 67.2 (C-5), 52.1 (CH_2Ph), 49.5 (C-2), 45.6 (C-1), 30.7 (C-6), 21.3 (NHCOCH$_3$). **ESIMS**: *m/z*

354.1 $[M + H]^+$, 376.1 $[M + Na]^+$. Anal. Calcd for $C_{16}H_{20}FN_3O_3S.HCl$: C 49.29, H 5.43, N 10.78, S 8.22. Found: C, 49.14; H, 5.53; N, 10.62; S, 7.99.

(*Z*)-2-Acetamido-5-*N*,6-*S*-(*N'*-*o*-azidomethylbenzyliminomethylidene)-1,2-dideoxy-6-thionojirimycin Hydrochloride (21). Column chromatography, eluent: 70:10:1 DCM-MeOH-H_2O. Yield: 105 mg (quantitative). $[\alpha]_D$ +26.4 (*c* 1.00, MeOH). R_f 0.75 (50:10:1 DCM-MeOH-H_2O).

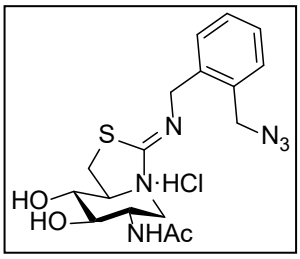

^{1}H NMR (300 MHz, CD_3OD): δ 7.31-7.13 (m, 4 H, CH_{arom}), 4.36 (s, 2H, NC*H*$_2$Ph), 4.33 (bd, 2H, CH_2N_3), 4.07 (dd, 1 H, $J_{1a,1b}$ = 12.9 Hz, $J_{1a,2}$ = 5.2 Hz, H-1a), 3.73 (m, 1 H, H-2), 3.37 (bdd, 1 H, $J_{6a,6b}$ = 11.1 Hz, $J_{5,6a}$ = 6.2 Hz, H-6a), 3.33 (m, 1 H, H-5), 3.26 (m, 2 H, H-3, H-4), 3.10 (dd, 1 H, H-6b), 2.50 (dd, 1 H, $J_{1b,2}$ = 11.3 Hz, H-1b), 1.86 (s, 3 H, NHCOC*H*$_3$). **^{13}C NMR** (75.5 MHz, CD_3OD): δ 172.2 (CO), 162.9 (CN), 138.5, 133.4, 129.3, 128.5, 128.2, 126.8 (C_{arom}), 75.5 (C-3), 73.8 (C-4), 64.7 (C-5), 54.8 (*C*H_2Ph), 51.9 (CH_2N_3), 49.9 (C-2), 45.7 (C-1), 29.9 (C-6), 21.3 (NHCO*C*H_3). **ESIMS**: *m/z* 391.1 $[M + H]^+$. Anal. Calcd for $C_{17}H_{22}N_6O_3S.HCl$: C 47.83, H 5.43, N 19.69, S 7.51. Found: C, 47.51; H, 5.19; N, 19.33; S, 7.14.

(*Z*)-2-Acetamido-5-*N*,6-*S*-(*N'*-*m*-azidomethylbenzyliminomethylidene)-1,2-dideoxy-6-thionojirimycin Hydrochloride (22). Column chromatography, eluent: 70:10:1 DCM-MeOH-H_2O. Yield: 105 mg (quantitative). $[\alpha]_D$ +37.4 (*c* 1.00, MeOH). R_f 0.75 (50:10:1 DCM-MeOH-H_2O).

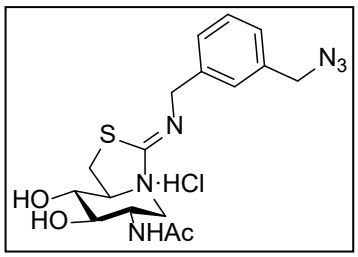

^{1}H NMR (300 MHz, CD_3OD): δ 7.38-7.22 (m, 4 H, CH_{arom}), 4.42 (bd, 2H, NC*H*$_2$Ph), 4.36 (s, 2H, CH_2N_3), 4.18 (dd, 1 H, $J_{1a,1b}$ = 12.9 Hz, $J_{1a,2}$ = 5.2 Hz, H-1a), 3.87 (m, 1 H, H-2), 3.50 (bdd, 1 H, $J_{6a,6b}$ = 11.1 Hz, $J_{5,6a}$ = $J_{5,6b}$ = 6.2 Hz, H-6a), 3.45 (m, 1 H, H-5), 3.39 (m, 2 H, H-3, H-4), 3.22 (dd, 1 H, H-6b), 2.65 (dd, 1 H, $J_{1b,2}$ = 11.3 Hz, H-1b), 1.99 (s, 3 H, NHCOC*H*$_3$). **^{13}C NMR** (75.5 MHz, CD_3OD): δ 172.2 (CO), 162.9 (CN), 140.4, 135.8, 128.4, 127.0, 126.4 (C_{arom}), 75.5 (C-3), 73.9 (C-4), 64.9 (C-5), 56.8 (*C*H_2Ph), 54.1 (CH_2N_3), 49.9 (C-2), 45.8 (C-1), 30.0 (C-6), 21.3 (NHCO*C*H_3). **ESIMS**: *m/z* 391.1 $[M + H]^+$. Anal. Calcd for $C_{17}H_{22}N_6O_3S.HCl$: C 47.83, H 5.43, N 19.69, S 7.51. Found: C, 47.69; H, 5.24; N, 19.39; S, 7.20.

(*Z*)-2-Acetamido-5-*N*,6-*S*-(*N'-p*-azidomethylbenzyliminomethylidene)-1,2-dideoxy-6-thionojirimycin Hydrochloride (23). Column chromatography, eluent: 70:10:1 DCM-MeOH-H_2O. Yield: 105 mg (quantitative). $[\alpha]_D$ +1.07 (*c* 1.00, MeOH). R_f 0.75 (50:10:1 DCM-MeOH-H_2O).

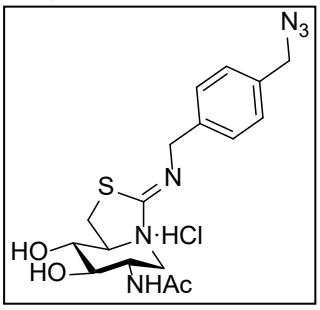

^{1}H NMR (400 MHz, CD_3OD): δ 7.35 (d, 2 H, $J_{H,H}$ =8.3 Hz, CH_{arom}), 7.30 (d, 2 H, CH_{arom}), 4.40 (bt, 2 H, $^2J_{H,H}$ = 15.0 Hz, NC*H*$_2$Ph), 4.34 (s, 2 H, CH_2N_3), 4.18 (dd, 1 H, $J_{1a,1b}$ = 12.9 Hz, $J_{1a,2}$ = 5.2 Hz, H-1a), 3.88 (m, 1 H, H-2), 3.47 (m, 1 H, H-5), 3.39 (m, 2 H, H-3, H-4), 3.34 (m, 1 H, H-6a), 3.19 (dd, 1 H, $J_{6a,6b}$ = 11.1 Hz, $J_{5,6b}$ = 6.8 Hz, H-6b), 2.61 (dd, 1 H, $J_{1b,2}$ = 11.3 Hz, H-1b), 2.00 (s, 3 H, NHCOC*H*$_3$). **^{13}C NMR** (100.6 MHz, CD_3OD): δ 172.2 (CO), 161.9 (CN), 140.4, 134.0, 128.0, 127.5 (C_{arom}), 75.6 (C-3), 74.0 (C-4), 64.6 (C-5), 54.2 (*C*H$_2$Ph), 53.9 (CH_2N_3), 49.9 (C-2), 45.8 (C-1), 29.8 (C-6), 21.3 (NHCO*C*H$_3$). **ESIMS**: *m/z* 391.1 $[M + H]^+$. Anal. Calcd for $C_{17}H_{22}N_6O_3S.HCl$: C 47.83, H 5.43, N 19.69, S 7.51. Found: C, 47.49; H, 5.19; N, 19.43; S, 7.19**.**

(*Z*)-2-Acetamido-5-*N*,6-*S*-(*N'-2*-phenylethyliminomethylidene)-1,2-dideoxy-6-thionojirimycin Hydrochloride (24). Column chromatography, eluent: 70:10:1 DCM-MeOH-H_2O. Yield: 94 mg (quantitative). $[\alpha]_D$ +2.84 (*c* 1.00, MeOH). R_f 0.30 (70:10:1 DCM-MeOH-H_2O).

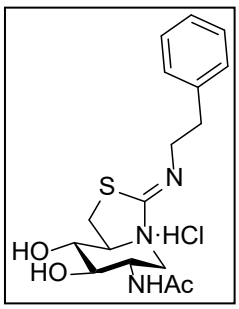

^{1}H NMR (300 MHz, CD_3OD): δ 7.24-7.09 (m, 4 H, CH_{arom}), 3.97 (dd, 1 H, $J_{1a,1b}$ = 12.9 Hz, $J_{1a,2}$ = 5.2 Hz, H-1a), 3.73 (m, 1 H, H-2), 3.67 (m, 1 H, H-5), 3.48 (dd, 1 H, $J_{6a,6b}$ = 11.4 Hz, $J_{5,6a}$ = 7.3 Hz, H-6a), 3.39 (m, 3 H, H-3, CH_2C*H*$_2$Ph), 3.20 (m, 1 H, H-4, H-6b), 2.80 (m, 3 H, C*H*$_2$CH$_2$Ph, H-1b), 1.90 (s, 3 H, NHCOC*H*$_3$). **^{13}C NMR** (75.5 MHz, CD_3OD): δ 172.4 (CO), 168.1 (CN), 138.0, 128.7, 128.3, 126.3 (C_{arom}), 74.4 (C-3), 73.1 (C-4), 66.8 (C-5), 52.2 (CH_2*C*H$_2$Ph), 49.6 (C-2), 45.5 (C-1), 35.5 (C-6), 30.1 (*C*H$_2$CH$_2$Ph), 21.3 (NHCO*C*H$_3$). **ESIMS**: *m/z* 372.1 $[M + Na]^+$, 350.1 $[M + H]^+$. Anal. Calcd for $C_{17}H_{23}N_3O_3S.HCl$: C 52.91, H 6.27, N 10.89, S 8.31. Found: C, 52.56; H, 6.08; N, 10.55; S, 7.99.

Synthesis of DNJC-thiazolidines 28-32

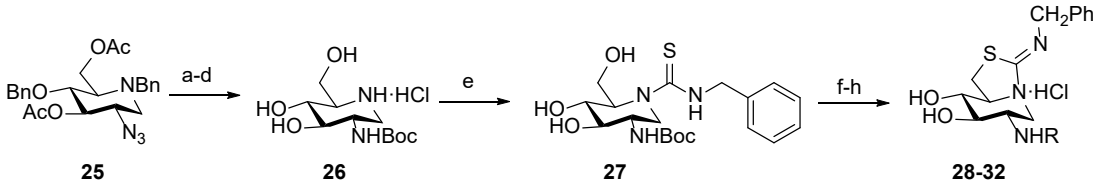

25 **26** **27** **28-32**

Supplemental scheme 6. Reagents and conditions: a. NaOMe, MeOH, RT, 18 h; b. PPh_3, THF-NH_4OH, 60 ºC, 18 h; c. Boc_2O, Et_3N, dioxane, RT, 18 h; d. H_2, Pd/C, MeOH, RT, 18 h; e. BnNCS, Et_3N, MeCN, RT, 18 h; f. HCl, MeOH, RT, 18 h; g. TFA, 1:1 DCM-H_2O, RT, 18 h. RCOCl or RNCS, Et_3N, MeOH, RT, 18 h, quant.

2-*tert*-Butoxycarbonylamino-1,2-dideoxynojirimycin (26). 2-Azido-3,6-di-*O*-acetyl-4-*O*-benzyl-1,2,5-trideoxy-1,5-imino-D-glucitol[1] **25** (207 mg, 0.45 mM) was dissolved in MeOH (4.5 mL) and MeONa (5 mg, 0.09 mM) was added. The mixture was stirred overnight at RT. Then, dry ice was added until neutral pH and the solvent was evaporated. The deacetylated product was dissolved in THF-NH_4OH (3:1, 4 mL) and reduced with PPh_3 (192 mg, 0.73 mM) overnight at 60 ºC. The solvent was evaporated and the crude amine was dissolved in dioxane (4.8 mL). Boc_2O (213 mg, 0.978 mM) and Et_3N (131 µL, 0.978 mM) were added and the mixture stirred overnight. The reaction mixture was concetrated to dryness, the crude Boc-protected derivative was dissolved in MeOH (4.5 mL) and debenzymated by treatment with Pd/C 10% (50 mg) overnight under H_2 atmosphere. The mixture was filtered over celite, evaporated and suspended in H_2O (10 mL). The insoluble PPh_3O precipitate was filtered and the aqueous solution was lyophilized to give **26**. Yield: 58 mg (49%, 4 steps). R_f 0.30 (6:3:1 MeCN-H_2O-NH_4OH).

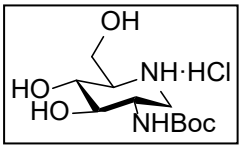

^{1}H NMR (500 MHz, CD_3OD): δ 3.93 (dd, 1 H, $J_{6a,6b}$ = 11.8 Hz, $J_{5,6a}$ = 2.8 Hz, H-6a), 3.86 (dd, 1 H, $J_{5,6b}$ = 5.3 Hz, H-6b), 3.69 (m, 1 H, H-2), 3.55 (bt, 1 H, $J_{3,4}$= 9.6 Hz, H-4), 3.45 (bt, 1 H, H-3), 3.39 (dd, 1 H, $J_{1a,1b}$ = 12.2, $J_{1a,2}$ = 4.7 Hz, H-1a), 3.07 (m, 1 H, H-5), 2.89 (bt, 1 H, $J_{1b,2}$ = 12 Hz, H-1b), 1.46 (s, 9 H, $COCMe_3$). **^{13}C NMR** (125.7 MHz, CD_3OD): δ 156.5 (CO), 79.3 (*C*Me_3), 73.8 (C-3), 68.9 (C-4), 60.5 (C-5), 57.7 (C-6), 49.7 (C-2), 44.8 (C-1), 27.2 (C*Me*$_3$). **HRMS** (ESI) *m/z* [M + H]$^+$ calcd for $[C_{11}H_{22}N_2O_5]^+$ 263.1601; found 263.1605.

2-*tert*-Butoxycarbonylamino-5-*N*-(*N'*-methylbenzylthiocarbamoyl)-1,2-dideoxynojirimicin (27). Compound **26** (58 mg, 0.22 mM) in MeCN (2.2 mL) was treated with Et_3N (62 µL, 0.44 mmol) and benzyl isothiocyanate (44 µL, 0.331 mM). The mixture was stirred at RT overnight and concentrated to dryness. The crude product was purified by column cromatography using 100:10:1 DCM-MeOH-H_2O as eluent. Yield: 47 mg (52%). R_f 0.40 (70:10:1 DCM-MeOH-H_2O).

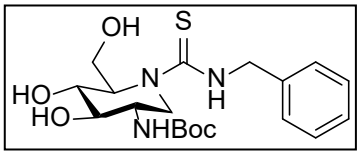

^{1}H NMR (600 MHz, CD_3OD): δ 7.36-7.22 (CH_{arom}), 4.90 (m, 2 H, H-1a, C*H*$_2$Ph), 4.80 (d, 1 H, $^2J_{H,H}$ = 15 Hz, C*H*Ph), 4.49 (m, 1 H, H-5), 3.97 (dd, 1 H, $J_{6a,6b}$ = 11.4 Hz, $J_{5,6a}$ = 8.7 Hz, H-6a), 3.82 (dd, 1 H, $J_{5,6b}$ = 3.6 Hz, H-6b), 3.73 (t, 1 H, $J_{3,4}$ = $J_{4,5}$ = 5.1 Hz, H-4), 3.66 (m, 1 H, H-2), 3.61 (t, 1 H, $J_{2,3}$ = 5.1 Hz, H-3), 3.52 (dd, 1 H, $J_{1a,1b}$ = 14.3 Hz, $J_{1b,2}$ = 3.8 Hz, H-1b), 1.45 (s, 9 H, CO_2Me_3). **^{13}C NMR** (150 MHz, CD_3OD): δ 185.5 (CS), 156.3 (CO), 138.7, 128.0, 127.2, 126.6 (C_{arom}), 79.0

(*C*Me$_3$), 70.8 (C-3), 69.2 (C-4), 64.3 (C-5), 60.4 (C-6), 52.0 (C-2), 49.2 (*C*H$_2$Ph), 43.9 (C-1), 27.3 (C*Me*$_3$). **HRMS** (ESI) *m/z* [M + H]$^+$ calcd for [$C_{19}H_{29}N_3O_5S$]$^+$ 412.1901; found 412.1904.

General procedure for the preparation of the DNJC-thiazolidines 28-32. Compound **27** (47 mg, 0.11 mM) was dissolved in MeOH (2 mL) and concentrated HCl was dropwise added until pH 1. The mixture was stirred at rt overnight and monitored by ESIMS to confim total conversion into the corresponding cyclic isourea. The reaction mixture was concentrated and the crude product was dissolved in 1:1 DCM-H_2O (2 mL). TFA (30 μL, 0.38 mM, 3 eq) was then added and the solution was stirred overnight. The mixture was evaported, co-evaporated with toluene (3 x 5 mL) and lyophilized. The free amine derivative thus obtained was engaged in the nex reactions without further purification. Thus, 10 mg (0.034 mM) of this material was dissolved in MeOH (3 mL) and reacted with either propionyl, butyryl or isobutyryl chorideor ethyl or propyl isothiocyanate (1.2 eq) in the presence of Et_3N (3 eq). The reaction mixtures were stirred at RT overnight, the solvent was evaporated and the crude product was purified as indicated for each compound.

(*Z*)-2-Propionamido-5-*N*,6-*S*-(*N'*-benzyliminomethylidene)-1,2-dideoxy-6-thionojirimycin Hydrochloride (28). Column chromatography, eluent: 70:10:1 DCM-MeOH-H_2O. Yield: 94 mg (quantitative). $[\alpha]_D$ +31.9 (*c* 1.00, MeOH). R_f 0.30 (70:10:1 DCM-MeOH-H_2O).

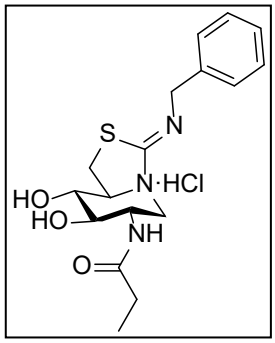

^{1}H NMR (500 MHz, CD_3OD): δ 7.18-7.08 (m, 5 H, CH_{arom}), 4.26 (d, 2 H, $^3J_{H,H}$ = 15 Hz, C*H*$_2$Ph), 4.05 (dd, 1 H, $J_{1a,1b}$ = 12.6 Hz, $J_{1a,2}$ = 5.3 Hz, H-1a), 3.75 (m, 1 H, H-2), 3.36 (dd, 1 H, $J_{6a,6b}$ = 11.2 Hz, $J_{5,6a}$ = 7.3 Hz, H-6a), 3.29 (m, 1 H, H-5), 3.23 (m, 2 H, H-3, H-4), 3.08 (dd, 1 H, H-6b), 2.51 (dd, 1 H, $J_{1b,2}$ = 11.7 Hz, H-1b), 2.13 (q, 2 H, COC*H*$_2$CH$_3$), 1.03 (t, 3 H, COCH$_2$C*H*$_3$). **^{13}C NMR** (125.7 MHz, CD_3OD): δ 177.4 (CO), 163.7 (CN), 141.3, 129.3, 128.5, 127.8 (C_{arom}), 77.0 (C-3), 75.5 (C-4), 66.2 (C-5), 58.8 (C*H*$_2$Ph), 51.2 (C-2), 47.3 (C-1), 31.4 (C-6) 30.3 (CO*C*H$_2$CH$_3$), 10.3 (COCH$_2$*C*H$_3$). **ESIMS**: *m/z* 350.1 [M + H]$^+$. Anal. Calcd for $C_{17}H_{23}N_3O_3S$.HCl: C 52.91, H 6.27, N 10.89, S 8.31. Found: C, 52.98; H, 6.40; N, 10.71; S, 8.52.

(*Z*)-2-Butyramido-5-*N*,6-*S*-(*N'*-benzyliminomethylidene)-1,2-dideoxy-6-thionojirimycin (29). Column chromatography, eluent: 100:10:1 DCM-MeOH-H_2O. Yield: 98 mg (quantitative). R_f 0.50 (70:10:1 DCM-MeOH-H_2O).

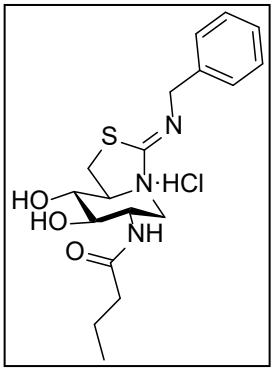

^{1}H NMR (600 MHz, CD_3OD): δ 7.31-7.20 (m, 5 H, CH_{arom}), 4.37 (d, 2 H, $^3J_{H,H}$ = 15.0 Hz, CH_2Ph), 4.16 (dd, 1 H, $J_{1a,1b}$ = 12.6 Hz, $J_{1a,2}$ = 5.3 Hz , H-1a), 3.88 (m, 1 H, H-2), 3.48 (dd, 1 H, $J_{6a,6b}$ = 11.2 Hz, $J_{5,6a}$ = 7.3 Hz, H-6a), 3.40 (m, 1 H, H-5), 3.37 (m, 2 H, H-3, H-4), 3.19 (dd, 1 H, H-6b), 2.61 (dd, 1 H, $J_{1b,2}$ = 11.2 Hz, H-1b), 2.49, 1.66 (m, 4 H, C$H_2$$CH_3$), 0.97 (t, 3 H, CH_2CH_3). **^{13}C NMR** (150 MHz, CD_3OD): δ 175.0 (CO), 162.1 (CN), 140.0, 127.8, 127.1, 126.3 (C_{arom}), 75.5 (C-3), 74.2 (C-4), 64.7 (C-5), 57.6 (CH_2Ph), 49.7 (C-2), 45.8 (C-1), 37.7 (C-6), 29.9, 18.9 (CH_2CH_3), 12.5 (CH_2CH_3). **HRMS** (ESI) *m/z* $[M + H]^+$ calcd for $[C_{18}H_{25}N_3O_3S]^+$ 364.1689; found 364.1696.

2-Isobutyramido-5-*N*,6-*S*-(*N'*-benzyliminomethylidene)-1,2-dideoxy-6-thionojirimycin Hydrochloride (30). Column chromatography, eluent: 70:10:1 DCM-MeOH-H_2O. Yield: 98 mg (quantitative). $[\alpha]_D$ +36.2 (*c* 1.04, MeOH). R_f 0.50 (70:10:1 DCM-MeOH-H_2O).

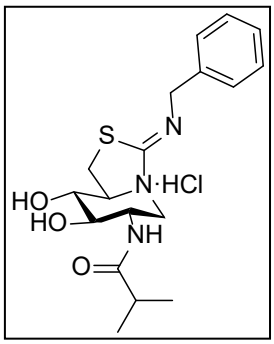

^{1}H NMR (500 MHz, CD_3OD): δ 7.31-7.20 (m, 5 H, CH_{arom}), 4.39 (d, 2 H, $^3J_{H,H}$ = 15.0 Hz, CH_2Ph), 4.17 (dd, 1 H, $J_{1a,1b}$ = 12.6 Hz, $J_{1a,2}$ = 5.3 Hz, H-1a), 3.87 (m, 1 H, H-2), 3.49 (dd, 1 H, $J_{6a,6b}$ = 11.2 Hz, $J_{5,6a}$ = 7.3 Hz, H-6a), 3.47 (m, 1 H, H-5), 3.39 (m, 2 H, H-3, H-4), 3.20 (dd, 1 H, H-6b), 2.64 (dd, 1 H, $J_{1b,2}$ = 11.7 Hz, H-1b), 2.49 (q, 2 H, COC$H_2$$Me_2$), 1.15 (t, 6 H, $COCH_2Me_2$). **^{13}C NMR** (125.7 MHz, CD_3OD): δ 180.6 (CO), 163.8 (CN), 141.2, 129.3, 128.6, 127.8 (C_{arom}), 76.9 (C-3), 75.7 (C-4), 66.2 (C-5), 58.8 (CH_2Ph), 51.1 (C-2), 47.1 (C-1), 36.4 (C-6) 31.4 (CO*C*HMe_2), 20.0, 19.7 ($COCHMe_2$). **ESIMS**: *m/z* 364.1 $[M + H]^+$. Anal. Calcd for $C_{18}H_{25}N_3O_3S$.HCl: C, 54.06; H, 6.55; N, 10.51; S, 8.02. Found: C, 53.79; H, 6.47; N, 10.32; S, 7.72.

(*Z*)-2-*N'*-Ethylthioureido-5-*N*,6-*S*-(*N'*-benzyliminomethylidene)-1,2-dideoxy-6-thionojirimycin (31). Column chromatography, eluent: 100:10:1 DCM-MeOH-H_2O. Yield: 102 mg (quantitative). R_f 0.50 (70:10:1 DCM-MeOH-H_2O).

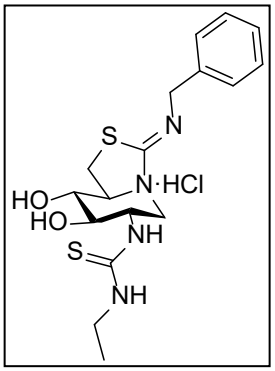

^{1}H NMR (600 MHz, CD_3OD): δ 7.33-7.21 (m, 5 H, CH_{arom}), 4.37 (d, 3 H, $^{3}J_{H,H}$ = 15.0 Hz, C*H*$_2$Ph, H-1a), 3.47 (m, 3 H, H-6a, CH_2N), 3.41 (m, 1 H, H-2), 3.37 (m, 3 H, H-3, H-4, H-5), 3.20 (dd, 1 H, H-6b), 2.60 (dd, 1 H, $J_{1b,2}$ = 11.2 Hz, H-1b), 1.16 (t, 3 H, CH_2CH_3). **^{13}C NMR** (150 MHz, CD_3OD): δ 161.7 (CN), 140.2, 127.8, 127.1, 126.2 (C_{arom}), 76.3 (C-3), 73.8 (C-4), 64.5 (C-5), 57.7 (C*H*$_2$Ph), 48.1 (CH_2N, C-2), 45.7 (C-1), 29.7 (C-6), 13.2 (CH_2CH_3). **HRMS** (ESI) *m/z* $[M + H]^+$ calcd for $[C_{17}H_{24}N_4O_2S_2]^+$ 381.1413; found 381.1424.

(*Z*)-2-Propylthioureido-5-*N*,6-*S*-(*N'*-benzyliminomethylidene)-1,2-dideoxy-6-thionojirimycin (32). Column chromatography, eluent: 100:10:1 DCM-MeOH-H_2O. Yield: 106 mg (quantitative). R_f 0.51 (70:10:1 DCM-MeOH-H_2O).

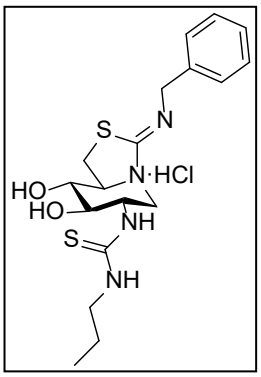

^{1}H NMR (600 MHz, CD_3OD): δ 7.33-7.20 (m, 5 H, CH_{arom}), 4.38 (d, 3 H, $^{3}J_{H,H}$ = 15.0 Hz, C*H*$_2$Ph, H-1a), 3.48 (m, 3 H, H-6a, CH_2N), 3.42 (m, 1 H, H-2), 3.37 (m, 3 H, H-3, H-4, H-5), 3.21 (dd, 1 H, H-6b), 2.62 (dd, 1 H, $J_{1b,2}$ = 11.2 Hz, H-1b), 1.58 (t, 3 H, C*H*$_2$CH$_3$), 0.94 (t, 3 H, CH_2CH_3). **^{13}C NMR** (150 MHz, CD_3OD): δ 162.0 (CN), 140.0, 127.8, 127.1, 126.3 (C_{arom}), 76.3 (C-3), 73.8 (C-4), 64.5 (C-5), 57.8 (C*H*$_2$Ph), 48.1 (CH_2N, C-2), 45.7 (C-1), 29.7 (C-6), 21.9 (*C*H$_2$CH$_3$), 10.2 (CH_2CH_3). **HRMS** (ESI) *m/z* $[M + H]^+$ calcd for $[C_{18}H_{26}N_4O_2S_2]^+$ 395.1570; found 395.1567.

Synthesis of DNJC-thiazolidines 37 and 38.

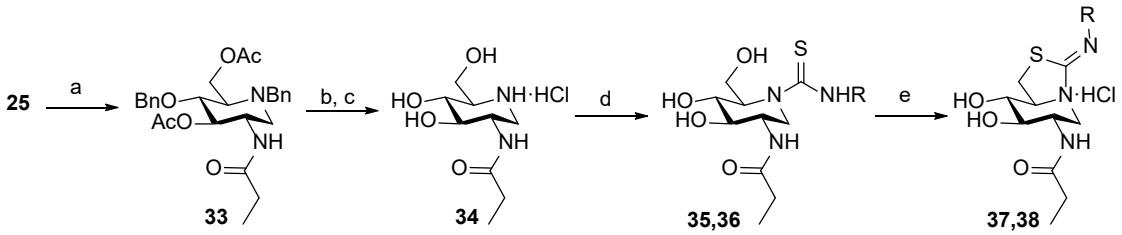

Supplemental scheme 7. Reagents and conditions: a. Zn, $CuSO_{4(aq)}$, THF-PrOH-Pr_2O, RT, 20 min; b. NaOMe, MeOH, RT, 18 h; c. H_2, Pd/C, MeOH, RT, 18 h; d. R-NCS, Et_3N, MeCN, RT, 18 h; e. HCl, MeOH, RT, 18 h.

2-Propionamide-3,6-di-*O*-acetyl-1-*N*,4-*O*-dibenzyl-1,2-dideoxynojirimycin (33). Powdered zinc (373 mg, 5.74 mM) was added to a solution of the azide **25**[1] (130 mg, 0.28 mM) in 3:2:1 THF-propionic acid-propionic anhydride (3.5 mL) and stirred vigorously before the dropwise addition of a saturated copper (II) sulfate solution (0.9 mL) to initiate the reaction. After 20 min, t.l.c. analysis (1:2 EtOAc-CyHex) indicated the complete consumption of the starting material (R_f 0.50) and the formation of a major product (R_f 0.10). The reaction mixture was filtered through Celite®, concentrated *in vacuo* and the crude residue purified by flash chromatography (50:1, DCM-MeOH) to afford the propanamide **33** (109 mg, 79%). $[\alpha]_D$ +8.80 (*c* 1, MeOH). R_f 0.50 (20:1 DCM-MeOH).

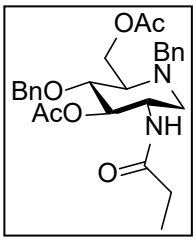

^{1}H NMR (300 MHz, $CDCl_3$): δ 7.36-7.23 (m, 10 H, CH_{arom}), 6.07 (s, 1 H, $J_{NH,2}$ = 8.7 Hz, NH), 4.90 (dd, 1 H, $J_{2,3} = J_{3,4}$ = 8.6 Hz, H-3), 4.65 (dd, 2 H, $^2J_{H,H}$ = 11.1 Hz, O*C*H_2Ph), 4.51 (dd, 1 H, $J_{6a,6b}$ = 12.1 Hz, $J_{5,6a} = J_{5,6b}$ = 4.1 Hz, H-6a), 4.37 (dd, 1 H, H-6b), 4.15 (m, 1 H, H-2), 3.92 (dd, 2 H, J_{gem} = 13.6 Hz, NC*H*$_2$Ph), 3.73 (t, 1 H, $J_{4,3} = J_{4,5}$ = 6.7 Hz, H-4), 3.05 (dd, 1 H, $J_{1a,1b}$ = 12.0 Hz, $J_{1a,2}$ = 3.7 Hz, H-1a), 2.86 (m, 1 H, H-5), 2.18 (dd, 1 H, $J_{1b,2}$ = 7.8 Hz, H-1b), 2.05 (m, 2 H, COC*H*$_2$CH$_3$), 2.04 (s, 6 H, $COCH_3$), 1.02 (t, 3 H, CO*C*H_2C*H*$_3$). **^{13}C NMR** (75.5 MHz, $CDCl_3$): δ 173.1, 170.9, 170.7 (*C*OCH_3, NH*C*OCH_2), 138.1-127.3 (C_{arom}), 75.5 (C-4), 74.4 (C-3), 73.9 (O*C*H_2Ph), 61.9 (C-5), 59.7 (C-6), 57.3 (N*C*H_2Ph), 51.6 (C-1), 47.9 (C-2), 29.7 (CO*C*H_2CH_3), 20.9, 20.8 ($COCH_3$), 9.5 ($COCH_2CH_3$). **ESIMS**: 483.3 $[M + H]^+$, 505.3 $[M+Na]^+$. Anal. Calcd for $C_{27}H_{34}N_2O_6$: C 67.20, H 7.10, N 5.81. Found: C, 67.33; H, 7.26; N, 5.74.

2-Propionamido-5-*N*-(*N'*-1-naphthylmethylthiocarbamoyl)-1,2-dideoxynojirimycin (35). Column chromatography, eluent 100:10:1 DCM-MeOH-H_2O. Yield: 90 mg (60%). R_f 0.40 (70:10:1 DCM-MeOH-H_2O).

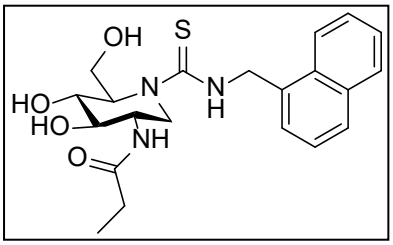

^{1}H NMR (600 MHz, CD_3OD): δ 8.10-7.42 (m, 8 H, CH_{arom}), 5.27 (bs, 2 H, CH_2Naph), 4.98 (m, 1 H, H-1a), 4.31 (m, 1 H, H-5), 3.95 (dd, 1 H, $J_{6a,6b}$ = 11.2 Hz, $J_{5,6a}$ = 8.8 Hz, H-6a), 3.95 (m, 1 H, H-2), 3.75 (dd, 1 H, $J_{5,6b}$ = 3.5 Hz, H-6b), 3.67 (t, 1 H, $J_{3,4}$ = $J_{4,5}$= 5.7 Hz, H-4), 3.62 (t, 1 H, $J_{2,3}$ = 5.4 Hz, H-3), 3.54 (dd, 1 H, $J_{1a,1b}$ = 14.1 Hz, $J_{1b,2}$ = 3.8 Hz, H-1b), 2.22 (q, 2 H, CH_2CH$_3$), 1.14 (t, 3 H, CH$_2$CH_3). **^{13}C NMR** (150 MHz, CD_3OD): δ 185.4 (CS), 175.1 (CO), 133.9-123.2 (C_{arom}), 70.7 (C-3), 69.1 (C-4), 64.8 (C-5), 60.3 (C-6), 51.3 (C-2, *C*H$_2$Naph), 43.6 (C-1), 29.1 (*C*H$_2$CH$_3$), 8.6 (CH$_2$*C*H$_3$). **HRMS** (ESI) *m/z* [M + Na]$^+$ calcd for [$C_{21}H_{27}N_3NaO_4S$]$^+$ 440.1614; found 440.1607

2-Propionamido-5-*N*-(*N'*-(1-Boc-indol-5-ylmethyl)thiocarbamoyl)-1,2-dideoxynojirimycin (36). Column chromatography, eluent 100:10:1 DCM-MeOH-H_2O. Yield: 90 mg (65%). [α]$_D$ -54.6 (*c* 1.0, MeOH). R_f 0.60 (70:10:1 DCM-MeOH-H_2O).

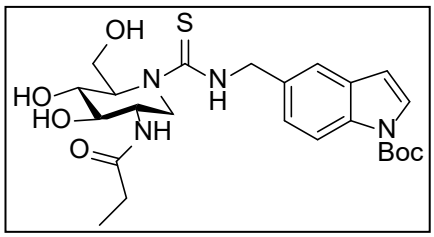

^{1}H NMR (500 MHz, CD_3OD): δ 8.04-6.55 (m, 5 H, CH_{arom}), 4.88 (d, 3 H, $^3J_{H,H}$ = 15.0 Hz, CH_2Ph), 4.84 (m, 1 H, H-1a), 4.40 (m, 1 H, H-5), 3.95 (dd, 1 H, $J_{6a,6b}$ = 11.2 Hz, $J_{5,6a}$ = 8.8 Hz, H-6a), 3.92 (m, 1 H, H-2), 3.80 (dd, 1 H, $J_{5,6b}$ = 3.6 Hz, H-6b), 3.69 (t, 1 H, $J_{3,4}$ = $J_{4,5}$= 5.2 Hz, H-4), 3.60 (t, 1 H, $J_{2,3}$ = 5.4 Hz, H-3), 3.51 (dd, 1 H, $J_{1a,1b}$ = 14.3 Hz, $J_{1b,2}$ = 3.6 Hz, H-1b), 2.17 (q, 2 H, CH_2CH$_3$), 1.68 (s, 9 H, CO_2Me_3), 1.07 (t, 3 H, CH$_2$CH_3). **^{13}C NMR** (125.7 MHz, CD_3OD): δ 185.4 (CS), 175.1 (CO_{amide}), 149.6 ($CO_{carbamate}$), 149.6-106.9 (C_{arom}), 83.5 (*C*CH$_3$), 70.7 (C-3), 69.2 (C-4), 64.6 (C-5), 60.2 (C-6), 51.3 (C-2), 49.2 (*C*H$_2$Ph), 43.6 (C-1), 29.1 (*C*H$_2$CH$_3$), 26.9 (CO_2*Me$_3$*), 8.6 (CH$_2$*C*H$_3$). **HRMS** (ESI) *m/z* [M + Na]$^+$ calcd for [$C_{24}H_{34}N_4NaO_6S$]$^+$ 529.2091; found 529.2082

(*Z*)-2-Propionamido-5-*N*,6-*S*-(*N'*-1-naphthymethyliminomethylidene)-1,2-dideoxy-6-thionojirimycin Hydrochloride (37). Column chromatography, eluent: 70:10:1 DCM-MeOH-H_2O. Yield: 104 mg (quantitative). R_f 0.62 (50:10:1 DCM-MeOH-H_2O).

^{1}H NMR (500 MHz, 1:1 CD_3OD-$CDCl_3$): δ 8.03-7.43 (m, 8 H, CH_{arom}), 4.90 (bs, 2H, CH_2Naph), 4.22 (dd, 1 H, $J_{1a,1b}$ = 13.1 Hz, $J_{1a,2}$ = 5.2 Hz, H-1a), 3.86 (m, 1 H, H-2), 3.65 (m, 1 H, H-5), 3.58

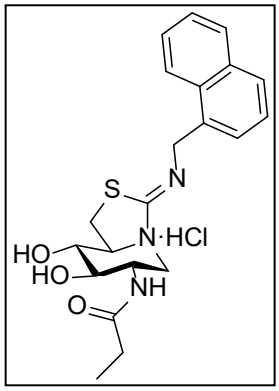

(m, 1 H, H-6a), 3.47 (t, 1 H, $J_{2,3} = J_{3,4} = 9.9$, H-3), 3.40 (t, 1 H, H-4), 3.33 (m, 1 H, H-6b), 2.78 (dd, 1 H, $J_{1b,2} = 11.5$ Hz, H-1b), 2.25 (q, 2 H, CH_2CH$_3$), 1.14 (t, 3 H, CH$_2$CH_3). **^{13}C NMR** (125.7 MHz, 1:1 CD_3OD-$CDCl_3$): δ 176.3 (CO), 165.1 (CN), 133.8-122.9 (C_{arom}), 75.1 (C-3), 73.8 (C-4), 65.8 (C-5), 53.6 (CH_2Naph), 49.8 (C-2), 45.9 (C-1), 30.5 (C-6), 29.0 (CH_2CH$_3$), 9.2 (CH$_2$CH_3). **HRMS** (ESI) *m/z* $[M + H]^+$ calcd for $[C_{21}H_{26}N_3O_3S]^+$ 400.1689; found 400.1683. Anal. Calcd for $C_{21}H_{26}N_3O_3S.HCl$: C 57.86, H 6.01, N 9.64, S 7.35. Found: C, 57.54; H, 5.82; N, 9.30; S, 7.03.

(*Z*)-2-Propionamido-5-*N*,6-*S*-(*N'*-5-indolylmethyliminomethylidene)-1,2-dideoxy-6-thionojirimycin Hydrochloride (38). Column chromatography, eluent: 70:10:1 DCM-MeOH-H_2O. Yield: 104 mg (quantitative). R_f 0.40 (50:10:1 DCM-MeOH-H_2O).

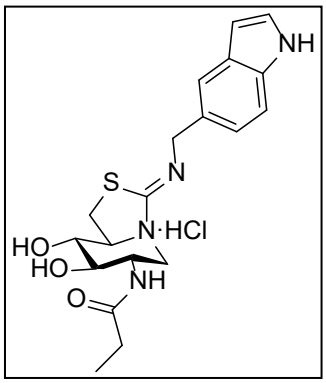

^{1}H NMR (500 MHz, CD_3OD): δ 7.57-6.46 (m, 5 H, CH$_{arom}$), 4.60 (bs, 2H, CH_2Ph), 4.18 (dd, 1 H, $J_{1a,1b} = 13.3$ Hz, $J_{1a,2} = 5.3$ Hz, H-1a), 3.88 (m, 1 H, H-2), 3.83 (m, 1 H, H-5), 3.68 (m, 1 H, $J_{6a,6b} = 11.3$ Hz, $J_{5,6a} = 7.4$ Hz, H-6a), 3.52 (t, 1 H, $J_{2,3} = J_{3,4} = 9.0$, H-3), 3.42 (m, 2 H, H-4, H-6b), 2.93 (dd, 1 H, $J_{1b,2} = 11.5$ Hz, H-1b), 2.29 (q, 2 H, CH_2CH$_3$), 1.16 (t, 3 H, CH$_2$CH_3). **^{13}C NMR** (125.7 MHz, CD_3OD): δ 177.7 (CO), 169.9 (CN), 137.4-102.5 (C_{arom}), 75.9 (C-3), 75.1 (C-4), 68.4 (C-5), 55.8 (CH_2Ph), 51.0 (C-2), 47.2 (C-1), 32.2 (C-6), 30.3 (CH_2CH$_3$), 10.4 (CH$_2$CH_3). **HRMS** (ESI) *m/z* $[M + H]^+$ calcd for $[C_{19}H_{25}N_4O_3S]^+$ 389.1642; found 389.1637. Anal. Calcd for $C_{19}H_{25}N_4O_3S.HCl$: C 53.70, H 5.93, N 13.18, S 7.54. Found: C, 53.48; H, 5.70; N, 12.86; S, 7.21.

Synthesis of DNJNAc-6S-NBn-Biotin probe

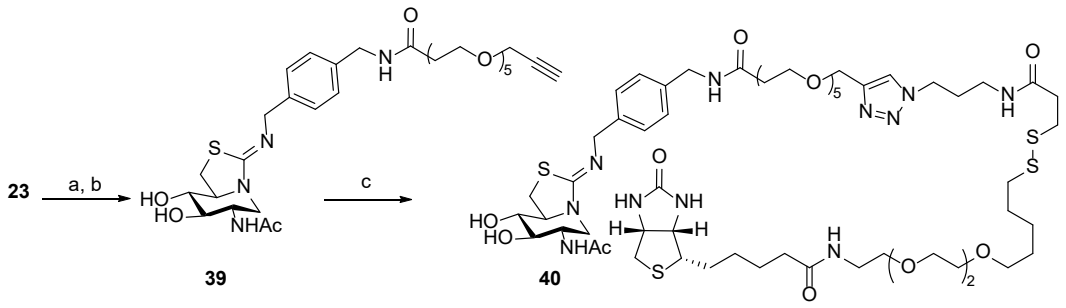

Supplemental scheme 8. Reagents and conditions: a. PPh_3, THF-H_2O, RT, 18 h; b. alkyne-PEG4-acid, HBTU, DIPEA, DMF, RT, 24 h; c. biotin-azide, sodium ascorbate, $CuSO_4 \cdot 5H_2O$, DMF-H_2O, RT, 18 h.

Alkyne intermediate (39). A mixture of inhibitor **23** (13.5 mg, 0.0316 mM) and PPh_3 (9.1 mg, 0.0348 mM) in 4:1 THF-H_2O (2.5 mL) was stirred overnight and then concentrated with co-evaporation with 1:1 toluene-^{i}PrOH. The residue was dried under vacuum for 2.5 h. To the residue was added HBTU (16.8 mg, 0.0442 mM) and alkyne-PEG4-acid (12.5 mg, 0.0411 mM) followed by anhydrous DMF (1.5 mL) and DIPEA (16.6 µL, 0.0948 mM). The reaction mixture was stirred overnight and then concentrated with co-evaporation with toluene. The resulting residue was purified by CombiFlash (dry load, 4 g RediSep Gold Column, 18 mL/min) using a gradient of 1:0:0→6:3:1 EtOAc-MeOH-H_2O to give intermediate **39** (12.9 mg, 64%) as a clear viscous oil. R_f 0.41 (9:3:1 EtOAc-MeOH-H_2O).

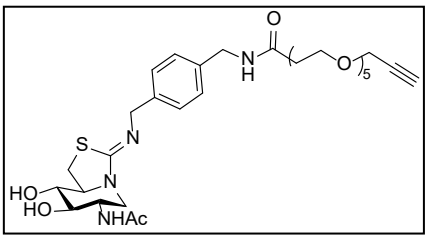

^{1}H NMR (600 MHz, CD_3OD): δ 7.27 (d, 2 H, *J* = 8.3 Hz, CH-arom), 7.25 (d, 2 H, *J* = 8.6 Hz, CH_{arom}), 4.39 (d, 1 H, *J* = 14.8 Hz, PhC*H*$_2$N), 4.38 (s, 2 H, PhC*H*$_2$N), 4.33 (d, 1 H, *J* = 14.9 Hz, ArC*H*$_2$N), 4.19 (s, 2 H, OC*H*$_2$C), 4.16 (dd, 1 H, *J* = 12.7, 5.2 Hz, H-1), 3.86 (ddd, 1 H, *J* = 11.2, 10.2, 5.2 Hz, H-2), 3.77 (t, 2 H, *J* = 6.0 Hz, $COCH_2CH_2O$), 3.71–3.62 (m, 16 H, 8 × OC*H*$_2$), 3.47 (dd, 1 H, *J* = 10.9, 5.9 Hz, H-6), 3.40 (dd, 1 H, *J* = 10.2, 8.4 Hz, H-3), 3.36–3.32 (m, 2 H, H-4, H-5), 3.18 (dd, 1 H, *J* = 10.8, 7.1 Hz, H-6'), 2.89 (t, 1 H, *J* = 2.4 Hz, C_qCH), 2.59 (dd, 1 H, *J* = 12.8, 11.3 Hz, H-1'), 2.51 (t, 2 H, *J* = 6.0 Hz, $COCH_2CH_2O$), 1.99 (s, 3 H, COC*H*$_3$). **^{13}C NMR** (150 MHz, CD_3OD): δ 172.5, 172.2 (CO), 161.8 (CN), 139.2, 136.9, 127.2, 127.1 (C_{arom}), 79.2 (C_qCH),75.6 (C3), 74.1 (C4), 70.1 (OCH_2), 70.0 (OCH_2), 69.9 (OCH_2), 68.7 (OCH_2), 66.9 ($COCH_2CH_2O$), 64.6 (C5), 57.6 (O*C*H$_2$C$_q$, N*C*H$_2$Ar), 57.5 (N*C*H$_2$Ar), 49.9 (C2), 45.8 (C1), 36.3 ($COCH_2CH_2$), 29.9 (C6), 21.4 (CO*C*H$_3$). **HRMS (ESI)** *m/z* $[M+H]^+$ calcd for $C_{31}H_{47}N_4O_9S$: 651.3064, found 651.3631.

DNJNAc-6S-NBn-Biotin (40). To a mixture of intermediate **39** (4.7 mg, 0.0072 mmol) and biotin-SS-azide (5.5 mg, 0.0079 mM) obtained from ClickChemistryTools (1168-25,) in DMF (250 µL) was added a solution of sodium ascorbate (1.4 mg, 0.00722 mM) and $CuSO_4 \cdot 5H_2O$ (0.9 mg, 0.00361 mM) in H_2O (250 µL). The reaction mixture was stirred overnight at RT. The mixture was concentrated and co-evaporated with a 1:1 toluene-^{i}PrOH solution, then dried under vacuum for 1 h. The resulting residue was purified by HPLC (XDB C18 semi-prep column) to give the final DNJNAc-6S-NBn-Biotin (**40**) (3.0 mg, 31%) as a colorless oil. R_f 0.20 (4:3:1 EtOAc-MeOH-H_2O).

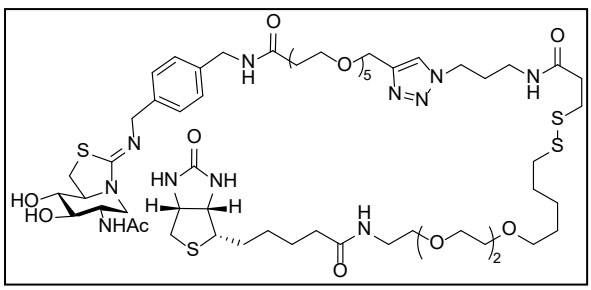

^{1}H NMR (600 MHz, CD_3OD): δ 8.05 (s, 1 H, CH_{arom}), 7.39–7.32 (m, 4 H, CH_{arom}), 4.64 (s,

2 H, OCH_2Ph), 4.60 (s, 2 H, NCH_2Ph), 4.52 (dd, 1H, J = 13.3, 5.1 Hz, CHN$_{biotin}$), 4.47 (t, 2 H, J = 6.8 Hz, N$_{Ar}$CH_2CH$_2$CH$_2$), 4.42 (s, 2 H, ArCH_2N), 4.33 (dd, 1 H, J = 7.9, 4.4 Hz, CHN$_{biotin}$), 4.18 (dd, 1 H, J = 12.4, 5.2 Hz, H-1), 4.09 (app. q, 1 H, J = 8.3 Hz, H-5), 3.86 (ddd, 1 H, J = 11.9, 10.7, 5.1 Hz, H-2), 3.81–3.75 (m, 3 H, H-6, COCH$_2$CH_2O$_{L1}$), 3.73–3.45 (m, 28 H, H-3, H-4, COCH$_2$CH_2O$_{L2}$, 13 × OCH$_2$), 3.42–3.37 (m, 4H, OCH$_2$CH_2N$_{L2}$, SCH$_2$CH_2N$_{L2}$), 3.26–3.21 (m, 3 H, CHS$_{biotin}$, CH$_2$CH$_2$CH_2N$_{(L2)}$), 3.08 (dd, 1 H, J = 12.2, 12.2 Hz, H-1'), 3.03–2.91 (m, 5 H, CH_2S$_{biotin}$, CH$_2$CH_2S$_{L2}$, SCH_2CH$_{2(L2)}$), 2.73 (d, 1 H, J = 12.7 Hz, CH_2'S$_{biotin}$), 2.66–2.61 (m, 4 H, COCH_2CH$_2$S$_{L2}$, COCH_2CH$_2$O$_{L2}$), 2.52 (t, 2 H, J = 5.8 Hz, COCH_2CH$_2$O$_{L1}$), 2.24 (t, 2 H, J = 7.3 Hz, NCOCH_2CH$_{2(biotin)}$), 2.13 (app. t, 2 H, J = 6.8 Hz, NCH$_2$CH_2CH$_2$N $_{L2}$), 2.02 (s, 3 H, COCH$_3$), 1.83–1.55 (m, 4 H, CH$_{2(biotin)}$, CH$_{2(biotin)}$), 1.49–1.44 (m, 2 H, CH$_{2(biotin)}$). **^{13}C NMR** (150 MHz, CD$_3$OD): δ 174.7, 172. 7, 172.5, 172.3, 172.0, 139.4, 133.5, 127.7, 127.6, 73.8, 73.2, 70.2, 70.1 (4×), 70.0 (2×), 69.8 (3×), 69.4, 69.2, 69.1, 68.1, 66.9, 62.0, 60.2, 55.6, 51.1, 49.5, 45.6, 42.2, 39.7, 39.1, 39.0, 36.4, 36.1, 35.4, 35.1, 35.0 (2×), 33.7, 33.6, 31.1, 29.7, 28.4, 28.1, 25.5, 21.3. **HRMS (ESI)** *m/z* [M+NH$_4$]$^+$ calcd for C$_{59}$H$_{101}$N$_{12}$O$_{15}$S$_4$: 1345.5828, found 1345.5766.

Morrison K_i determination against human OGA, HexA and HexB

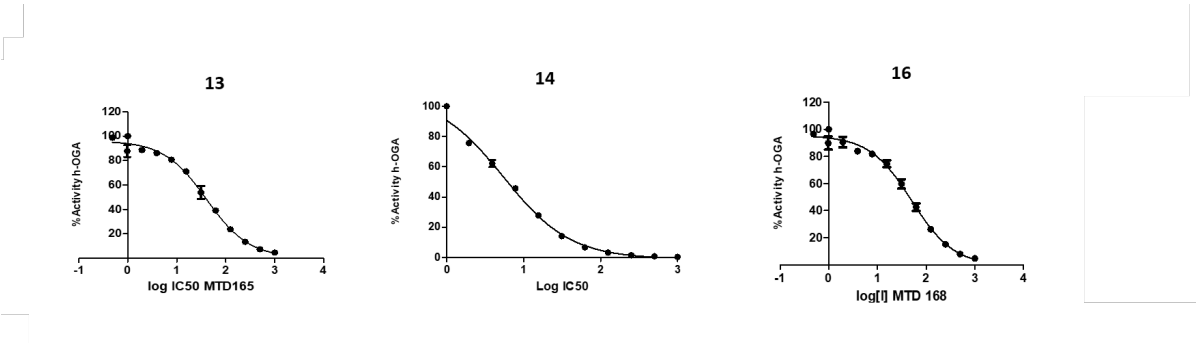

Supplemental Figure 1. K_i determination of **13** (24 ± 8 nM), **14** (20 ± 7 nM) and **16** (3 ± 1 nM) against hOGA.

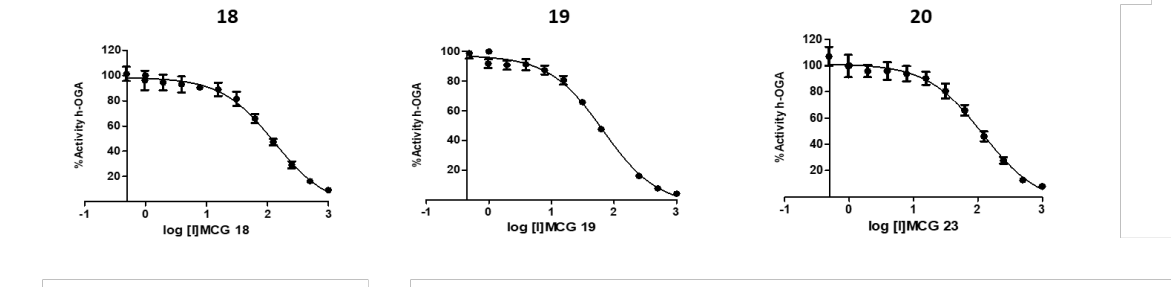

Supplemental Figure 2. K_i determination of **18** (50 ± 20 nM), **19** (30 ± 10 nM), and **20** (50 ± 20 nM), against hOGA.

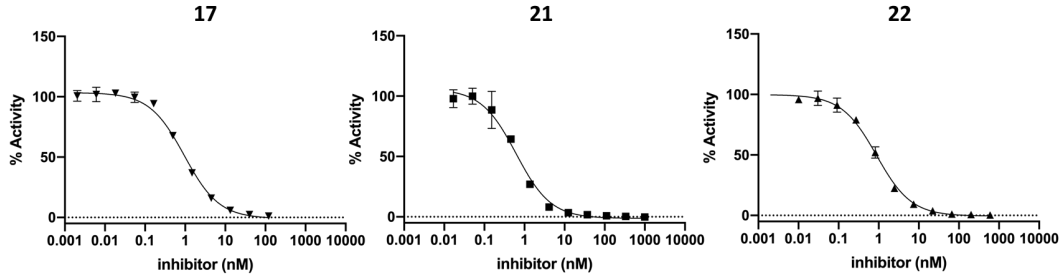

Supplemental Figure 3. K_i determination of **17** (0.3 ± 0.1 nM), **21** (0.27 ± 0.09.nM), and **22** (0.22 ± 0.07 nM), against hOGA.

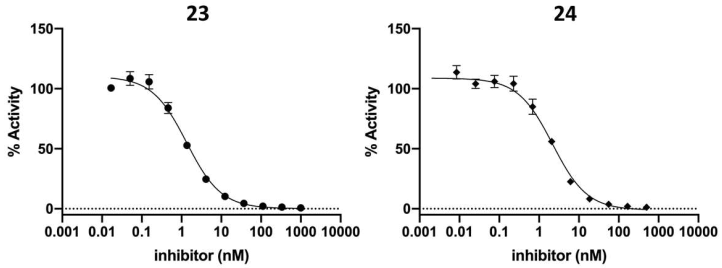

Supplemental Figure 4. K_i determination of **23** (0.4 ± 0.2 nM), and **24** (0.9 ± 0.3 nM), against hOGA.

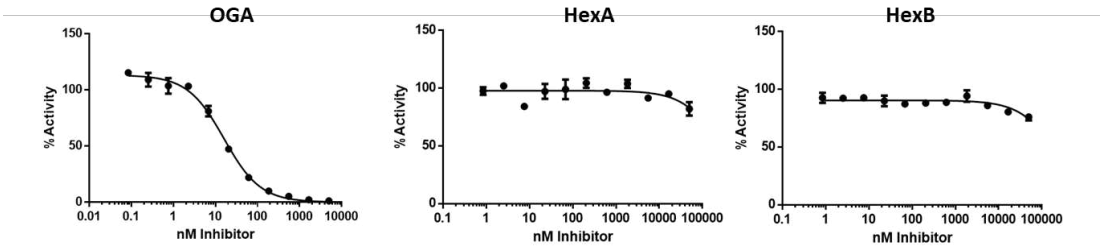

Supplemental Figure 5. K_i determination of **28** against hOGA (8 ± 3 nM), HexA (<100 μM) and HexB (<100 μM).

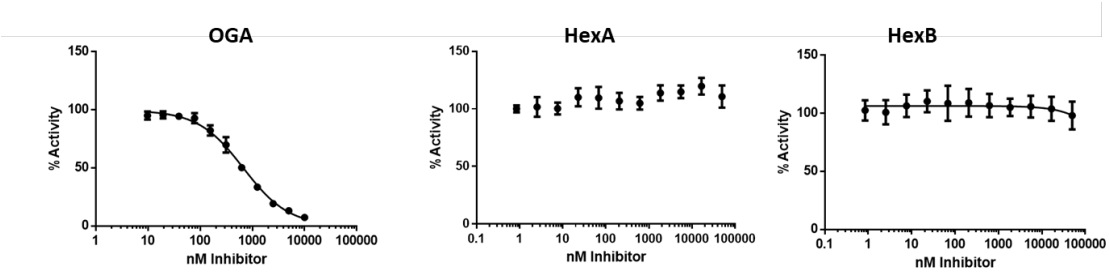

Supplemental Figure 6. K_i determination of **29** (900 ± 300 nM) against hOGA, HexA (<100 μM) and HexB (<100 μM).

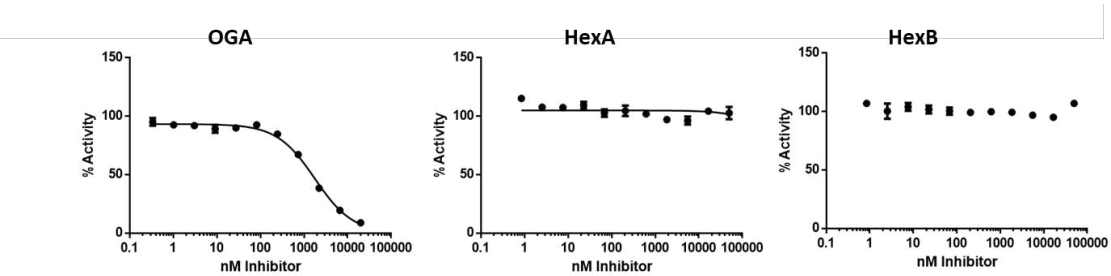

Supplemental Figure 7. K_i determination of **30** (300 ± 100 nM) against hOGA, HexA (<100 μM) and HexB (<100 μM).

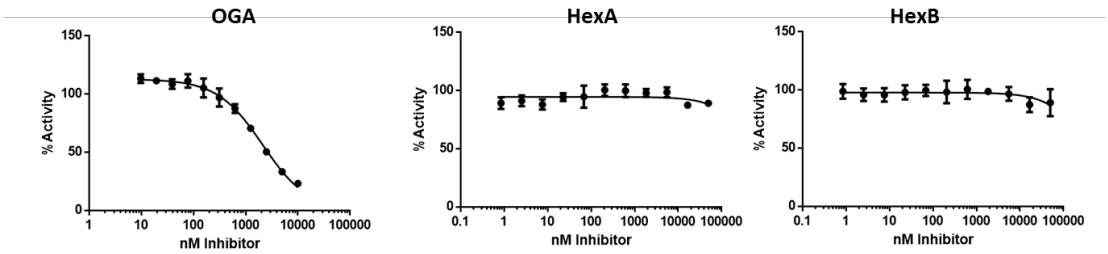

Supplemental Figure 8. K_i determination of **31** against hOGA (1000 ± 400 nM), HexA (<100 μM) and HexB (<100 μM).

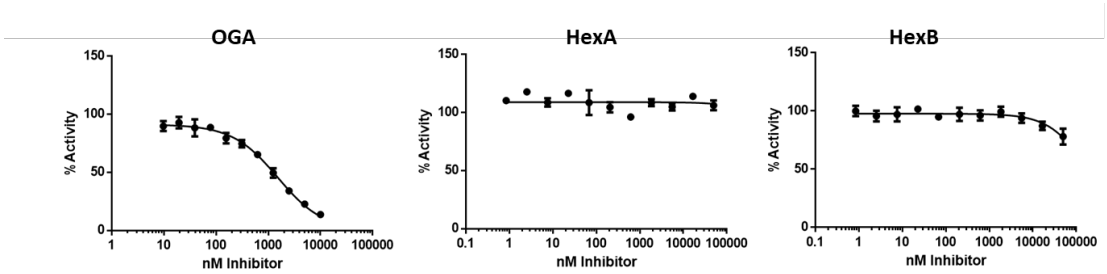

Supplemental Figure 9. K_i determination of **32** against hOGA (800 ± 300 nM), HexA (<100 μM) and HexB (<100 μM).

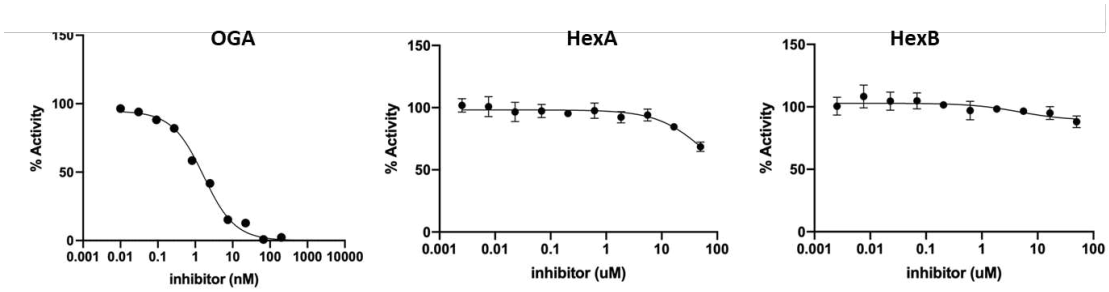

Supplemental Figure 10. K_i determination of **37** against hOGA (0.8 ± 0.2 nM), HexA (<100 μM) and HexB (<100 μM).

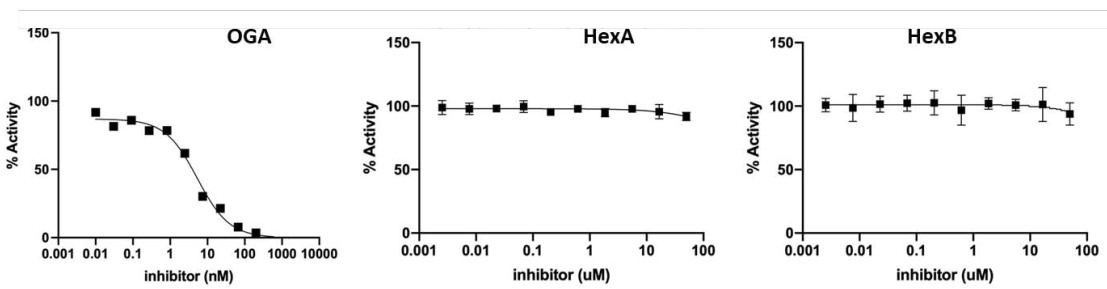

Supplemental Figure 11. K_i determination of **38** against hOGA (2.4 ± 0.9 nM), HexA (<100 μM) and HexB (<100 μM).

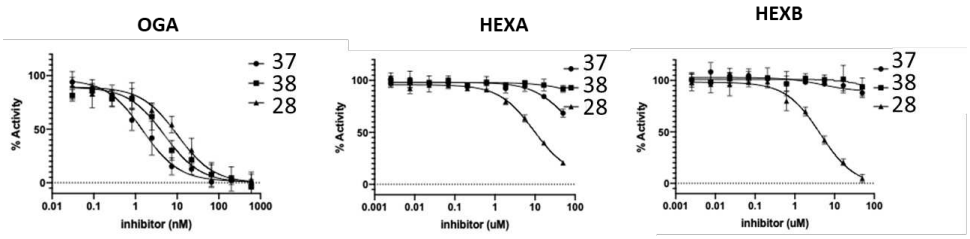

Supplemental Figure 12. Comparative K_i determination of **28, 37 and 38** against hOGA, HexA (<100 μM) and HexB (<100 μM).

Inhibition of compounds 1-24 against commercial hexosaminidases.

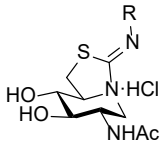

Supplemental Table 1. Inhibition constants (Ki) for DNJNAc-thiazolidines **13-24** against commercial hexosaminidases

Compound	Structure (R)	Bovine kidney Hex K_i (μM)	Human placenta Hex K_i (μM)
13	$(CH2)_3CH_3$	0.57 ± 0.04	0.24 ± 0.02
14	$(CH2)_7CH_3$	0.19 ± 0.02	0.24 ± 0.02
15	Ph	0.70 ± 0.05	0.58 ± 0.04
16	CH_2Ph	0.46 ± 0.03	0.42 ± 0.03
17	CH_2-1-naphthyl	0.89 ± 0.8	n.d.[a]
18	CH_2p-FPh	1.5 ± 0.2	0.28 ± 0.02
19	CH_2p-OMePh	1.2 ± 0.1	0.73 ± 0.04
20	CH_2p-CF_3Ph	0.43 ± 0.04	0.40 ± 0.03
21	CH_2o-CH_2N_3Ph	0.91 ± 0.09	n.d.[a]
22	CH_2m-CH_2N_3Ph	0.83 ± 0.06	n.d.[a]
23	CH_2p-CH_2N_3Ph	0.72 ± 0.05	n.d.[a]
24	CH_2CH_2Ph	1.4 ± 0.12	n.d.[a]

X-Ray structure solution methods for hOGA and *Bt*GH84 in complex with compound 16

hOGA was produced and purified as a split construct, DNA encoding residues 11-396 and 535-715 was inserted in two separate plasmids, according to the protocol published by Roth, *et al.* 2017[6]. hOGA was crystallised by hanging drop vapour diffusion method at a concentration of 30 mg mL^{-1} under the conditions of 200 mM Triammonium citrate pH 7.5 and 24% Polyethylene glycol 3350. A seed stock was added at 20x diluted concentration in a 1 : 0.2 : 0.8 µL ratio of protein : seed stock : reservoir. *Bt*GH84 was produced and purified as described previously by Dennis *et al*, 2006[7]. *Bt*GH84 was crystallised by sitting drop vapour diffusion method at a concentration of 12 mg mL^{-1} under the conditions of 125 mM imidazole pH8, 8% PEG 8000, 3% trimethylamine N-oxide dehydrate, 15% ethylene glycol in a 1:1 ratio of protein to reservoir solution. Crystals were soaked with compound **16** at a final concentration of 5 mM for either 2 hours or 7 days, *Bt*GH84 and hOGA respectively. Diffraction data were collected on the I03 and I04-1 beamlines at Diamond Light Source (DLS). The data were indexed, integrated and scaled using Xia2[8] and reintegrated using Aimless[9,10] from the CCP4 software[11]; the data collection statistics are shown in table 2. Molecular replacement was conducted using Molrep[12] with coordinates 5M7R and 5ABE for hOGA and *Bt*GH84, respectively. The model was adjusted and refined using alternating cycles of manual model building and real space refinement in Coot[13] and reciprocal space refinement in Refmac[14–17]. Data quality was assessed by the multimeric model geometry validation programme[18] in CCP4 and Privateer[19] was used to assess the confidence of the carbohydrate ligand conformation. Figures were produced using CCP4mg[20].

Supplemental Table 2. Data collection and refinement statistics for hOGA and BtGH84 enzymes in complex with compound **16**.

	*h*OGA_**16**	*Bt*GH84_**16**
PDB code	**7OU6**	**7OU8**
Data collection		
Beamline	Diamond I03	Diamond I04-1
Wavelength (Å)	0.9763	0.9159
Space group	$P\ 4_3\ 2_1\ 2$	$P\ 2\ 2_1\ 2_1$
Cell dimensions: *a*, *b*, *c* (Å)	101.29, 101.29, 284.52	51.53, 160.62, 224.51
α, β, γ (°)	90.00, 90.00, 90.00	90.00, 90.00, 90.00
Resolution (Å)	58.21-2.41 (2.48-2.41)	75.62-1.50 (1.53-1.50)
R_{merge}	0.05 (2.28)	0.07 (0.81)
R_{pim}	0.01 (0.59)	0.03 (0.37)
CC (1/2)	1.00 (0.56)	1.00 (0.65)
$I / \sigma I$	26.5 (1.5)	12.3 (1.5)
Completeness (%)	100.0 (100.0)	100.0 (100.0)
Redundancy	15.8 (15.6)	7.5 (5.8)
Refinement		
Resolution (Å)	58.21-2.41 (2.48-2.41)	75.62-1.50 (1.53-1.50)
No. reflections	58168	298007
R_{work} / R_{free}	0.22/0.27	0.21/0.23
No. atoms		
Protein	6704	11529
Ligands/Ions	46	50/1
Water	18	903
B-factors (Å^2)		
Protein	89	28
Ligand/Ions	82	19/23
Water	65	31
R.m.s. deviations		

Bond lengths (Å)	0.007	0.011
Bond angles (°)	1.52	1.74
Ramachandran		
Favoured (%)	94.2	95.8
Allowed (%)	4.7	3.6
Outliers (%)	1.1	0.6

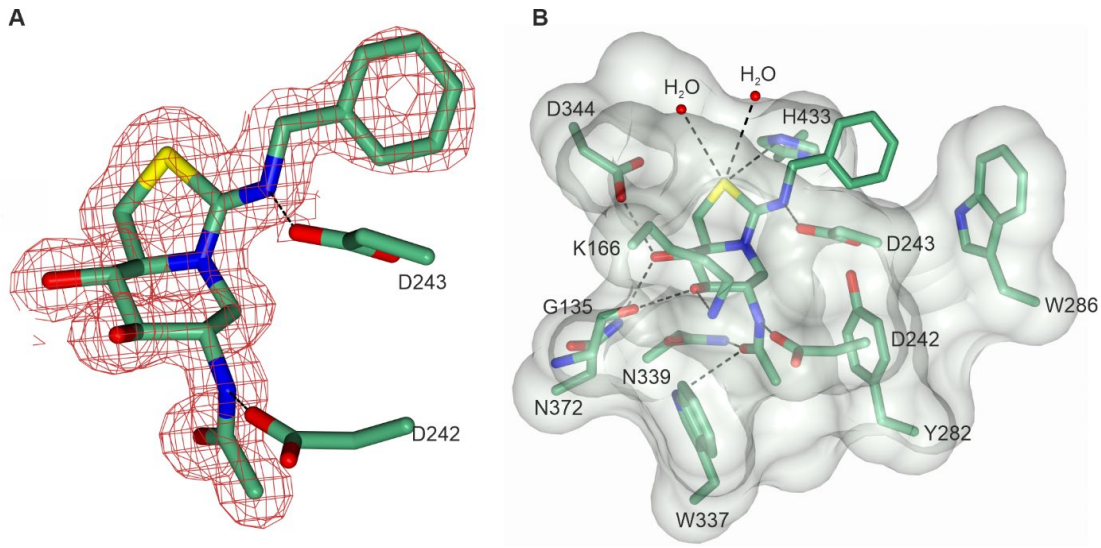

Supplemental Figure 13. Structure of *Bt*GH84 in complex with compound **16**. Active site residues of *Bt*GH84 are shown in green. (A) **16** is shown in dark green with the corresponding REFMAC maximum-likelihood/σA-weighted $2F_o$-F_c map, shown in red, contoured at 0.46 electrons Å^{-3}. (B) Surface representation of the active site pocket of *Bt*GH84 with neighbouring residues, waters and hydrogen bond interactions highlighted.

Chemoproteomic and mapping of post-transcriptional modifications

Preliminary pull-down experiments with recombinant hOGA. Recombinant hOGA was added to lysis buffer (25 mM HEPES, 150 mM NaCl, 5 mM EDTA, 5% glycerol, pH 7.1) containing protease inhibitor cocktail (Roche cOmplete™, EDTA free) at a concentration of 100 nM at 4°C. DNJNAc-6S-NBn-Biotin was added at concentration of 500 nM and incubated with rotation for 1 h at 4 °C. The sample was then incubated with the streptavidin beads (Tri-Link Biotechnologies) for 1 h at 4 °C. The beads were separated and washed with lysis buffer 5 times at 4 °C. The beads were then eluted with 100 mM DTT in lysis buffer.

Large scale precipitation of bovine OGA. Bovine brains were obtained from Animal Technologies, Inc. The lysate was prepared using a 4:1 lysis buffer: dry cell extractions. The entire brain was homogenized by cryomilling under liquid nitrogen. The brain tissue was processed using a dounce homogenizer in 4:1 lysis buffer (25 mM HEPES, 133 mM KCl, 5 mM MgCl2, 5 mM EDTA, 10% Glycerol, pH 7.1, SIGMAFAST™ Protease Inhibitor Cocktail) to dry tissue, at 4 °C. The lysate was cleared by centrifugation (Sorvall RC-6 Plus) at 20,000 RPM for 30 min at 4 °C. The supernatant was collected and the remaining debris was removed by ultra-centrifugation (Beckman Optima Ultracentrifuge L-80 XP) at 45,000 RPM for 45 min at 4 °C. The supernatant was collected and separated into fresh tubes. The samples were incubated for 30 min at 4 °C with streptavidin beads to deplete endogenously biotinylated proteins. The sample was centrifuged and the supernatant collected to remove the beads from the sample after which 128 nM of DNJNAc-6S-NBn-Biotin was added and the sample was mixed by rotation for 1 hr at 4 °C. A parallel control experiment was performed in which we added a high concentration of Thiamet-G (1 mM) to block binding to the DNJNAc-6S-NBn-Biotin ligand. The sample and control were then incubated with the beads (200 µL) for 1 hr at 4 °C. The beads were separated and washed with cold lysis buffer 5 times at 4 °C. The affinity purified protein and control were then eluted by addition of DTT in lysis buffer to provide a final concentration of 60 mM and the samples were mixed using a thermomixer (Eppendorf) at 37 °C for 10 min.

LC-MS/MS sample preparation and analysis. The samples were loaded onto 12% SDS-PAGE minigels (Bio-Rad), electrophoresed, and stained with Coomassie blue G-250 (Thermo Fisher Scientific). The band corresponding to OGA at the 130 kDa range was excised, destained, protein disulfide bonds were reduced (10 mM DTT in 50 mM NH_4HCO_3, 45 min, 56 °C), after which thiols were alkylated (55 mM iodoacetamide in 50 mM NH_4HCO_3, dark, 30 min, room temperature). Protein was subsequently digested (trypsin, Promega, in 50 mM NH_4HCO_3, overnight, 37 °C) and the resulting peptides were extracted with a gradient of acetonitrile solutions starting with aqueous 0.1% formic acid. Peptide mixtures were purified by solid-phase extraction

using C18 StageTips (Thermo Fisher Scientific). 200 ng of sample was injected into LC-MS/MS, analysis was performed using a Bruker timfTOF coupled to a Bruker nanoElute UHPLC system (Thermo Fisher Scientific).

Acquired data was then searched against the Uniprot protein database for Bos taurus using the Byonic™ (v4.0.12 – ProteinMetrics Inc.) search algorithm from Protein Metrics Inc, with 15 ppm and 40 ppm mass accuracies for precursor and product ion masses respectively, and a 1% false discovery rate cut-off. Assigning of peptide and protein identifications included carbamidomethyl @ C (fixed), oxidation @ M (common1) and deamidation @ N,Q (common1) modifications, RK fully specific digestion (maximum two missed cleavages), 15 and 40 ppm precursor and fragment mass tolerance. Several variable modifications were selected for a second pass search, these can be found in Supplemental Spreadsheet. Focusing on the enzymatic modifications, an FDR criterion was defined for the modifications identified on a peptide hits as those with a |Log Prob| > 1.52 (3%FDR), and high-confidence modifications were assigned as |Log Prob| > 2.0 (1% FDR). (Additional information regarding search parameters selected can be found in Supplemental Spreadsheet)

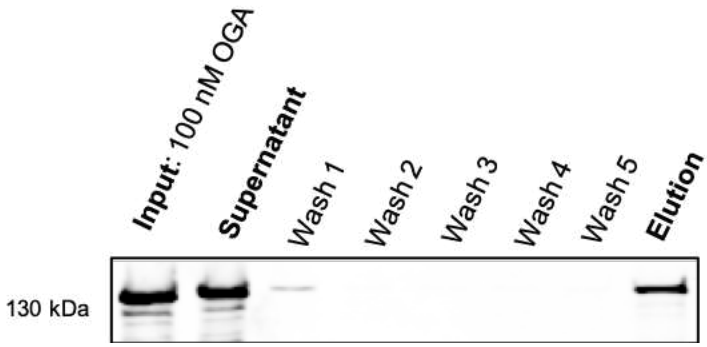

Supplemental Figure 14. Small scale validation experiment showing **DNJNAc-6S-NBn-Biotin** enables enrichment of recombinant hOGA as determined using immunoblot assay.

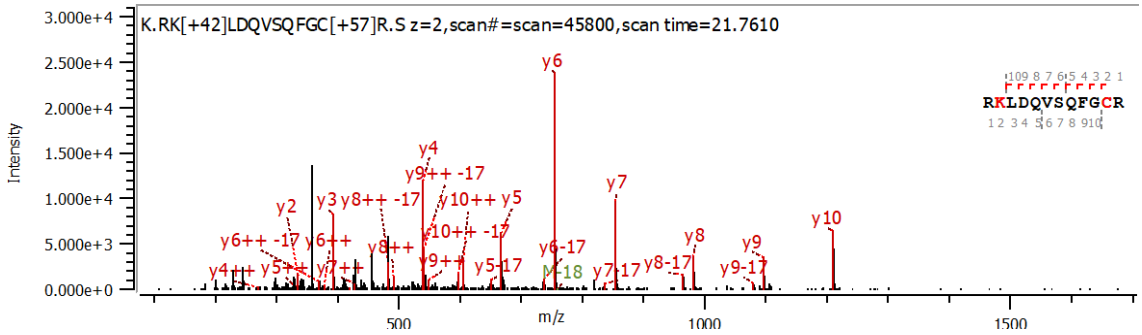

Supplemental Figure 15. MS/MS spectrum for acetylation identified at K157.

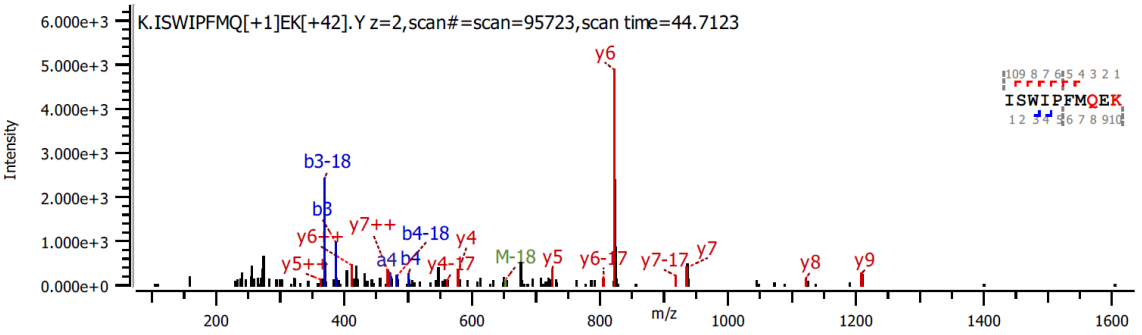

Supplemental Figure 16. MS/MS spectrum for acetylation identified at K805.

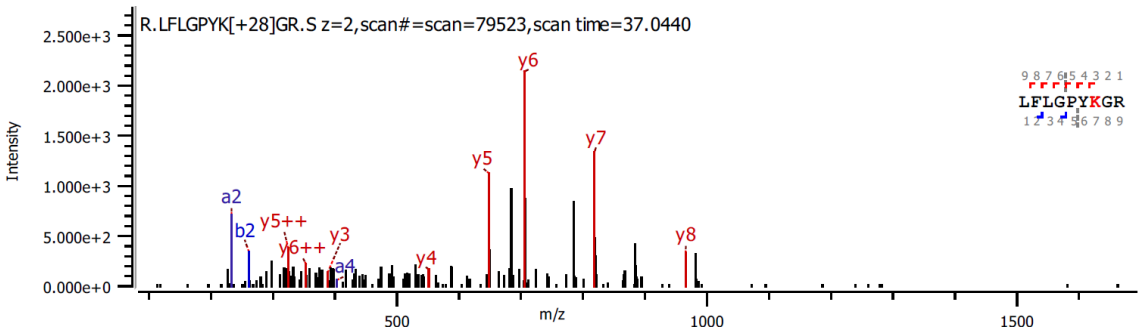

Supplemental Figure 17. MS/MS spectrum for formylation identified at K297.

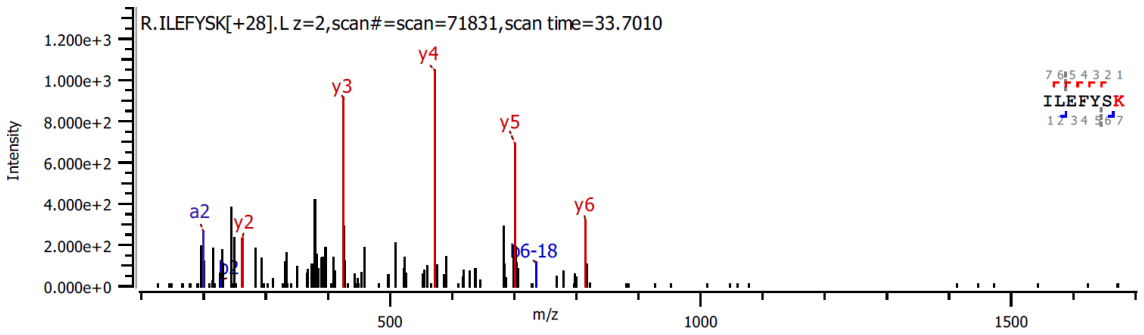

Supplemental Figure 18. MS/MS spectrum for formylation identified at K893.

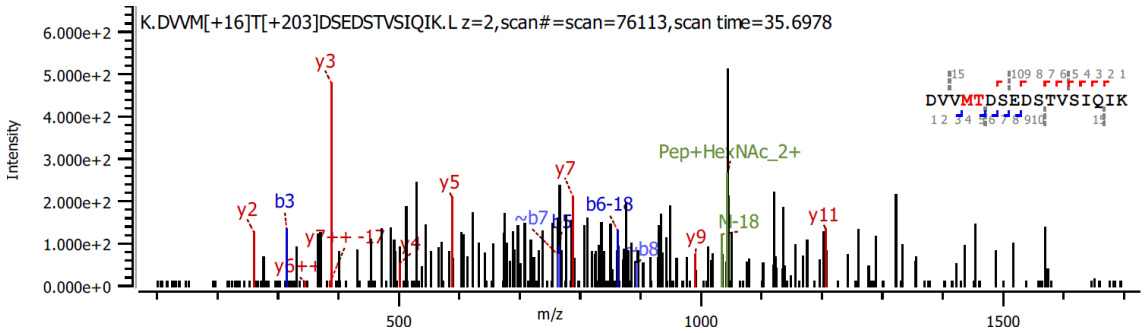

Supplemental Figure 19. MS/MS spectrum for O-GlcNAcylation identified at T346.

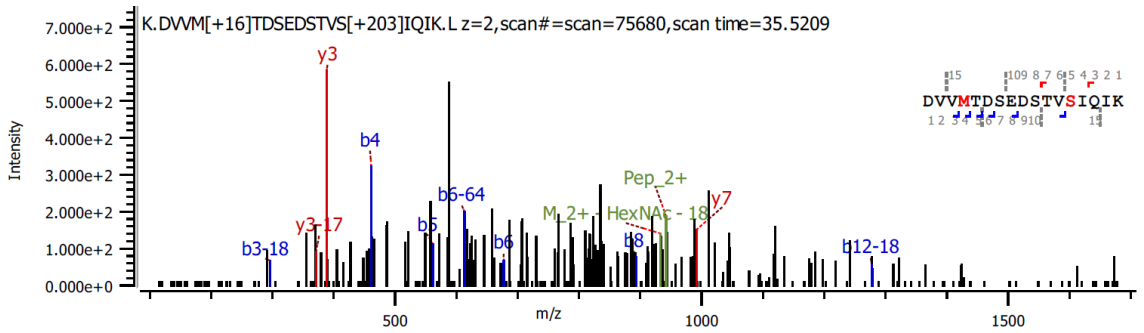

Supplemental Figure 20. MS/MS spectrum for O-GlcNAcylation identified at S354.

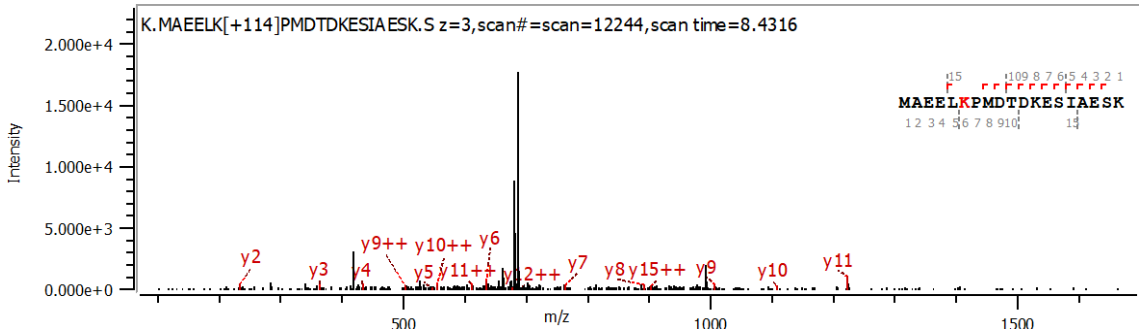

Supplemental Figure 21. MS/MS spectrum for N-ubiquitination identified at K497.

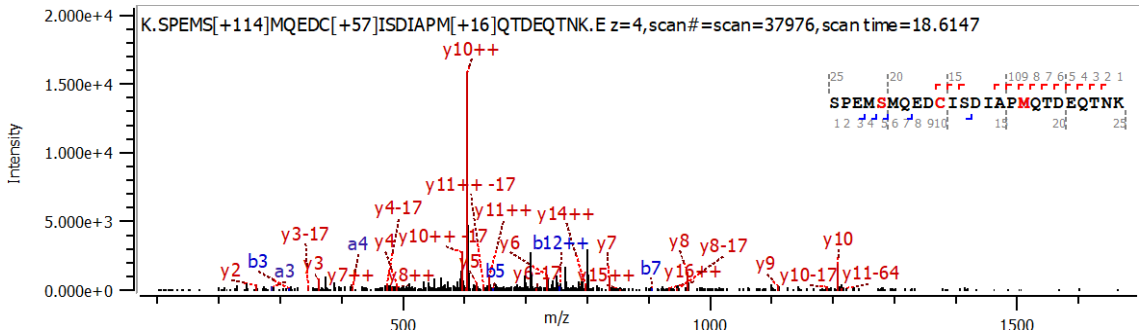

Supplemental Figure 22. MS/MS spectrum for O-ubiquitination identified at S515.

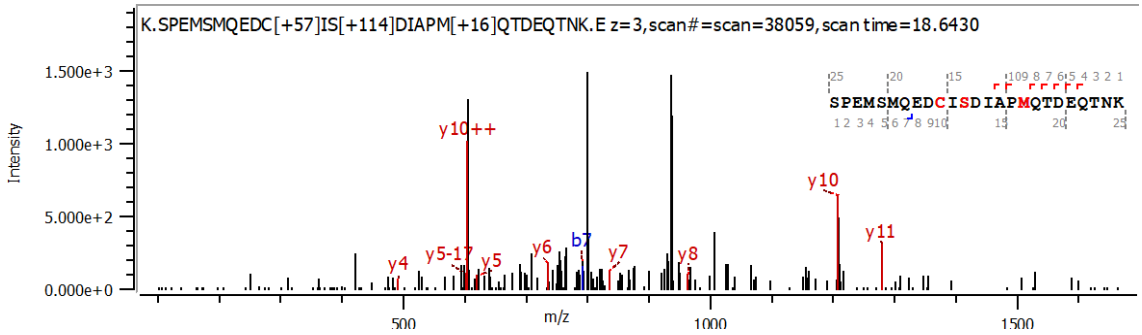

Supplemental Figure 23. MS/MS spectrum for O-ubiquitination identified at S522.

Supplemental Table 3. Fragment ion series of mass spectra from acetylated Lys157 peptide.

#	a calc.	a obs.	a delta	b calc.	b obs.	b delta	b-18 calc.	b-18 obs.	b-18 delta	Seq.	y calc.	y obs.	y delta	y++ calc.	y++ obs.	y++ delta	#
1	129.1135			157.1084			139.0978			R							12
2	299.219			327.2139			309.2033			K	1379.6736			690.3404			11
3	412.3031			440.298			422.2874			L	1209.5681	1209.5676	-0.0005	605.2877	605.2874	-0.0002	10
4	527.33			555.3249			537.3143			D	1096.484	1096.4829	-0.0011	548.7456	548.743	-0.0027	9
5	655.3886			683.3835			665.3729			Q	981.4571	981.4567	-0.0004	491.2322	491.2281	-0.0041	8
6	754.457			782.4519			764.4413			V	853.3985	853.3932	-0.0053	427.2029	427.1967	-0.0062	7
7	841.489			869.4839			851.4734			S	754.3301	754.328	-0.002	377.6687	377.664	-0.0047	6
8	969.5476			997.5425			979.5319			Q	667.298	667.2953	-0.0027	334.1527	334.1502	-0.0025	5
9	1116.616			1144.6109			1126.6004			F	539.2395	539.2367	-0.0028	270.1234	270.1241	0.0007	4
10	1173.6375			1201.6324			1183.6218			G	392.1711	392.1692	-0.0019	196.5892			3
11	1333.6681			1361.663			1343.6525			C	335.1496	335.1479	-0.0017	168.0784			2
12										R	175.119			88.0631			1

Supplemental Table 4. Fragment ion series of mass spectra from acetylated Lys805 peptide.

#	a calc.	a obs.	a delta	b calc.	b obs.	b delta	b-18 calc.	b-18 obs.	b-18 delta	Seq.	y calc.	y obs.	y delta	y++ calc.	y++ obs.	y++ delta	#
1	86.0964			114.0913			96.0808			I							10
2	173.1285			201.1234			183.1128			S	1208.5656	1208.5888	0.0232	604.7864			9
3	359.2078	359.2091	0.0013	387.2027	387.1984	-0.0042	369.1921	369.1891	-0.0031	W	1121.5336	1121.5592	0.0256	561.2704			8
4	472.2918	472.2934	0.0016	500.2867	500.2866	-0.0002	482.2762			I	935.4543	935.4616	0.0073	468.2308			7
5	569.3446			597.3395			579.3289			P	822.3702	822.3776	0.0074	411.6887	411.6924	0.0036	6
6	716.413			744.4079			726.3973			F	725.3174	725.3282	0.0107	363.1624			5
7	847.4535			875.4484			857.4378			M	578.249	578.2581	0.009	289.6282			4
8	976.4961			1004.491			986.4804			Q	447.2086			224.1079			3
9	1105.5387			1133.5336			1115.523			E	318.166			159.5866			2
10										K	189.1234			95.0653			1

Supplemental Table 5. Fragment ion series of mass spectra from formylated Lys297 peptide.

#	a calc.	a obs.	a delta	b calc.	b obs.	b delta	b-18 calc.	b-18 obs.	b-18 delta	Seq.	y calc.	y obs.	y delta	y++ calc.	y++ obs.	y++ delta	#
1	86.0964			114.0913			96.0808			L							9
2	233.1648	233.1635	-0.0014	261.1597	261.1567	-0.0031	243.1492			F	965.5203	965.5163	-0.004	483.2638			8
3	346.2489			374.2438			356.2332			L	818.4519	818.4503	-0.0016	409.7296			7
4	403.2704	403.2642	-0.0061	431.2653			413.2547			G	705.3678	705.3676	-0.0002	353.1876	353.1834	-0.0042	6
5	500.3231			528.318			510.3075			P	648.3464	648.3451	-0.0013	324.6768	324.6788	0.002	5
6	663.3864			691.3814			673.3708			Y	551.2936	551.2972	0.0036	276.1504			4
7	819.4763			847.4712			829.4607			K	388.2303	388.2242	-0.0061	194.6188			3
8	876.4978			904.4927			886.4821			G	232.1404			116.5738			2
9										R	175.119			88.0631			1

Supplemental Table 6. Fragment ion series of mass spectra from formylated Lys893 peptide.

#	a calc.	a obs.	a delta	b calc.	b obs.	b delta	b-18 calc.	b-18 obs.	b-18 delta	Seq.	y calc.	y obs.	y delta	y++ calc.	y++ obs.	y++ delta	#
1	86.0964			114.0913			96.0808			I							7
2	199.1805	199.183	0.0025	227.1754	227.1735	-0.0019	209.1648			L	814.3981	814.3996	0.0015	407.7027			6
3	328.2231			356.218			338.2074			E	701.3141	701.3176	0.0035	351.1607			5
4	475.2915			503.2864			485.2758			F	572.2715	572.265	-0.0064	286.6394			4
5	638.3548			666.3497			648.3392			Y	425.2031	425.2002	-0.0029	213.1052			3
6	725.3868			753.3818			735.3712	735.3912	0.02	S	262.1397	262.14	0.0003	131.5735			2
7										K	175.1077			88.0575			1

Supplemental Table 7. Fragment ion series of mass spectra from O-GlcNAcylated Thr346 peptide.

#	a calc.	a obs.	a delta	b calc.	b obs.	b delta	b-18 calc.	b-18 obs.	b-18 delta	Seq.	y calc.	y obs.	y delta	y++ calc.	y++ obs.	y++ delta	#
1	88.0393			116.0342			98.0237			D							17
2	187.1077			215.1026			197.0921			V	1970.9474			985.9773			16
3	286.1761			314.171	314.1609	-0.0101	296.1605			V	1871.879			936.4431			15
4	433.2115			461.2064			443.1959			M	1772.8106			886.9089			14
5	737.3386			765.3335	765.3178	-0.0157	747.3229			T	1625.7752			813.3912			13
6	852.3655			880.3604			862.3499	862.3284	-0.0214	D	1321.6482			661.3277			12
7	939.3975			967.3925			949.3819			S	1206.6212	1206.6213	0.0001	603.8142			11
8	1068.4401			1096.435			1078.4245			E	1119.5892			560.2982			10
9	1183.4671			1211.462			1193.4514			D	990.5466	990.5421	-0.0045	495.7769			9
10	1270.4991			1298.494			1280.4835			S	875.5197			438.2635			8
11	1371.5468			1399.5417			1381.5311			T	788.4876	788.4909	0.0033	394.7474			7
12	1470.6152			1498.6101			1480.5995			V	687.4399			344.2236	344.237	0.0134	6
13	1557.6472			1585.6421			1567.6316			S	588.3715	588.3682	-0.0033	294.6894			5
14	1670.7313			1698.7262			1680.7156			I	501.3395	501.3279	-0.0116	251.1734			4
15	1798.7899			1826.7848			1808.7742			Q	388.2554	388.2561	0.0006	194.6314			3
16	1911.8739			1939.8688			1921.8583			I	260.1969	260.1967	-0.0002	130.6021			2
17										K	147.1128			74.06			1

Supplemental Table 8. Fragment ion series of mass spectra from O-GlcNAcylated Ser354 peptide.

#	a calc.	a obs.	a delta	b calc.	b obs.	b delta	b-18 calc.	b-18 obs.	b-18 delta	Seq.	y calc.	y obs.	y delta	y++ calc.	y++ obs.	y++ delta	#
1	88.0393			116.0342			98.0237			D							17
2	187.1077			215.1026			197.0921			V	1970.9474			985.9773			16
3	286.1761			314.171			296.1605	296.1571	-0.0034	V	1871.879			936.4431			15
4	433.2115			461.2064	461.1902	-0.0162	443.1959			M	1772.8106			886.9089			14
5	534.2592			562.2541	562.2681	0.014	544.2436			T	1625.7752			813.3912			13
6	649.2861			677.2811	677.2795	-0.0016	659.2705			D	1524.7275			762.8674			12
7	736.3182			764.3131			746.3025			S	1409.7006			705.3539			11
8	865.3608			893.3557	893.3476	-0.0081	875.3451			E	1322.6686			661.8379			10
9	980.3877			1008.3826			990.3721			D	1193.626			597.3166			9
10	1067.4197			1095.4146			1077.4041			S	1078.599			539.8031			8
11	1168.4674			1196.4623			1178.4518			T	991.567	991.5449	-0.0221	496.2871			7
12	1267.5358			1295.5307			1277.5202	1277.5149	-0.0052	V	890.5193			445.7633			6
13	1557.6472			1585.6421			1567.6316			S	791.4509			396.2291			5
14	1670.7313			1698.7262			1680.7156			I	501.3395			251.1734			4
15	1798.7899			1826.7848			1808.7742			Q	388.2554	388.2532	-0.0022	194.6314			3
16	1911.8739			1939.8688			1921.8583			I	260.1969			130.6021			2
17										K	147.1128			74.06			1

Supplemental Table 9. Fragment ion series of mass spectra from N-ubiquitinated Lys497 peptide.

#	a calc.	a obs.	a delta	b calc.	b obs.	b delta	b++ calc.	b++ obs.	b++ delta	Seq.	y calc.	y obs.	y delta	y++ calc.	y++ obs.	y++ delta	#
1	104.0528			132.0478			66.5275			M							19
2	175.09			203.0849			102.0461			A	2135.0172			1068.0122			18
3	304.1325			332.1275			166.5674			E	2063.9801			1032.4937			17
4	433.1751			461.17			231.0887			E	1934.9375			967.9724			16
5	546.2592			574.2541			287.6307			L	1805.8949			903.4511	903.4276	-0.0235	15
6	788.3971			816.392			408.6996			K	1692.8109			846.9091			14
7	885.4498			913.4448			457.226			P	1450.673			725.8401			13
8	1016.4903			1044.4852			522.7463			M	1353.6202			677.3137	677.3246	0.0109	12
9	1131.5173			1159.5122			580.2597			D	1222.5797	1222.5854	0.0057	611.7935	611.7944	0.0009	11
10	1232.5649			1260.5599			630.7836			T	1107.5528	1107.5622	0.0094	554.28	554.2744	-0.0056	10
11	1347.5919			1375.5868			688.297			D	1006.5051	1006.5058	0.0007	503.7562	503.7531	-0.0031	9
12	1475.6868			1503.6818			752.3445			K	891.4782	891.4658	-0.0123	446.2427			8
13	1604.7294			1632.7243			816.8658			E	763.3832	763.3694	-0.0138	382.1952			7
14	1691.7615			1719.7564			860.3818			S	634.3406	634.3441	0.0034	317.6739			6
15	1804.8455			1832.8404			916.9239			I	547.3086	547.3073	-0.0013	274.1579			5
16	1875.8826			1903.8775			952.4424			A	434.2245	434.2194	-0.0052	217.6159			4
17	2004.9252			2032.9201			1016.9637			E	363.1874	363.183	-0.0045	182.0973			3
18	2091.9573			2119.9522			1060.4797			S	234.1448	234.1478	0.003	117.5761			2
19										K	147.1128			74.06			1

Supplemental Table 10. Fragment ion series of mass spectra from O-ubiquitinated Ser515 peptide.

#	a calc.	a obs.	a delta	b calc.	b obs.	b delta	b++ calc.	b++ obs.	b++ delta	Seq.	y calc.	y obs.	y delta	y++ calc.	y++ obs.	y++ delta	#
1	60.0444			88.0393			44.5233			S							25
2	157.0972			185.0921			93.0497			P	2928.2002			1464.6037			24
3	286.1397	286.1367	-0.0031	314.1347	314.1301	-0.0046	157.571			E	2831.1474			1416.0773			23
4	417.1802	417.1868	0.0066	445.1751			223.0912			M	2702.1048			1351.556			22
5	618.2552			646.2501	646.2548	0.0047	323.6287			S	2571.0643			1286.0358			21
6	749.2957			777.2906			389.1489			M	2369.9894			1185.4983			20
7	877.3542			905.3492	905.3553	0.0062	453.1782			Q	2238.9489			1119.9781			19
8	1006.3968			1034.3917			517.6995			E	2110.8903			1055.9488			18
9	1121.4238			1149.4187			575.213			D	1981.8477			991.4275			17
10	1281.4544			1309.4493			655.2283			C	1866.8208			933.914	933.9101	-0.004	16
11	1394.5385			1422.5334			711.7703			I	1706.7901			853.8987	853.9253	0.0265	15
12	1481.5705			1509.5654			755.2863	755.3037	0.0173	S	1593.7061			797.3567	797.3519	-0.0047	14
13	1596.5974			1624.5924			812.7998			D	1506.6741			753.8407			13
14	1709.6815			1737.6764			869.3418			I	1391.6471			696.3272			12
15	1780.7186			1808.7135			904.8604			A	1278.5631			639.7852	639.7825	-0.0026	11
16	1877.7714			1905.7663			953.3868			P	1207.5259	1207.5258	-0.0002	604.2666	604.2647	-0.0019	10
17	2024.8068			2052.8017			1026.9045			M	1110.4732	1110.4827	0.0095	555.7402			9
18	2152.8654			2180.8603			1090.9338			Q	963.4378	963.439	0.0013	482.2225	482.2222	-0.0003	8
19	2253.913			2281.9079			1141.4576			T	835.3792	835.3736	-0.0056	418.1932	418.1956	0.0024	7
20	2368.94			2396.9349			1198.9711			D	734.3315	734.3222	-0.0093	367.6694			6
21	2497.9826			2525.9775			1263.4924			E	619.3046	619.2951	-0.0095	310.1559			5
22	2626.0411			2654.0361			1327.5217			Q	490.262	490.2578	-0.0042	245.6346			4
23	2727.0888			2755.0837			1378.0455			T	362.2034	362.2053	0.0019	181.6053			3
24	2841.1318			2869.1267			1435.067			N	261.1557	261.1527	-0.0031	131.0815			2
25										K	147.1128			74.06			1

Supplemental Table 11. Fragment ion series of mass spectra from O-ubiquitinated Ser522 peptide.

#	a calc.	a obs.	a delta	b calc.	b obs.	b delta	b++ calc.	b++ obs.	b++ delta	Seq.	y calc.	y obs.	y delta	y++ calc.	y++ obs.	y++ delta	#
1	60.0444			88.0393			44.5233			S							25
2	157.0972			185.0921			93.0497			P	2928.2002			1464.6037			24
3	286.1397			314.1347			157.571			E	2831.1474			1416.0773			23
4	417.1802			445.1751			223.0912			M	2702.1048			1351.556			22
5	504.2123			532.2072			266.6072			S	2571.0643			1286.0358			21
6	635.2527			663.2476			332.1275			M	2484.0323			1242.5198			20
7	763.3113			791.3062	791.3231	0.0169	396.1568			Q	2352.9918			1176.9995			19
8	892.3539			920.3488			460.678			E	2224.9332			1112.9703			18
9	1007.3808			1035.3758			518.1915			D	2095.8907			1048.449			17
10	1167.4115			1195.4064			598.2068			C	1980.8637			990.9355			16
11	1280.4955			1308.4905			654.7489			I	1820.8331			910.9202			15
12	1481.5705			1509.5654			755.2863			S	1707.749			854.3781			14
13	1596.5974			1624.5924			812.7998			D	1506.6741			753.8407			13
14	1709.6815			1737.6764			869.3418			I	1391.6471			696.3272			12
15	1780.7186			1808.7135			904.8604			A	1278.5631	1278.5622	-0.0008	639.7852			11
16	1877.7714			1905.7663			953.3868			P	1207.5259	1207.5212	-0.0047	604.2666	604.2566	-0.01	10
17	2024.8068			2052.8017			1026.9045			M	1110.4732			555.7402			9
18	2152.8654			2180.8603			1090.9338			Q	963.4378	963.4367	-0.0011	482.2225			8
19	2253.913			2281.9079			1141.4576			T	835.3792	835.3679	-0.0113	418.1932			7
20	2368.94			2396.9349			1198.9711			D	734.3315	734.3225	-0.009	367.6694			6
21	2497.9826			2525.9775			1263.4924			E	619.3046	619.2927	-0.0119	310.1559			5
22	2626.0411			2654.0361			1327.5217			Q	490.262	490.2635	0.0015	245.6346			4
23	2727.0888			2755.0837			1378.0455			T	362.2034			181.6053			3
24	2841.1318			2869.1267			1435.067			N	261.1557			131.0815			2
25										K	147.1128			74.06			1

Brain permeability in vivo of compound 16

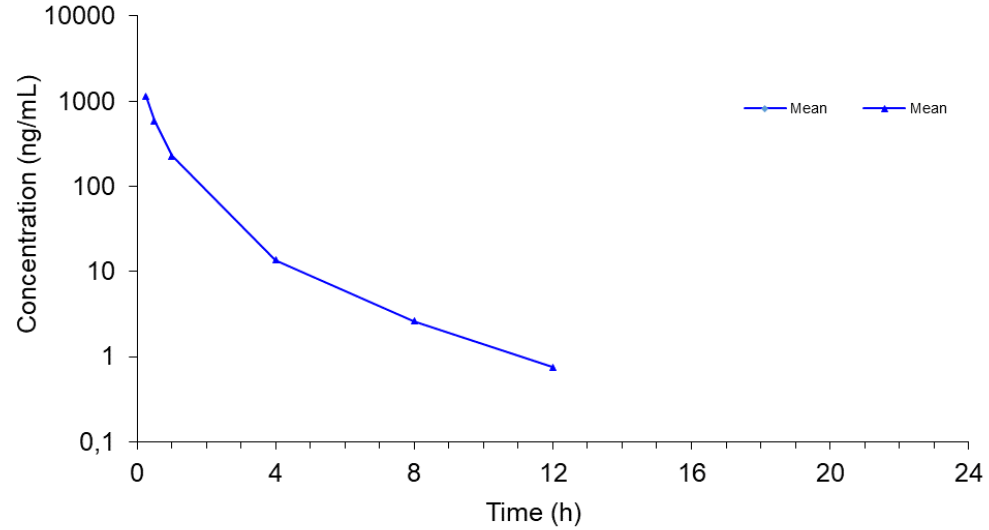

Supplemental Figure 24. Rat exposure in plasma from a single oral dose of **16** (3 mg/kg).

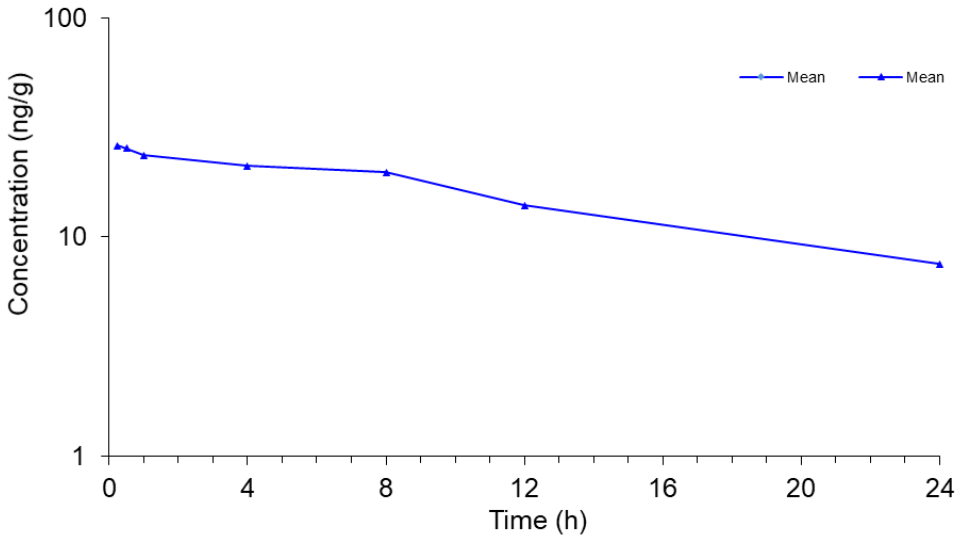

Supplemental Figure 25. Rat exposure in homogenized brain from a single oral dose of **16** (3 mg/kg).

Copies of ^{1}H and ^{13}C NMR and MS spectra

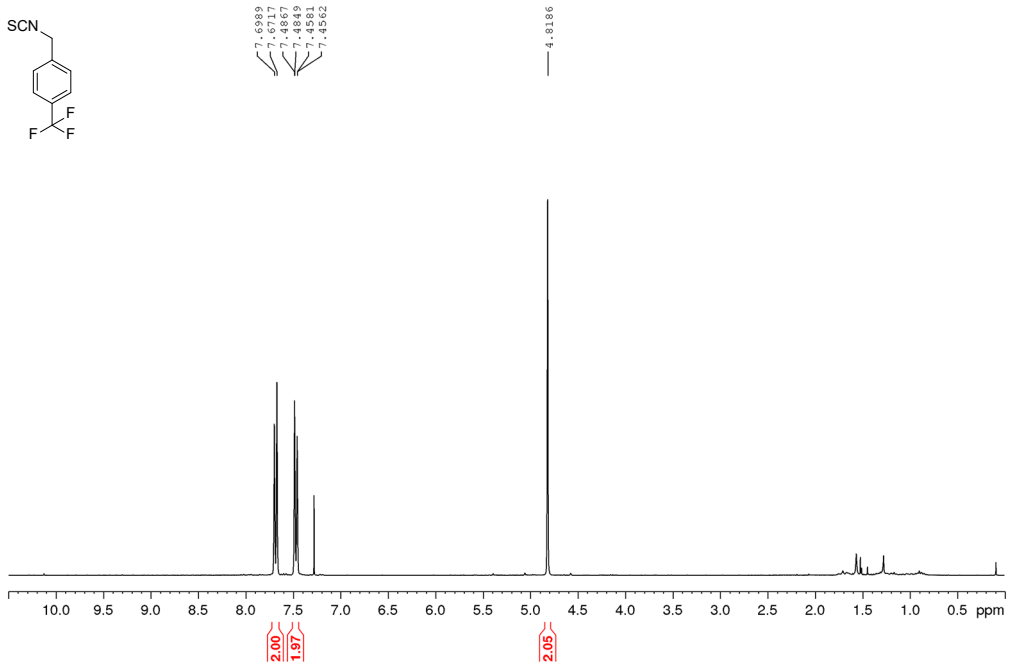

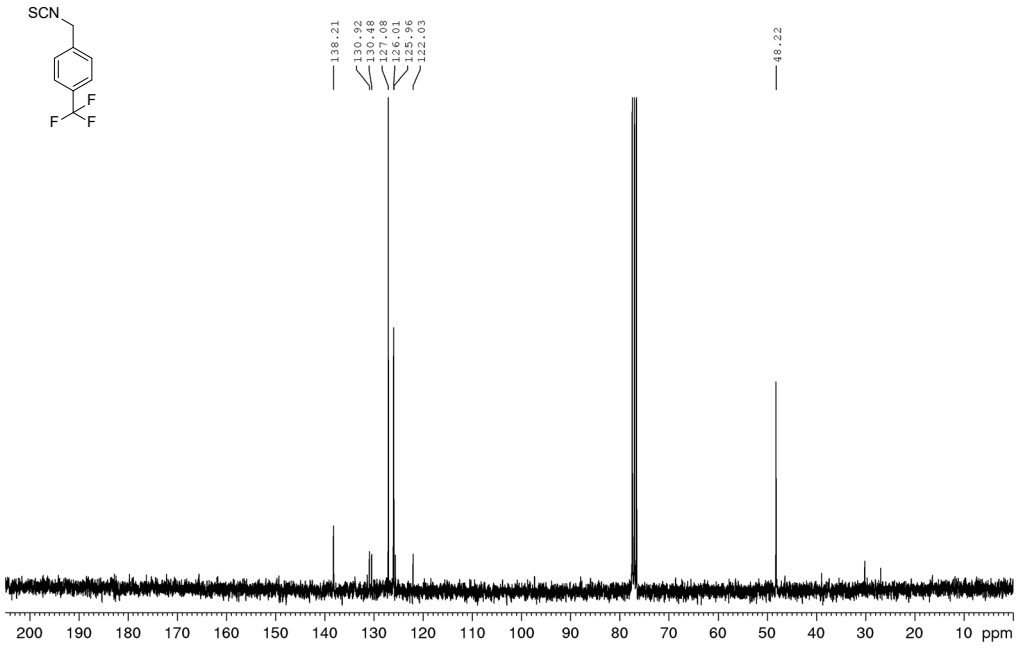

Supplemental Figure 26. ^{1}H NMR and ^{13}C NMR (300 MHz, 75.5 MHz $CDCl_3$) of **TFBNCS**

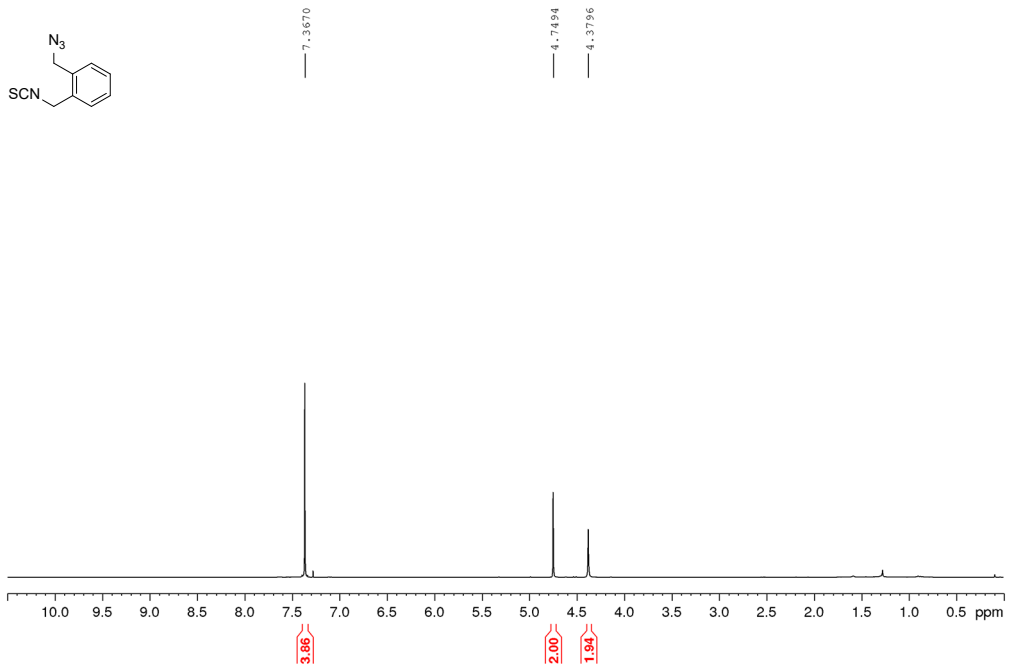

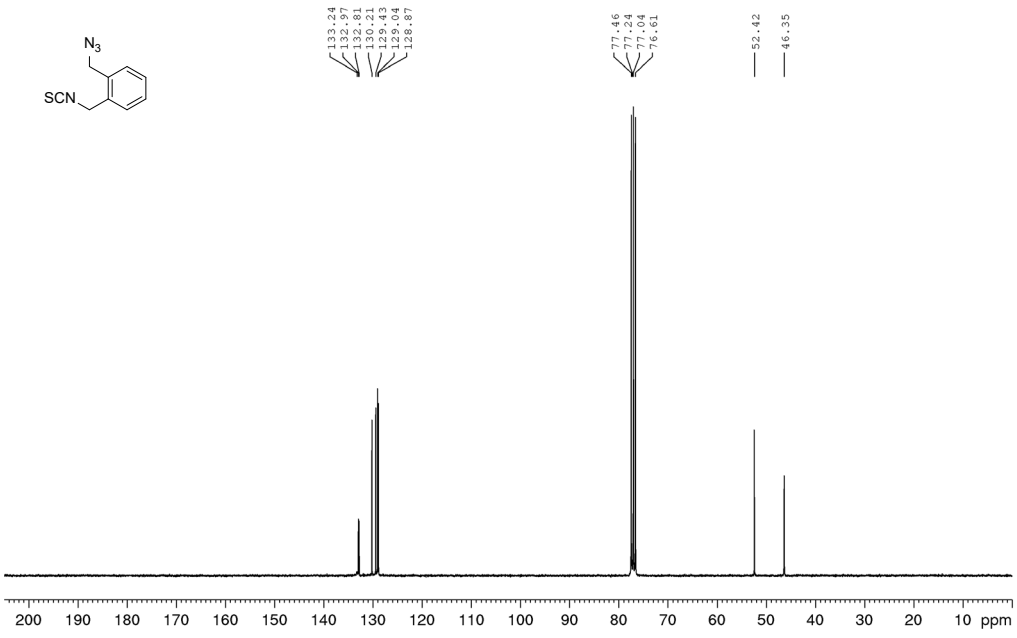

Supplemental Figure 27. ^{1}H NMR and ^{13}C NMR (300 MHz, 75.5 MHz $CDCl_3$) of ***o*-ABNCS**

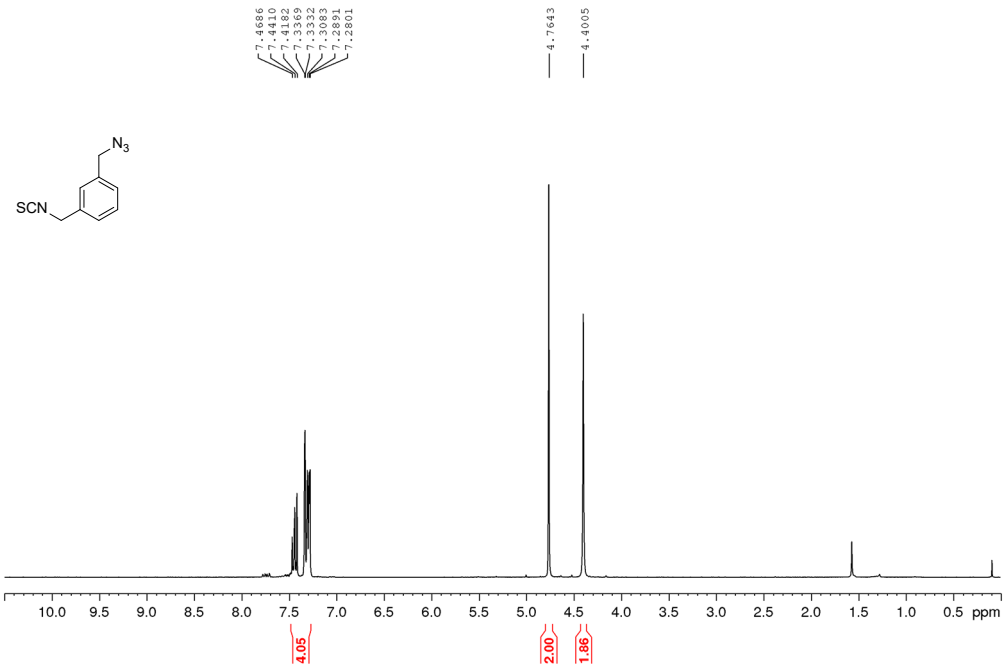

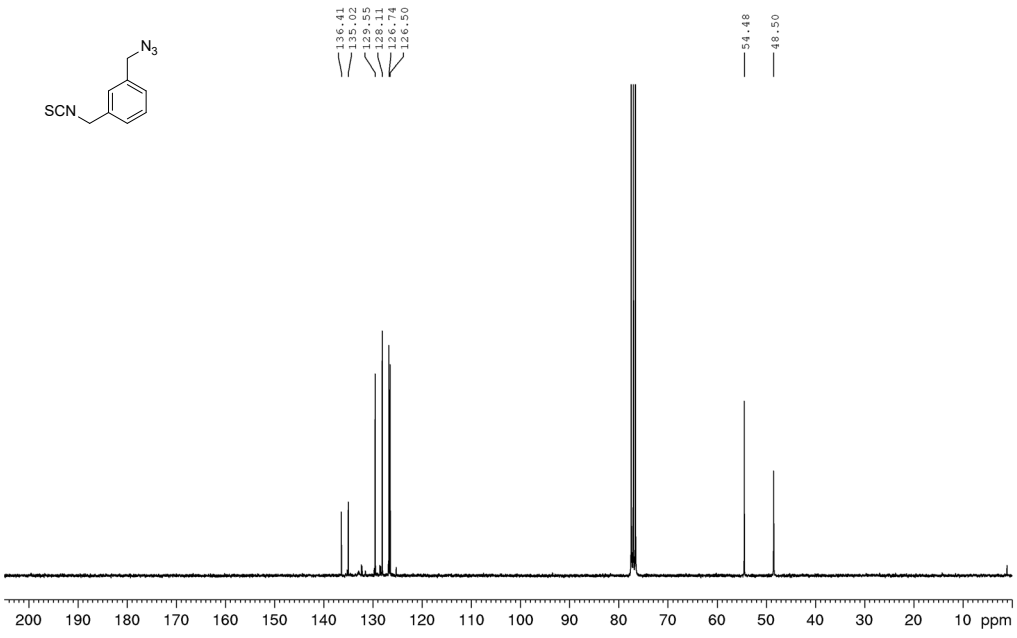

Supplemental Figure 28. ^{1}H NMR and ^{13}C NMR (300 MHz, 75.5 MHz $CDCl_3$) of ***m*-ABNCS**

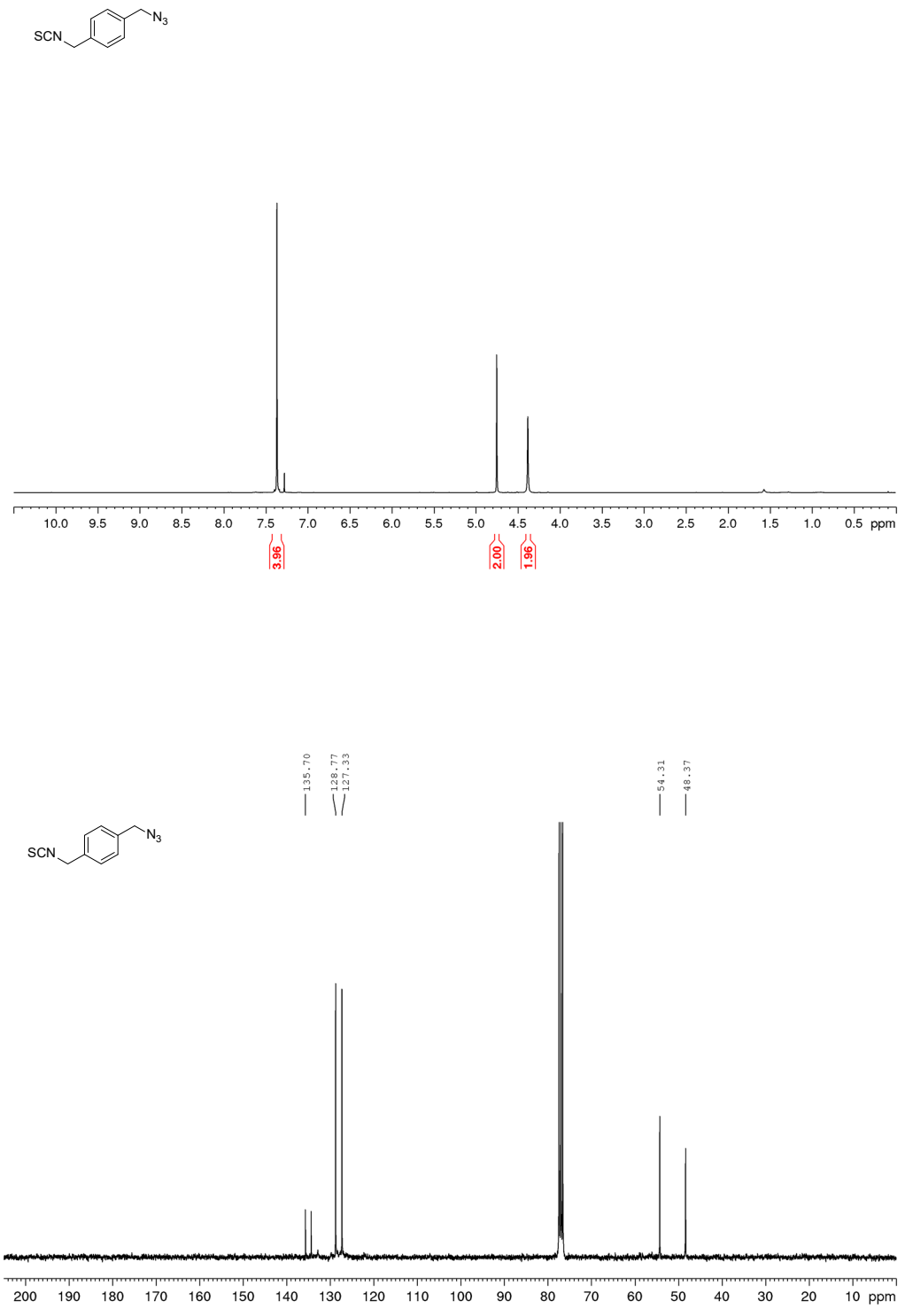

Supplemental Figure 29. ^{1}H NMR and ^{13}C NMR (300 MHz, 75.5 MHz $CDCl_3$) of ***p*-ABNCS**

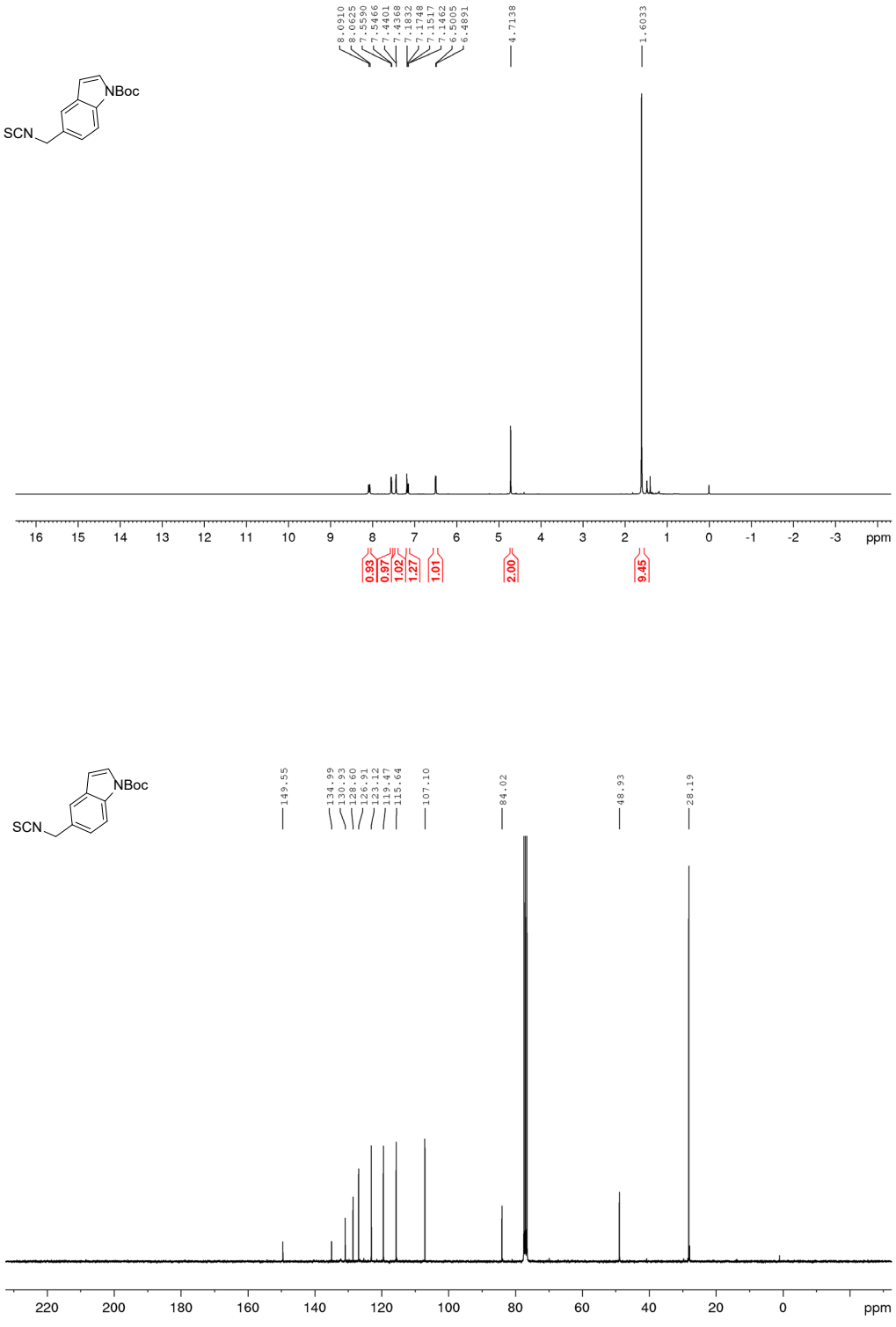

Supplemental Figure 30. ^{1}H NMR and ^{13}C NMR (300 MHz, 75.5 MHz CD_3OD) of **IBLCS**

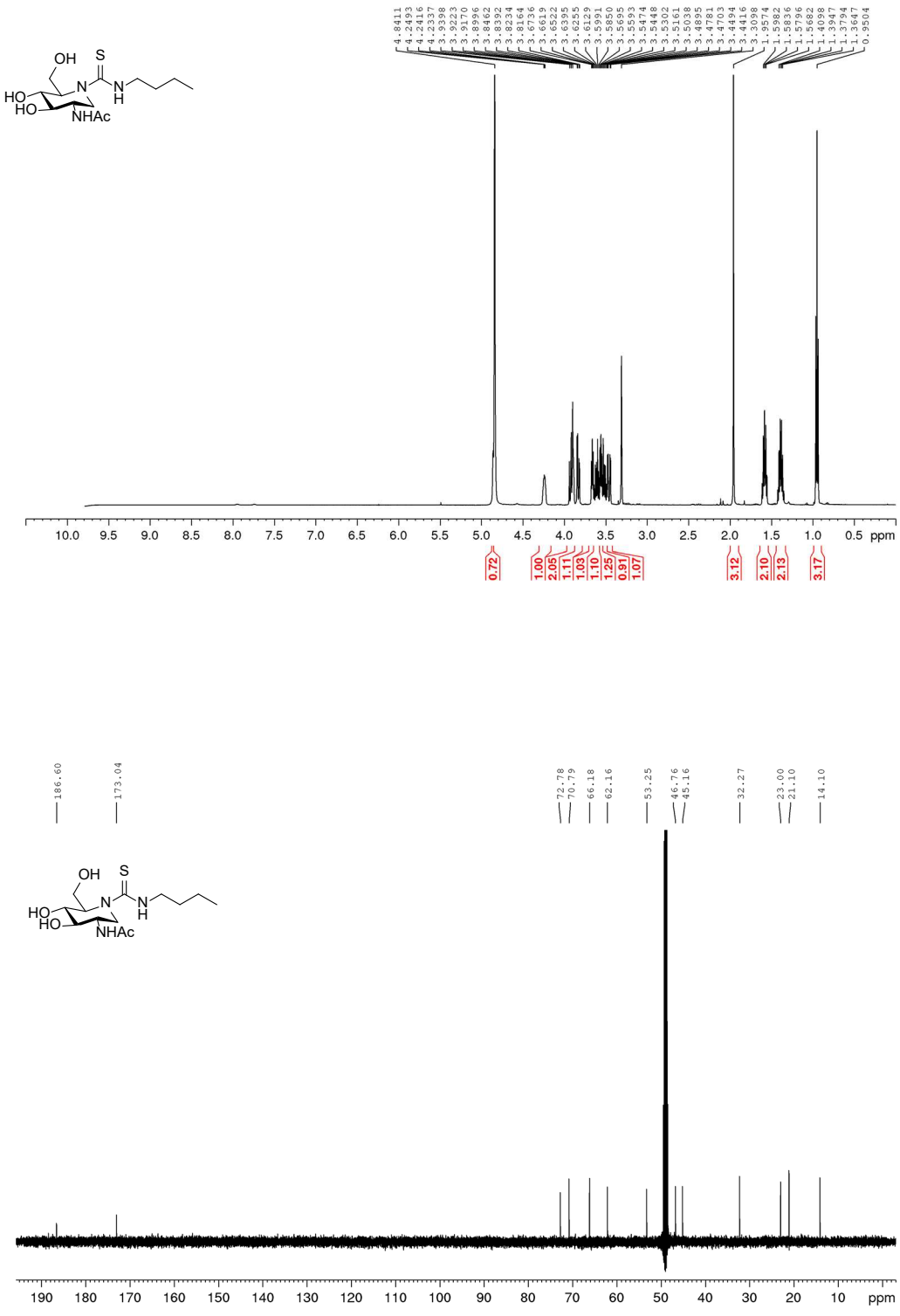

Supplemental Figure 31. ^{1}H NMR and ^{13}C NMR (500 MHz, 125.7 MHz CD_3OD) of **1**

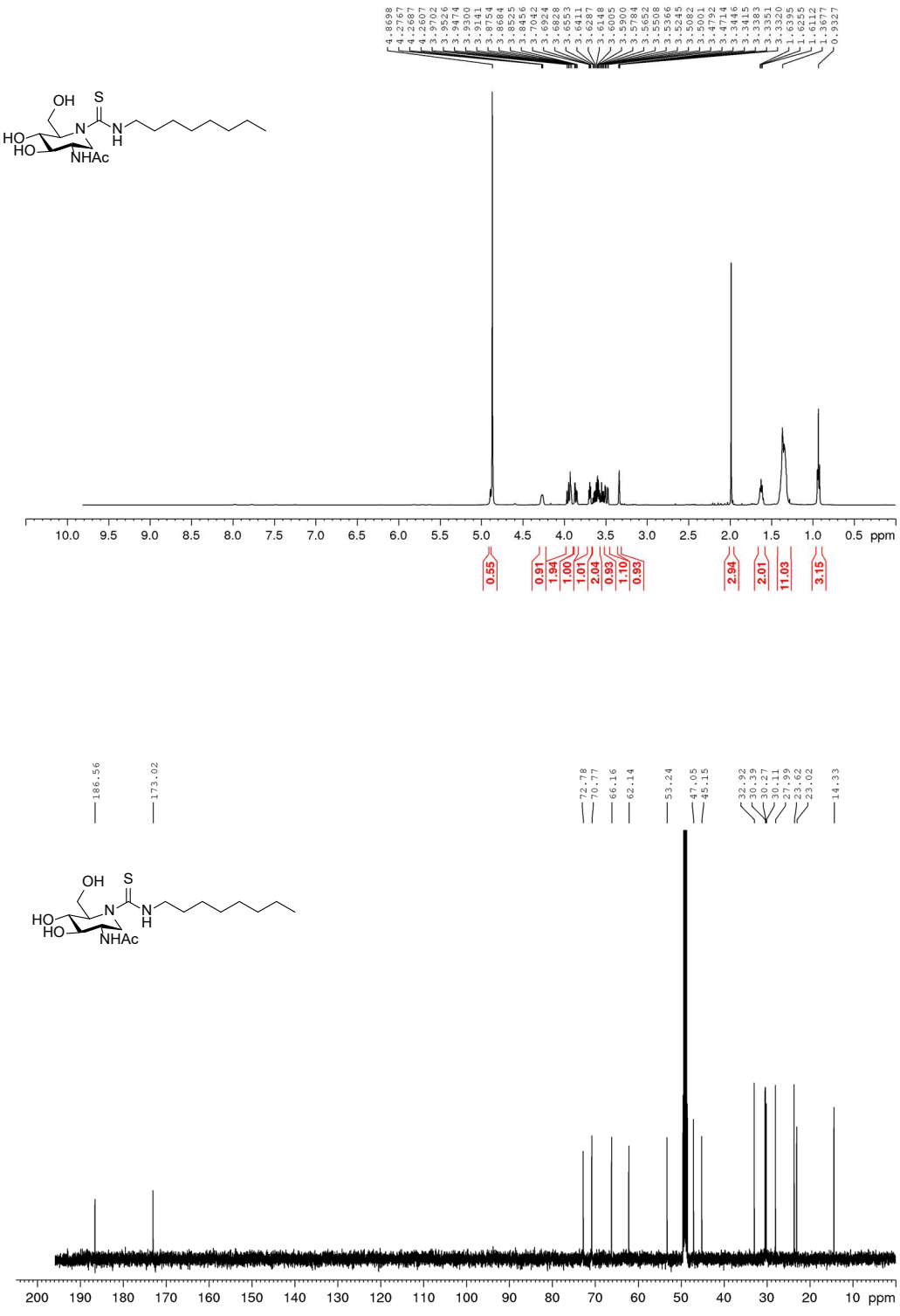

Supplemental Figure 32. ^{1}H NMR and ^{13}C NMR (500 MHz, 125.7 MHz CD_3OD) of **2**

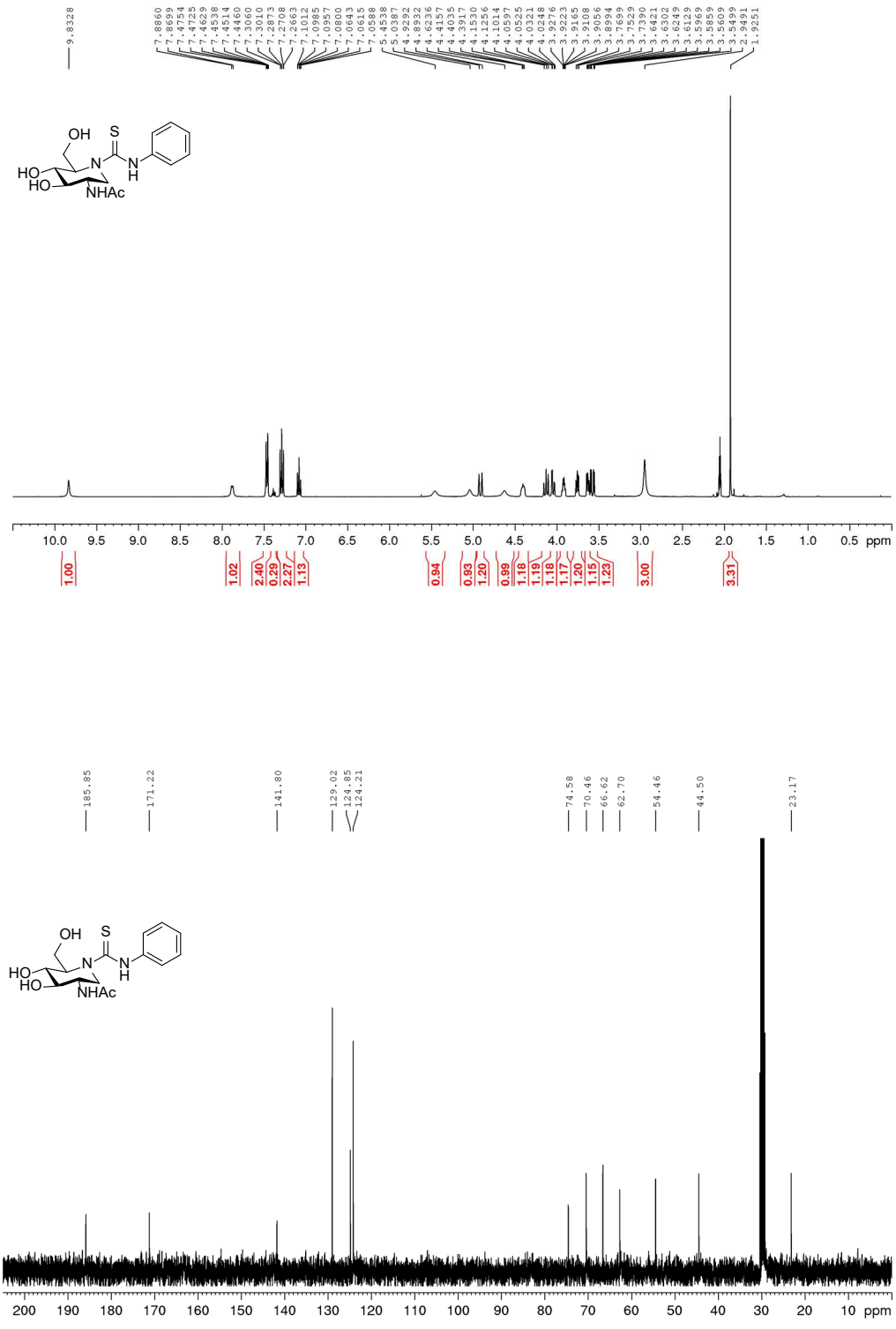

Supplemental Figure 33. ^{1}H NMR and ^{13}C NMR (400 MHz, 100.6 MHz acetone-d_6) of **3**

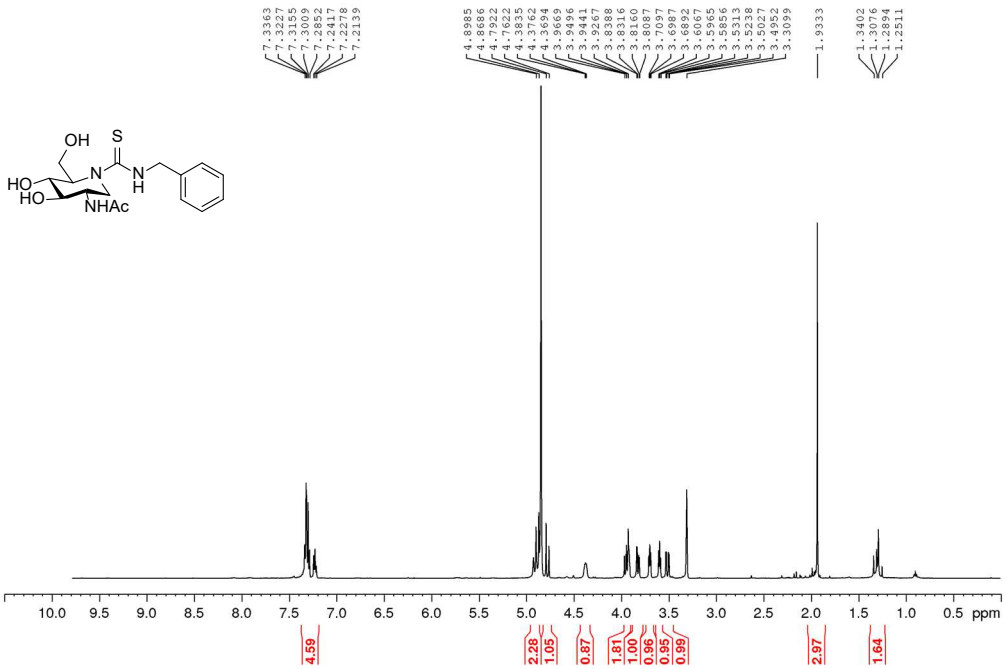

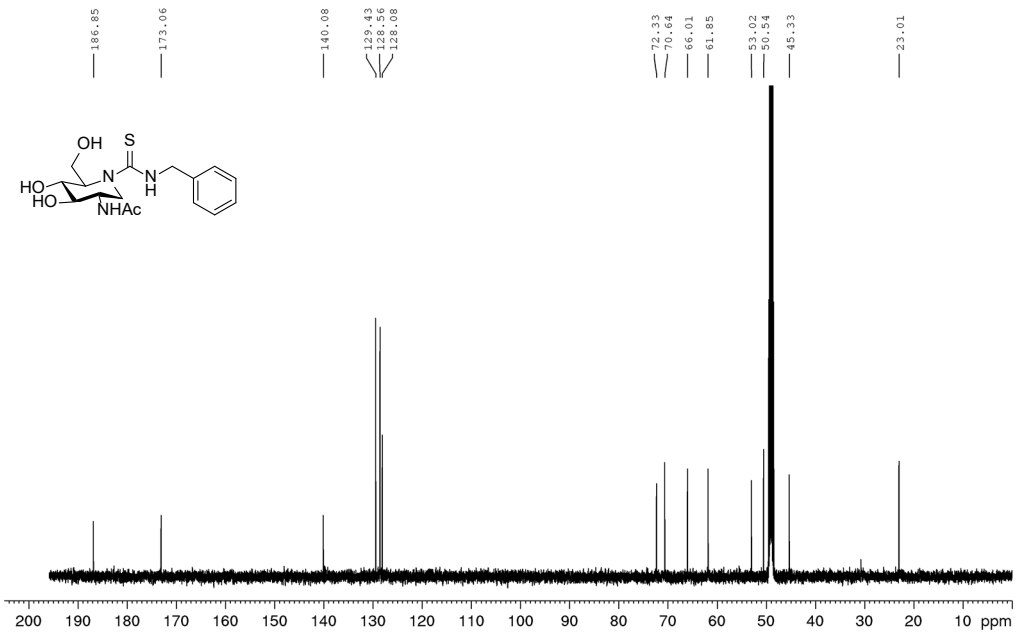

Supplemental Figure 34. ^{1}H NMR and ^{13}C NMR (500 MHz, 125.7 MHz CD_3OD) of **4**

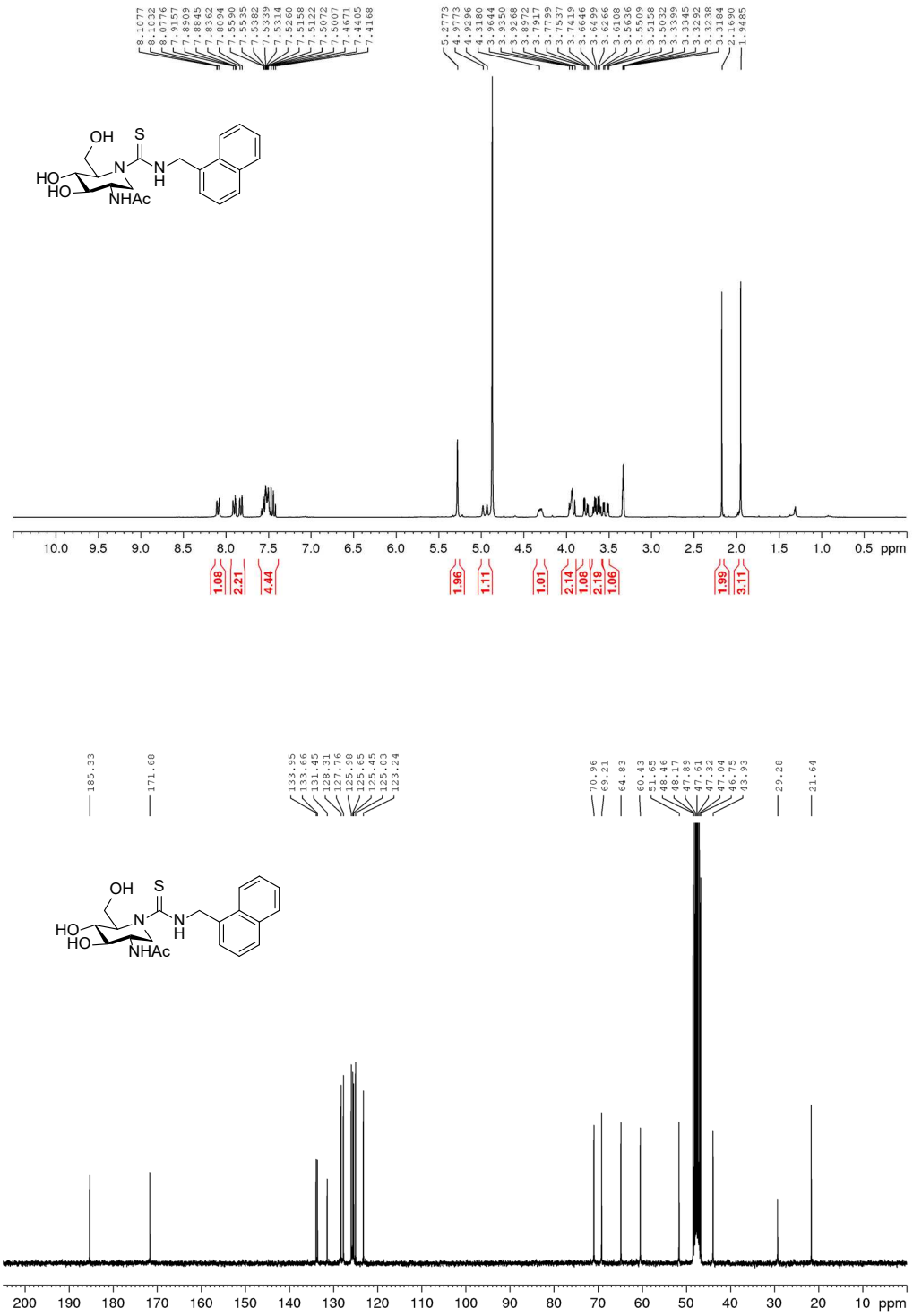

Supplemental Figure 35. ^{1}H NMR and ^{13}C NMR (300 MHz, 100.6 MHz CD_3OD) of **5**

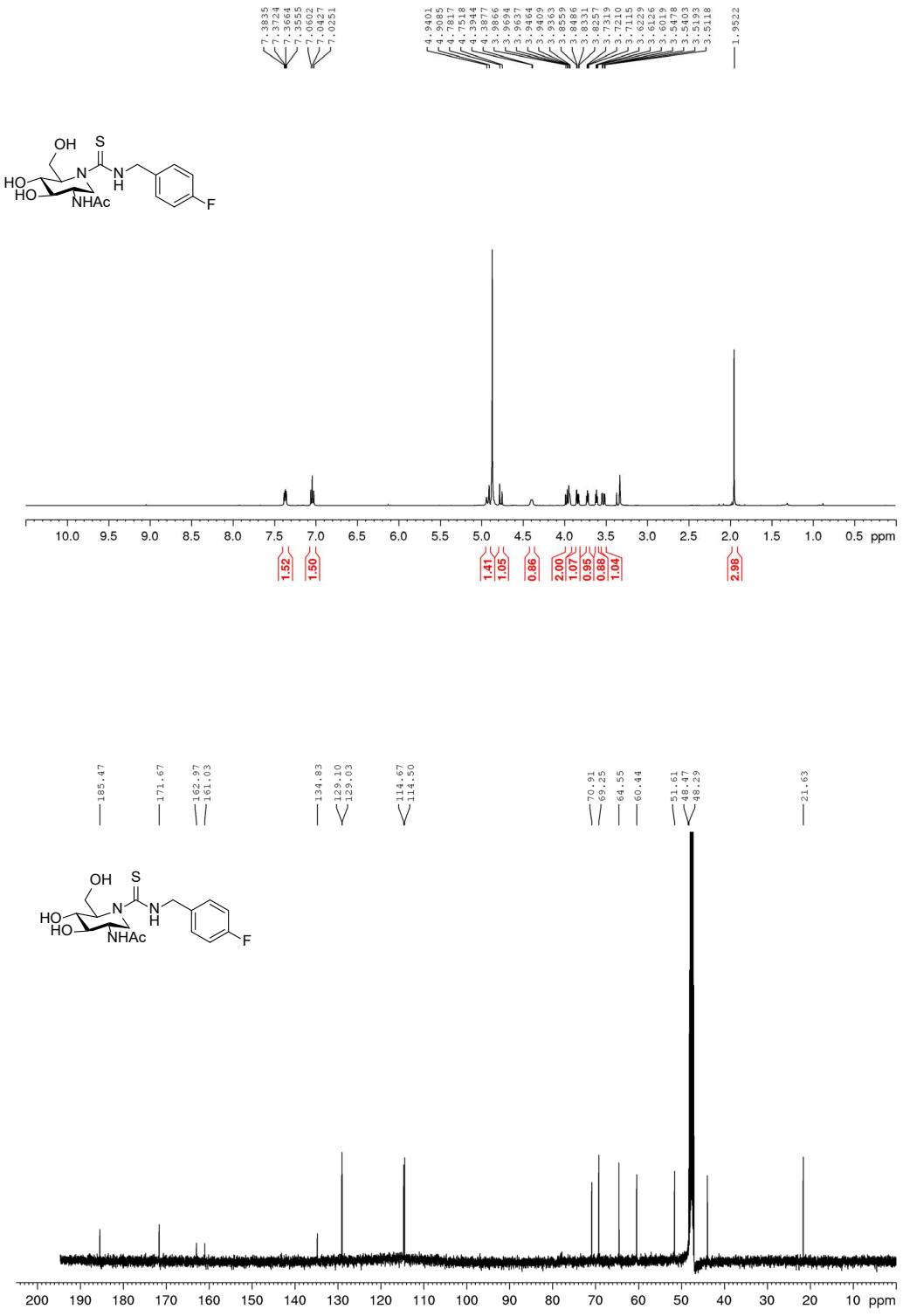

Supplemental Figure 36. ^{1}H NMR and ^{13}C NMR (500 MHz, 125.7 MHz CD_3OD) of **6**

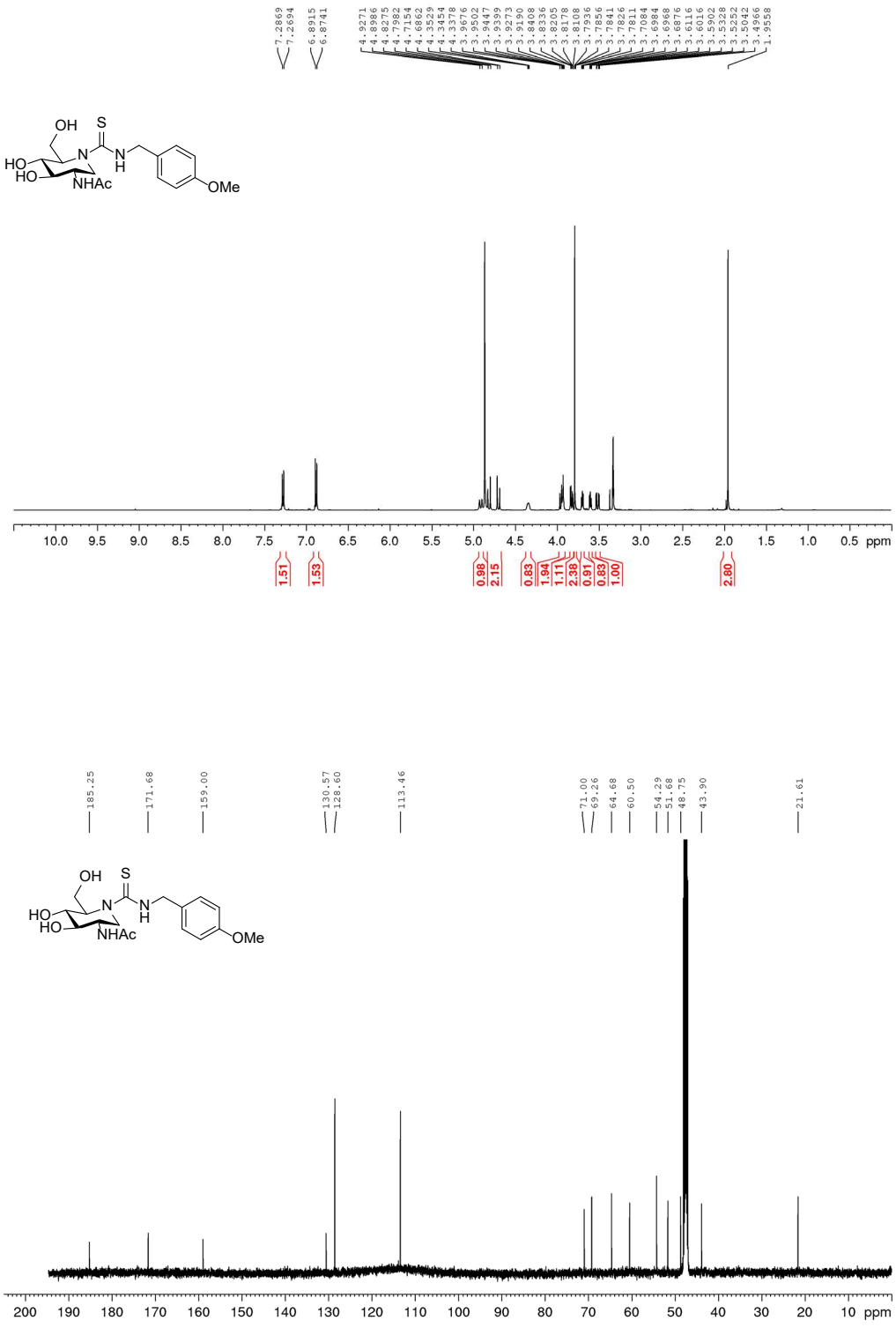

Supplemental Figure 37. ^{1}H NMR and ^{13}C NMR (500 MHz, 125.7 MHz CD_3OD) of **7**

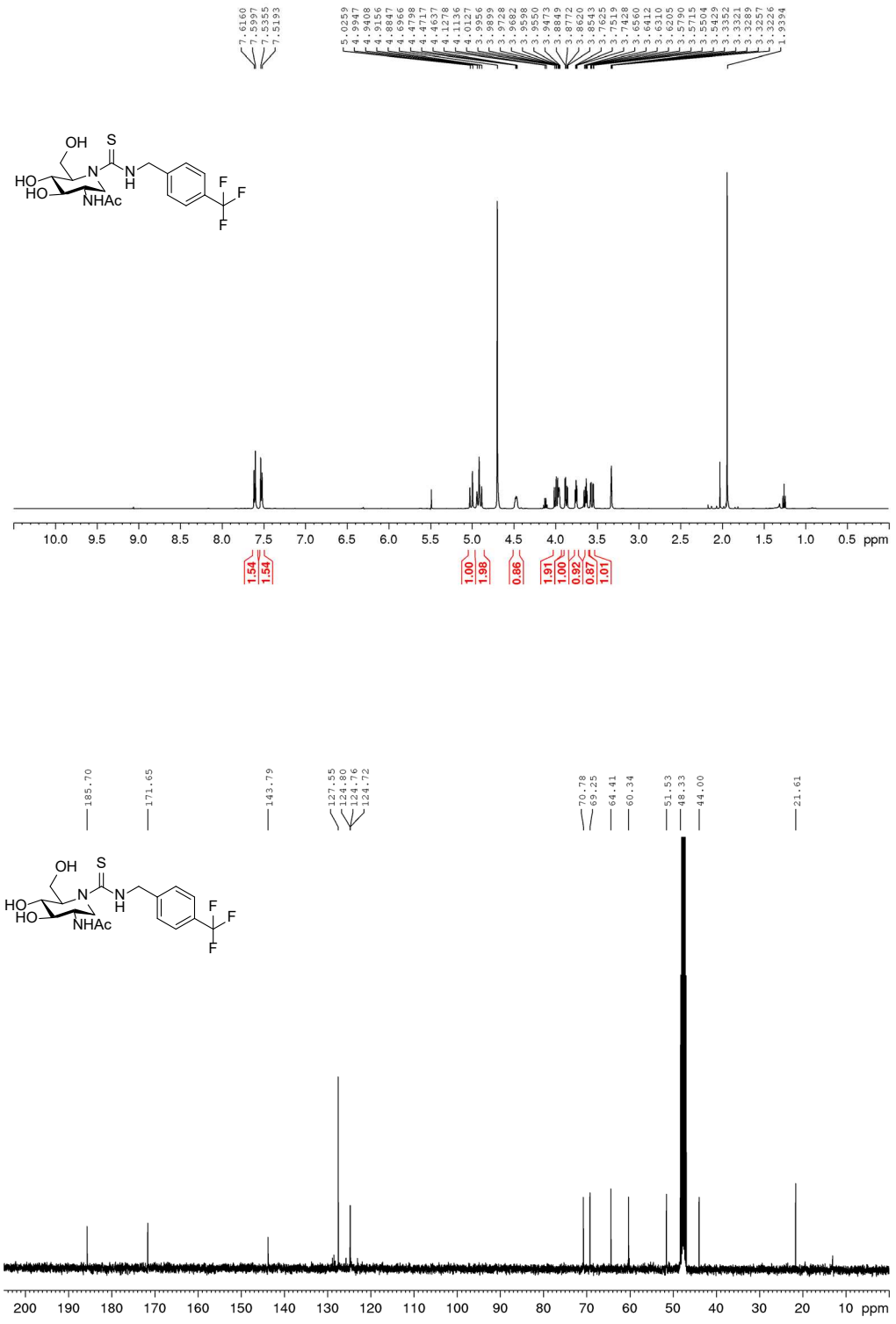

Supplemental Figure 38. ^{1}H NMR and ^{13}C NMR (500 MHz, 125.7 MHz CD_3OD) of **8**

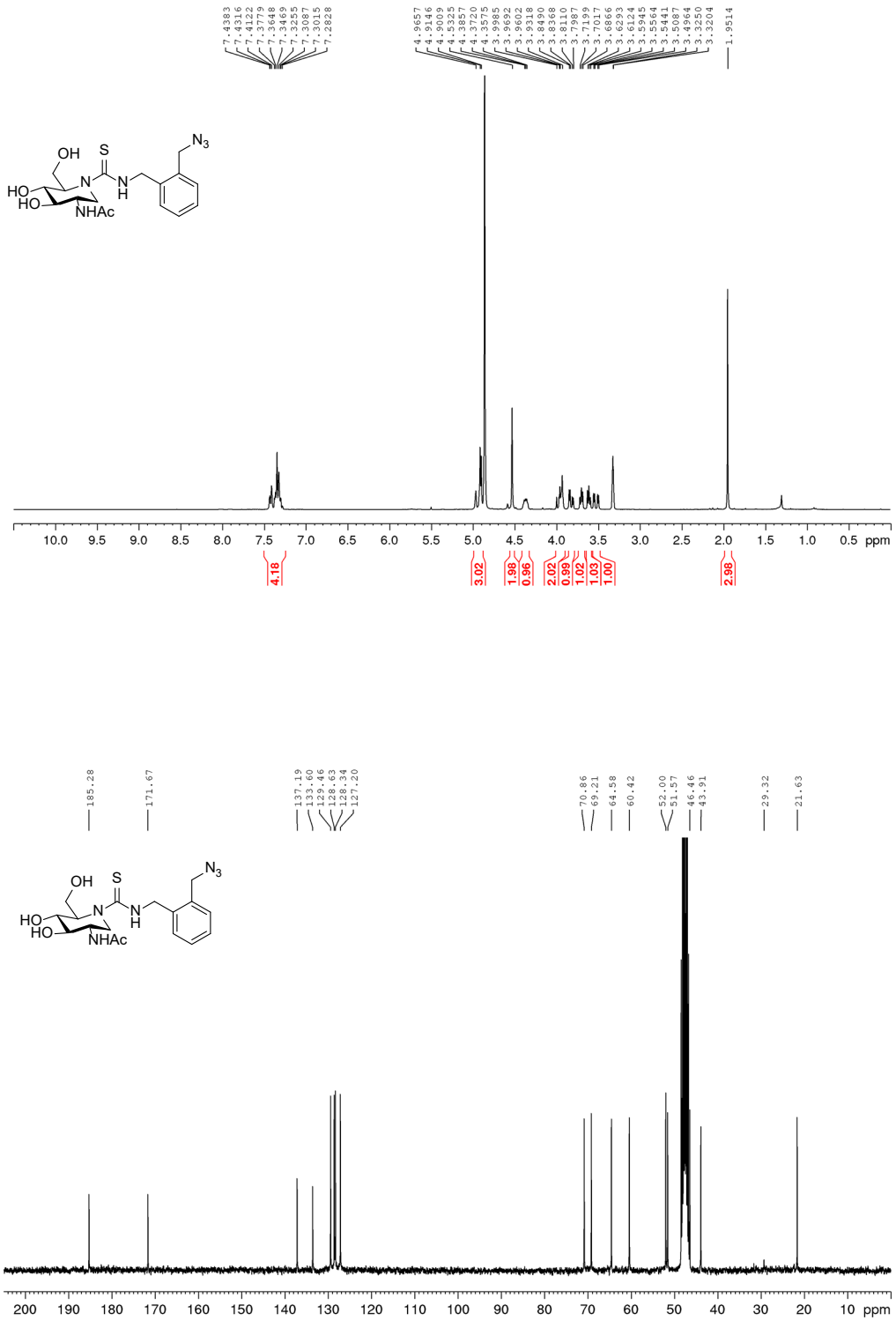

Supplemental Figure 39. ^{1}H NMR and ^{13}C NMR (300 MHz, 100.6 MHz CD_3OD) of **9**

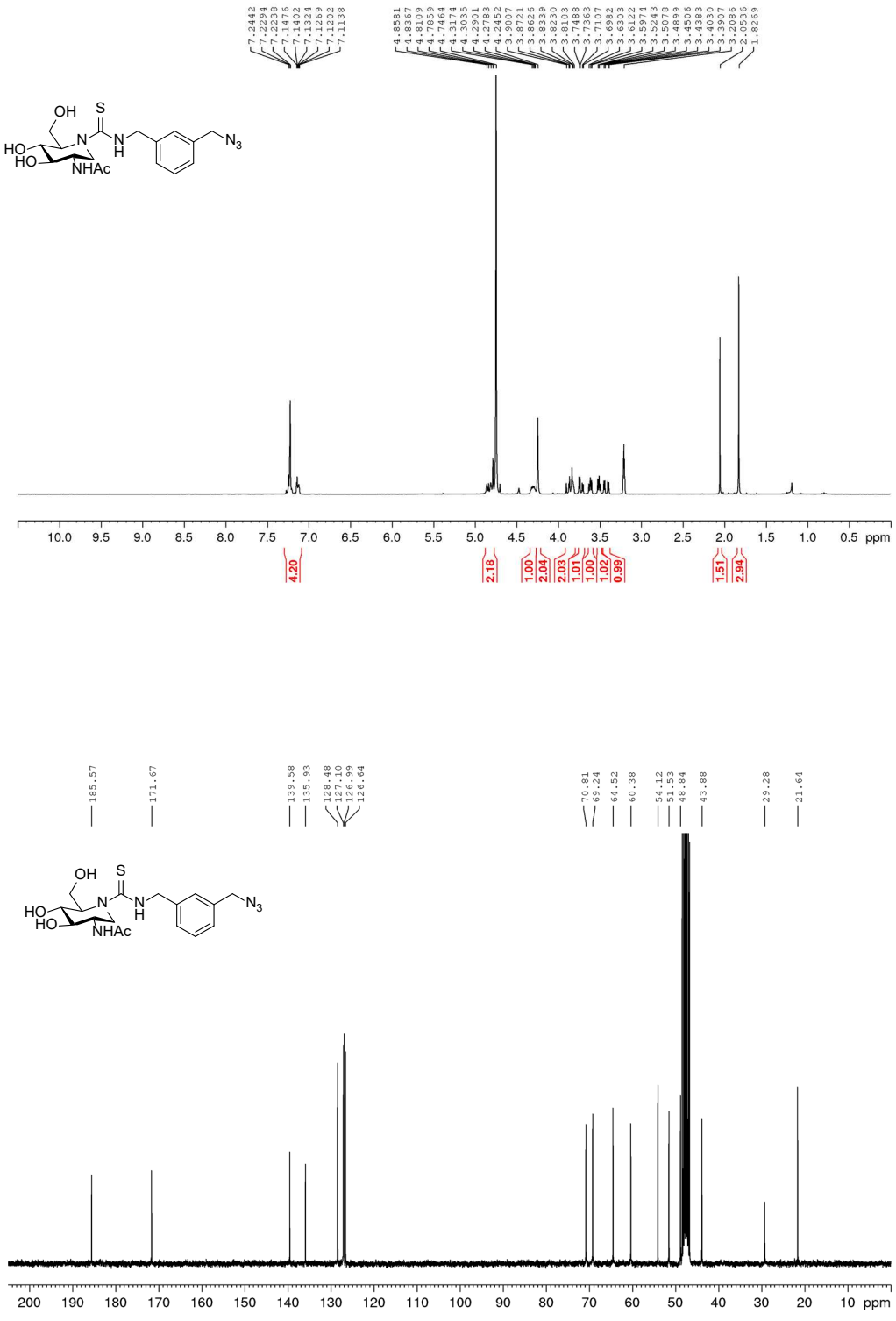

Supplemental Figure 40. ^{1}H NMR and ^{13}C NMR (300 MHz, 100.6 MHz CD_3OD) of **10**

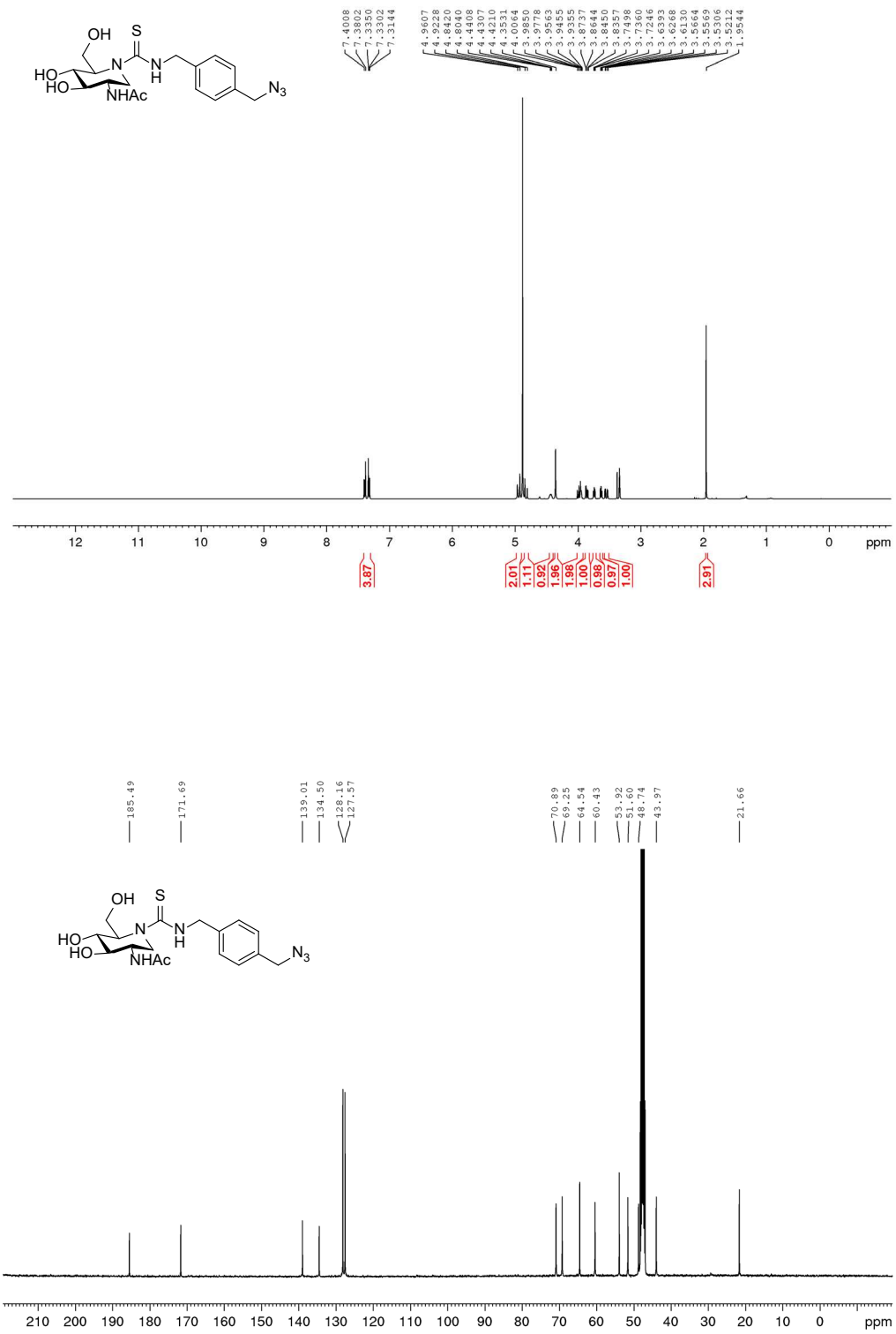

Supplemental Figure 41. ^{1}H NMR and ^{13}C NMR (400 MHz, 100.6 MHz CD_3OD) of **11**

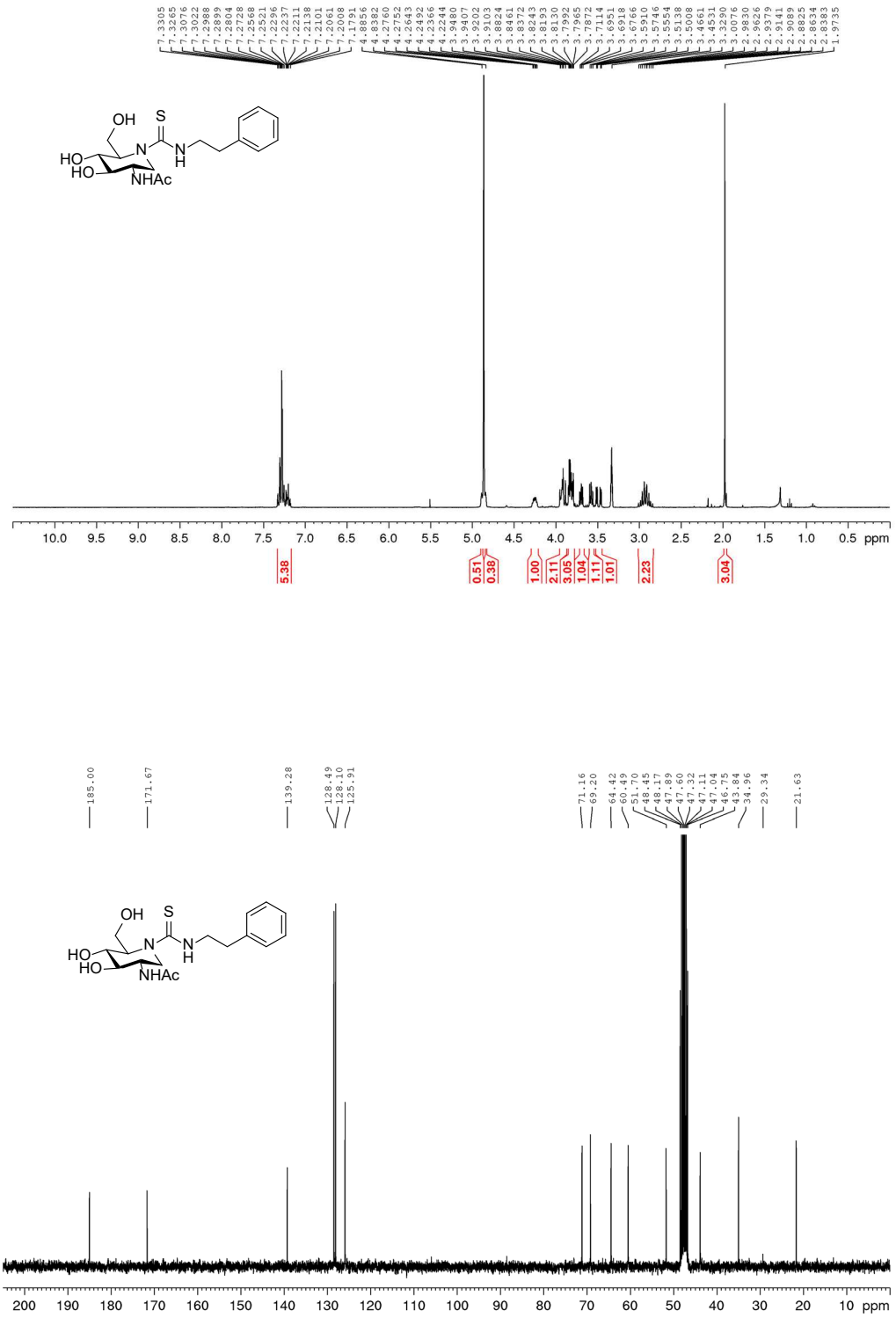

Supplemental Figure 42 ^{1}H NMR and ^{13}C NMR (300 MHz, 75.5 MHz CD_3OD) of 1**2**

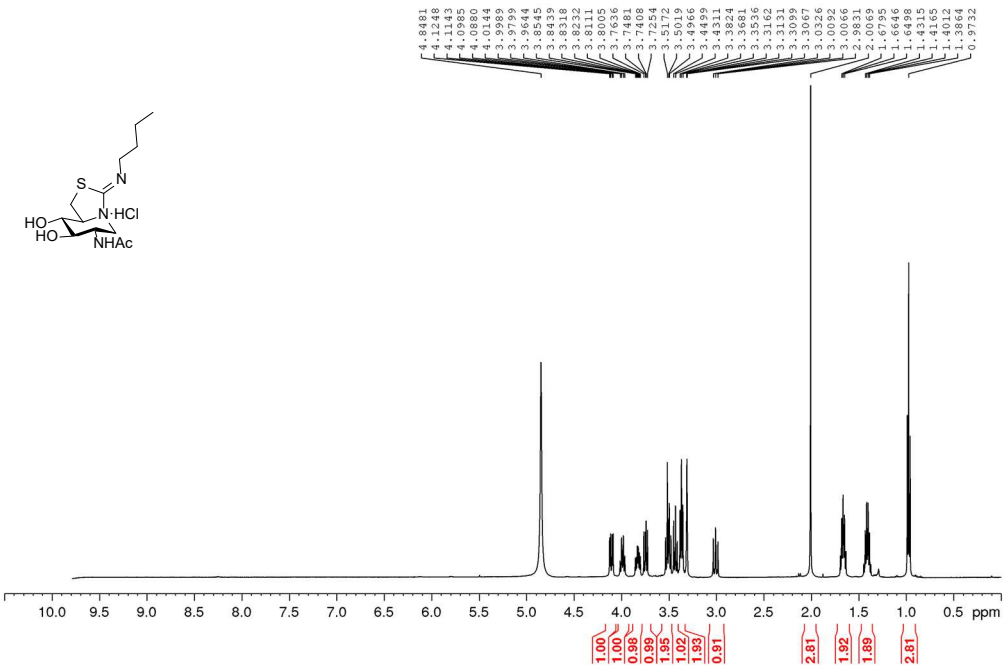

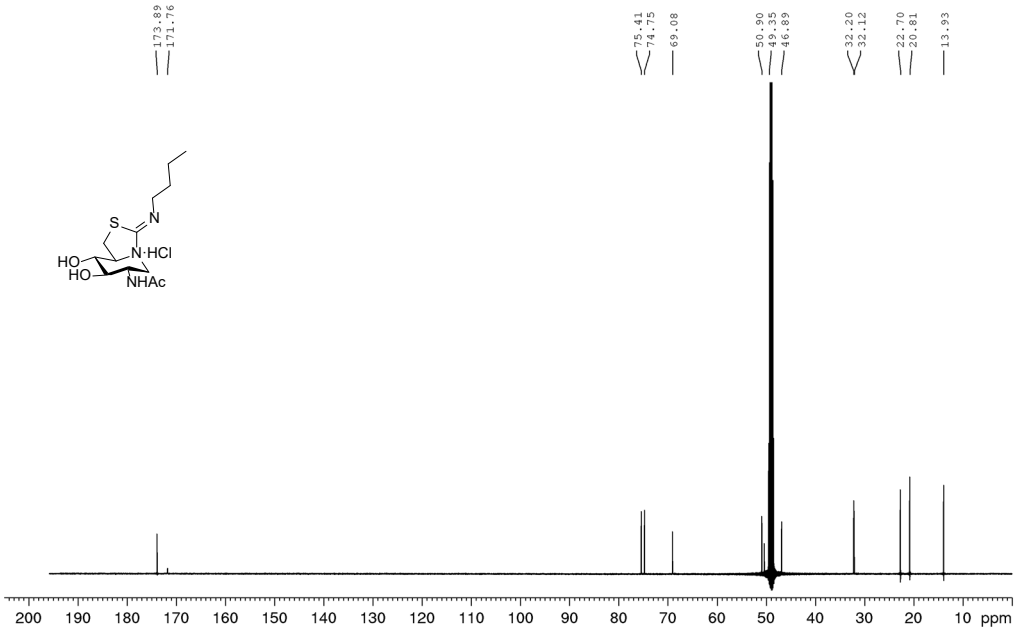

Supplemental Figure 43. ^{1}H NMR and ^{13}C NMR (500 MHz, 125.7 MHz CD_3OD) of **13**

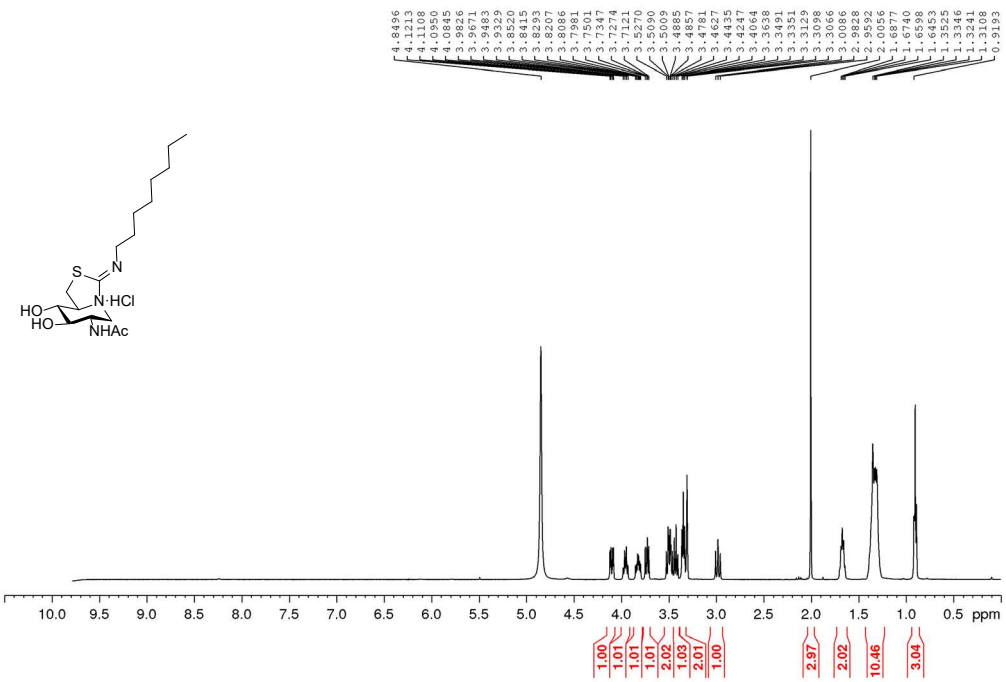

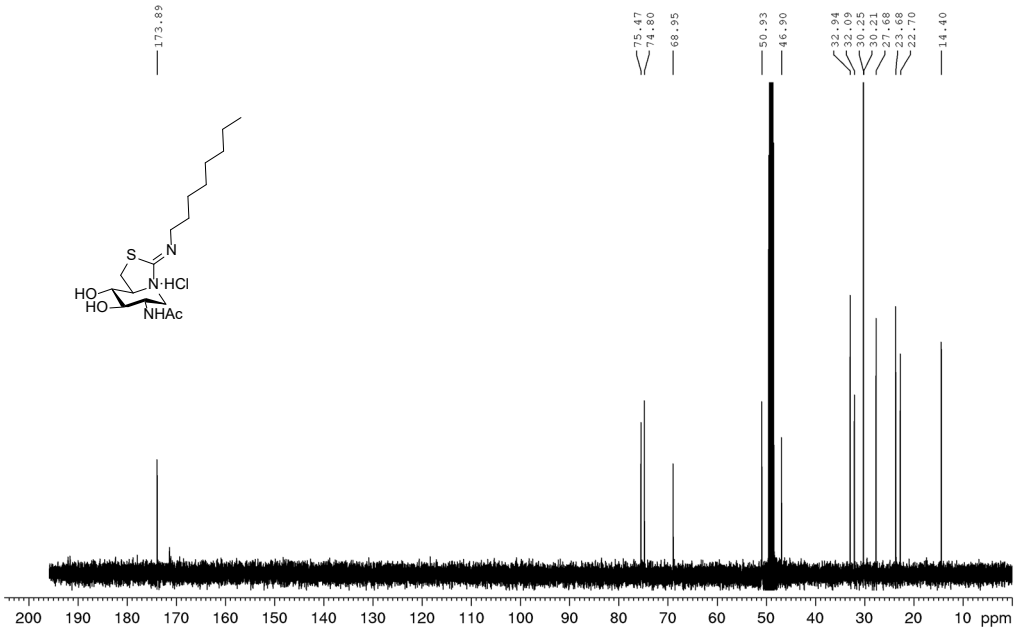

Supplemental Figure 44. ^{1}H NMR and ^{13}C NMR (500 MHz, 125.7 MHz CD_3OD) of **14**

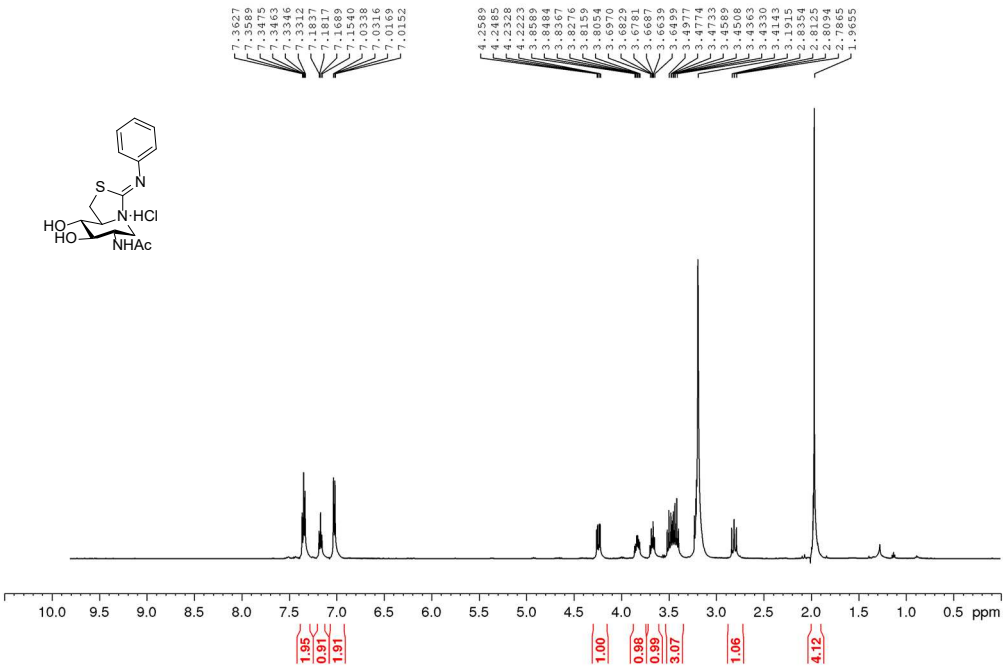

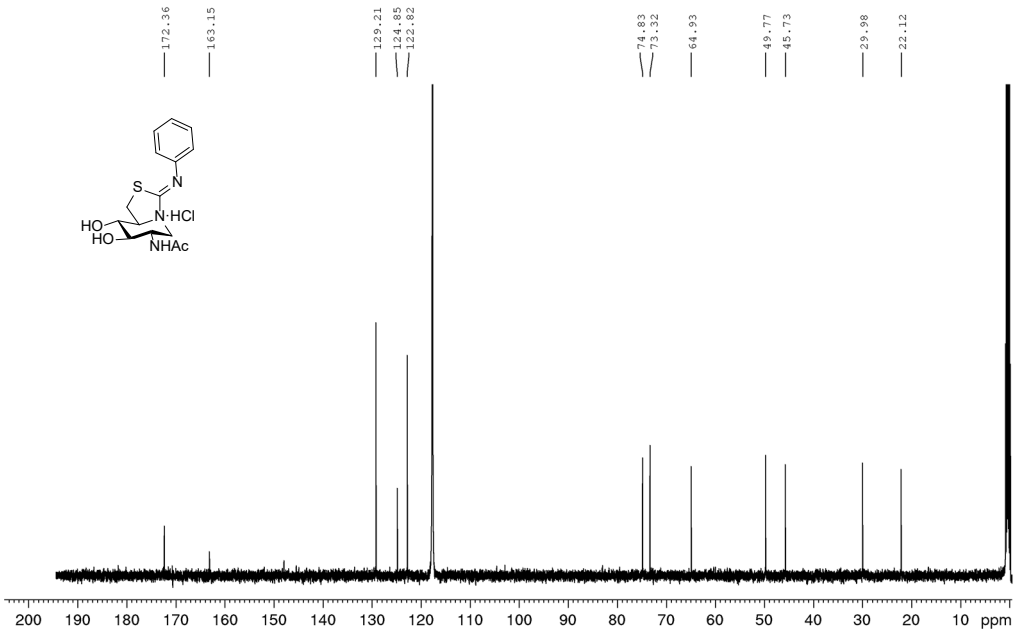

Supplemental Figure 45. ^{1}H NMR and ^{13}C NMR (500 MHz, 125.7 MHz 1:10 CD_3CN-D_2O) of **15**

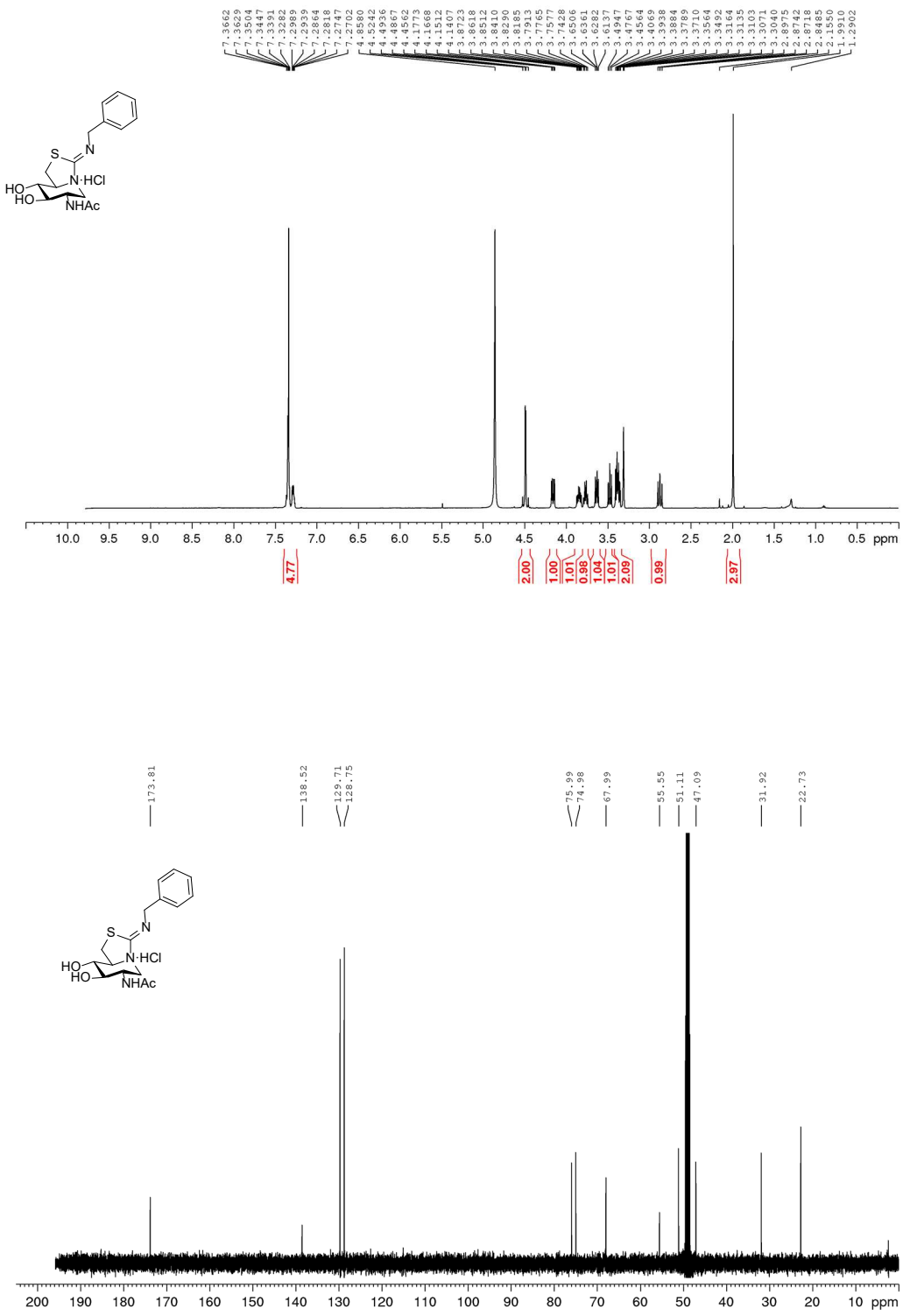

Supplemental Figure 46. ^{1}H NMR and ^{13}C NMR (500 MHz, 125.7 MHz CD_3OD) of **16**

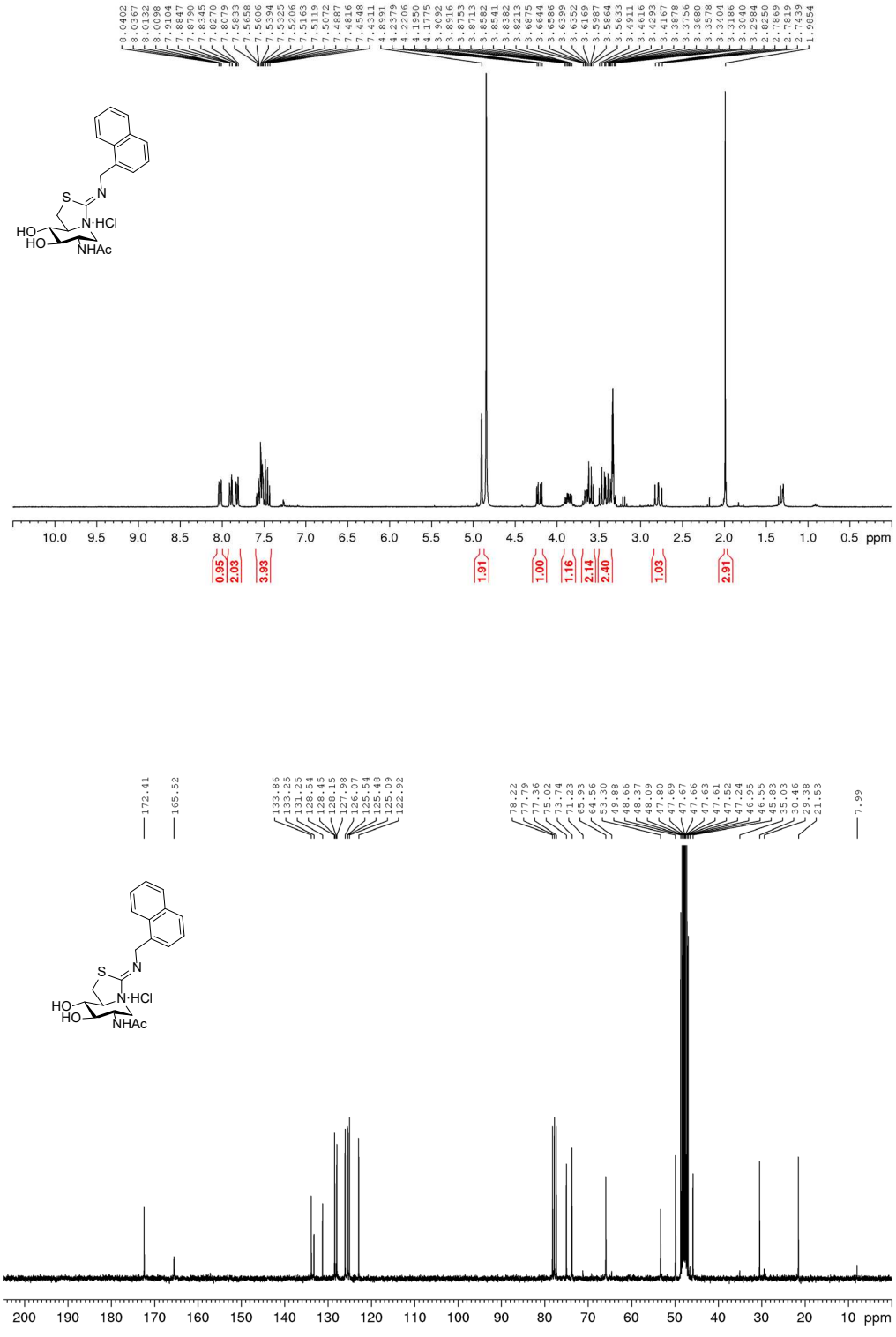

Supplemental Figure 47. ^{1}H NMR and ^{13}C NMR (300 MHz, 100.6 MHz 8:1 CD_3OD-$CDCl_3$) of **17**

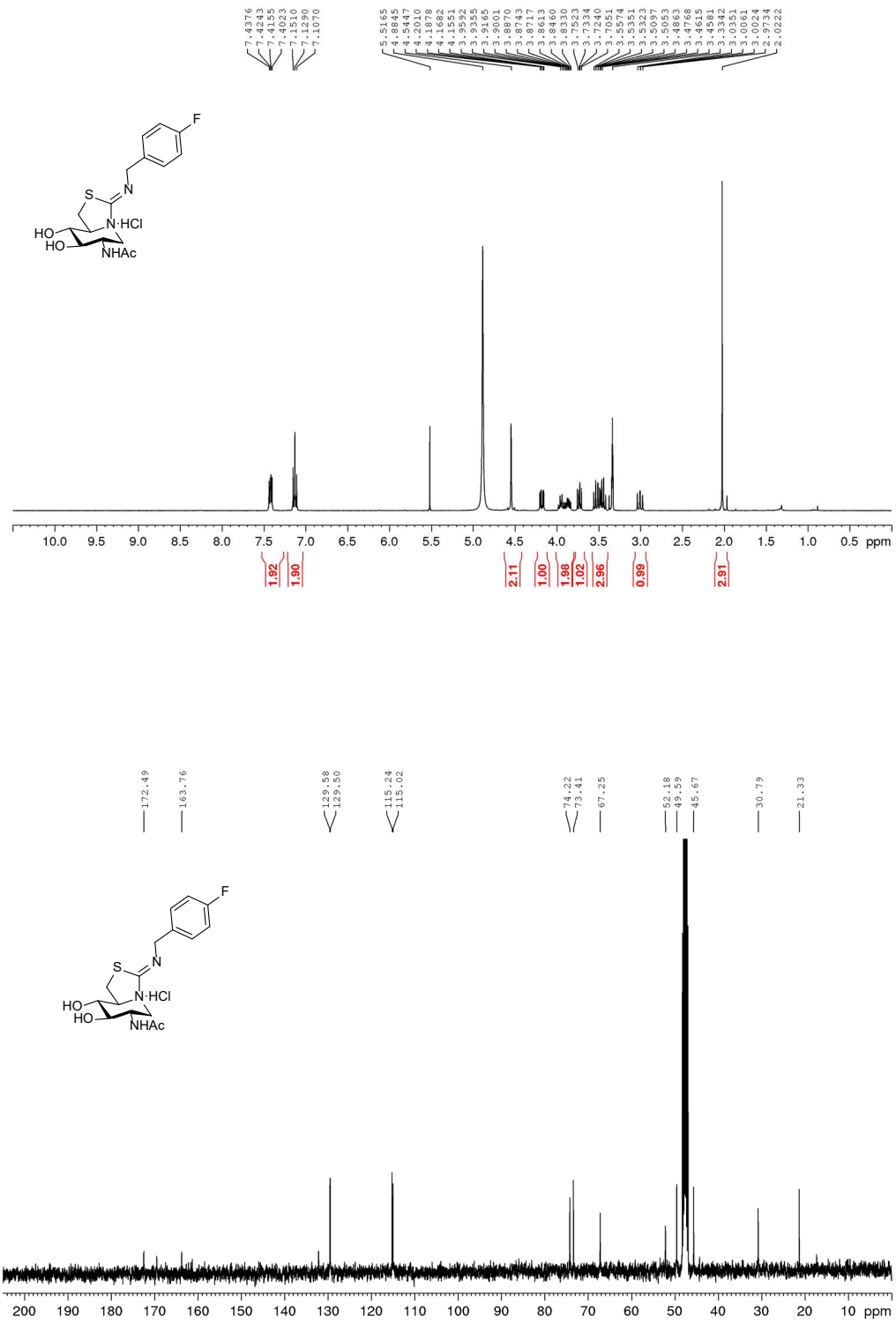

Supplemental Figure 48. ^{1}H NMR and ^{13}C NMR (500 MHz, 125.7 MHz CD_3OD) of **18**

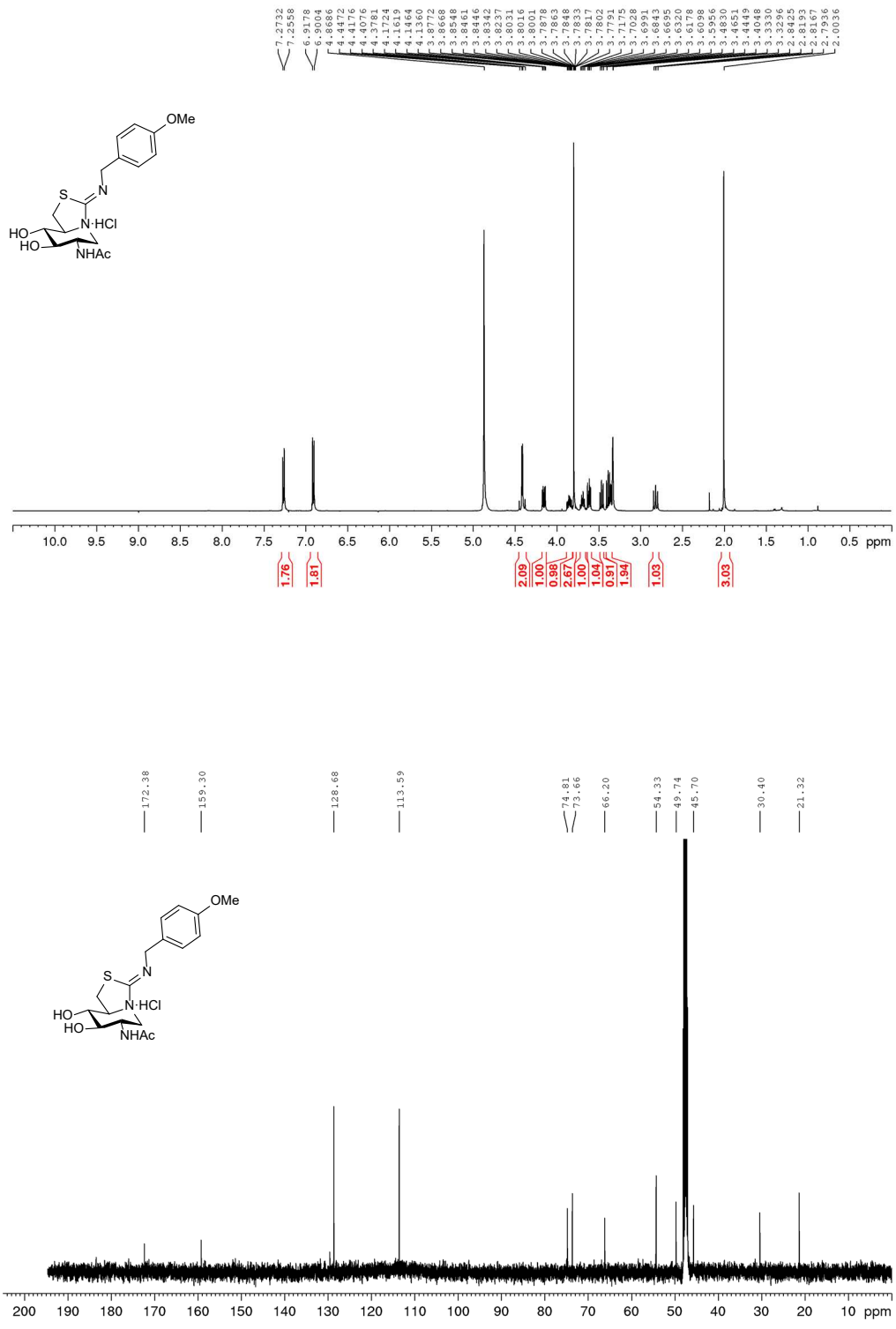

Supplemental Figure 49. ^{1}H NMR and ^{13}C NMR (500 MHz, 125.7 MHz CD_3OD) of **19**

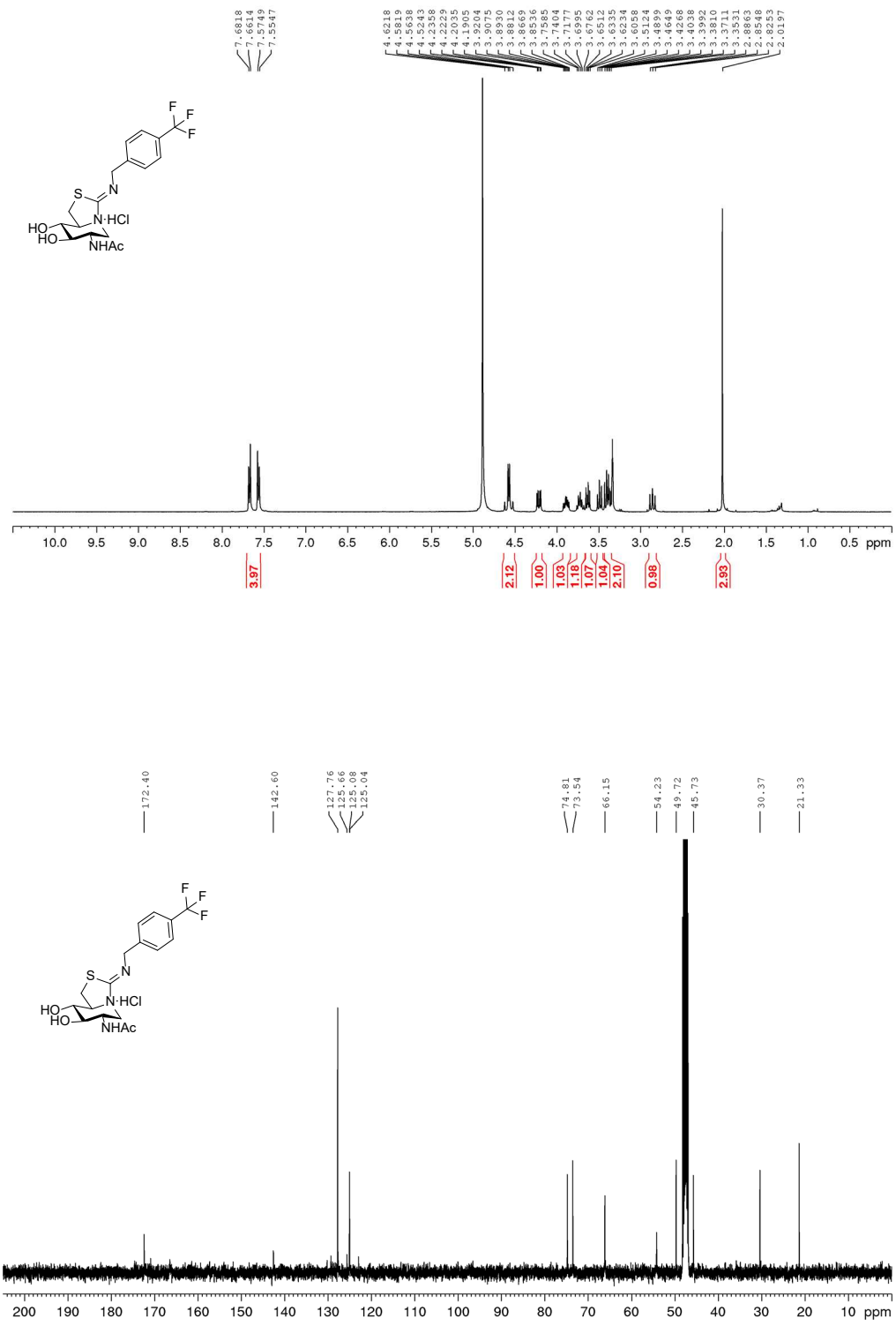

Supplemental Figure 50. ^{1}H NMR and ^{13}C NMR (500 MHz, 125.7 MHz CD_3OD) of **20**

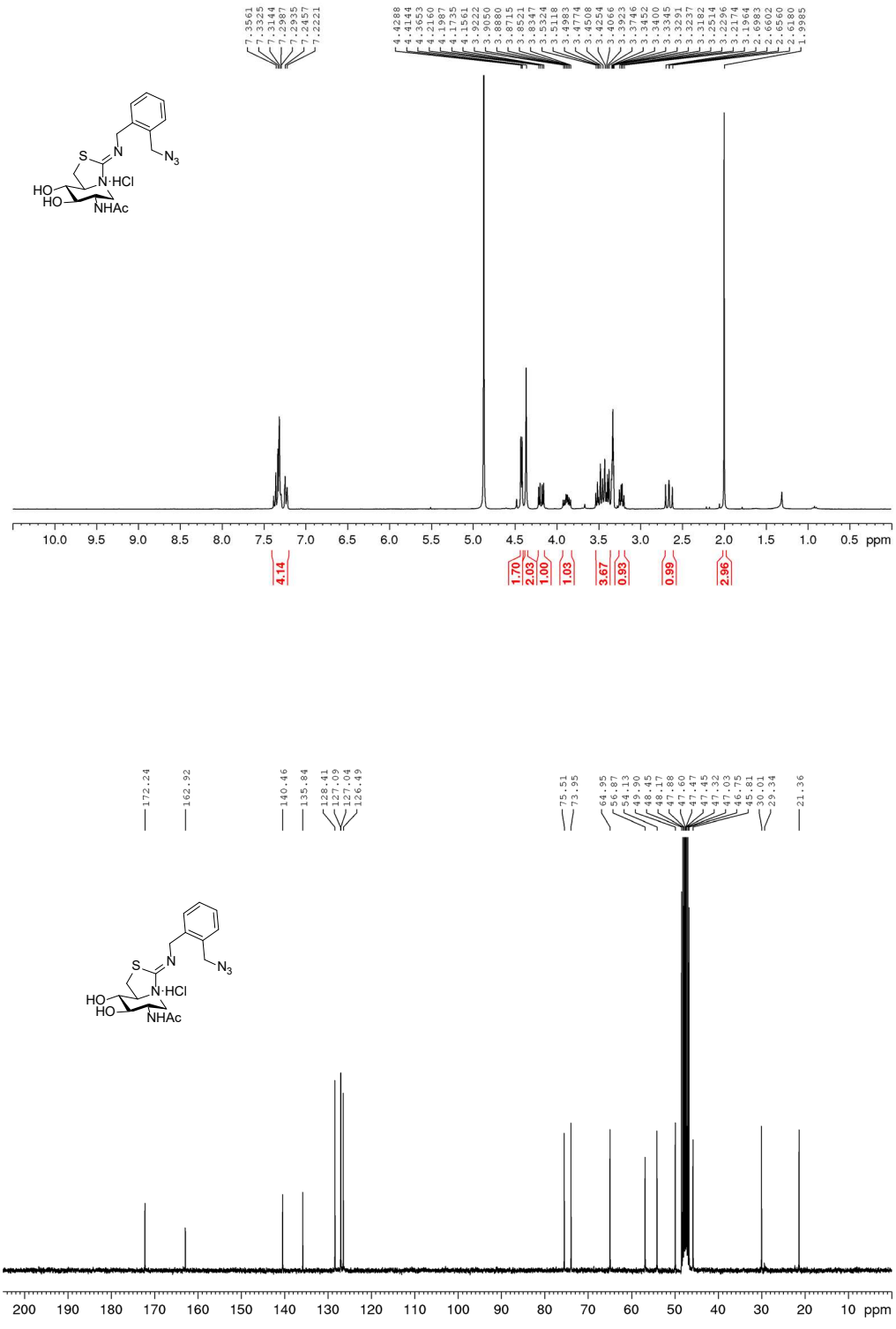

Supplemental Figure 51. ^{1}H NMR and ^{13}C NMR (300 MHz, 75.5 MHz CD_3OD) of **21**

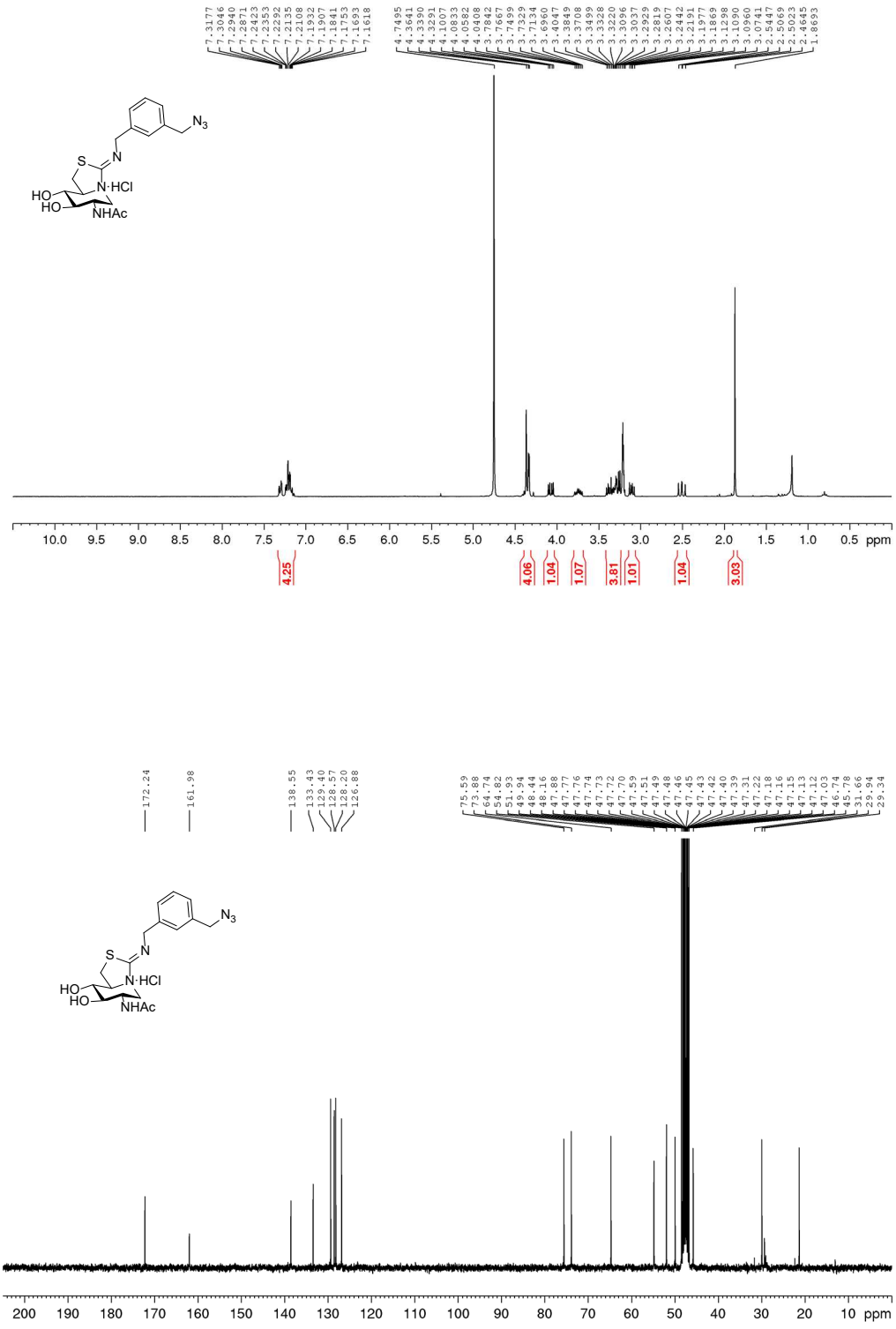

Supplemental Figure 52. ^{1}H NMR and ^{13}C NMR (300 MHz, 75.5 MHz CD_3OD) of **22**

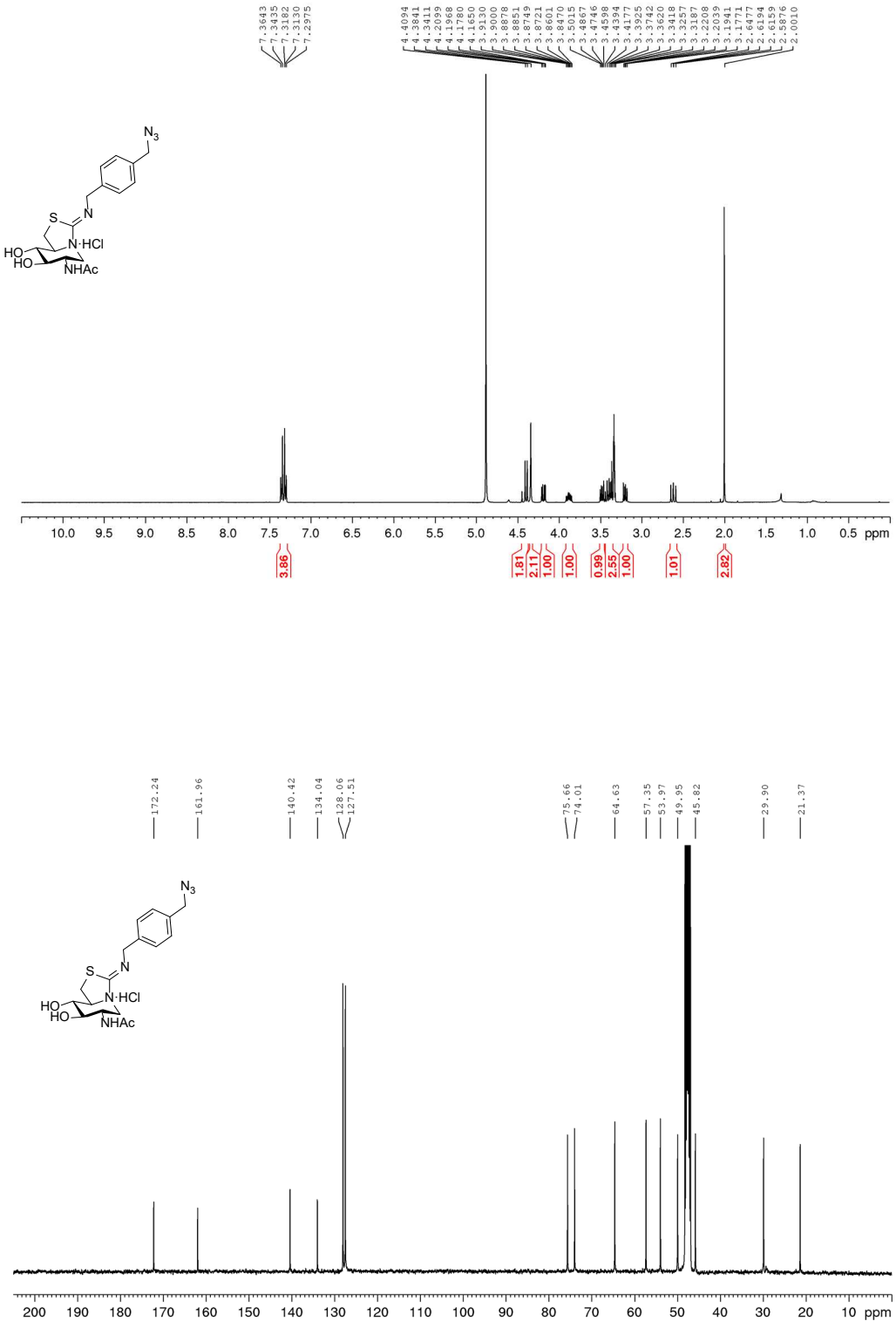

Supplemental Figure 53. ^{1}H NMR and ^{13}C NMR (400 MHz, 100.6 MHz CD_3OD) of **23**

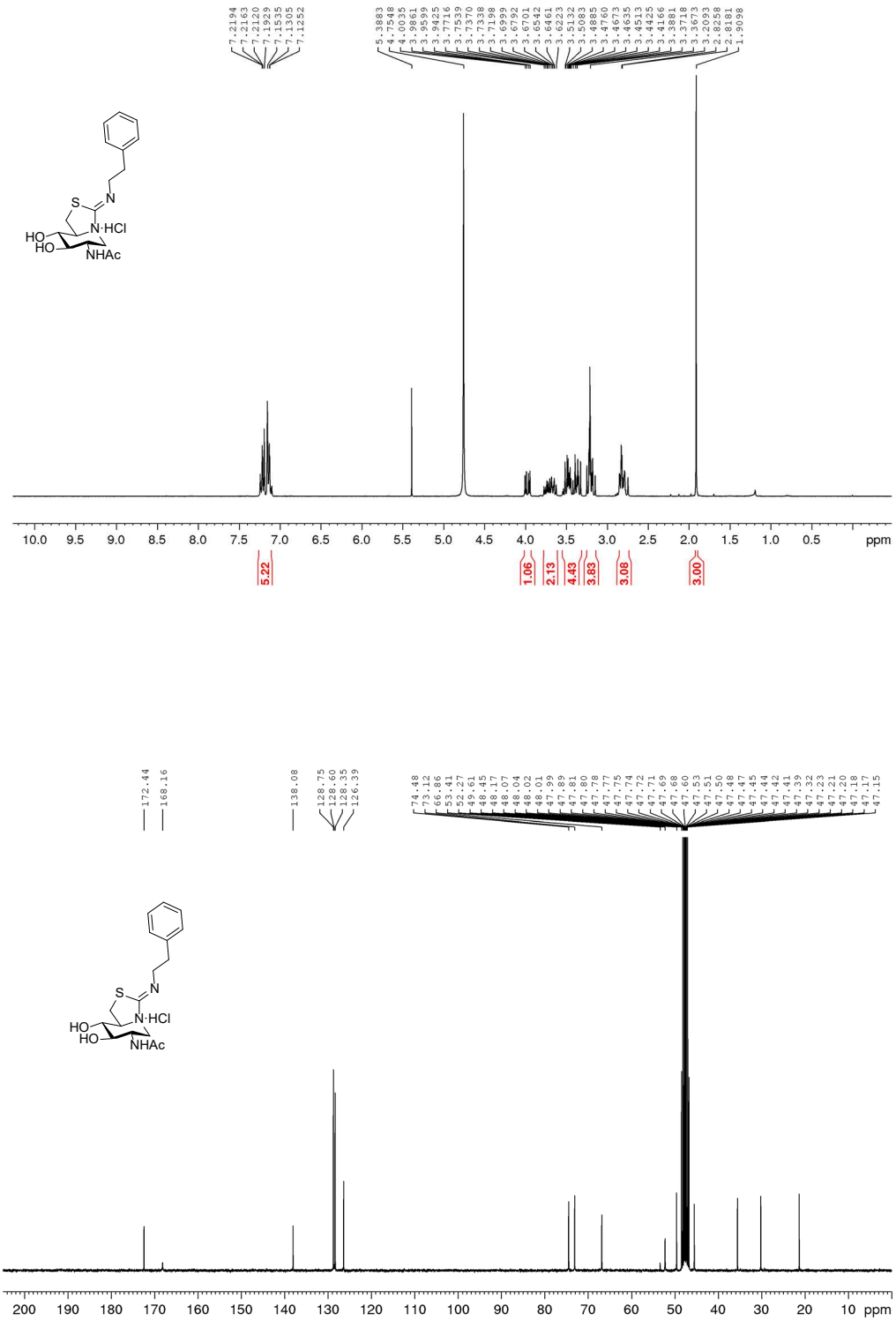

Supplemental Figure 54. ^{1}H NMR and ^{13}C NMR (300 MHz, 75.5 MHz CD_3OD) of **24**

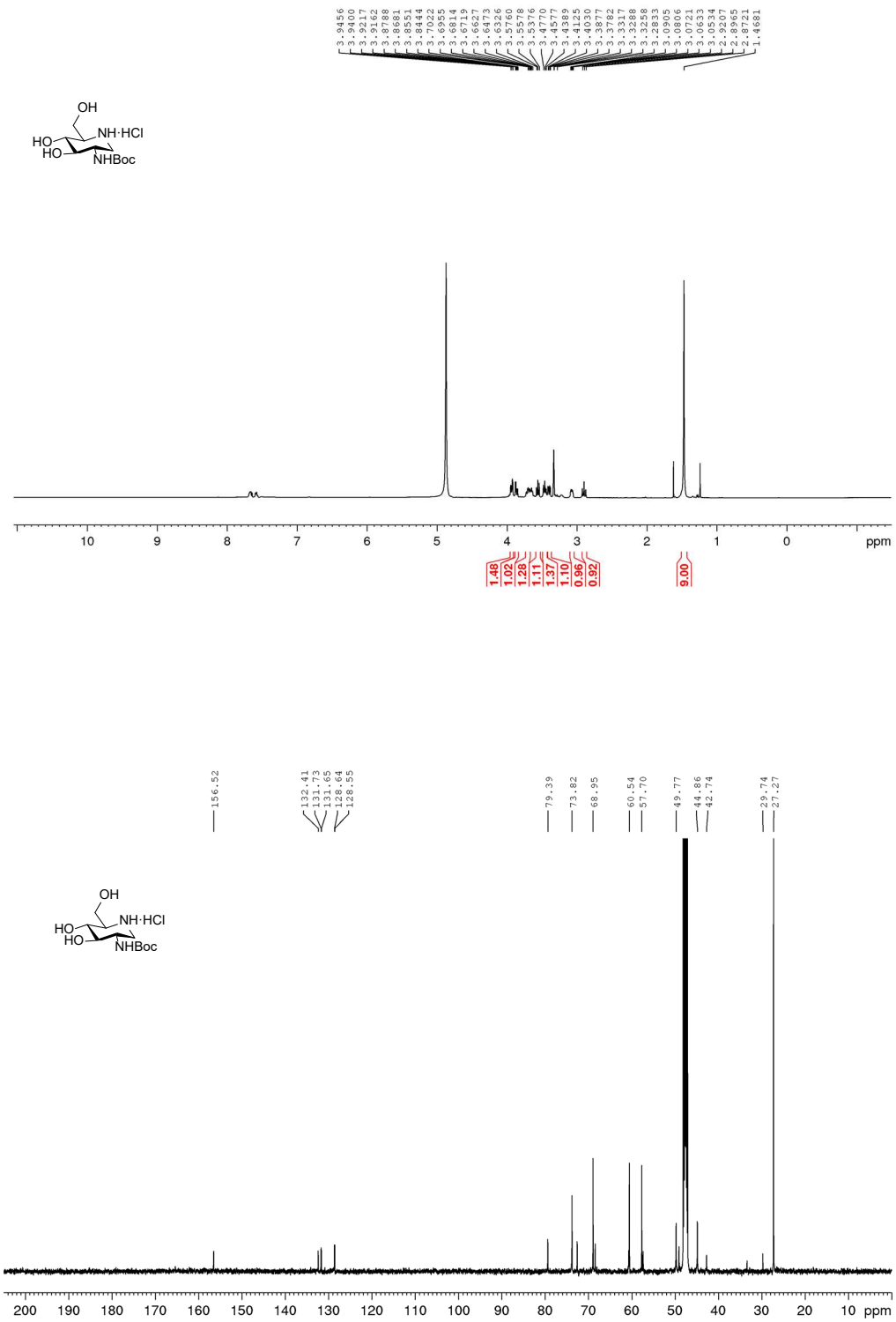

Supplemental Figure 55. ^{1}H NMR and ^{13}C NMR (500 MHz, 125.7 MHz CD_3OD) of **26**

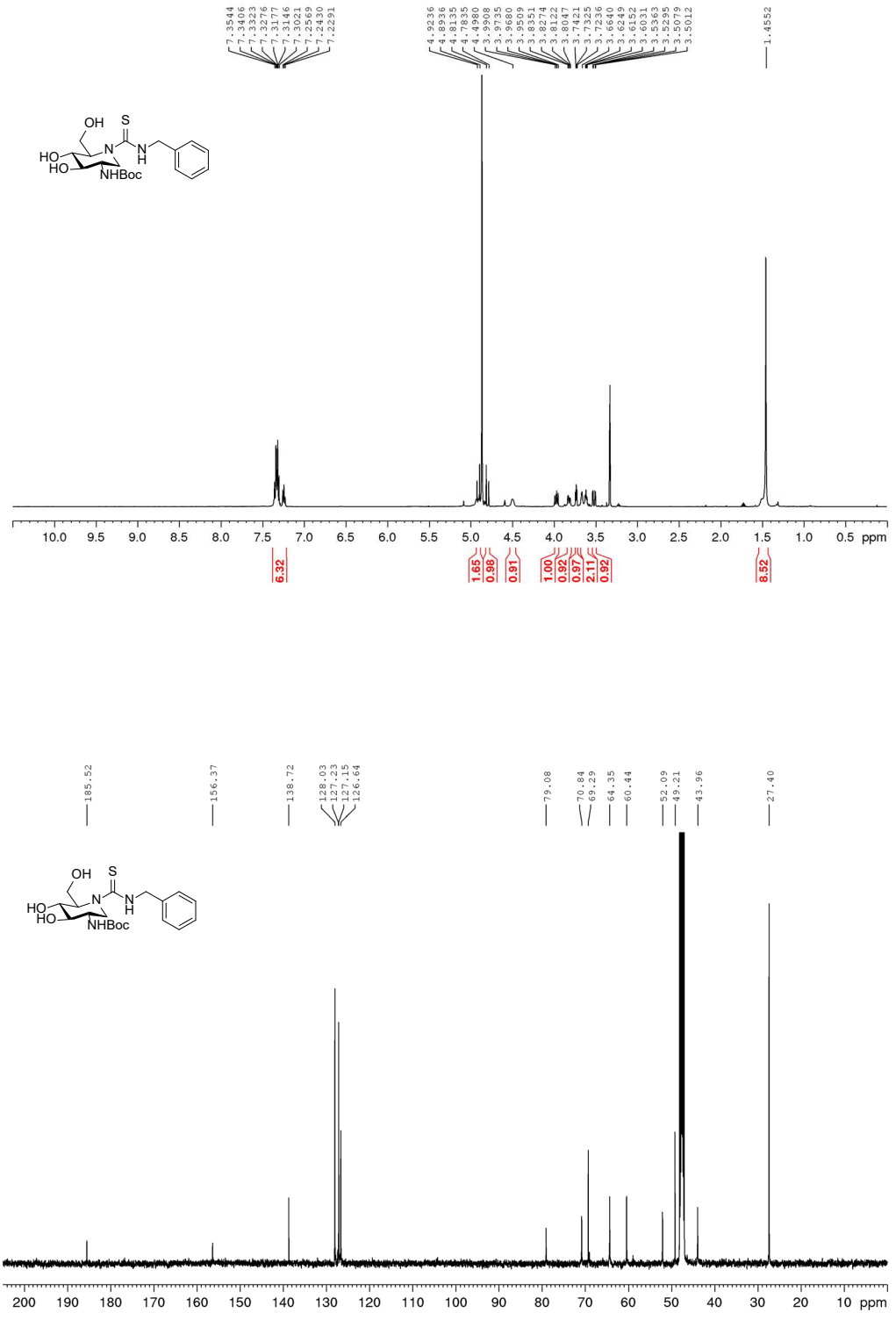

Supplemental Figure 56. ^{1}H NMR and ^{13}C NMR (600 MHz, 150 MHz CD_3OD) of **27**

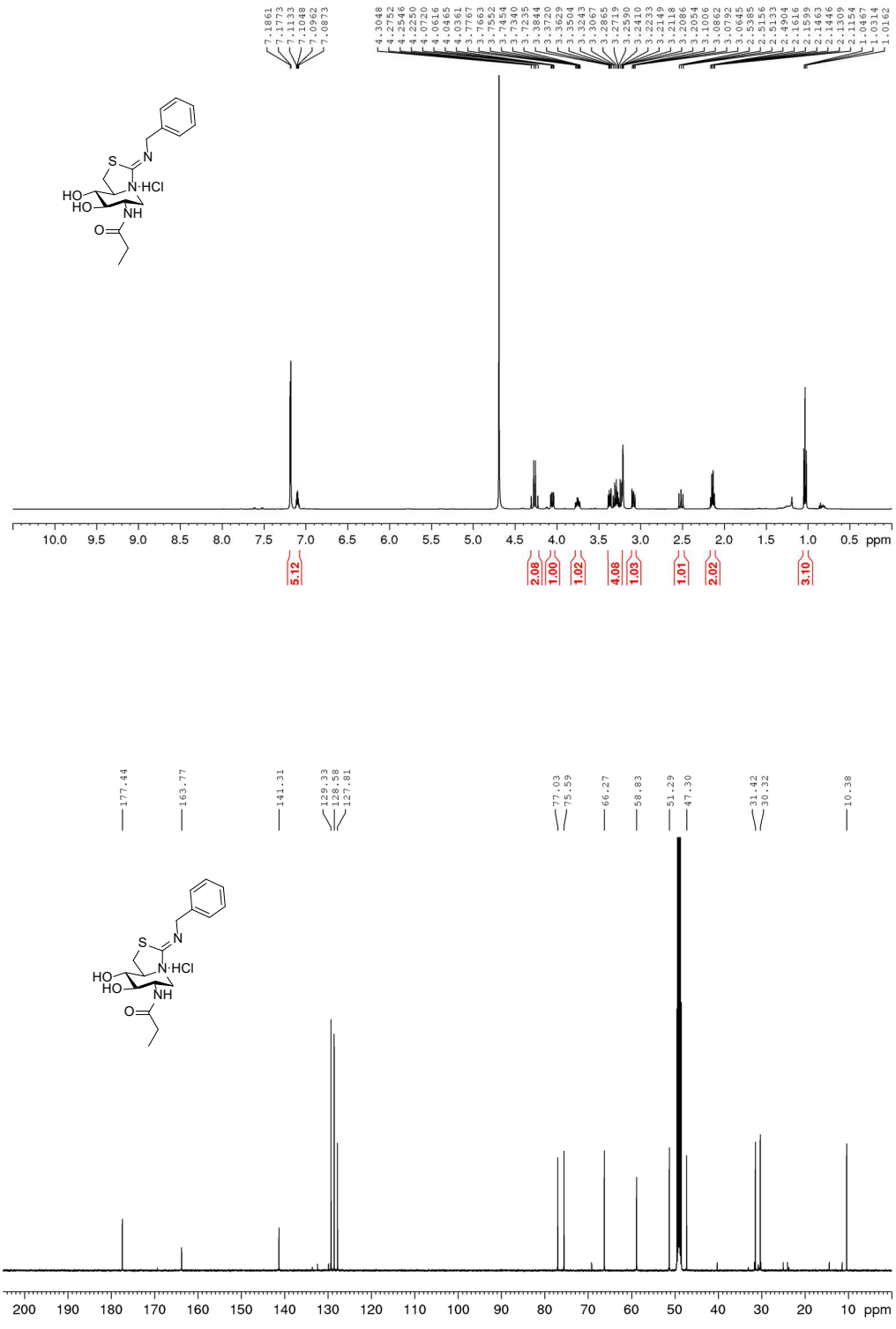

Supplemental Figure 57. ^{1}H NMR and ^{13}C NMR (500 MHz, 125.7 MHz CD_3OD) of **28**

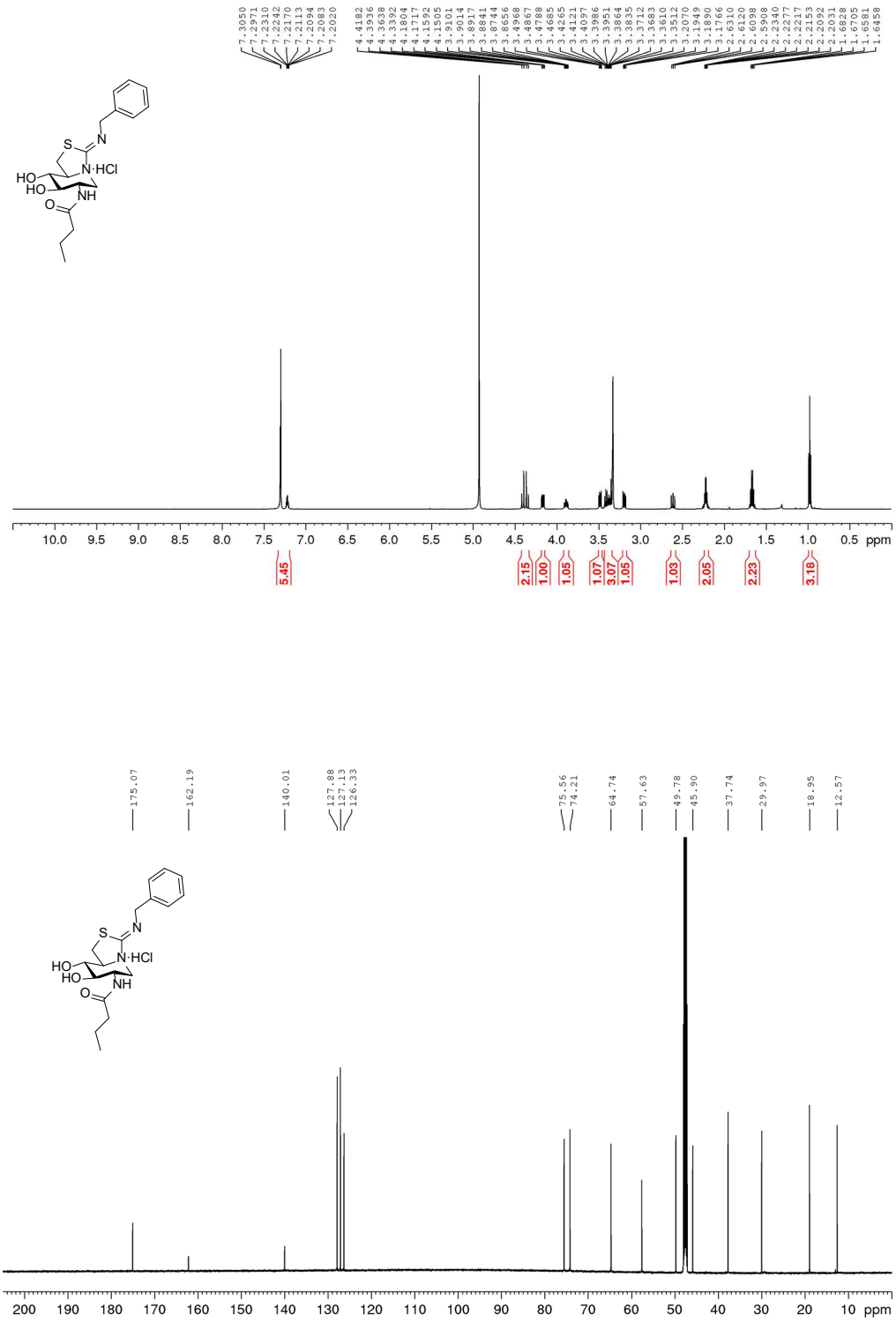

Supplemental Figure 58. ^{1}H NMR and ^{13}C NMR (600 MHz, 150 MHz CD_3OD) of **29**

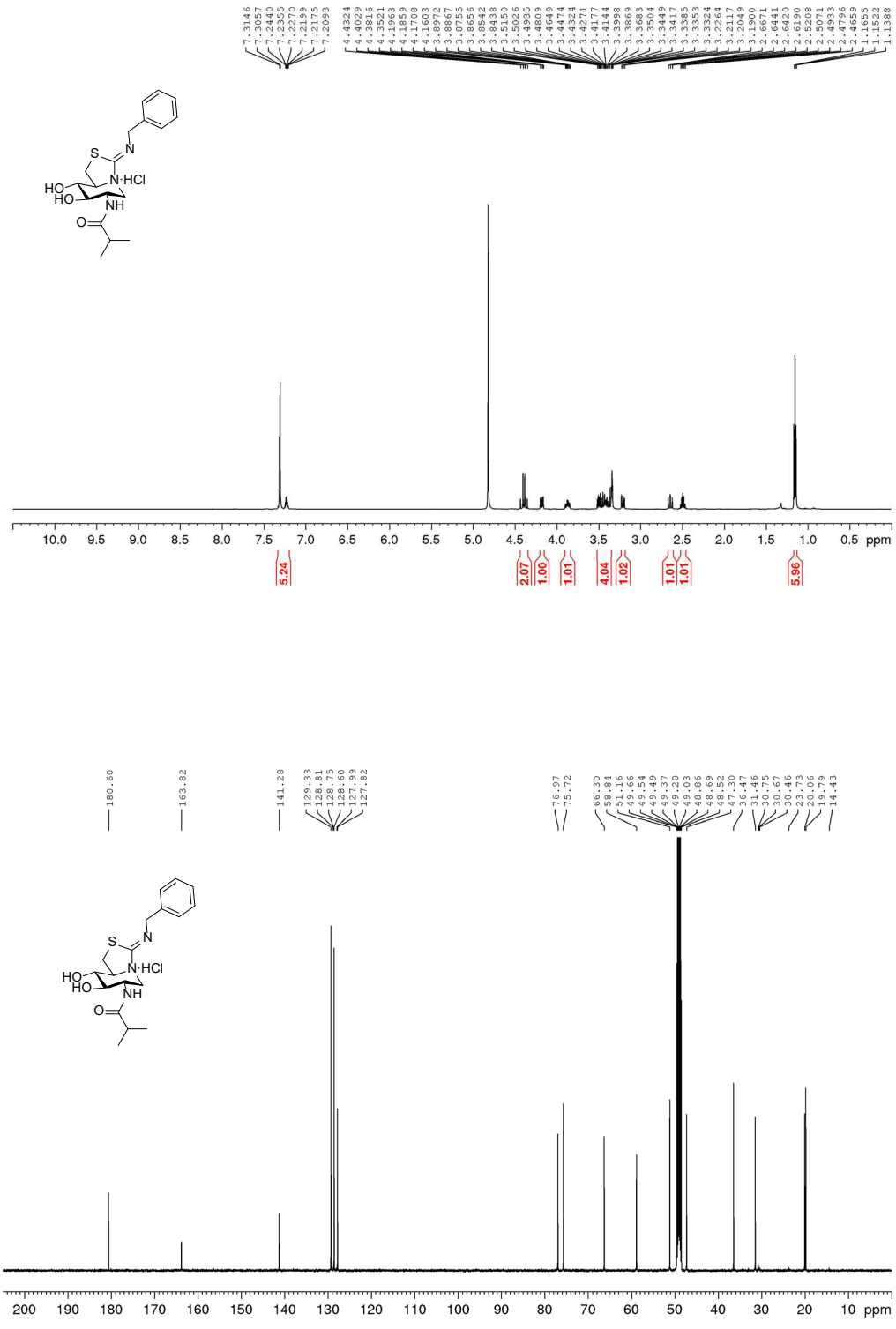

Supplemental Figure 59. ^{1}H NMR and ^{13}C NMR (500 MHz, 125.7 MHz CD_3OD) of **30**

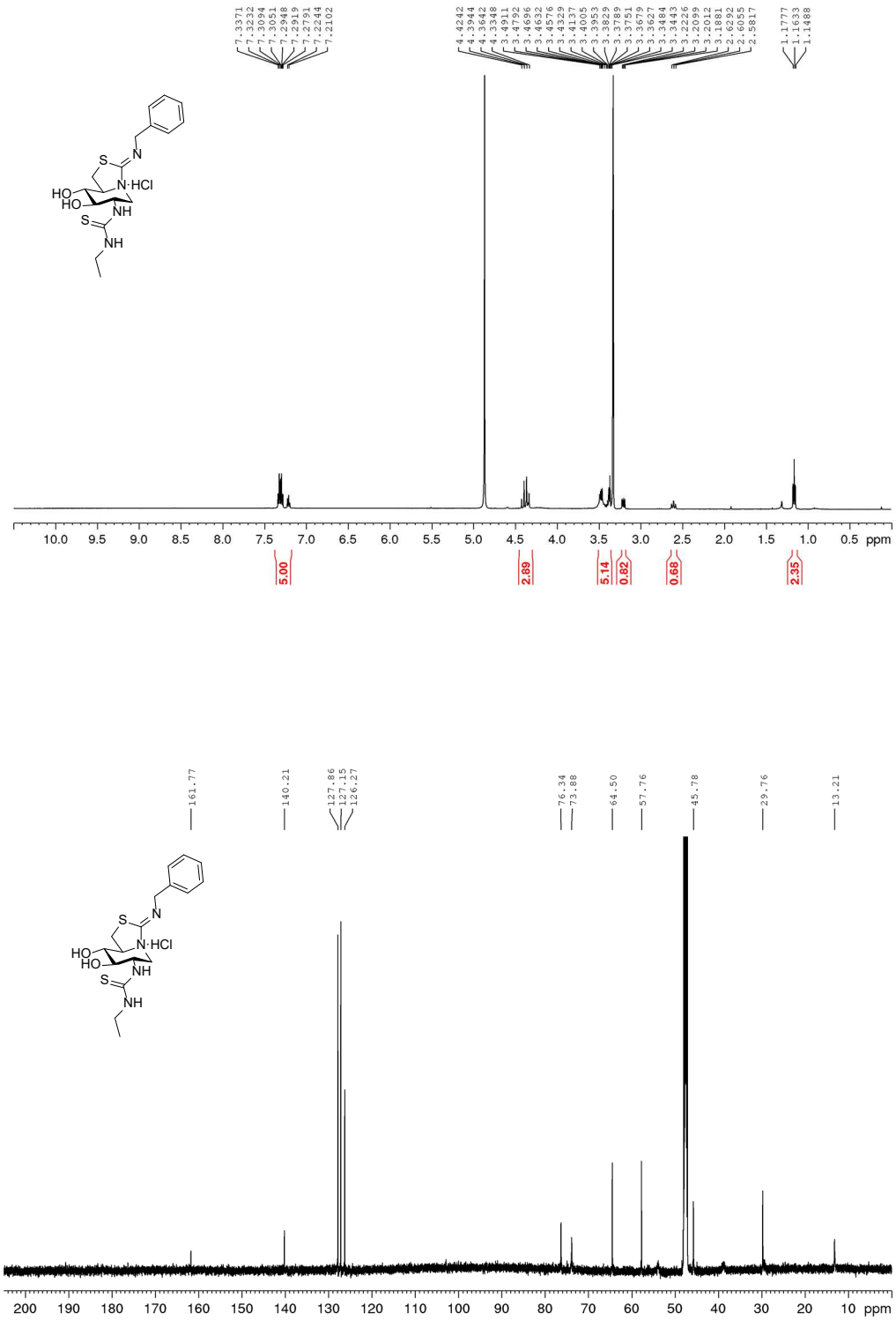

Supplemental Figure 60. ^{1}H NMR and ^{13}C NMR (600 MHz, 150 MHz CD_3OD) of **31**

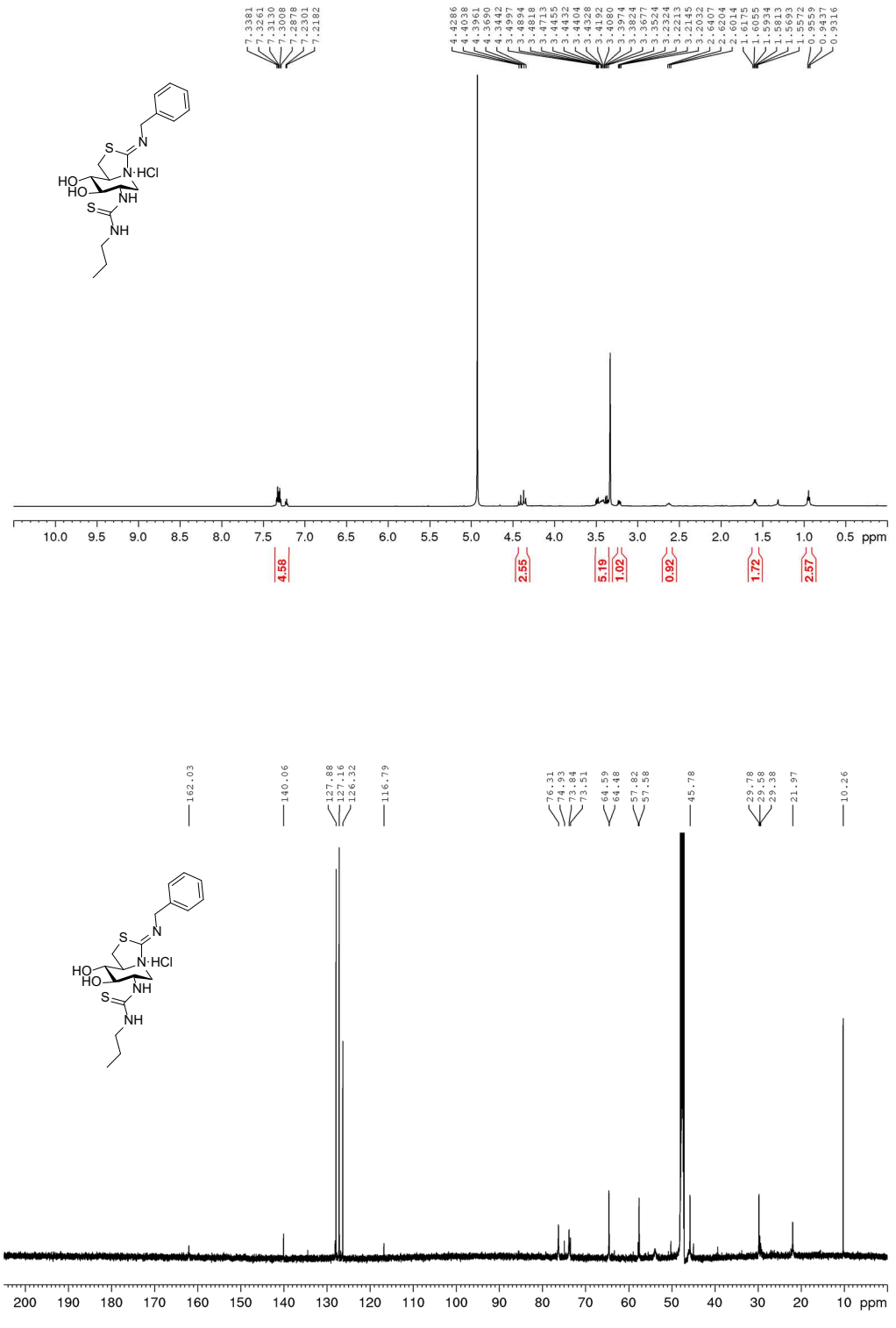

Supplemental Figure 61. ^{1}H NMR and ^{13}C NMR (600 MHz, 150 MHz CD_3OD) of **32**

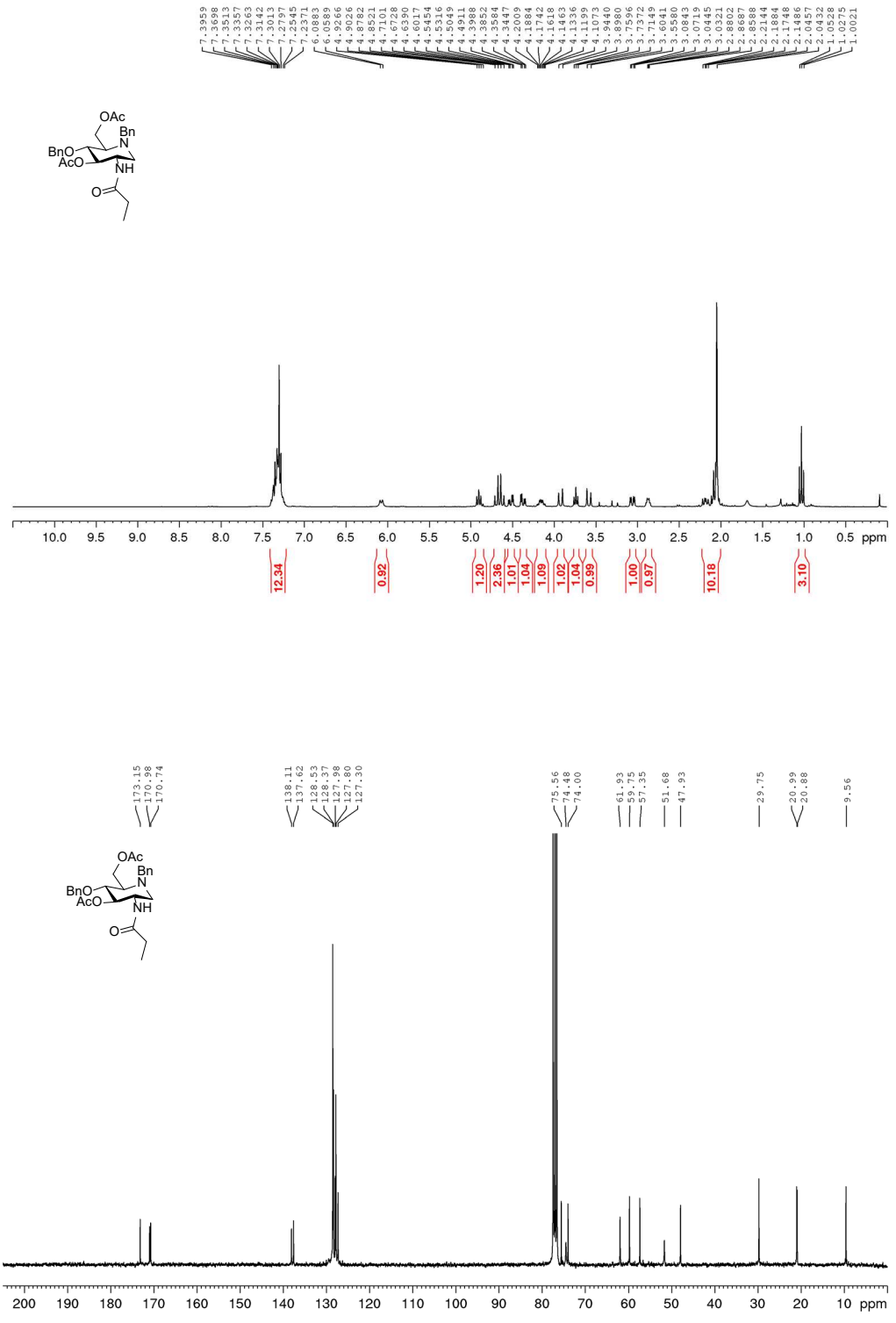

Supplemental Figure 62. ^{1}H NMR and ^{13}C NMR (300 MHz, 75.5 MHz CD_3OD) of **33**

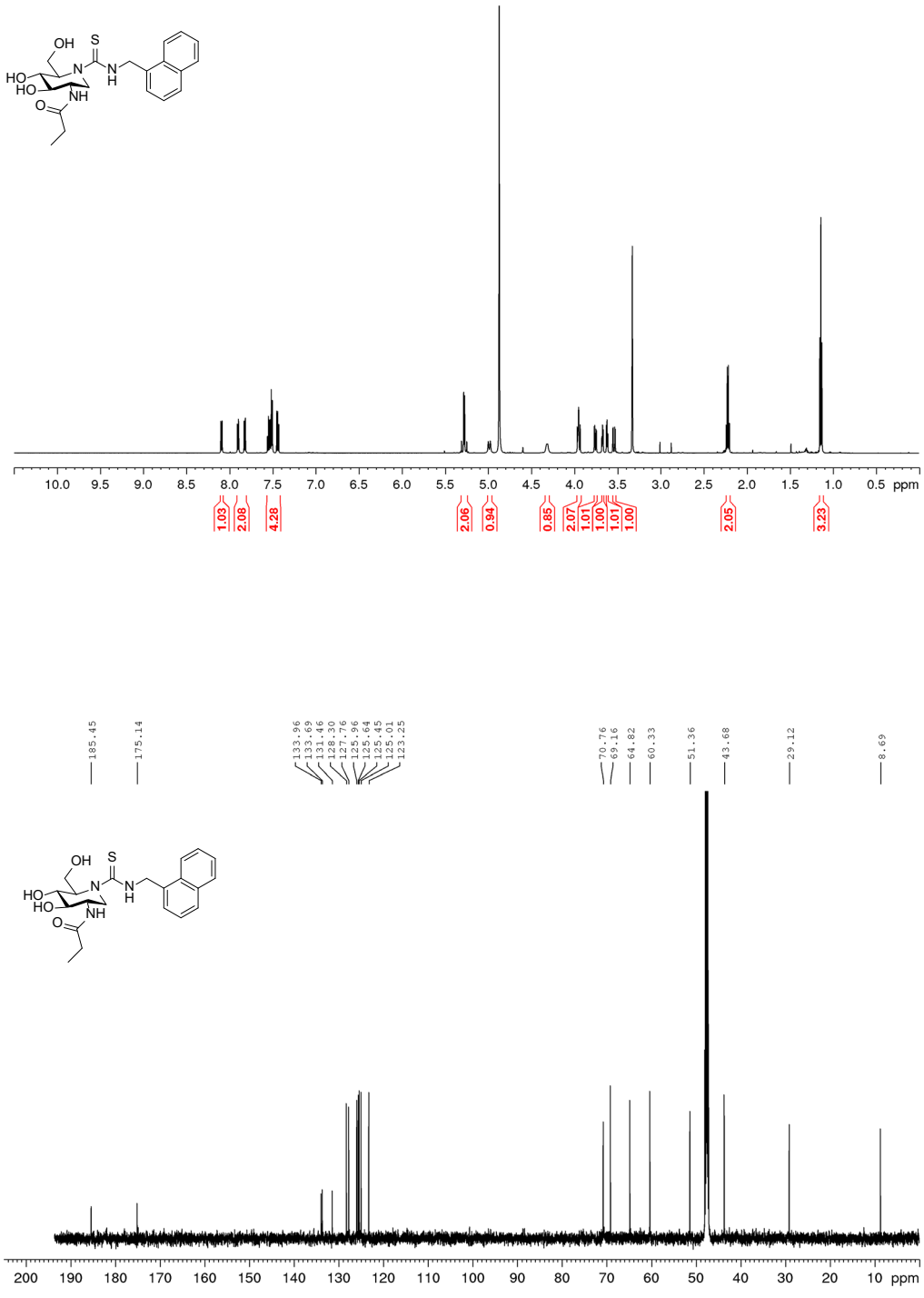

Supplemental Figure 63. ^{1}H NMR and ^{13}C NMR (600 MHz, 150 MHz CD_3OD) of **35**

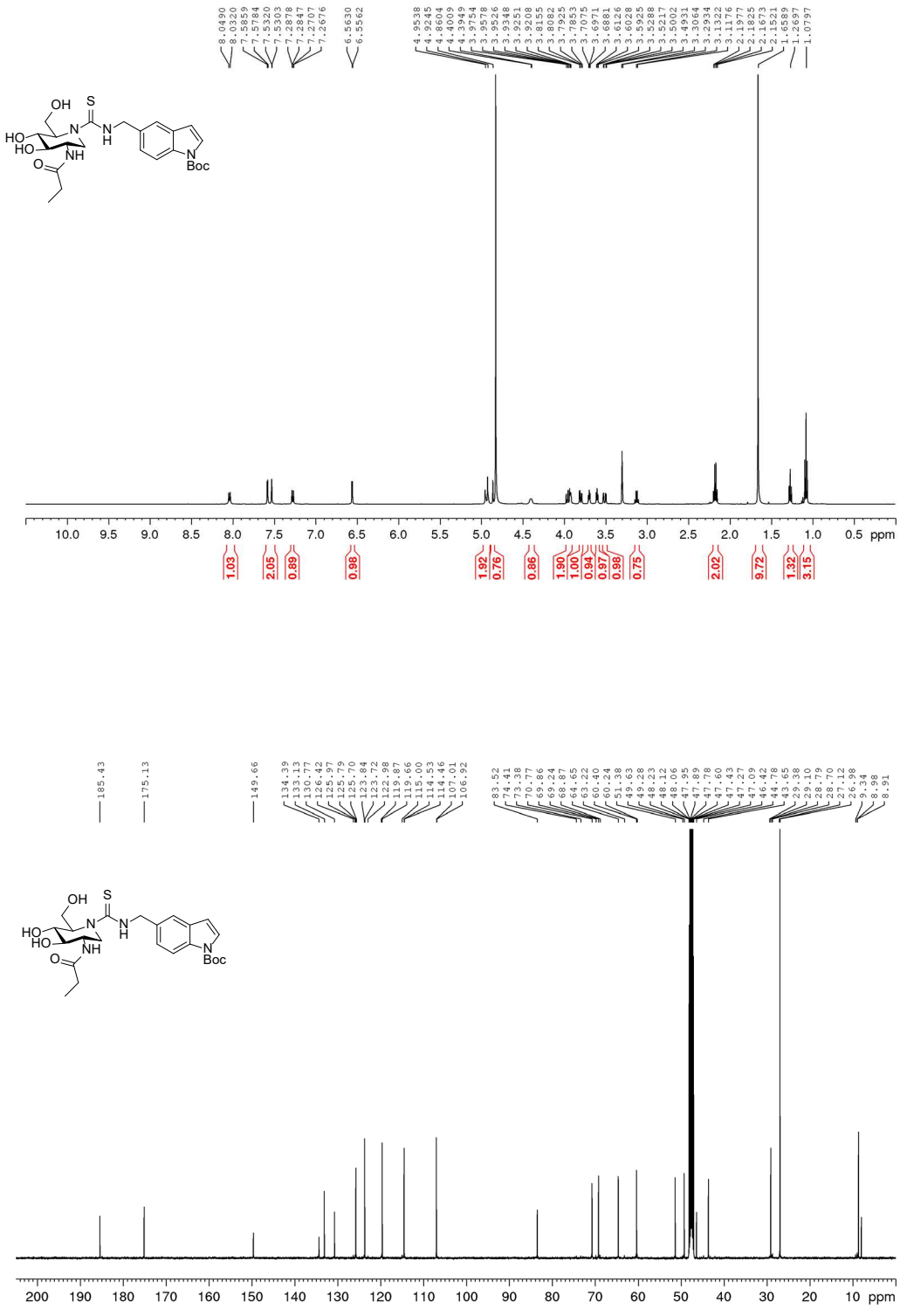

Supplemental Figure 64. ^{1}H NMR and ^{13}C NMR (500 MHz, 125.7 MHz CD_3OD) of **36**

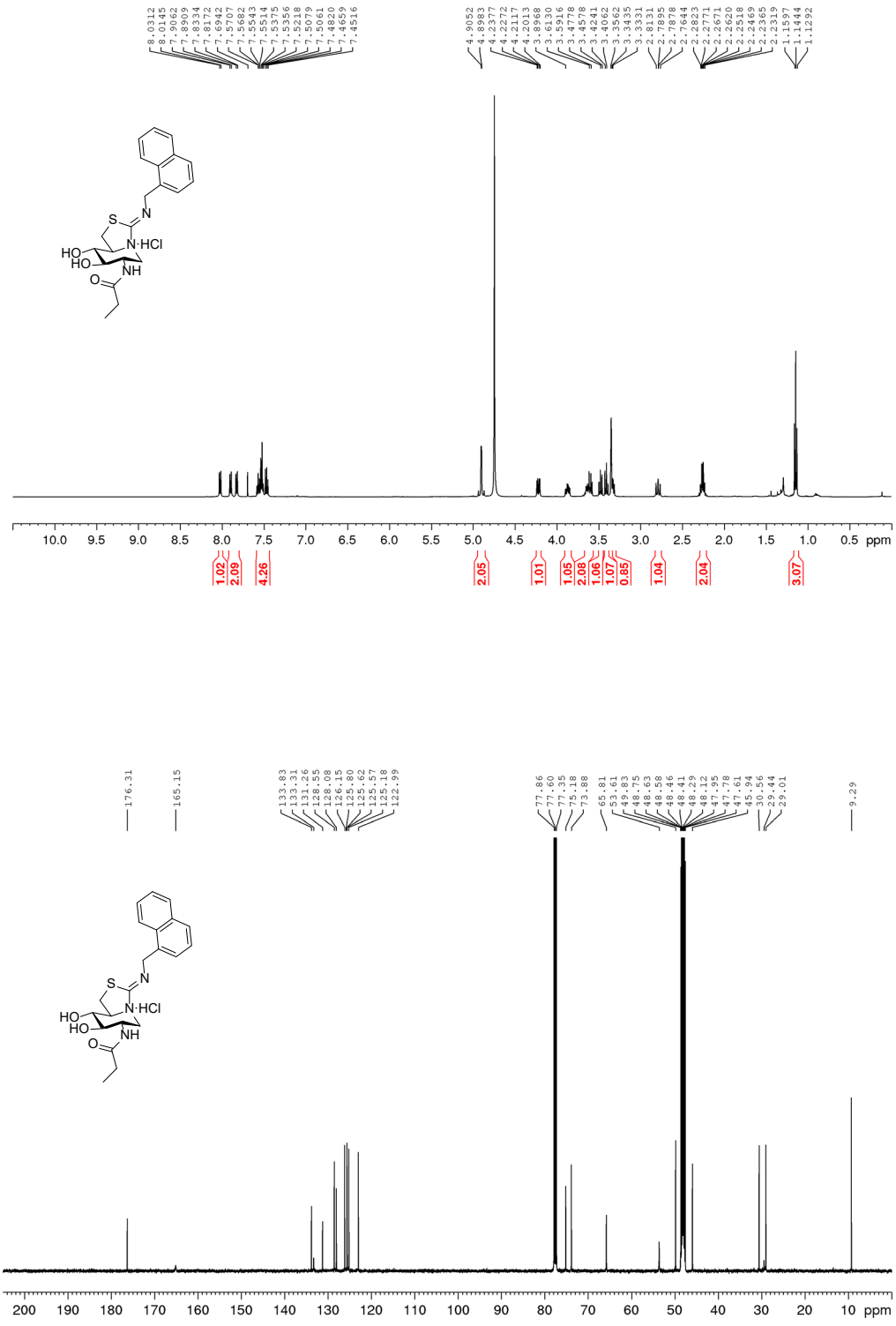

Supplemental Figure 65. ^{1}H NMR and ^{13}C NMR (500 MHz, 125.7 MHz 1:1 CD_3OD-$CDCl_3$) of **37**

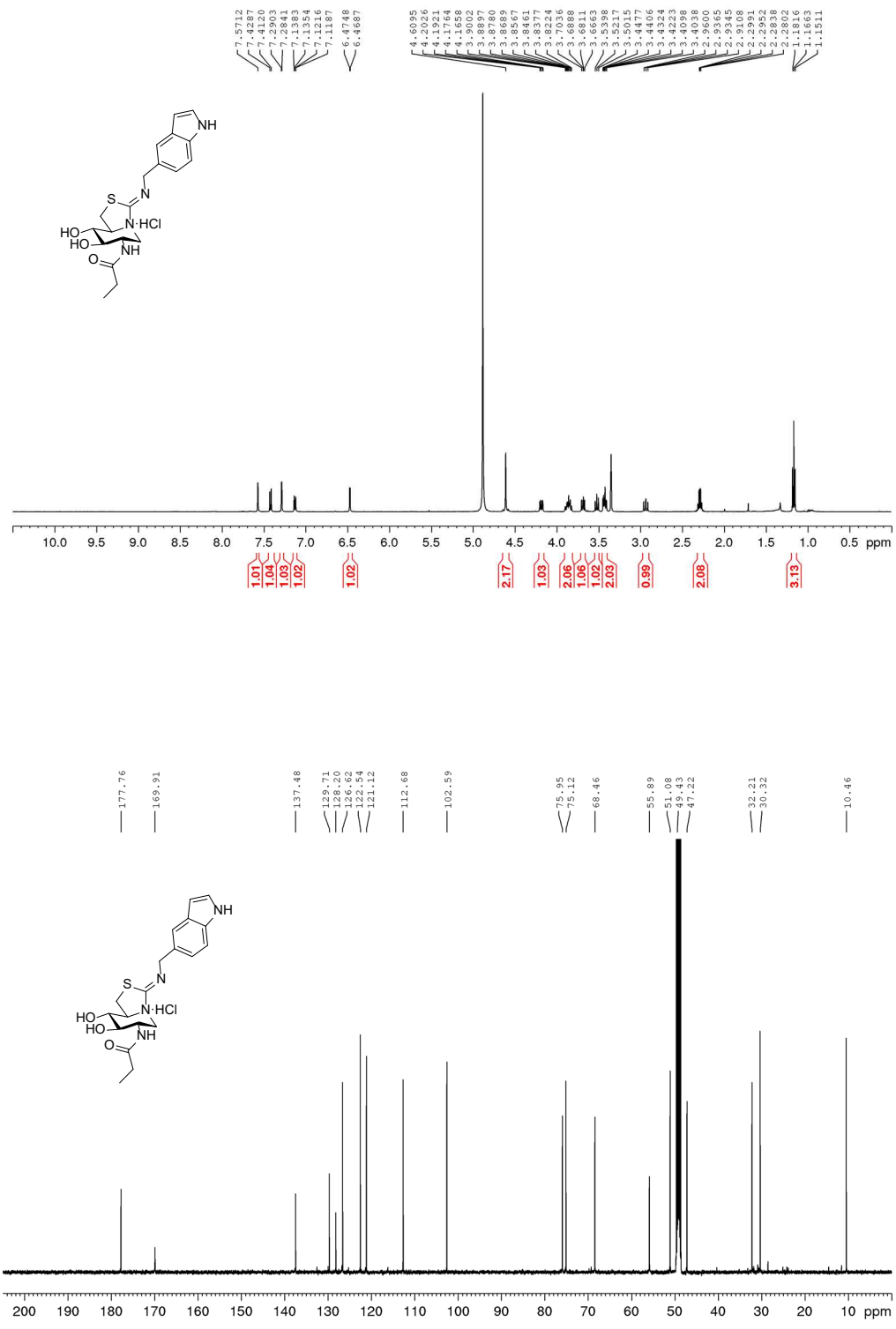

Supplemental Figure 66. ^{1}H NMR and ^{13}C NMR (500 MHz, 125.7 MHz CD_3OD) of **38**

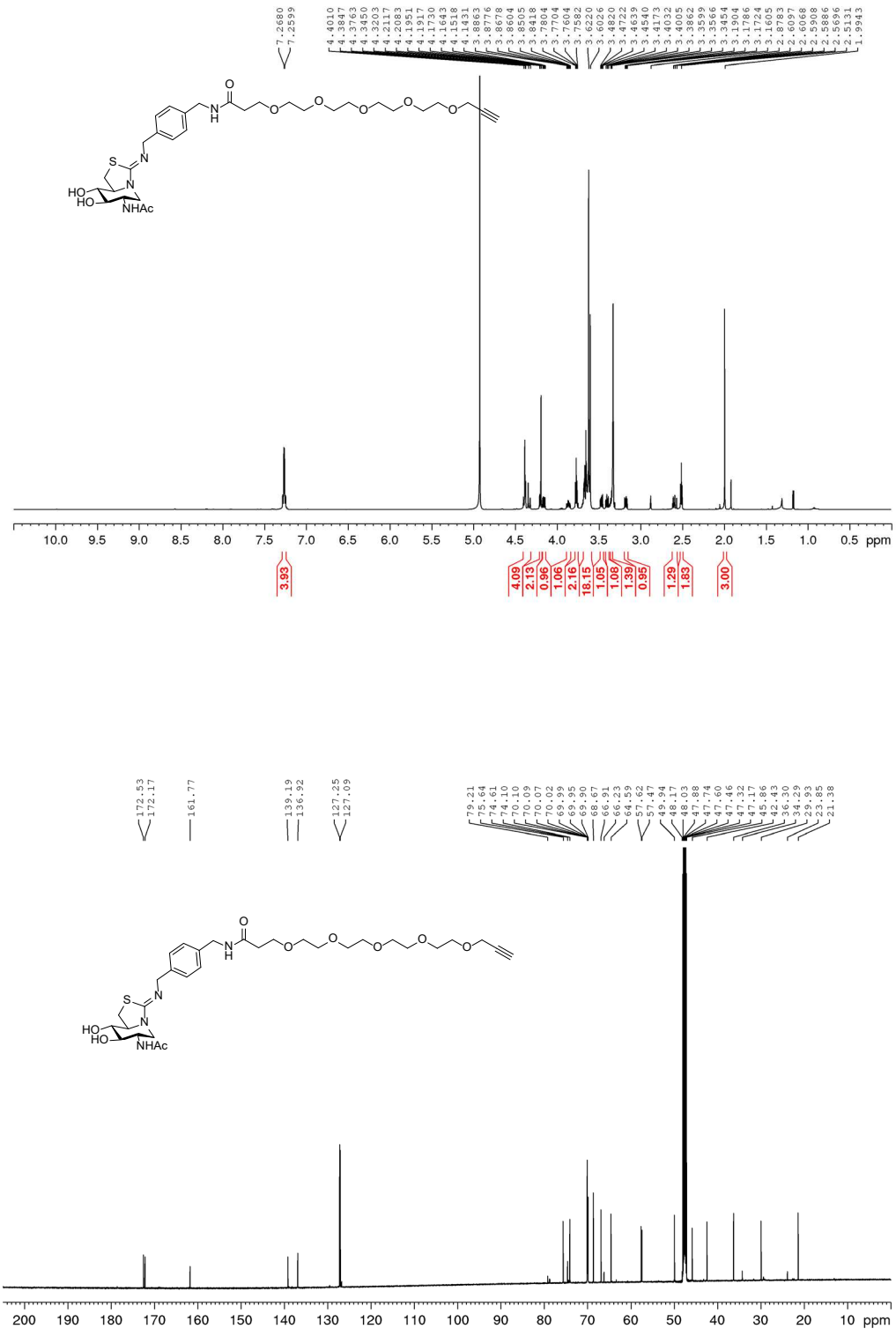

Supplemental Figure 67. ^{1}H NMR and ^{13}C NMR (600 MHz, 150 MHz CD_3OD) of **39**

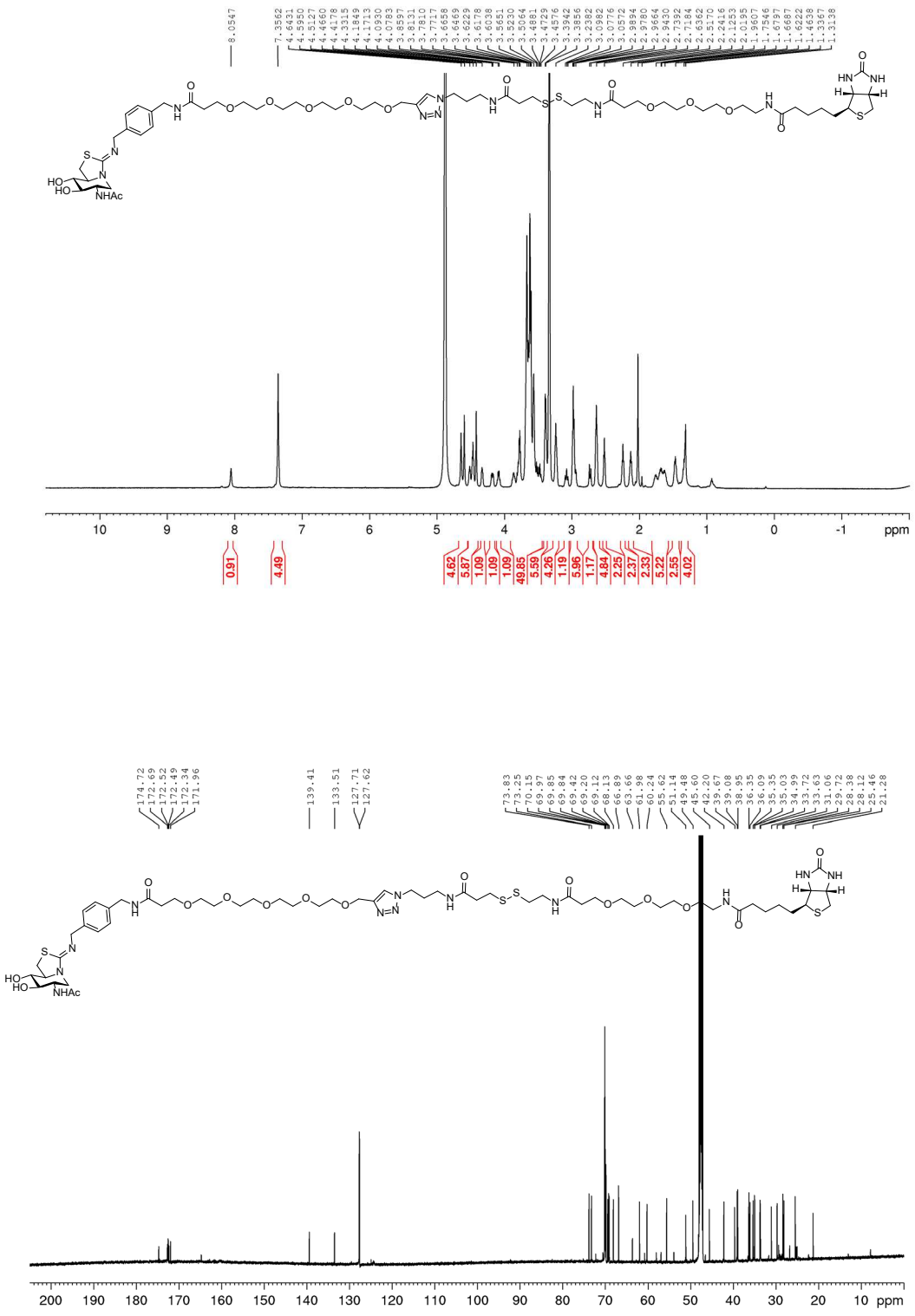

Supplemental Figure 68. ^{1}H NMR and ^{13}C NMR (600 MHz, 150 MHz CD_3OD) of **40**

References

(1) A. F. G. Glawar, D. Best, B. J. Ayers, S. Miyauchi, S. Nakagawa, M. Aguilar-Moncayo, J. M. García Fernández, C. Ortiz Mellet, E. V. Crabtree, T. D. Butters, F. X. Wilson, A. Kato, G. W. J. Fleet. Scalable Syntheses of Both Enantiomers of DNJNAc and DGJNAc from Glucuronolactone: The Effect of N-Alkylation on Hexosaminidase Inhibition. *Chem. Eur. J*. **2012**, *18*, 9341–9359.

(2) J. R. Thomas, X. Liu, P. J. Hergenrother. Size-Specific Ligands for RNA Hairpin Loops. *J. Am. Chem. Soc*. **2005**, *127*, 12434–12435.

(3) K. N. Farrugia, D. Makuc, A. Podborska, K. Szaciłowski, J. Plavec, D. C. Magri. Colorimetric Naphthalene-Based Thiosemicarbazide Anion Chemosensors with an Internal Charge Transfer Mechanism. *Eur. J. Org. Chem*. **2016**, *16*, 4415–4422.

(4) K. A. Stubbs, J. P. Bacik, G. E. Perley-Robertson, G. E. Whitworth, T. M. Gloster, D. J. Vocadlo, B. L. Mark. The Development of Selective Inhibitors of Nagz: Increased Susceptibility of Gram-Negative Bacteria to β-Lactams. *ChemBioChem* **2013**, *14*, 1973–1981.

(5) K. N. Lau, H. F. Chow, M. C. Chan, K. W. Wong. Dendronized Polymer Organogels from Click Chemistry: A Remarkable Gelation Property Owing to Synergistic Functional-Group Binding and Dendritic Size Effects. *Angew. Chem. Int. Ed*. **2008**, *47*, 6912–6916.

(6) C. Roth, S. Chan, W. A. Offen, G. R. Hemsworth, L. I. Willems, D. T. King, V. Varghese, R. Britton, D. J. Vocadlo, G. J. Davies. Structural and Functional Insight into Human O-GlcNAcase. *Nat. Chem. Biol*. **2017**, *13*, 610-612.

(7) R. J. Dennis, E. J. Taylor, M. S. Macauley, K. A. Stubbs, J. P. Turkenburg, S. J. Hart, G. N. Black, D. J. Vocadlo, G. J. Davies. Structure and Mechanism of a Bacterial β-Glucosaminidase Having O-GlcNAcase Activity. *Nat. Struct. Mol. Biol*. **2006**, *13*, 365-371.

(8) G. Winter, J. Appl. Xia2 : An Expert System for Macromolecular Crystallography Data Reduction. *Crystallogr*. **2010**, *43*, 186-190.

(9) P. Evans. Scaling and Assessment of Data Quality. *Acta Crystallogr. Sect. D Biol. Crystallogr*. **2006**, *62*, 72-82.

(10) P. R. Evans, G. N. Murshudov. How Good Are My Data and What Is the Resolution? *Acta Crystallogr. Sect. D Biol. Crystallogr*. **2013**, *69*, 1204-1214.

(11) M. D. Winn, C. C. Ballard, K. D. Cowtan, E. J. Dodson, P. Emsley, P. R. Evans, R. M. Keegan, E. B. Krissinel, A. G. W. Leslie, A. McCoy, S. J. McNicholas, G. N. Murshudov, N. S. Pannu, E. A. Potterton, H. R. Powell, R. J. Read, A. Vagin, K. S. Wilson. Overview of the CCP 4 Suite and Current Developments. *Acta Crystallogr. Sect. D Biol. Crystallogr*. **2011**, *67*, 235-242.

(12) A. Vagin, A. Teplyakov. Molecular Replacement with MOLREP. *Acta Crystallogr. Sect. D Biol. Crystallogr*. **2010**, *66*, 22-25.

(13) P. Emsley, B. Lohkamp, W. G. Scott, K. Cowtan. Features and Development of Coot. *Acta Crystallogr. Sect. D Biol. Crystallogr*. **2010**, *66*, 486-501.

(14) G. N. Murshudov, A. A. Vagin, E. J. Dodson. Refinement of Macromolecular Structures by the Maximum-Likelihood Method. *Acta Crystallogr. Sect. D Biol. Crystallogr*. **1997**, *53*, 240-255.

(15) G. N. Murshudov, P. Skubák, A. A. Lebedev, N. S. Pannu, R. A. Steiner, R. A. Nicholls, M. D. Winn, F. Long, A. A. Vagin. REFMAC 5 for the Refinement of Macromolecular Crystal Structures. *Acta Crystallogr. Sect. D Biol. Crystallogr*. **2011**, *67*, 355-367.

(16) N. S. Pannu, G. N. Murshudov, E. J. Dodson, R. J. Read. Incorporation of Prior Phase Information Strengthens Maximum-Likelihood Structure Refinement. *Acta Crystallogr. Sect. D Biol. Crystallogr*. **1998**, *54*, 1285-1292.

(17) A. A. Vagin, R. A. Steiner, A. A. Lebedev, L. Potterton, S. McNicholas, F. Long, G. N. Murshudov. REFMAC 5 Dictionary: Organization of Prior Chemical Knowledge and Guidelines for Its Use. *Acta Crystallogr. Sect. D Biol. Crystallogr*. **2004**, *60*, 2184-2195.

(18) C. J. Williams, J. J. Headd, N. W. Moriarty, M. G. Prisant, L. L. Videau, L. N. Deis, V. Verma, D. A. Keedy, B. J. Hintze, V. B. Chen, S. Jain, S. M. Lewis, W. B.

Arendall, J. Snoeyink, P. D. Adams, S. C. Lovell, J. S. Richardson, D. C. Richardson. MolProbity: More and Better Reference Data for Improved All-Atom Structure Validation. *Protein Sci*. **2018**, *27*, 293-315.

(19) J. Agirre, J. Iglesias-Fernández, C. Rovira, G. J. Davies, K. S. Wilson, K. D. Cowtan. Privateer: Software for the Conformational Validation of Carbohydrate Structures. *Nat. Struct. Mol. Biol*. **2015**, *22*, 833-834.

(20) S. McNicholas, E. Potterton, K. S. Wilson, M. E. M. Noble. Presenting Your Structures: The CCP 4 Mg Molecular-Graphics Software. *Acta Crystallogr. Sect. D Biol. Crystallogr*. **2011**, *67*, 386-394.